Stochastic models for variability changes in neuronal point processes

Dissertation
zur Erlangung des Doktorgrades
der Naturwissenschaften

vorgelegt beim Fachbereich 12 (Informatik und Mathematik)
der Johann Wolfgang Goethe-Universität
in Frankfurt am Main

von
Stefan Albert
aus Bad Homburg v. d. Höhe

Frankfurt am Main 2018
(D30)

Vom Fachbereich 12 (Informatik und Mathematik) der
Johann Wolfgang Goethe-Universität als Dissertation angenommen.

Dekan:
Prof. Dr. Andreas Bernig

Gutachter:
Prof. Dr. Gaby Schneider
Prof. Dr. Anton Wakolbinger

Datum der Disputation:
13.07.2018

Acknowledgements

I would like to thank my advisor Prof. Dr. Gaby Schneider for giving me the opportunity to work on this thesis and join her research group. Moreover, I am very grateful for her constant support, her innovative ideas and the fruitful and motivating discussions. She guided me into the world of science and shared her valuable experience in interdisciplinary research.

I thank Dr. Michael Messer for always being a source of new ideas, his great technical help and all the hints for improving the presentation of mathematical results. Additionally, thanks to Dr. Brooks Ferebee for inspring discussions.

For a pleasant and stimulating collaboration and the preparation of the data used in the second part of this thesis I thank Dr. Katharina Schmack and Prof. Dr. Philipp Sterzer. Additionally, I thank Dr. Julia Schiemann for collecting the data used in the first part of this thesis.

I thank Prof. Dr. Ralph Neininger and Prof. Dr. Anton Wakolbinger for always promoting me during the course of my studies.

Furthermore, I thank my room mates Matthias Gärtner and Benjamin Straub for the manifold discussions and the wonderful working atmosphere.

I am grateful to Rebecca Büchner for proofreading the thesis in detail and giving numerous detailed and very helpful hints to improve the argumentation and presentation.

This work was supported by the BMBF within the framework of the e:Med research and funding concept (grant number 01ZX1404B). I would like to express my gratitude for this financial support.

In the end I would like to thank my family for the constant support of my studies.

Contents

Chapter 1

Introduction and outline

1.1 Motivation

Time series of events play an important role in neuroscience and are often described by point processes on the real line. A first and far-reaching example is information processing in the brain. By integration of input from adjoining cells or from sensory organs such as the ears and eyes, nerve cells (also called neurons) transmit electric signals – so-called spikes – to adjacent cells so that information is processed. In precise terms, spikes are short periods (of length 1-2ms) of a typical increase in the neuron's membrane potential. As the duration and the height of this increase do not differ remarkably, it is commonly assumed that the information content of neuronal activity is mainly coded by the temporal sequence of spiking the so-called neuronal **spike train**. For the understanding of the nervous system, it is therefore crucial to develop a deep insight into neural firing activity. A detailed explanation of the role of neurons and the whole nervous system can be found in, e.g., the textbooks of Kandel et al. (2000) and Berg et al. (2007).

Formally, a spike train is given by the sequence $(t_1, t_2, \ldots, t_n)$ of spike times in a recording interval $[0,T]$ (with $0 < t_1 < t_2 < \ldots < t_n < T < \infty$). The intervals between consecutive spike times are called inter-spike intervals or life times. Spike trains with usually hundreds of events are a well studied object in computational neuroscience, where statistical models based on point processes like renewal processes are used frequently (Johnson, 1996; Dayan and Abbott, 2005; Kass et al., 2005; Nawrot et al., 2008; Grün and Rotter, 2010).

Often stationarity of the process parameters like rate or variance of the life times is required for further analyses such as coordination between parallel point processes (e.g., Grün and Rotter, 2010). Change points in the rate may cause misinterpretations of serial correlations when assuming a constant rate (Farkhooi et al., 2009). The impact of neglecting non-constant parameters on techniques assuming stationarity is further discussed in, e.g., Brody (1999); Grün et al. (2003). Hence, it is crucial to capture potential change points, and non-stationary spike trains are in a preprocessing step often split up into sections with approximately constant parameters (Schneider, 2008; Staude et al., 2010; Quiroga-Lombard et al., 2013). To detect changes in the rate, considerable research has been conducted, e.g., by Fryzlewicz (2014); Messer et al. (2014); Eichinger and Kirch (2018), compare also the reviews of Khodadadi and Asgharian (2008); Aue and Horváth (2013); Jandhyala et al. (2013). Little is known about the detection of variance change points, especially with rate change points being present. To the best of our knowledge, the only theoretical work dealing with variance changes in presence of

a non constant mean is Dette et al. (2015). An example of a spike train with both – rate and variance changes – is given in Figure 1.1. The occurrence times of the spikes are symbolized by the vertical bars.

Figure 1.1: A point process with a non-stationary rate and variance profile.

Detected changes of the rate or the variance not only improve statistical analysis by separating stationary periods but might also contain important information themselves. Different firing patterns as described, e.g., in Bingmer et al. (2011) are connected to changes in variability. For instance, in dopamine neurons the firing patterns often switch between a low-rate regular or irregular single spike background pattern and short so-called "bursty" periods with a large number of spikes. These bursty periods represent a possible change in variance and have been shown to be coupled to an increase in dopamine release (e.g., Gonon, 1988; Schiemann et al., 2012).

A second example showing the application of time series of events in neuroscience are **response patterns** to behavioral experiments like ambiguous stimuli. The perception of ambiguous stimuli changes spontaneously in an unpredictable and subjective manner. Traditional examples of ambiguous stimuli are the Necker cube (Necker, 1832) or Rubin's vase (Rubin, 1915), see Figure 1.2. In these examples, there are two possible perceptions such that we also speak of bistable perception.

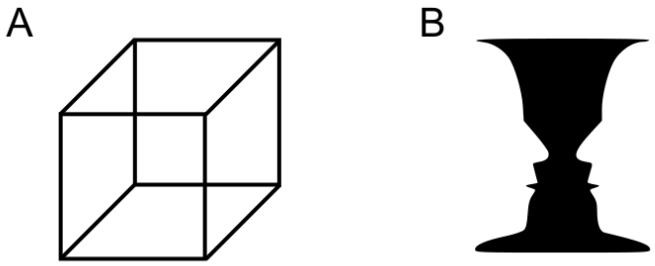

Figure 1.2: Necker Cube (A) and Rubin's vase (B). *In the Necker Cube either the upper-right or the lower-left square can be interpreted as front side. Rubin's vase may be perceived as vase or as two faces looking at each other. The graph is slightly modified from https://commons.wikimedia.org/wiki/File:Multistability.svg (Public Domain license).*

Recently, also rotating spheres with switching perceived rotation direction were used in bistable perception experiments, e.g., Schmack et al. (2013, 2015). The increasing sequence of perceptual reversal points $(t_1, t_2, \ldots, t_n)$ in a recording interval $[0, T]$ is called response pattern, and the periods of constant perception are called **dominance times**. Examples for continuous and intermittent presentation (i.e., with short blank displays between the presentation phases of the stimulus) are shown in Figure 1.3.
We observe an increase in variability from continuous (green) to intermittent presentation (blue) in Figure 1.3 compared to the respective mean dominance times. During continuous

presentation the dominance times appear to be unimodal distributed, whereas during intermittent stimulation phases of rapidly changing perception interchange with long stable phases (reported also by Brascamp et al., 2009). Modeling these different types of response patterns as well as linking them to possible underlying neuronal mechanisms in a model with only a few interpretable parameters such that also possible differences between groups can be explained is a challenging task. Current approaches often use detailed assumptions and large parameter sets, which complicate parameter estimation.

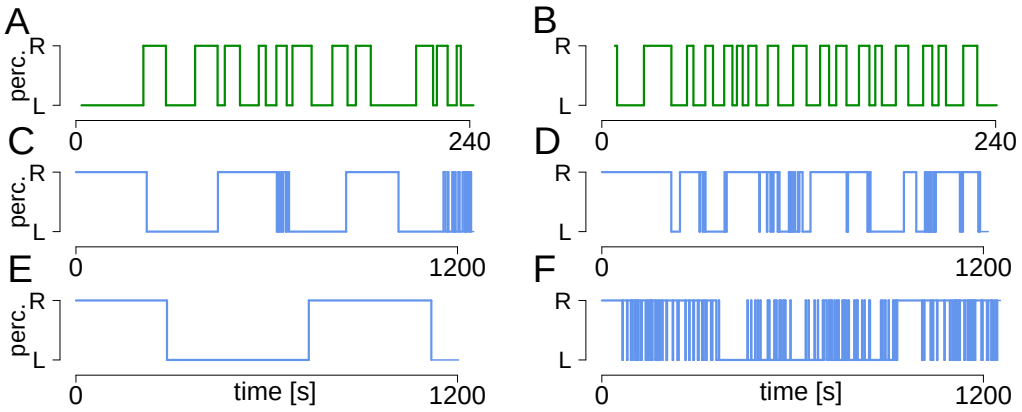

Figure 1.3: Examples of response patterns to a bistable stimulus. Response patterns to continuous (green, A,B) and intermittent (blue, C-F) presentation from the data set reported in Schmack et al. (2015). *Each of the six response patterns shows the responses of one individual to continuous presentation (recording time 240s, green) or intermittent presentation (recording time 1200s, blue) of the bistable stimulus. While the distribution of dominance times tends to be unimodal in the continuous case, stable and unstable phases seem to interchange in intermittent stimulation. In addition, response patterns can be highly variable across subjects.*

Main goals of the thesis

The overall goal of the thesis is to describe and detect different kinds of variability changes in point processes on the real line analyzed in neuroscience as introduced above. The thesis is divided into two parts. In the first part, we focus on the detection of non-stationarities in the rate and variance (of the life times) of point processes like neuronal spike trains. The main goal is to extend the multiple filter method proposed by Messer et al. (2014) to detect changes in the variance in multiple time scales in presence of rate change points where we assume the rate to be a step function. The method uses a non-parametric approach that is applicable to a wide range of inter spike (or life time) distributions if there are enough events.
The subject of inquiry in the second part are the aforementioned response patterns to bistable stimuli, where in particular data of Schmack et al. (2013, 2015) are used. The main goal of this part is to develop a model that builds a bridge between empirical data analysis and mechanistic modeling and that captures the change in variability from continuous to intermittent presentation. Thus, the model should be able to describe both the response patterns to continuous presentation (with a one-peaked distribution of dominance times) and the response patterns to intermittent presentation where the distribution of dominance times is

rather bimodal (compare Figure 1.3). Moreover, the model should be fittable to typically short experimental data such that statistical investigation of differences between clinical groups is possible, and the model should allow for neuronal correlates.
In summary, variability changes in point processes should be described in both parts of the thesis, where in the first part a broadly applicable method for change point detection in the rate and the variance is presented, and in the second part we focus on a direct modeling approach with a model enabling links to neuronal processes and describing the variability change in response patterns from continuous to intermittent presentation of a bistable stimulus.

1.2 Outline of the thesis

1.2.1 Outline of Part I

Part I deals with the detection of non-stationarities in point processes like neuronal spike trains. The multiple filter test and algorithm (MFT and MFA) developed by Messer et al. (2014) in order to detect changes in the rate of a wide class of point processes with a certain variability in the variance of life times are explained. The key idea of the MFT is to use the filtered derivative approach (e.g., Bertrand, 2000), i.e., to compare the estimated rate in two adjacent windows, to slide these windows over the process and to use multiple window sizes such that small as well as fast changes can be detected. We extend this idea in Chapter 3 to detect changes also in the variance in the potential presence of rate change points by regarding the scaled difference

$$G_{h,t} := \frac{\hat{\sigma}^2_{\text{ri}} - \hat{\sigma}^2_{\text{le}}}{\sqrt{\widehat{\mathbb{V}\text{ar}}(\hat{\sigma}^2_{\text{ri}} - \hat{\sigma}^2_{\text{le}})}},$$

where $\hat{\sigma}^2_{\text{ri}}$ and $\hat{\sigma}^2_{\text{le}}$ are estimators of the variances in two adjacent windows of size h incorporating potential rate change points. Two limit results for the derivation of the rejection threshold identify under the null hypothesis of variance homogeneity Gaussian limit processes of $(G_{h,t})_t$ for the case of constant rate and one rate change point (Theorems 3.4 and 3.6). The limit process $\widetilde{L}$ in the case of one rate change point depends on unknown point process parameters but is closely related to the limit process L emerging in the rate homogeneous case and being independent of process parameters. Both are centered Gaussian processes with unit variance where only the covariance structures slightly differ in the neighborhood of the rate change point (Figure 5.4). In case of more than one rate change point the limit process is similar to $\widetilde{L}$. Thus, in practice L can be used which is also supported by simulation results. Detailed proofs using a Functional Central Limit Theorem (FCLT), continuous mapping and the consistency of the estimator in the denominator of $G_{h,t}$ are given in Section 4. The procedure can also be extended to higher order moments assuming constant lower order moments (Corollary 3.5).
In case of rate change points we propose to estimate these change points first (by an application of the MFA that combines the change points detected by different window sizes preferring change points detected by smaller windows) and then include them in the analysis of variances (Section 5.2.1). The empirical properties of this asymptotic procedure are evaluated in Chapter 5 showing that for the smallest window containing at least about 150 events the asymptotic significance level is kept also in case of an inhomogeneous rate (Figure 5.1). Moreover, the detection probability of variance change points is considerably large (Figure 5.5) and is hardly effected by the necessity to estimate potential rate change points. Finally, the two-step procedure to detect rate and variance change points is applied to a data set of neuronal spike

trains reported in (Schiemann et al., 2012) to underline the practical applicability of the method (Chapter 6). In the majority of spike trains, rate and/or variance change points were detected.

Part I is published most widely in Albert et al. (2017a) and partly builds on Albert (2014). The `R`-code of the MFT for the variances is part of the `MFT` package available on CRAN (https://CRAN.R-project.org/package=MFT, Messer et al. (2017)).

1.2.2 Outline of Part II

In the second part of the thesis, two models to describe response patterns to bistable stimulation (as, e.g., recorded by Schmack et al. (2013, 2015)) are developed. We start in Chapter 9 by applying for the first time a simple Hidden Markov Model (HMM) to the response patterns, whereby there is one state for the response patterns to continuous presentation, and two states for the intermittent case. The transition between the hidden states is modeled by a hidden Markov chain and the observable emissions depend on the state. During intermittent presentation one state describes the short dominance times during periods of perception changing rapidly, and the other state models the long stable dominance times. The parameter estimation is described in Chapters 9.3 and 9.4 for the assumptions of Gamma and inverse Gaussian distributed life times (Wilson, 2007; Gigante et al., 2009; Gershman et al., 2012; Cao et al., 2016). Basically, maximum likelihood estimation is used, where in the case of the two-state HMM an expectation maximization algorithm is applied for iterative likelihood maximization. Theoretical results (like first passage times, number of perceptual changes or stationarity properties) for the resulting point process of perceptual reversals are derived in Chapter 10. The estimation precision and the fitting to the data set of Schmack et al. (2015) are quite good (chapters 9.6 and 14.1). However, the HMM is a descriptive approach that lacks connections to possible underlying neuronal processes.
That is why we introduce a hierarchical Brownian model (HBM) in Chapter 11, which allows us to connect the descriptive analysis of response patterns with potential underlying neuronal processes. The key idea of the model is to describe the activity difference P_t between conflicting neuronal populations as Brownian motion with drift ν_0 fluctuating between two borders $\pm\, b$ as follows

$$dP_t = S_t \nu_0 dt + dW_t, \quad \text{where} \quad P_0 = -b,$$

with S_t describing the sign of the drift and W_t as standard Brownian motion. Each first passage time leads to a change in perception and in the sign of the drift S_t (Chapter 11.1). In addition to this perception process, a background process is modeled during intermittent presentation that is responsible for the type of state, stable or unstable, by modeling the drift and border of the perception process (Chapter 11.2). The parameters of the HBM for continuous presentation are estimated via maximum likelihood (ML) exploiting the inverse Gaussian distribution of first hitting times by a Brownian motion with drift (Chapter 12.1). The likelihood in the case of intermittent presentation is expressed using forward variables and maximized as described in detail in Chapter 12.2. Using the Viterbi algorithm, the hidden state of each dominance time can be estimated (Chapter 12.5). Moreover, theoretical results concerning the resulting point processes are derived (Chapter 13). Especially the relative time spent by the hidden process $\tilde{Y}$ in the stable state is of interest. Finally, the model is applied to the data set Schmack et al. (2013, 2015) showing good model fit and yielding potential

explanations for observed behavioral differences between a group of controls and a group of patients with schizophrenia (Chapter 14.2).

A condensed version of Part II (including the most important content of chapters 9, 11, 12, 14 and 15) has been published by Albert et al. (2017b).

The computations have been performed using the statistical software RStudio basing on the programming language `R`. We mainly used a Mac Pro with a 2.7 GHz 12-Core Intel Xeon E5 processor and 32 GB working memory. Operating system was OS X El Capitan, Version 10.11.6.

Part I

Multi-scale detection of variance changes in renewal processes in the presence of rate change points

Chapter 2

Introduction

Motivation

Non-stationarity of the rate or variance of events is a well-known problem in the description and analysis of time series of events. For example, neuronal spike trains are often analyzed with point process models (Dayan and Abbott, 2005; Kass et al., 2005; Grün and Rotter, 2010). As such analyses can be affected by changes in process parameters, it is often necessary to use preprocessing steps that divide the processes into sections with approximately constant parameters (Grün et al., 2002; Schneider, 2008; Staude et al., 2010; Quiroga-Lombard et al., 2013). These preprocessing steps use models with step functions for the parameters and aim at detecting the points in time when the parameters change, i.e., the change points.

For the detection of change points in the rate (or equivalently change points in the mean of sequences of random variables), several techniques have been developed, e.g., moving sums (MOSUM, using parts of the data in moving windows, Eichinger and Kirch, 2018), which are also called filtered derivative (Bertrand, 2000; Bertrand et al., 2011), cumulative sums (CUSUM, similar to likelihood ratios and referring to the entire data, Horváth et al., 2008) or penalized least squares (minimizing the quadratic deviations from the mean values and using the number of change points as penalty, Lavielle and Moulines, 2000). Interesting multi scale methods have been proposed by Fryzlewicz (2014); Matteson and James (2014); Messer et al. (2014); Frick et al. (2014) using wild binary segmentation (basing on CUSUM statistics on randomly chosen intervals), E-Divisive (comparing the time series using a distance function on all adjacent intervals), filtered derivative and likelihood-ratio statistics. For a general survey about change point methods we refer to the books Basseville and Nikiforov (1993); Brodsky and Darkhovsky (1993); Csörgö and Horváth (1997); Brodsky (2017) or the review articles of Aue and Horváth (2013); Jandhyala et al. (2013).

Some of these techniques can also be applied to the detection of variance change points (by studying the quadratic deviations from the mean). Other approaches to the analysis of variance homogeneity use CUSUM (Hsu, 1977; Inclan and Tiao, 1994; Whitcher et al., 2000), Bayesian ideas (Inclan, 1993), binary segmentation (Chen and Gupta, 1997), penalized likelihoods (Killick et al., 2010), ratio tests of cumulative sums (Zhao et al., 2010), likelihood methods (Noorossana and Heydari, 2012), wavelet based methods (wavelets are oscillating functions with some desirable properties, Killick et al., 2013; Nam et al., 2015) and wild binary segmentation (Korkas and Fryzlewicz, 2017).

However, most available methods use specific assumptions on the underlying distribution, e.g., Gaussian sequences (Inclan, 1993; Chen and Gupta, 1997; Whitcher et al., 2000; Killick

et al., 2010; Noorossana and Heydari, 2012), or aim at detecting at most one change point like Hsu (1977); Chen and Gupta (1997); Zhao et al. (2010). In addition, they usually assume the rate to be constant (sometimes even a known rate is claimed). Few applied approaches simultaneously deal with potential rate and variance changes (Hawkins and Zamba, 2005; Rodionov, 2005) using control charts or sequential F-tests. Recently, Dette et al. (2015) proposed a CUSUM based test for the null hypothesis of constant variance in the presence of a smoothly varying mean. However, we are not aware of a method that can detect multiple rate and variance changes occurring on different time scales in point processes with a wide variety of life time distributions.

Main goals

The goal of this first part of the thesis is the (further) development of a technique to detect both rate and variance change points (see Figure 2.1) that may occur in multiple time scales. The structure of the underlying point process is unknown and can be highly diverse including weak and strong changes of the rate and/or the variance as well as changes occurring slowly or fast. The procedure should be applicable to renewal processes with a wide range of life time distributions, i.e., we use a non-parametric approach.

Figure 2.1: A point process with a non-stationary rate and variance profile.

To that end, we propose a two-step procedure that first tests the null hypothesis of rate homogeneity allowing for an inhomogeneous variance and that estimates change points in the rate if the null hypothesis is rejected. In the second step, we test the null hypothesis of variance homogeneity and estimate variance change points. As this step requires estimation of the underlying rate, we propose to plug in the estimated rate change points derived in the first step. In our setting we are not restricted to the alternative of at most one change-point and allow for change points in the rate such that the rate is given by a step function.

The multiple filter test (MFT)

The procedure builds on the multiple filter test (MFT) (Messer et al., 2014) and a corresponding algorithm (MFA). These were originally designed for the detection of change points in the rate on different time scales in a wide class of point processes which allows for a certain variability in the variance of the life times and are thus considered suitable candidates for the first step of rate change detection here. They will be modified in the second step to allow for the detection of variance changes. The filtered derivative idea used in the MFT works as follows. Assume that each life time ξ_i of a point process on $(0, T]$ depends on a parameter ϑ_i of which change points are to be detected. For a window of size h and each time t in the analysis region $\tau_h := [h, T - h]$, compare the information about ϑ in the left and right window denoted here by $J_{\text{le}} := J(t - h, t]$ and $J_{\text{ri}} := J(t, t + h]$, using a scaled process $G := (G_{h,t})_t$ with

$$G_{h,t} := \frac{J_{\text{ri}} - J_{\text{le}}}{\hat{s}_t}, \tag{2.1}$$

where $\hat{s}$ is an appropriate estimator for the standard deviation of the numerator under the null hypothesis of no change point in ϑ. Figure 2.2 visualizes the idea.

For example, Messer et al. (2014) use the numbers of events in the left and right window in order to detect change points in the mean of the life times. Under mild assumptions (especially fulfilled by renewal processes), the process G converges weakly under the null hypothesis to a process $L := (L_{h,t})_t$ given by

$$L_{h,t} := \frac{(W_{t+h} - W_t) - (W_t - W_{t-h})}{\sqrt{2h}}, \tag{2.2}$$

for a standard Brownian motion $(W)_{t\geq 0}$, if the window size h grows linearly with the total time T. Note that the process L does not depend on the parameters of the point process.

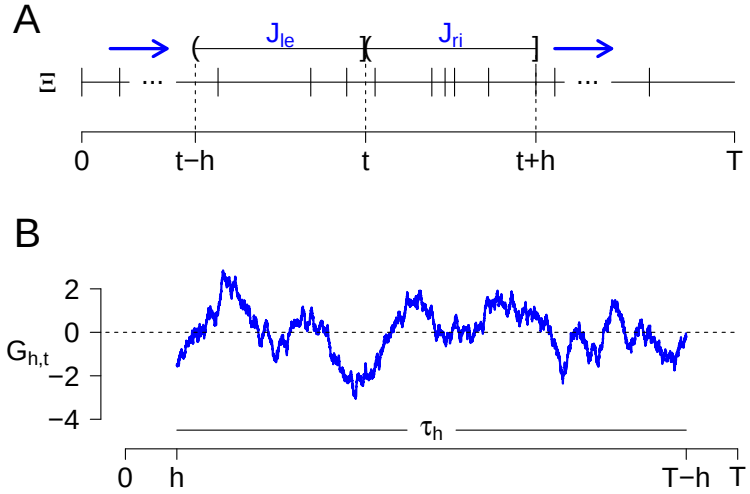

Figure 2.2: Schematic representation of the derivation of $G_{h,t}$ (A) and an exemplary $(G_{h,t})_{t\in\tau_h}$-process (B). *(A) At each time $t \in \tau_h$ the information J_{le} about ϑ in the left window is compared to the information J_{ri} about ϑ in the right window. $G_{h,t}$ is the scaled difference of J_{le} and J_{ri}. The double window slides along the process visualized by the blue arrows such that the process $(G_{h,t})_{t\in\tau_h}$ is obtained. (B) An example of a process $(G_{h,t})_{t\in\tau_h}$ with $T = 2500$ and $h = 200$ which is derived using the number of events in the left and the right window as information from a stationary Poisson process Ξ on $(0, T]$ with independent exponential(2) distributed lifetimes. The figure is based on Figure 3.3 in Messer (2014).*

While under the null hypothesis G fluctuates around zero, a change in ϑ at time t should cause systematic deviations from zero. Therefore, a large temporal maximum $M_h := \max_t |G_{h,t}|$ indicates a change point in ϑ. Using a finite set of multiple windows $H = \{h_1, \ldots, h_k\} \subset (0, T/2]$ simultaneously, the MFT allows for the detection of change points on different time scales. The global maximum M of all processes $(G_{h,t})_{h\in H}$ serves as a test statistic whose distribution can be approximated from the corresponding limit processes $(L_{h,t})_{h\in H}$, i.e.,

$$M := \max_{h\in H} M_h = \max_{h\in H} \max_{t\in[h,T-h]} |G_{h,t}| \sim \max_{h\in H} \max_{t\in[h,T-h]} |L_{h,t}|.$$

By simulating these limit processes $(L_{h,t})_{h\in H}$ as functionals of the same underlying Brownian motion, the rejection threshold Q of the MFT can be obtained. We stress that the derivation

of the quantile Q works in two steps: First, we use that the maximum of all processes $(G_{h,t})_t$ over all windows h converges to the maximum of the limit processes $(L_{h,t})_t$ over all windows h, the latter being a functional of a standard Brownian motion and particularly independent from parameters of the input spike train. Then, in a second step, we simulate Q as a quantile of the limit law. (To the best of our knowledge, there is no closed formula expression for the limit law where we could directly read Q from.) The main reason for this two step approach is that it allows for the simultaneous application of multiple windows, which helps to improve the detection of change points that appear on different time scales: small windows are more sensitive to frequent change points, while larger windows have higher power and thus improve the detection of parameter changes of smaller magnitude.

The MFT for variance changes – outline of Part I

In order to perform the second step of change point detection in the variance, we extend the MFT here, where now the relevant information J in the process G from (2.1) is an estimator of σ^2 (Section 3.1),

$$G_{h,t} := \frac{\hat{\sigma}^2_{\text{ri}} - \hat{\sigma}^2_{\text{le}}}{\hat{s}_t}, \tag{2.3}$$

where $\hat{s}_t$ denotes an estimator of the standard deviation of the numerator. Assuming first rate homogeneity with independent identically distributed (i.i.d.) life times, we show that under the null hypothesis of constant variance, G converges weakly in Skorokhod topology to the same limit process L (eq. (2.2)) (Section 3.2). This enables to test for and estimate change points in the variance analogously to rate change points, applying the modified process G from equation (2.3). This procedure can also be extended to higher order moments assuming constant lower order moments (Section 3.3). We then deal with processes that contain rate and variance changes by investigating the impact of one rate change point on the limit behavior of G in Section 3.4. Under the null of constant variance, the limit process is a continuous, $2h$-dependent zero-mean, unit-variance Gaussian process $\widetilde{L}$ similar to L (Theorem 3.6), with slight changes in the covariance structure in the neighborhood of a rate change point. The proofs are outsourced to Chapter 4 using a Functional Central Limit Theorem, continuous mapping and the consistency of the estimator $\hat{s}_t$. As the process $\widetilde{L}$ depends on unknown point process parameters, we suggest to use L to derive the rejection threshold of the test. This is supported by our theoretical and simulation results.
The practical performance of the MFT and the corresponding MFA (Messer et al., 2014) for the detection of variance change points is presented in Chapter 5. As the MFT is an asymptotic method, we study the empirical significance level. Our simulations suggest that in case of about 150 events in the smallest window of H the significance level of the MFT for variance changes is kept for a wide range of parameter settings also in cases with multiple unknown rate changes (Chapters 5.1 and 5.2). Further, the detection probability of variance change points is considerable and barely affected by the necessity to estimate rate change points. The detection probability depends on the magnitude of the variance change as well as on the regularity of the process (Chapter 5.3). We present an example for the MFA on rate and variance change point detection and illustrate the importance of including existing rate change points in the estimation of variance change points. Finally, we use the MFA in Chapter 6 to estimate rate and variance change points in spike train recordings obtained in the substantia nigra of anesthetized mice as reported partly in Schiemann et al. (2012). In about 50% of the cases both null hypotheses of constant rate and constant variance are rejected and

different change points are detected by different window sizes. In Chapter 7 we summarize and discuss the results of Part I of this thesis.

Notation

We state basic notation used in this first part of the thesis. For $p \in (0, \infty)$ we call a real-valued random variable X p-times integrable if $\mathbb{E}[|X|^p] := \int_{\mathbb{R}} |x|^p dP_X(x) < \infty$. $\mathscr{L}^p$ is the set of all p-times integrable random variables. If X is integrable, we denote the expectation of X by $\mathbb{E}[X]$ and in case of X being twice integrable $\mathbb{V}\text{ar}(X) := \mathbb{E}[X^2] - \mathbb{E}[X]^2$ is the variance of X. The m-th moment of a random variable $X \in \mathscr{L}^p$ is given by $\mathbb{E}[X^m]$, for all $m = 1, 2, \ldots, p$. We use $\xrightarrow[d]{}$ to denote weak convergence and $\xrightarrow[\mathbb{P}]{}$ to abbreviate convergence in probability. *almost surely* is abbreviated by a.s.
For $\tau > 0$ we denote the set of all càdlàg functions on $[0, \tau]$ by $D[0, \tau]$. $d_{||\cdot||}$ serves as abbreviation for the metric induced by the supremum norm. The Skorokhod metric on $D[0, \tau]$ is abbreviated by d_{SK}. We use $D[0, \infty)$ with the Skorokhod metric. Note the fact that convergence in $(D[0, \infty), d_{||\cdot||})$ implies convergence in $(D[0, \infty), d_{SK})$. For details on the Skorokhod metric we refer to Billingsley (1968). Furthermore, for an a.s. constant stochastic process in $D[0, \tau]$ with value c we abbreviate the process $(c)_{t \in [0,\tau]}$ with c. Note that uniform a.s. convergence interchanges with sums in general and with products if the limits are constant.

In both parts of the thesis, we use the well-known Gamma distribution. It is, for example, discussed in Lehmann and Casella (1998). Note that, in this thesis, we use a non-standard parametrization of the Gamma distribution (Remark 2.3).

Definition 2.1. ***Gamma and Exponential distribution***
The Gamma distribution $\Gamma(p, \theta)$ for the two parameters $p > 0, \theta > 0$ is given by the probability density function

$$f(x) = \frac{\theta^p}{\Gamma(p)} x^{p-1} e^{-\theta x}, \text{if } x > 0,$$

and $f(x) = 0$ else.
$\Gamma(p)$ is the value of the Gamma function at p:

$$\Gamma(p) := \int_0^\infty t^{p-1} e^{-t} dt$$

A Gamma distribution with parameter $p = 1$ is also called Exponential distribution.

Proposition 2.2. ***Moments of the Gamma distribution***
Let X be a Gamma-distributed random variable with parameters p and θ. Then, we have

$$\mathbb{E}[X] = \frac{p}{\theta}, \qquad \mathbb{V}ar(X) = \frac{p}{\theta^2}.$$

Remark 2.3. ***Reparametrization of the Gamma distribution***
In this thesis, we will speak of a Gamma distribution with mean $\mu > 0$ and standard deviation $\sigma > 0$ (and density $f^{\Gamma}_{\mu,\sigma}$) to simplify interpretation. Using the parameter transformations $p = \mu^2/\sigma^2$ and $\theta = \mu/\sigma^2$, one obtains the notation of Definition 2.1.

Point and renewal processes Point and renewal processes are crucial for this thesis. Therefore, we briefly state corresponding notation.
Instead of giving the detailed and technical definition of (general) point processes we restrict us to the following Notation 2.4 and refer for details to Daley and Vere-Jones (1988).

Notation 2.4. ***Description of point processes on the line***
Two equivalent ways to describe a point process Ξ on $\mathbb{R}$ are

1. *Sequence of occurrences $\{T_i : i \in \mathbb{Z}\}$.*
2. *First occurrence time T_1 together with the sequence of intervals (life times) $\xi_i = T_{i+1} - T_i, \forall i \in \mathbb{Z}$: $\{\xi_i : i \in \mathbb{Z}\} \cup \{T_1\}$.*

Moreover, we require the famous concept of a renewal process (e.g., Ross, 1996).

Definition 2.5. ***Renewal process***
Let Ξ be a point process on the positive line with i.i.d., positive life times $(\xi_i)_{i=1,2,\ldots}$ with mean $\mu > 0$. Further, let $S_0 := 0$ and $S_n := \sum_{i=1}^{n} \xi_i$ be the time of the n-th event. The corresponding counting process

$$N_t := \max\{n \geq 0 : S_n \leq t\}, \quad t \geq 0,$$

is called a ***renewal*** *process.*

Chapter 3

The MFT for testing variance homogeneity

Here, we derive the limit distribution of the filtered derivative process G when testing for variance homogeneity. The rejection threshold of the statistical test can be obtained as described in the introduction by simulation of the respective functional of the limit process. We first define the model assumptions. Section 3.1 then elaborates on the explicit structure of G when testing for variance homogeneity. Limit results for G under constant rate and under one change point in the rate are given in Sections 3.2 and 3.4, respectively. An extension to the detection of changes in higher order moments assuming constant lower order moments is presented in Section 3.3.
First we define a class $\mathscr{R}$ of renewal processes on the positive line with $\xi_i \in \mathscr{L}^4$ (Definition 3.1). The models with change points in the mean and/or variance considered here are then given as piecewise elements of $\mathscr{R}$ (Definition 3.3).

Definition 3.1. ***The class*** $\mathscr{R}$
The class of point processes with i.i.d., a.s. positive life times $(\xi_i)_{i\geq 1}$ *with* $\xi_1 \in \mathscr{L}^4$ *is called* $\mathscr{R}$.

A process $\Xi \in \mathscr{R}$ whose life times have mean μ and variance σ^2 and $\nu^2 := \mathbb{V}\mathrm{ar}((\xi_1 - \mu)^2)$ is therefore denoted by $\Xi(\mu, \sigma^2) := \Xi(\mu, \sigma^2, \nu^2)$. The inverse of the mean, μ^{-1}, is termed the rate of Ξ.

Remark 3.2. ***Explicit expression for*** $\boldsymbol{\nu^2}$
Using the assumption of finite fourth moments, the parameter ν^2 *of a renewal process* $\Xi(\mu, \sigma^2, \nu^2)$ *can be derived as follows*

$$\begin{aligned}\nu^2 = \mathbb{V}ar((\xi_i - \mu)^2) &= \mathbb{E}[(\xi_i - \mu)^4] - (\mathbb{E}[(\xi_i - \mu)^2])^2 \\ &= \mathbb{E}[{\xi_i}^4] - 4\mu\mathbb{E}[{\xi_i}^3] + 6\mu^2\mathbb{E}[{\xi_i}^2] - 4\mu^3\mathbb{E}[\xi_i] + \mu^4 - \sigma^4 \\ &= \mathbb{E}[{\xi_i}^4] - 4\mu\mathbb{E}[{\xi_i}^3] + 3\mu^4 + 6\mu^2\sigma^2 - \sigma^4.\end{aligned}$$

As an example assume a Gamma distribution with expectation μ *and standard deviation* σ. *Then, we obtain*

$$\nu^2 = \frac{\sigma^6}{\mu^2}\left(2\frac{\mu^2}{\sigma^2} + 6\right),$$

where the exact derivation can be found in Albert (2014).

A class of processes that are piecewise elements of $\mathscr{R}$ is used in order to introduce rate and/or variance changes.

Definition 3.3. ***Renewal process with change points in the mean or variance*** *For $T > 0$ let $C := \{c_1, \ldots, c_k\}$ be a set of change points with $0 < c_1 < \ldots < c_k < T$. At time $t = 0$ start $k+1$ independent elements of $\mathscr{R}$*

$$\Xi_1\left(\mu_1, \sigma_1^2\right), \ldots, \Xi_{k+1}\left(\mu_{k+1}, \sigma_{k+1}^2\right),$$

with $(\mu_i, \sigma_i^2) \neq (\mu_{i+1}, \sigma_{i+1}^2)$. Let $c_0 := 0$, $c_{k+1} := T$ and define

$$\Xi := \bigcup_{j=1}^{k+1} \Xi_j|_{(c_{j-1}, c_j]},$$

where $\Xi_j|_{(c_{j-1}, c_j]}$ denotes the restriction of Ξ_j to the interval $(c_{j-1}, c_j]$.

The family of processes which derive according to Definition 3.3 is called $\mathscr{M}$ (see Figure 3.1 for an example). For $\Xi \in \mathscr{M}$, at each change point c_i the rate and/or the variance changes, such that the rate and variance constitute step functions.
Thus, we test the null hypothesis

$$H_0 : \sigma_1^2 = \ldots = \sigma_{k+1}^2$$

against the alternative

$$H_A : \exists i, j : \sigma_i^2 \neq \sigma_j^2,$$

where we allow for an unknown number of potential additional change points in the rate that may or may not occur simultaneously with rate changes. Note that we require the mean in order to estimate the variances $(\hat{\sigma}_{\text{ri}}^2, \hat{\sigma}_{\text{le}}^2)$ and to derive the test statistic G. We therefore first formulate the theory without explicit assumptions on the mean, letting $\mu^{(i)}$ denote the mean of
and the case where the mean follows a step function, and we investigate the behavior under estimation of $\mu^{(i)}$.

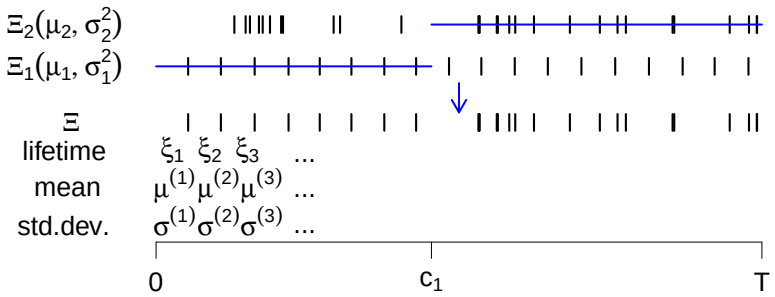

Figure 3.1: A realization of a process Ξ according to Definition 3.3. *Ξ originates from two processes $\Xi_1(\mu_1, \sigma_1^2)$ and $\Xi_2(\mu_2, \sigma_2^2) \in \mathscr{R}$. Each life time ξ_i has mean $\mu^{(i)}$ and standard deviation $\sigma^{(i)}$. Before the change point c_1 the mean of the life times is μ_1 and the standard deviation is σ_1, and afterwards mean and standard deviation change to μ_2 and σ_2, respectively.*

3.1 Filtered derivative approach for the variances

As explained in the introduction, we test the null hypothesis using a window size $h > 0$ and the filtered derivative process from (2.3) for $t \in \tau_h$ defined as

$$G_{h,t} := \frac{\hat{\sigma}^2_{\text{ri}} - \hat{\sigma}^2_{\text{le}}}{\hat{s}_t}$$

if $\hat{s}_t > 0$ and $G_{h,t} := 0$ otherwise. The numerator is given by the standard variance estimators (eq. (3.3)), and $\hat{s}_t$ is a local estimator of the standard deviation of the numerator (eq. (3.4)). We use the notation

$$V_i := (\xi_i - \mu^{(i)})^2 \tag{3.1}$$

with $\mu^{(i)} := \mathbb{E}[\xi_i]$, $(\sigma^{(i)})^2 := \mathbb{E}[V_i] = \mathbb{V}ar(\xi_i)$ and $(\nu^{(i)})^2 := \mathbb{V}ar(V_i)$ (Figure 3.1). Now we include estimated rates, using an estimator $\hat{\mu}^{(i)}$ of $\mu^{(i)}$ and define the estimator of V_i as

$$\hat{V}_i := (\xi_i - \hat{\mu}^{(i)})^2. \tag{3.2}$$

As estimator $\hat{\mu}^{(i)}$ we later use a global estimator derived as the mean of all life times (Theorem 3.4) or a local estimator derived between estimated change points (Theorem 3.6).
If $\hat{I}_{\text{le}}$ and $\hat{I}_{\text{ri}}$ denote the sets of life times in $(t-h, t]$ and $(t, t+h]$ which do not overlap a rate change point, the standard variance estimators are given by

$$\hat{\sigma}^2_{\text{le}} := \frac{1}{|\hat{I}_{\text{le}}|} \sum_{i \in \hat{I}_{\text{le}}} \hat{V}_i \qquad \text{and} \qquad \hat{\sigma}^2_{\text{ri}} := \frac{1}{|\hat{I}_{\text{ri}}|} \sum_{i \in \hat{I}_{\text{ri}}} \hat{V}_i \tag{3.3}$$

if $|\hat{I}_{\text{ri}}|, |\hat{I}_{\text{le}}| > 0$ and zero otherwise. The estimator $\hat{s}^2_t$ of $\mathbb{V}ar(\hat{\sigma}^2_{\text{ri}} - \hat{\sigma}^2_{\text{le}})$ in the denominator of G is defined as

$$\hat{s}^2_t := \frac{\hat{\nu}^2_{\text{ri}}}{h/\hat{\mu}_{\text{ri}}} + \frac{\hat{\nu}^2_{\text{le}}}{h/\hat{\mu}_{\text{le}}}, \tag{3.4}$$

where $\hat{\mu}_{\text{ri}}$ and $\hat{\mu}_{\text{le}}$ are the means of the life times in $\hat{I}_{\text{ri}}$ and $\hat{I}_{\text{le}}$ and the numerators are estimated as

$$\hat{\nu}^2_{\text{le}} := \frac{1}{|\hat{I}_{\text{le}}|} \sum_{i \in \hat{I}_{\text{le}}} (\hat{V}_i - \hat{\sigma}^2_{\text{le}})^2 \qquad \text{and} \qquad \hat{\nu}^2_{\text{ri}} := \frac{1}{|\hat{I}_{\text{ri}}|} \sum_{i \in \hat{I}_{\text{ri}}} (\hat{V}_i - \hat{\sigma}^2_{\text{ri}})^2 \tag{3.5}$$

for $|\hat{I}_{\text{le}}| > 0$ and $|\hat{I}_{\text{ri}}| > 0$ and zero otherwise. This is motivated by the Central Limit Theorem $\sqrt{t/\mu}(\hat{\sigma}^2_t - \sigma^2) \xrightarrow{d} N(0, \nu^2)$ as $t \to \infty$, where $\hat{\sigma}^2_t$ denotes the empirical variance of all life times up to time t.

3.2 Limit behavior of G under a constant rate

If the mean of the life times is constant μ, one can show the following Theorem 3.4, which allows application of the multiple filter approach. We use the extended filtered derivative process $G^{(n)} := (G^{(n)}_{h,t})_t := (G_{nh,nt})_t$ from (2.3) where the window size and the time grow linearly in n (compare Figure 3.2).
Furthermore, we use the globally estimated mean $\hat{\mu} := \hat{\mu}_{nT} := (1/N_{nT}) \sum_{i=1}^{N_{nT}} \xi_i$ as estimator for each $\mu^{(i)}$, where N_t denotes the number of events up to time t.

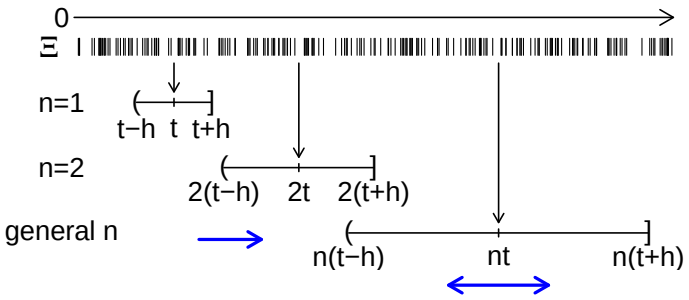

Figure 3.2: Asymptotic setting for the derivation of the limit processes. *The time and the window size grow linearly in n. Thus, an increase in n shifts the windows to the right and simultaneously increases their size. The figure is based on Figure 3.4 in Messer (2014).*

Theorem 3.4. ***Constant rate: Convergence of G***
Let $T > 0$ and $h \in (0, T/2]$ be a window size. If $\Xi \in \mathscr{M}$ with constant μ and σ^2 using the globally estimated mean $\hat{\mu}$ we have in $(D[h, T-h], d_{SK})$ for $n \to \infty$

$$G^{(n)} \xrightarrow{d} L,$$

with L as defined in (2.2).

Sketch of proof: Here, the proof is sketched briefly. For the detailed proof we refer to Section 4.1.
We show weak convergence of the filtered derivative process

$$G_t^{(n)} := G_{h,t}^{(n)} = \frac{1}{\hat{s}_t^{(n)}} \left(\frac{1}{N_{n(t+h)} - N_{nt} - 1} \sum_{i=N_{nt}+2}^{N_{n(t+h)}} \hat{V}_i - \frac{1}{N_{nt} - N_{n(t-h)} - 1} \sum_{i=N_{n(t-h)}+2}^{N_{nt}} \hat{V}_i \right).$$

In step 1, we assume a known mean μ and a known $s_t^{(n)} = 2\nu^2\mu/(nh)$ and thus use an auxiliary process $\Gamma^{(n)} := \Gamma_t^{(n)}$ defined as follows

$$\Gamma_t^{(n)} := \Gamma_{\mathrm{ri},t}^{(n)} - \Gamma_{\mathrm{le},t}^{(n)} = \frac{1}{s_t^{(n)}} \left(\frac{1}{N_{n(t+h)} - N_{nt} - 1} \sum_{i=N_{nt}+2}^{N_{n(t+h)}} V_i - \frac{1}{N_{nt} - N_{n(t-h)} - 1} \sum_{i=N_{n(t-h)}+2}^{N_{nt}} V_i \right). \tag{3.6}$$

Applying the Anscombe-Donsker-Theorem and continuous mapping, we show that in $(D[h, T-h] \times D[h, T-h], d_{SK} \otimes d_{SK})$ it holds as $n \to \infty$

$$\left(\left(\Gamma_{\mathrm{ri},t}^{(n)} \right)_{t \in \tau_h}, \left(\Gamma_{\mathrm{le},t}^{(n)} \right)_{t \in \tau_h} \right) \xrightarrow{d} \left(\left(\frac{W_{t+h} - W_t}{\sqrt{2h}} \right)_{t \in \tau_h}, \left(\frac{W_t - W_{t-h}}{\sqrt{2h}} \right)_{t \in \tau_h} \right), \tag{3.7}$$

which yields $\Gamma^{(n)} \xrightarrow{d} L$.
In step 2, the true mean μ occurring in the left side of (3.7) is replaced by the globally estimated mean $\hat{\mu}$ and s is replaced by $\hat{s}$ thereby showing that $G^{(n)} \xrightarrow{d} L$ holds true. □
This assertion holds particularly for a constant and known mean, i.e., if $\hat{\mu}^{(i)} = \mu_1 \ \forall i \geq 1$.

3.3 Changes in the k-th moments

Extending the results of the latter section, we can also test the null hypothesis of homogeneity of the k-th order moments $m_k := \mathbb{E}[\xi_1^k]$ of the life times $(\xi_i)_{i\geq 1}$ for every fixed k under the assumption that all lower order moments are constant. In this case, the scaled process G from (2.1) uses the standard estimators of the k-th order moments $\hat{m}_k$ in the two windows in the numerator

$$\hat{m}_{k,\mathrm{le}} := \frac{1}{|\hat{I}_{\mathrm{le}}|} \sum_{i \in \hat{I}_{\mathrm{le}}} \xi_i^k \qquad \text{and} \qquad \hat{m}_{k,\mathrm{ri}} := \frac{1}{|\hat{I}_{\mathrm{ri}}|} \sum_{i \in \hat{I}_{\mathrm{ri}}} \xi_i^k.$$

In detail, we get

$$G_{h,t} := \frac{\hat{m}_{k,\mathrm{ri}} - \hat{m}_{k,\mathrm{le}}}{\hat{s}}, \quad \text{with} \quad \hat{s}^2 := \frac{\widehat{\mathbb{V}ar}\left(\xi_1^k\right)_{\mathrm{ri}}}{h/\hat{\mu}_{\mathrm{ri}}} + \frac{\widehat{\mathbb{V}ar}\left(\xi_1^k\right)_{\mathrm{le}}}{h/\hat{\mu}_{\mathrm{le}}}, \tag{3.8}$$

where the numerators in $\hat{s}^2$ are the standard variance estimators

$$\widehat{\mathbb{V}ar}\left(\xi_1^k\right)_{\mathrm{le}} := \frac{1}{|\hat{I}_{\mathrm{le}}|} \sum_{i \in \hat{I}_{\mathrm{le}}} (\xi_i^k - \hat{m}_{k,\mathrm{le}})^2 \qquad \text{and} \qquad \widehat{\mathbb{V}ar}\left(\xi_1^k\right)_{\mathrm{ri}} := \frac{1}{|\hat{I}_{\mathrm{ri}}|} \sum_{i \in \hat{I}_{\mathrm{ri}}} (\xi_i^k - \hat{m}_{k,\mathrm{ri}})^2.$$

Under the null hypothesis of constant k-th order moment we find convergence of $(G_{h,t})$ to the same limit process L.

Corollary 3.5. ***Changes in the k-th moments: Convergence of G***
Let $T > 0$, $h \in (0, T/2]$ be a window size. For $k \in \mathbb{N}$ let $\Xi \in \mathscr{R}$ (Def. 3.1) with $\xi_1 \in \mathscr{L}^{2k}$. Let $G^{(n)} := G_{nh,nt}$ be as in (3.8). Then it holds in $(D[h, T-h], d_{SK})$ as $n \to \infty$

$$G^{(n)} \xrightarrow{d} L.$$

Proof: By replacing V_i by ξ_i^k and using the known

$$s^2 := \frac{\mathbb{V}ar\left(\xi_1^k\right)_{\mathrm{ri}}}{h/\mu_{\mathrm{ri}}} + \frac{\mathbb{V}ar\left(\xi_1^k\right)_{\mathrm{le}}}{h/\mu_{\mathrm{le}}}$$

the first step of the proof is analogous to the first step of the proof of Theorem 3.4. In the second step, s is again substituted by $\hat{s}$, where the consistency of $\hat{s}$ is proven analogously to Corollary 4.4 and applying the same techniques as for the consistencies of $(\hat{\mu})_t$ and $(\hat{\sigma}^2)_t$ in Messer et al. (2014, Lemma A.15 and A.16). □

In commonly used distributions, however, for example, the change in third moments when leaving the first and second moment constant in general is very small and very difficult to detect in practice. The same holds for higher moments. Therefore, Corollary 3.5 is primarily of theoretical interest.

3.4 Limit behavior of G with one rate change point

In this section, we extend Theorem 3.4 allowing for one rate change point, while testing the null hypothesis of variance homogeneity. Assuming a process with at most one rate change point, the process G can be shown to converge against a limit process $\widetilde{L}$ (Theorem 3.6), which

is, like L, a zero-mean $2h$-dependent Gaussian process with unit variance (Corollary 3.7). It differs from L only in the covariance in the $3h$-neighborhood of a change point c (see Section 5.2 and Fig. 5.4 C,D).

Theorem 3.6. ***One rate change point: Convergence of G***
Let $\Xi^{(n)} \in \mathscr{M}$ (Def. 3.3) with at most one rate change and no variance change, as follows. Let $\Xi_1(\mu_1, \sigma_1^2, {\nu_1}^2), \Xi_2(\mu_2, \sigma_2^2, {\nu_2}^2) \in \mathscr{R}$ with $\mu_1 \neq \mu_2$, $\sigma_1^2 = \sigma_2^2$. For $c \in (0, T]$ and $n = 1, 2, \ldots$ let

$$\Xi^{(n)} := \Xi_1|_{[0,nc]} + \Xi_2|_{(nc,nT]}, \tag{3.9}$$

meaning that $\Xi^{(n)}$ fulfills H_0. Assume a consistent estimator $\hat{c}$ of c with

$$|\hat{c} - c| = o_{\mathbb{P}}(1/\sqrt{n}) \tag{3.10}$$

where $o_{\mathbb{P}}(\cdot)$ is the small o-notation with respect to convergence in probability. Let $G^{(n)}$ be the filtered derivative process associated with $\Xi^{(n)}$ using the empirical means $\hat{\mu}_1^{\hat{c}}$, $\hat{\mu}_2^{\hat{c}}$ estimated in the intervals $[0, \hat{c})$ and $[\hat{c}, T]$. Then with $\widetilde{L}$ from (3.11), as $n \to \infty$, we have

$$G^{(n)} \xrightarrow{d} \widetilde{L},$$

where $\xrightarrow{d}$ denotes weak convergence in the Skorokhod topology. The marginals $\widetilde{L}_{h,t}$ of the limit process $\widetilde{L}$ equal L outside the h-neighborhood of c and are given by

$$\widetilde{L}_{h,t} = \begin{cases} L_{h,t}, & |t-c| > h, \\ \frac{\sqrt{(\mu_{\mathrm{ri}}\nu_2)^2/(\mu_2 h^2)}(W_{t+h}-W_c)+\sqrt{(\mu_{\mathrm{ri}}\nu_1)^2/(\mu_1 h^2)}(W_c-W_t)-\sqrt{\mu_1{\nu_1}^2/h^2}(W_t-W_{t-h})}{s_t^{(1)}}, & t \in [c-h, c], \\ \frac{\sqrt{\mu_2{\nu_2}^2/h^2}(W_{t+h}-W_t)-\sqrt{(\mu_{\mathrm{le}}\nu_2)^2/(\mu_2 h^2)}(W_t-W_c)-\sqrt{(\mu_{\mathrm{le}}\nu_1)^2/(\mu_1 h^2)}(W_c-W_{t-h})}{s_t^{(1)}}, & t \in (c, c+h], \end{cases} \tag{3.11}$$

for a standard Brownian motion $(W_t)_{t\geq 0}$. The functions $\mu_{\mathrm{ri}} := \mu_{\mathrm{ri},h,t}, \mu_{\mathrm{le}} := \mu_{\mathrm{le},h,t}$ are the limits of the empirical means $\hat{\mu}_{\mathrm{ri}}, \hat{\mu}_{\mathrm{le}}$ and are given by $\mu_{\mathrm{ri},h,t} := \mu_1$ for $t \leq c-h$, $\mu_{\mathrm{ri},h,t} := \mu_2$ for $t > c$ and

$$\mu_{\mathrm{ri},h,t} := \frac{h}{(c-t)/\mu_1 + (t+h-c)/\mu_2}, \tag{3.12}$$

for $t \in (c-h, c]$ and analogously for μ_{le}. The true order of scaling $\left((s_t^{(n)})^2\right)_{t\in\tau_h}$ is defined by $\frac{2{\nu_1}^2}{nh/\mu_1}$ for $t < c-h$, by $\frac{2{\nu_2}^2}{nh/\mu_2}$ for $t > c+h$ and for $|t-c| \leq h$ by the following linear interpolation

$$(s_t^{(n)})^2 := (s_{h,t}^{(n)})^2 := \begin{cases} \frac{1}{n}\left(\frac{\mu_1{\nu_1}^2}{h} + \frac{(c-t)}{h^2\mu_1}(\mu_{\mathrm{ri}}\nu_1)^2 + \frac{(t+h-c)}{h^2\mu_2}(\mu_{\mathrm{ri}}\nu_2)^2\right), & \text{if } c-h \leq t \leq c, \\ \frac{1}{n}\left(\frac{(c-(t-h))}{h^2\mu_1}(\mu_{le}\nu_1)^2 + \frac{(t-c)}{h^2\mu_2}(\mu_{\mathrm{le}}\nu_2)^2 + \frac{\mu_2{\nu_2}^2}{h}\right), & \text{if } c < t \leq c+h. \end{cases} \tag{3.13}$$

Sketch of proof: Again, we sketch the proof and refer for the detailed proof version to Section 4.2.

The key ingredients are the Anscombe-Donsker-Theorem and continuous mapping. In addition to the proof of Theorem 3.4, a change point in the rate requires separate considerations for

different intervals in the neighborhood of a change point. Like in the proof of Theorem 3.4 we first assume known process parameters and use the modified filtered derivative process Γ

$$\Gamma_t^{(n)} = \Gamma_{\mathrm{ri},t}^{(n)} - \Gamma_{\mathrm{le},t}^{(n)}, \tag{3.14}$$

which is comparable to the process $\Gamma_t^{(n)}$ defined in equation (3.6). The detailed definitions are given in Section 4.2. Moreover, we decompose the limit process $\widetilde{L} \sim \widetilde{L}_{\mathrm{ri}} - \widetilde{L}_{\mathrm{le}}$, where $\sim$ denotes equality in distribution and refer again for detailed definitions to Section 4.2. The first step of the proof will be to show convergence of the processes

$$\widetilde{\Gamma}_{\mathrm{ri}}^{(n)} := \left(\frac{N_{n(t+h)} - N_{nt} - 1}{nh/\mu_{\mathrm{ri}}} \right)_t \cdot \Gamma_{\mathrm{ri}}^{(n)}$$

and $\widetilde{\Gamma}_{\mathrm{le}}$ against $\left(\widetilde{L}_{\mathrm{ri}}, \widetilde{L}_{\mathrm{le}}\right)$ using the Donsker-Ascombe-Theorem and continuous mapping. With Lemma 4.5, we can then conclude

$$\left(\Gamma_{\mathrm{ri}}^{(n)}, \Gamma_{\mathrm{le}}^{(n)}\right) \xrightarrow{d} \left(\widetilde{L}_{\mathrm{ri}}, \widetilde{L}_{\mathrm{le}}\right),$$

and using continuous mapping again yields for $t \in \tau_h$

$$\Gamma^{(n)} = \Gamma_{\mathrm{ri}}^{(n)} - \Gamma_{\mathrm{le}}^{(n)} \xrightarrow{d} \widetilde{L}_{\mathrm{ri}} - \widetilde{L}_{\mathrm{le}} \sim \widetilde{L}.$$

In step two of the proof, we first replace the true means μ_1, μ_2 in the numerator by their estimators to define the process $\hat{\Gamma}^{(n)}$ and show

$$\hat{\Gamma}^{(n)} - \Gamma^{(n)} \xrightarrow{\mathbb{P}} (0)_t. \tag{3.15}$$

Then, we use Lemma 4.6 to substitute the scaling $s_t^{(1)}$ used in $\hat{\Gamma}$ by the estimator $\hat{s}_t^{(n)}$ to prove the assertion. □

We show that $\widetilde{L}$ is a Gaussian process with zero mean and unit variance.

Corollary 3.7. ***Marginal distribution of*** $\widetilde{L}$
Let $\widetilde{L}$ *be defined as in* (3.11). *For all* $t \in \tau_h$ *it holds* $\widetilde{L}_{h,t} \sim N(0,1)$.

Proof: As the increments of a standard Brownian motion $(W_t)_{t\geq 0}$ are independent and Gaussian distributed, $\widetilde{L}$ is Gaussian distributed. Moreover, the increments have zero expectation and thus the zero mean follows by the linearity of expectation. To show the unit variance, we analyse three cases. We use the independence of increments and the property that for $0 \leq s \leq t: \quad \mathbb{V}\mathrm{ar}(W_t - W_s) = t - s$. For $|t - c| > h$ the assertion follows directly. Now, let $t \in [c - h, c]$. We obtain

$$\mathbb{V}\mathrm{ar}(\widetilde{L}_{h,t}) = \frac{\frac{\mu_{\mathrm{ri}}^2 \nu_2^2}{\mu_2 h^2}(t + h - c) + \frac{\mu_{\mathrm{ri}}^2 \nu_1^2}{\mu_1 h^2}(c - t) + \frac{\mu_1 \nu_1^2}{h^2} h}{\frac{\mu_1 {\nu_1}^2}{h} + \frac{(\mu_{\mathrm{ri}}\nu_1)^2}{h^2 \mu_1}(c - t) + \frac{(\mu_{\mathrm{ri}}\nu_2)^2}{h^2 \mu_2}(t + h - c)} = 1.$$

The case $t \in (c, c + h]$ is shown analogously. □

Note that analogous results to Theorem 3.6 hold if there are several rate change points with pairwise distances each larger than $2h$ as shown in Figure 3.3 for two rate change points.

In the h-neighborhood of each rate change point the marginals of the corresponding limit process are similar to the marginals of $\widetilde{L}$ around c and in between the marginals are identical to the marginals of L. In case of rate change points with distance smaller than or equal to $2h$, the structure of the limit process becomes more complicated but is still comparable to the structure of $\widetilde{L}$. Furthermore, note that the proof of Theorem 3.6 is based on a Functional Central Limit Theorem and a consistent estimator of s_t. Therefore the result can be shown not only for renewal processes but also for a subclass of renewal processes with varying variance (RPVV) as introduced in Messer et al. (2014).

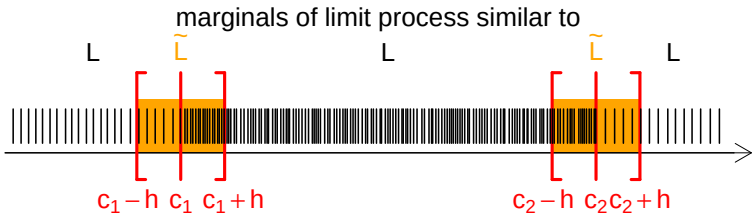

Figure 3.3: Limit process in the case of two rate cps with distance larger than 2h. *The marginals of the limit process resemble in the h-neighborhoods of the two rate change points c_1, c_2 the marginals of the process $\tilde{L}$ around its rate change point, and outside they are identical to the marginals of L.*

As the marginals of L and $\widetilde{L}$ differ only in the h-neighborhood of c and both processes are $2h$-dependent, their covariance structures differ in the $3h$-neighborhood of the rate change point c, which is illustrated in Figure 3.4. Our simulations in Section 5.2 suggest that the differences between L and $\widetilde{L}$ are typically small with respect to the 95%-quantile of their absolute maxima. We therefore suggest to use the parameter independent limit process L also in the situation of potential rate change points for the derivation of the rejection threshold in the statistical test. The simulations in Section 5 show that the MFT using L instead of $\widetilde{L}$ keeps the asymptotic significance level for most combinations of μ and σ even for the case of multiple unknown rate change points.

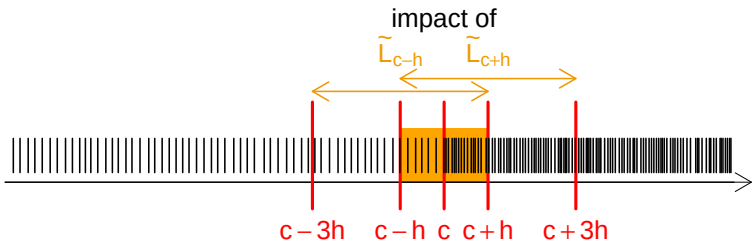

Figure 3.4: Impact of a rate change point on the covariance of $\widetilde{L}$. *The processes L and $\widetilde{L}$ are $2h$-dependent as visualized by orange arrows in the graph. As the marginals of L and $\widetilde{L}$ differ in the h-neighborhood of the rate change point c (colored orange), the covariance of $\widetilde{L}$ differs in a $3h$-neighborhood of the rate change point from the covariance of L.*

Chapter 4

Proofs of Theorems 3.4 and 3.6

In this section, we prove the key theoretical results of the first part of this thesis in detail. The proof of Theorem 3.4 in Section 4.1 uses the Anscombe-Donsker-Theorem, continuous mapping and the consistency of the estimator $\hat{s}^2$. In Section 4.2, we prove Theorem 3.6 basically using the same ideas as for the proof of Theorem 3.4.
We specify the sets of indices

$$\hat{I}_{\text{le}} := \{N_{n(t-h)} + 2, N_{n(t-h)} + 3, \ldots, N_{nt}\} \qquad \text{and} \qquad \hat{I}_{\text{ri}} := \{N_{nt} + 2, N_{nt} + 3, \ldots, N_{n(t+h)}\}.$$

The Anscombe-Donsker invariance principle is of central importance for the proofs. We state it here following Gut (2009, Theorem 2.1, p.158).

Theorem 4.1. ***Anscombe-Donsker-Theorem***
Let $(\xi_k)_{k\geq 1}$ be i.i.d. random variables with zero mean and variance $\sigma^2 < \infty$, $(\tilde{N}(t))_{t\geq 0}$ be a nondecreasing, right-continuous family of positive, integer valued random variables and set

$$Z_n(t) := \frac{1}{\sigma\sqrt{n}} \sum_{k=1}^{\tilde{N}_{nt}} \xi_k.$$

Suppose that

$$\frac{\tilde{N}(t)}{t} \xrightarrow[t\to\infty]{a.s.} \kappa \quad (0 < \kappa < \infty).$$

Then we have in $(D[0,\infty), d_{sk})$

$$\frac{Z_n}{\sqrt{\kappa}} \xrightarrow[t\to\infty]{d} W,$$

with W as standard Brownian motion.

Proof: Compare, e.g., Gut (2009). □

4.1 Proof of Theorem 3.4

Recall the sketch of proof directly following the statement of Theorem 3.4. The processes $\Gamma_{\mathrm{le}}^{(n)}$ and $\Gamma_{\mathrm{ri}}^{(n)}$ in equation (3.6) are in detail defined as

$$\Gamma_{\mathrm{ri},t}^{(n)} := \frac{1}{s_t^{(n)}} \left(\frac{1}{N_{n(t+h)} - N_{nt} - 1} \sum_{i=N_{nt}+2}^{N_{n(t+h)}} V_i - \mathbb{E}[V_1] \right),$$

$$\Gamma_{\mathrm{le},t}^{(n)} := \frac{1}{s_t^{(n)}} \left(\frac{1}{N_{nt} - N_{n(t-h)} - 1} \sum_{i=N_{n(t-h)}+2}^{N_{nt}} V_i - \mathbb{E}[V_1] \right).$$

Step 1: weak process convergence for known parameters
Recall $V_i = (\xi_i - \mu)^2$ for the life times $(\xi_i)_{i\geq 1}$ of a point process Ξ with a known mean μ. We apply the Anscombe-Donsker-Theorem to the process defined by

$$Y_t^{(n)} := \frac{1}{\nu\sqrt{n}} \sum_{i=1}^{N_{nt}} (V_i - \mathbb{E}[V_1]).$$

Since $N_t/t \to 1/\mu$ a.s. as $n \to \infty$, it follows that in $(D[0,\infty), d_{SK})$ it holds $(\sqrt{\mu} Y_t^{(n)})_t \xrightarrow{d} (W_t)_t$. Here, W denotes a standard Brownian motion.
Let $\varphi : (D[0,\infty), d_{SK}) \to (D[h, T-h] \times D[h, T-h], d_{SK} \otimes d_{SK})$ be defined by

$$(f(t))_{t\geq 0} \overset{\varphi}{\mapsto} \left(\left(\frac{(f(t+h) - f(t))}{\sqrt{2h}} \right)_{t\in\tau_h}, \left(\frac{(f(t) - f(t-h))}{\sqrt{2h}} \right)_{t\in\tau_h} \right).$$

This function is continuous. Mapping $\sqrt{\mu} Y^{(n)}$ via φ, the first component is given by

$$\left(\sqrt{\frac{\mu}{2nh\nu^2}} \left[\left(\sum_{i=N_{nt}+1}^{N_{n(t+h)}} V_i \right) - (N_{n(t+h)} - N_{nt}) \mathbb{E}[V_1] \right] \right)_{t\in\tau_h} \xrightarrow{d} \left(\frac{W_{t+h} - W_t}{\sqrt{2h}} \right)_{t\in\tau_h}.$$

By Slutsky's theorem this also implies

$$\left(\sqrt{\frac{\mu}{2nh\nu^2}} \left[\left(\sum_{i=N_{nt}+1}^{N_{n(t+h)}} V_i \right) - (N_{n(t+h)} - N_{nt} - 1) \mathbb{E}[V_1] \right] \right)_{t\in\tau_h} \xrightarrow{d} \left(\frac{W_{t+h} - W_t}{\sqrt{2h}} \right)_{t\in\tau_h}.$$

Now in $(D[h, T-h], d_{SK})$ it holds almost surely that $(N_{n(t+h)} - N_{nt} - 1)_t \sim (nh/\mu)_t$ as $n \to \infty$, see Lemma A.3.2 in Messer et al. (2014). Thus by Slutsky's theorem,

$$(\Gamma_{\mathrm{ri},t}^{(n)})_{t\in\tau_h} \xrightarrow{d} \left(\frac{W_{t+h} - W_t}{\sqrt{2h}} \right)_{t\in\tau_h}$$

(here, we also omitted one summand $i = N_{nt} + 1$, i.e., a term of order $o_{a.s.}(1)$). By exchanging t with $t - h$ and $t + h$ with t, we obtain the convergence for $\Gamma_{\mathrm{le}}^{(n)}$, which refers to the second component of $\varphi(\sqrt{\mu} Y^{(n)})$. Thus, we obtain (3.7). This implies $\Gamma^{(n)} \xrightarrow{d} L$ in $(D[h, T-h], d_{SK})$ as $n \to \infty$ by continuous mapping which is the assertion for a known mean μ.

Note that the expectation $\mathbb{E}[V_1]$ vanishes, since it appears in both summands.

Step 2: replacement of parameters by their estimators
In a second step we use the estimated mean $\hat{\mu}_{nT}$. We show that for

$$\hat{Y}_t^{(n)} := \frac{1}{\nu\sqrt{n}} \sum_{i=1}^{N_{nt}} (\hat{V}_i - \mathbb{E}[V_1])$$

in $(D[0,\infty), d_{SK})$ we also obtain

$$(\sqrt{\mu}\hat{Y}_t^{(n)})_{t\in[0,T]} \xrightarrow{d} (W_t)_{t\in[0,T]}. \tag{4.1}$$

Thus, the same arguments as in step 1 can be applied to show the assertion $G^{(n)} \to L$. Additionally, by Slutsky's theorem and Corollary 4.4 (given below), we can exchange the factor $(nh/2\mu\nu^2)^{1/2}$ with the estimator $1/\hat{s}(nt, nh)$ with the convergence holding true.
To show (4.1), we rewrite $\hat{Y}_t^{(n)} = Y_t^{(n)} + R_t^{(n)}$, with R given by

$$R_t^{(n)} := \frac{N_{nt}}{\nu\sqrt{n}} \left[(\hat{\mu}_{nT} - \hat{\mu}_{nt})^2 - (\hat{\mu}_{nt} - \mu)^2\right].$$

This decomposition holds true since

$$\begin{aligned}
\sum_{i=1}^{N_{nt}} \hat{V}_i \;=\; \sum_{i=1}^{N_{nt}} (\xi_i - \hat{\mu}_{nT})^2 &= \sum_{i=1}^{N_{nt}} \xi_i^2 - 2\hat{\mu}_{nT} \sum_{i=1}^{N_{nt}} \xi_i + N_{nt}\hat{\mu}_{nT}^2 \\
&= \sum_{i=1}^{N_{nt}} (\xi_i - \mu)^2 + 2(\mu - \hat{\mu}_{nT}) \sum_{i=1}^{N_{nt}} \xi_i + N_{nt}(\hat{\mu}_{nT}^2 - \mu^2) \\
&= \sum_{i=1}^{N_{nt}} V_i + N_{nt} \left[(\hat{\mu}_{nT} - \hat{\mu}_{nt})^2 - (\hat{\mu}_{nt} - \mu)^2\right].
\end{aligned}$$

We now show that in $(D[0,T], d_{||\cdot||})$ the remainder $R \to 0$ in probability as $n \to \infty$. Then, the convergence in (4.1) follows by Slutsky's theorem.
It suffices to show that $\sup_{t\in[0,T]} R_t^{(n)}$ vanishes in probability. Recall $\sigma^2 = \mathbb{V}ar(\xi_1)$ and set

$$Z_t^{(n)} := \frac{\sqrt{\mu}}{\sigma\sqrt{n}} \sum_{i=1}^{N_{nt}} (\xi_i - \mathbb{E}[\xi_i]) = \frac{\sqrt{\mu} N_{nt}}{\sigma\sqrt{n}} (\hat{\mu}_{nt} - \mu).$$

Then, by the Anscombe-Donsker-Theorem we find in $(D[0,T], d_{SK})$ that $(Z_t^{(n)})_{t\in[0,T]} \to (W_t)_{t\in[0,T]}$ weakly as $n \to \infty$, such that $\sup_{t\in[0,T]} Z_t^{(n)} \to \sup_{t\in[0,T]} W_t$ weakly. Applying the reflection principle, it is known that the distribution of $\sup_{t\in[0,T]} W_t$ directly derives from the normal distribution (e.g., Billingsley, 1968). Now, we first focus on the second summand of $R_t^{(n)}$ and show that its square root vanishes

$$\sup_{t\in[0,T]} \left[\left(\frac{N_{nt}}{\nu\sqrt{n}}\right)^{1/2} (\hat{\mu}_{nt} - \mu)\right] = \sup_{t\in[0,T]} \left[\left(\frac{n\sigma^4}{(\mu\nu N_{nt})^2}\right)^{1/4} Z_t^{(n)}\right] \xrightarrow{\mathbb{P}} 0,$$

as $n \to \infty$. This holds true since in $(D[0,T], d_{SK})$ it holds almost surely that $(N_{nt})_t \sim (nt/\mu)_t$ as $n \to \infty$, compare, e.g., Lemma A.3.2 in Messer et al. (2014). Thus, the first factor within the supreme itself vanishes such that the entire expression tends to zero. By continuous mapping theorem, this holds true for the squared expression, such that the second summand in $R_t^{(n)}$ uniformly tends to zero in probability. For the first summand in $R_t^{(n)}$, we decompose $(\hat{\mu}_{nT} - \hat{\mu}_{nt}) = (\hat{\mu}_{nT} - \mu) - (\hat{\mu}_{nt} - \mu)$ and apply the same argument as before to both summands. As a result R uniformly vanishes in probability. □

Now, we state the consistency of the variance estimator $\hat{s}$ in Corollary 4.4. Therefore, we need the consistency of the local estimators for μ and ν as stated in the following lemmata.

Lemma 4.2. *Let Ξ be an element of $\mathscr{R}$ with mean μ. Let $T > 0$, $h \in (0, T/2]$ and $\hat{\mu}_{le}$ and $\hat{\mu}_{ri}$ be defined as the empirical means of the life times in the left and the right window, respectively. Then it holds in $(D[h, T-h], d_{||\cdot||}))$ almost surely as $n \to \infty$ that*

$$(\hat{\mu}_{le})_{t\in\tau_h} \longrightarrow (\mu)_{t\in\tau_h} \qquad \text{and} \qquad (\hat{\mu}_{ri})_{t\in\tau_h} \longrightarrow (\mu)_{t\in\tau_h}.$$

Proof: This is a weaker version of Lemma A.15 in Messer et al. (2014). □

Lemma 4.3. *Let Ξ be an element of $\mathscr{R}$ with $\nu^2 = \mathbb{V}ar((\xi_1 - \mu)^2)$. Let $T > 0$, $h \in (0, T/2]$ and $\hat{\nu}_{le}^2$ and $\hat{\nu}_{ri}^2$ be defined as in (3.5) using the estimated global mean $\hat{\mu}^{(i)} = \hat{\mu}_{nT} = (1/N_{nT}) \sum_{i=1}^{N_{nT}} \xi_i \quad \forall i \geq 1$. Then it holds in $(D[h, T-h], d_{||\cdot||}))$ almost surely as $n \to \infty$ that*

$$(\hat{\nu}_{le}^2)_{t\in\tau_h} \longrightarrow (\nu^2)_{t\in\tau_h} \qquad \text{and} \qquad (\hat{\nu}_{ri}^2)_{t\in\tau_h} \longrightarrow (\nu^2)_{t\in\tau_h}. \tag{4.2}$$

Proof: For a known mean μ, i.e., V_i instead of $\hat{V}_i$ convergences (4.2) are shown using the same techniques as for the consistencies of $(\hat{\mu})_t$ and $(\hat{\sigma}^2)_t$ in Messer et al. (2014). A complete proof can be found in Albert (2014). To extend the result to the estimated global mean $\hat{\mu}_{nT}$ we derive

$$\begin{aligned}
\hat{\nu}_{\mathrm{ri}}^2 &= \frac{1}{N_{n(t+h)} - N_{nt} - 1} \sum_{i=N_{nt}+2}^{N_{n(t+h)}} ((\xi_i - \hat{\mu}_{nT})^2 - \hat{\sigma}_{\mathrm{ri}}^2)^2 \\
&= \frac{1}{N_{n(t+h)} - N_{nt} - 1} \sum_{i=N_{nt}+2}^{N_{n(t+h)}} (\xi_i^2 - 2\xi_i \hat{\mu}_{nT} + \hat{\mu}_{nT}^2 - \hat{\sigma}_{\mathrm{ri}}^2)^2 \\
&= \frac{\sum_{i=N_{nt}+2}^{N_{n(t+h)}} (\xi_i^4 - 4\xi_i^3 \hat{\mu}_{nT} + 6\xi_i^2 \hat{\mu}_{nT}^2 - 2\xi_i^2 \hat{\sigma}_{\mathrm{ri}}^2 - 4\xi_i \hat{\mu}_{nT}^3 + 4\xi_i \hat{\mu}_{nT} \hat{\sigma}_{\mathrm{ri}}^2 + \hat{\mu}_{nT}^4 - 2\hat{\mu}_{nT}^2 \hat{\sigma}_{\mathrm{ri}}^2 + \hat{\sigma}_{\mathrm{ri}}^4)}{N_{n(t+h)} - N_{nt} - 1}.
\end{aligned} \tag{4.3}$$

Using the summand with $\xi_i^3 \hat{\mu}_{nT}$ as an example, we explain that the difference between the summands with the estimators for μ and σ in the latter display and with the known values vanishes a.s. asymptotically for $n \to \infty$. It holds

$$\begin{aligned}
&\frac{1}{N_{n(t+h)} - N_{nt} - 1} \sum_{i=N_{nt}+2}^{N_{n(t+h)}} \xi_i^3 \hat{\mu}_{nT} - \frac{1}{N_{n(t+h)} - N_{nt} - 1} \sum_{i=N_{nt}+2}^{N_{n(t+h)}} \xi_i^3 \mu \\
&= \frac{1}{N_{n(t+h)} - N_{nt} - 1} \sum_{i=N_{nt}+2}^{N_{n(t+h)}} \xi_i^3 (\hat{\mu}_{nT} - \mu).
\end{aligned} \tag{4.4}$$

The strong consistency $(\hat{\mu}_{nT})_{t\in\tau_h} \to (\mu)_{t\in\tau_h}$ a.s. as $n \to \infty$ follows directly by Lemma 4.2 (note that in our situation regarding the fixed point in time T is sufficient) and thus it follows that $(\hat{\mu}_{nT} - \mu)_{t\in\tau_h}$ vanishes a.s. Moreover, with $\xi_i \in \mathscr{L}^4$ and the exact same techniques as in the consistency proof of $\hat{\sigma}_{\text{ri}}$ (Lemma A.16 in Messer et al., 2014) it can be shown that almost surely as $n \to \infty$

$$\left(\frac{1}{N_{n(t+h)} - N_{nt} - 1} \sum_{i=N_{nt}+2}^{N_{n(t+h)}} \xi_i^3 \right)_{t\in\tau_h} \longrightarrow (c)_{t\in\tau_h}$$

for some constant $c > 0$. This implies that the expression in (4.4) vanishes a.s. in $(D[h, T-h], d_{||\cdot||})$).

Similar arguments using also the strong consistency of $\hat{\sigma}_{\text{ri}}$ (where the replacement of the estimator $\hat{\mu}_{\text{ri}}$ by the estimator $\hat{\mu}_{nT}$ neither changes the correctness of Lemma A.16 in Messer et al. (2014) nor the arguments in its proof) hold for all other summands in equation (4.3). Consequently, the assertion follows by standard application of Slutsky's theorem. □

Lemma 4.3 directly implies the consistency of the variance estimator $\hat{s}^2$.

Corollary 4.4. *Let $\Xi \in \mathscr{R}$ with $\nu^2 = \mathbb{V}ar((\xi_1 - \mu)^2)$. Let $T > 0$, $h \in (0, T/2]$ and $\hat{s}^2(t,h)$ be defined as in (3.4). Then it holds in $(D[\tau_h], d_{||\cdot||})$ almost surely as $n \to \infty$ that*

$$\left(n\ \hat{s}^2(nt, nh)\right)_{t\in\tau_h} \longrightarrow \left(\frac{2\nu^2}{h/\mu}\right)_{t\in\tau_h}.$$

Proof: Recall equation (3.4)

$$\hat{s}_t^2 := \frac{\hat{\nu}_{\text{ri}}^2}{h/\hat{\mu}_{\text{ri}}} + \frac{\hat{\nu}_{\text{le}}^2}{h/\hat{\mu}_{\text{le}}}.$$

The assertion follows from the consistency of $\hat{\mu}_{\text{ri}}, \hat{\mu}_{\text{le}}$ (Lemma 4.2) and $\hat{\nu}_{\text{ri}}^2, \hat{\nu}_{\text{le}}^2$ (Lemma 4.3) by application of Slutsky's theorem. □

4.2 Proof of Theorem 3.6

The proof was already sketched on page 20 directly following the statement of Theorem 3.6. In addition to the previous proof, a change point in the rate requires separate considerations for different intervals in the neighborhood of a change point. These are different for the right and left window and therefore, we define auxiliary processes that correspond to the right and left window, respectively.

We recall the modified filtered derivative process Γ from (3.14)

$$\Gamma_t^{(n)} = \Gamma_{\text{ri},t}^{(n)} - \Gamma_{\text{le},t}^{(n)}.$$

The latter terms are given by $\Gamma_{\mathrm{ri}}^{(n)} =$

$$\begin{cases} \frac{\frac{1}{N_{n(t+h)}-N_{nt}-1}\left(\sum_{i=N_{nt}+2}^{N_{n(t+h)}}(\xi_i-\mu_1)^2\right)-\sigma^2}{s_t^{(n)}}, & \text{if } t < c-h, \\ \frac{\frac{1}{N_{n(t+h)}-N_{nt}-1}\left(\sum_{i=N_{nt}+2}^{N_{nc}}(\xi_i-\mu_1)^2+\sum_{i=N_{nc}+2}^{N_{n(t+h)}}(\xi_i-\mu_2)^2\right)-\sigma^2}{s_t^{(n)}}, & \text{if } c-h \le t < c, \\ \frac{\frac{1}{N_{n(t+h)}-N_{nt}-1}\left(\sum_{i=N_{nt}+2}^{N_{n(t+h)}}(\xi_i-\mu_2)^2\right)-\sigma^2}{s_t^{(n)}}, & \text{if } t \ge c, \end{cases}$$

and analogously for $\Gamma_{\mathrm{le}}^{(n)}$. Analogously, we decompose the limit process $\widetilde{L}_{\mathrm{ri}} - \widetilde{L}_{\mathrm{le}} \sim \widetilde{L}$, where $\sim$ denotes equality in distribution. With $(W_{1,t})_{t\ge0}$ and $(W_{2,t})_{t\ge0}$ independent standard Brownian motions the latter terms are given by $\widetilde{L}_{\mathrm{ri}} := \widetilde{L}_{\mathrm{ri},h,t} =$

$$\begin{cases} \frac{(W_{1,t+h}-W_{1,t})}{\sqrt{2h}}, & \text{if } t < c-h, \\ \frac{\sqrt{\mu_{\mathrm{ri},t}^2\nu_2^2/(h^2\mu_2)}(W_{2,t+h}-W_{2,c})+\sqrt{\mu_{\mathrm{ri},t}^2\nu_1^2/(h^2\mu_1)}(W_{1,c}-W_{1,t})}{s_t^{(1)}}, & \text{if } c-h \le t < c, \\ \frac{\sqrt{\mu_2\nu_2^2/h^2}(W_{2,t+h}-W_{2,t})}{s_t^{(1)}}, & \text{if } t \ge c, \end{cases}$$

and analogously for $\widetilde{L}_{\mathrm{le}}$.
The proof now follows the steps outlined on page 21.

Step 1: Proof of

$$\left(\widetilde{\Gamma}_{\mathrm{ri}}^{(n)}, \widetilde{\Gamma}_{\mathrm{le}}^{(n)}\right) \xrightarrow{d} \left(\widetilde{L}_{\mathrm{ri}}, \widetilde{L}_{\mathrm{le}}\right). \tag{4.5}$$

Let $(\xi_{1,i})_{i\ge1}$, $(\xi_{2,i})_{i\ge1}$ and $(\xi_i)_{i\ge1}$ denote the sequences of life times that correspond to Ξ_1, Ξ_2 and to the compound process Ξ, respectively. Analogously, let $(N_{1,t})_{t\ge0}$, $(N_{2,t})_{t\ge0}$ and $(N_t)_{t\ge0}$ denote the counting processes that correspond to Ξ_1, Ξ_2 and to Ξ. We use the abbreviated notation

$$V_{j,i} := (\xi_{j,i} - \mu_j)^2$$

for the individual processes Ξ_j, $j = 1, 2$. According to the Anscombe-Donsker-Theorem we observe in $(D[0,\infty), d_{SK})$ as $n \to \infty$

$$\left(Z_{j,t}^{(n)}\right)_{t\ge0} := \left(\frac{1}{\nu_j\sqrt{\frac{n}{\mu_j}}}\left(\sum_{i=1}^{N_{j,nt}}(V_{j,i} - \mathbb{E}[V_{j,i}])\right)\right)_{t\ge0} \xrightarrow{d} (W_{j,t})_{t\ge0}.$$

Using a different scaling it holds in $(D[0,\infty), d_{SK})$ as $n \to \infty$

$$\left(\widetilde{Z}_{j,t}^{(n)}\right)_{t\ge0} := \left(\sqrt{\frac{\nu_j^2}{nh^2\mu_j}}\frac{1}{s_t^{(n)}}Z_{j,t}^{(n)}\right)_{t\ge0} \xrightarrow{d} \left(\sqrt{\frac{\nu_j^2}{h^2\mu_j}}\frac{1}{s_t^{(1)}}W_{j,t}\right)_{t\ge0} \tag{4.6}$$

because $(\sqrt{\nu_j^2/(nh^2\mu_j)}/s_t^{(n)}))_t$ is continuous in t and does not depend on n. As Ξ_1 and Ξ_2 are independent, we also obtain joint convergence in $(D[0,\infty)\times D[0,\infty), d_{SK}\otimes d_{SK})$ as $n\to\infty$

$$\left(\left(\widetilde{Z}_{1,t}^{(n)}\right)_{t\geq 0},\left(\widetilde{Z}_{2,t}^{(n)}\right)_{t\geq 0}\right)\xrightarrow{d}\left(\left(\sqrt{\frac{\nu_1^2}{h^2\mu_1}}\frac{1}{s_t^{(1)}}W_{1,t}\right)_{t\geq 0},\left(\sqrt{\frac{\nu_2^2}{h^2\mu_2}}\frac{1}{s_t^{(1)}}W_{2,t}\right)_{t\geq 0}\right). \tag{4.7}$$

For $\mu_{\mathrm{ri}}(t)=\mu_{\mathrm{ri},t}$, $\mu_{\mathrm{le}}(t)=\mu_{\mathrm{le},t}$ (as in eq. (3.12)), we use the map
$\varphi:(D[0,\infty)\times D[0,\infty), d_{SK}\otimes d_{SK})\to(D[\tau_h]\times D[\tau_h], d_{SK}\otimes d_{SK})$ given by

$$\begin{aligned}((f(t))_{t\geq 0},(g(t))_{t\geq 0})\overset{\varphi}{\mapsto}\Bigg(&\begin{pmatrix}(f(t+h)-f(t))\mu_{\mathrm{ri}}(t)\mathbb{1}_{[h,c-h)}(t)\\ +(g(t+h)-g(c))+(f(c)-f(t))\mu_{\mathrm{ri}}(t)\mathbb{1}_{[c-h,c)}(t)\\ +(g(t+h)-g(t))\mu_{\mathrm{ri}}(t)\mathbb{1}_{[c,T-h)}(t)\end{pmatrix}_t,\\ &\begin{pmatrix}(f(t)-f(t-h))\mu_{\mathrm{le}}(t)\mathbb{1}_{[h,c)}(t)\\ +(g(t)-g(c))+(f(c)-f(t-h))\mu_{\mathrm{le}}(t)\mathbb{1}_{[c,c+h)}(t)\\ +(g(t)-g(t-h))\mu_{\mathrm{le}}(t)\mathbb{1}_{[c+h,T-h]}(t)\end{pmatrix}_t\Bigg).\end{aligned}$$

As both component functions are compositions of continuous functions, φ is also continuous. The Continuous-Mapping-Theorem explains why convergence (4.7) holds with map φ applied to both sides. φ applied to the right hand side of (4.7) equals $\left(\widetilde{L}_{\mathrm{ri}}(t),\widetilde{L}_{\mathrm{le}}(t)\right)$ in distribution, which is shown in the following for the first coordinate.
For $t\in[h,c-h)$ we obtain

$$\varphi\left(\left(\frac{\sqrt{\frac{\nu_1^2}{h^2\mu_1}}}{s_t^{(1)}}W_{1,t}\right)_{t\geq 0},\left(\frac{\sqrt{\frac{\nu_2^2}{h^2\mu_2}}}{s_t^{(1)}}W_{2,t}\right)_{t\geq 0}\right)\Bigg|_{1,t}=\frac{(W_{1,t+h}-W_{1,t})}{\sqrt{2h}}.$$

In the case $t\in[c-h,c)$ we obtain

$$\begin{aligned}&\varphi\left(\left(\frac{\sqrt{\frac{\nu_1^2}{h^2\mu_1}}}{s_t^{(1)}}W_{1,t}\right)_{t\geq 0},\left(\frac{\sqrt{\frac{\nu_2^2}{h^2\mu_2}}}{s_t^{(1)}}W_{2,t}\right)_{t\geq 0}\right)\Bigg|_{1,t}\\ &=\frac{\sqrt{\mu_{\mathrm{ri},t}^2\nu_2^2/(h^2\mu_2)}(W_{2,t+h}-W_{2,c})+\sqrt{\mu_{\mathrm{ri},t}^2\nu_1^2/(h^2\mu_1)}(W_{1,c}-W_{1,t})}{s_t^{(1)}}.\end{aligned}$$

For $t\in[c,T-h]$, it holds that

$$\varphi\left(\left(\frac{\sqrt{\frac{\nu_1^2}{h^2\mu_1}}}{s_t^{(1)}}W_{1,t}\right)_{t\geq 0},\left(\frac{\sqrt{\frac{\nu_2^2}{h^2\mu_2}}}{s_t^{(1)}}W_{2,t}\right)_{t\geq 0}\right)\Bigg|_{1,t}=\frac{\sqrt{\mu_2\nu_2^2/h^2}(W_{2,t+h}-W_{2,t})}{s_t^{(1)}}.$$

For the left hand side of (4.7), we show

$$\varphi\left(\left(\widetilde{Z}_{1,t}^{(n)}\right)_{t\geq 0},\left(\widetilde{Z}_{2,t}^{(n)}\right)_{t\geq 0}\right)=\left(\left(\widetilde{\Gamma}_{\mathrm{ri},t}^{(n)}\right)_{t\in\tau_h},\left(\widetilde{\Gamma}_{\mathrm{le},t}^{(n)}\right)_{t\in\tau_h}\right). \tag{4.8}$$

We make the first coordinate explicit. There, we again distinguish between the three cases $t\in[h,c-h)$, $t\in[c-h,c)$ and $t\in[c,T-h]$. For $t<c-h$, the first coordinate of the right

hand side in equation (4.8) is given by

$$\frac{1}{nh/\mu_{\text{ri}}}\sum_{i=N_{1,nt}+2}^{N_{1,n(t+h)}}(V_{1,i}-\mathbb{E}[V_{1,i}])\frac{1}{s_t^{(n)}}=\left(\frac{1}{nh/\mu_{\text{ri}}}\sum_{i=N_{nt}+2}^{N_{n(t+h)}}V_i-\frac{N_{n(t+h)}-N_{nt}-1}{nh/\mu_{\text{ri}}}\mathbb{E}[V_i]\right)\frac{1}{s_t^{(n)}}.$$

Exchanging subscripts yields analogous results for $t \geq c$. For $t \in [c-h, c)$ we obtain the first coordinate as

$$\begin{aligned}&\frac{1}{nh/\mu_{\text{ri}}}\left(\sum_{i=N_{1,nt}+2}^{N_{1,nc}}V_{1,i}-\mathbb{E}[V_{1,i}]+\sum_{i=N_{2,nc}+2}^{N_{2,n(t+h)}}V_{2,i}-\mathbb{E}[V_{2,i}]\right)\frac{1}{s_t^{(n)}}\\&=\left(\frac{1}{nh/\mu_{\text{ri}}}\left(\sum_{i=N_{nt}+2}^{N_{nc}}V_i+\sum_{i=N_{nc}+2}^{N_{n(t+h)}}V_i\right)-\frac{N_{n(t+h)}-N_{nt}-1}{nh/\mu_{\text{ri}}}\mathbb{E}[V_i]\right)\frac{1}{s_t^{(n)}}.\end{aligned}$$

In the latter displays we omitted the summands $i = N_{1,nt}+1$ and $i = N_{2,nc}+1$, i.e., terms of order $o_{a.s.}(1)$. Note that the life time $\xi_{N_{nc}+1}$ is not considered in the variance estimation as its distribution is a mixture of two distributions.
Thus, using the above arguments (Lemma 4.5, Slutsky's theorem and continuous mapping), we can conclude

$$\Gamma^{(n)}=\Gamma_{\text{ri}}^{(n)}-\Gamma_{\text{le}}^{(n)}\xrightarrow{d}\widetilde{L}_{\text{ri}}-\widetilde{L}_{\text{le}}\sim\widetilde{L},$$

as also the subscripts one and two of the Brownian motions $(W_{1,t})_{t\geq 0}$ and $(W_{2,t})_{t\geq 0}$ can be omitted without changing the distribution while preserving the continuity of sample paths. This is due to the fact that $\widetilde{L}_{\text{ri}}-\widetilde{L}_{\text{le}}$ is defined as a function of increments of disjoint intervals of the standard Brownian motions $(W_{1,t})_{t\geq 0}$ and $(W_{2,t})_{t\geq 0}$ and has continuous sample paths. It only remains to be shown that the true means μ_1, μ_2 and the true scaling s can be replaced by their estimators.

Step 2: replacement of parameters by their estimators

First, we show equation (3.15), i.e., $\hat{\Gamma}^{(n)}-\Gamma^{(n)}\xrightarrow{\mathbb{P}}(0)_t$. To obtain $\hat{\Gamma}^{(n)}$, we replace the true means by their estimators in the numerator of $\widetilde{\Gamma}^{(n)}$ and the true rate change point c by $\hat{c}$. Our aim is to show

$$\left(\frac{\sqrt{n}}{N_{n(t+h)}-N_{nt}-1}\left(\sum_{i=N_{nt}+2}^{N_{n(t+h)}}(\xi_i-\mu^{(i)})^2-\sum_{i=N_{nt}+2}^{N_{n(t+h)}}(\xi_i-\hat{\mu}^{(i)})^2\right)\right)_t\xrightarrow{\mathbb{P}}(0)_t \tag{4.9}$$

for the right window with analogous arguments for the left window.
To simplify notation we now restrict to $(D(c-h,c],d_{||\cdot||})$ and show that (4.9) holds. The corresponding convergences in $(D(0,c-h],d_{||\cdot||})$ and $(D(c,T-h],d_{||\cdot||})$ can be shown with similar arguments. For our notation we assume $(nt, nt+nh] \ni n\hat{c}$ where analogous arguments can be applied for the case $(nt, nt+nh] \not\ni n\hat{c}$. Moreover, we neglect for simplification that the summands with indices $i = N_{nc}+1$ and $i = N_{n\hat{c}}+1$ (i.e., terms of order $o_{a.s.}(1)$) are omitted in the exact expressions for $\Gamma^{(n)}$ and $\hat{\Gamma}^{(n)}$, respectively. We first use the local estimators

$$\hat{\mu}_{1,\text{loc},t}:=(N_{nc}-N_{nt}-1)^{-1}\sum_{i=N_{nt}+2}^{N_{nc}}\xi_i\quad\text{and}\quad\hat{\mu}_{1,\text{loc},t}^{\hat{c}}:=(N_{n\hat{c}}-N_{nt}-1)^{-1}\sum_{i=N_{nt}+2}^{N_{n\hat{c}}}\xi_i$$

and analogously for $\hat{\mu}_{2,\mathrm{loc},t}, \hat{\mu}^{\hat{c}}_{2,\mathrm{loc},t}$.
The terms inside the inner brackets of (4.9) write as

$$\begin{aligned}
&-2((N_{nc} - N_{nt} - 1)\mu_1\hat{\mu}_{1,\mathrm{loc},t} + (N_{n(t+h)} - N_{nc} - 1)\mu_2\hat{\mu}_{2,\mathrm{loc},t}) \\
&+ 2\left((N_{n\hat{c}} - N_{nt} - 1)(\hat{\mu}^{\hat{c}}_{1,\mathrm{loc},t})^2 + (N_{n(t+h)} - N_{n\hat{c}} - 1)(\hat{\mu}^{\hat{c}}_{2,\mathrm{loc},t})^2\right) \\
&+ (N_{nc} - N_{nt} - 1)\mu_1^2 + (N_{n(t+h)} - N_{nc} - 1)\mu_2^2 - (N_{n\hat{c}} - N_{nt} - 1)(\hat{\mu}^{\hat{c}}_{1,\mathrm{loc},t})^2 \\
&- (N_{n(t+h)} - N_{n\hat{c}} - 1)(\hat{\mu}^{\hat{c}}_{2,\mathrm{loc},t})^2 \\
&= (N_{nc} - N_{nt} - 1)\mu_1^2 + (N_{n(t+h)} - N_{nc} - 1)\mu_2^2 \\
&- 2((N_{nc} - N_{nt} - 1)\mu_1\hat{\mu}_{1,\mathrm{loc},t} + (N_{n(t+h)} - N_{nc} - 1)\mu_2\hat{\mu}_{2,\mathrm{loc},t}) \\
&+ ((N_{n\hat{c}} - N_{nt} - 1)(\hat{\mu}^{\hat{c}}_{1,\mathrm{loc},t})^2 + (N_{n(t+h)} - N_{n\hat{c}} - 1)(\hat{\mu}^{\hat{c}}_{2,\mathrm{loc},t})^2.
\end{aligned}$$

Applying the same arguments as for the second summand of $R_t^{(n)}$ in the proof of Theorem 3.4, we conclude that in $(D(c-h,c], d_{||\cdot||})$

$$\begin{aligned}
&\left(\frac{\sqrt{n}}{N_{n(t+h)} - N_{nt} - 1}((N_{nc} - N_{nt} - 1)(\mu_1 - \hat{\mu}_{1,\mathrm{loc},t})^2 + (N_{n(t+h)} - N_{nc} - 1)(\mu_2 - \hat{\mu}_{2,\mathrm{loc},t})^2)\right)_t \\
&\quad \xrightarrow{\mathbb{P}} (0)_t. \qquad (4.10)
\end{aligned}$$

Thus, we have to prove that the difference of (4.10) and (4.9) vanishes, i.e.,

$$\begin{aligned}
&\left(\frac{\sqrt{n}}{N_{n(t+h)} - N_{nt} - 1}\right)_t \times \Big(((N_{n\hat{c}} - N_{nt})\left(\hat{\mu}^{\hat{c}}_{1,\mathrm{loc},t}\right)^2 - (N_{nc} - N_{nt})\hat{\mu}^2_{1,\mathrm{loc},t} \\
&\qquad\qquad + (N_{n(t+h)} - N_{n\hat{c}})\left(\hat{\mu}^{\hat{c}}_{2,\mathrm{loc},t}\right)^2 - (N_{n(t+h)} - N_{nc})\hat{\mu}^2_{2,\mathrm{loc},t})\Big)_t \\
&\quad \xrightarrow{\mathbb{P}} (0)_t. \qquad (4.11)
\end{aligned}$$

We skipped the terms with -1 as they are of order $o_{\mathbb{P}}(1)$. Now, we concentrate on the first two terms with the argumentation for the other terms being similar and note that the corresponding terms in the previous line are the same as

$$\frac{\sqrt{n}}{N_{n(t+h)} - N_{nt} - 1}\left((N_{n\hat{c}} - N_{nc})\left(\hat{\mu}^{\hat{c}}_{1,\mathrm{loc},t}\right)^2 - (N_{nc} - N_{nt})\left(\hat{\mu}^2_{1,\mathrm{loc},t} - \left(\hat{\mu}^{\hat{c}}_{1,\mathrm{loc},t}\right)^2\right)\right). \quad (4.12)$$

Due to assumption (3.10) we derive $|\sum_{i=N_{nc}+1}^{N_{nc}} \xi_i| \leq |n(c-\hat{c})| = o_{\mathbb{P}}(\sqrt{n})$. Moreover, we have for the number of summands

$$N_{n\hat{c}} - N_{nc} = o_{\mathbb{P}}(\sqrt{n}) \qquad (4.13)$$

which results from using assumption (3.10) together with the Elementary Renewal Theorem (e.g., Ross, 1996) and Markov's inequality. (4.13) does not depend on t and consequently, it can be shown that the first summand in (4.12) vanishes using also the consistency of $\hat{\mu}^{\hat{c}}_{1,\mathrm{loc},t}$ (which follows from (4.14) below and the consistency of $\hat{\mu}_{1,\mathrm{loc},t}$). Defining $d_t^{(n)} := (\hat{\mu}_{1,\mathrm{loc},t} - \hat{\mu}^{\hat{c}}_{1,\mathrm{loc},t})$ we now show that $\left(|\sqrt{n}(\hat{\mu}^2_{1,\mathrm{loc},t} - (\hat{\mu}^{\hat{c}}_{1,\mathrm{loc},t})^2)|\right)_t = \left(|2\sqrt{n}\hat{\mu}^{\hat{c}}_{1,\mathrm{loc},t}d_t^{(n)} + \sqrt{n}(d_t^{(n)})^2|\right)_t$ converges

in probability in $(D(c-h,c],d_{||\cdot||})$ to zero and thus (4.11) holds. W.l.o.g. we assume $\hat{c}<c$ and observe

$$\sqrt{n}d_t^{(n)} = \sqrt{n}(N_{nc}-N_{nt}-1)^{-1}\left((N_{n\hat{c}}-N_{nc})\,(N_{n\hat{c}}-N_{nt}-1)^{-1}\sum_{i=N_{nt}+2}^{N_{n\hat{c}}}\xi_i+\sum_{i=N_{n\hat{c}}+1}^{N_{nc}}\xi_i\right). \tag{4.14}$$

One can show that $((\sum_{i=N_{nt}+2}^{N_{n\hat{c}}}\xi_i)(N_{n\hat{c}}-N_{nt}-1)^{-1})_t \to (\mu_1)_t$ holds in $(D[c-h,c],d_{||\cdot||})$ (using equation (4.13) and the a.s. consistency of the rate estimator in the rate constant case). Furthermore, using Lemma 4.5 and equation (4.13), we conclude that $((\sqrt{n}(N_{n\hat{c}}-N_{nc})(N_{nc}-N_{nt}-1)^{-1}))_t$ vanishes in probability in $(D[c-h,c],d_{||\cdot||})$. Together, this shows that the first summand in (4.14) vanishes. Together with assumption (3.10) explaining why the second summand of (4.14) converges to zero we can prove that $(\sqrt{n}d_t^{(n)})_t$ vanishes in $(D(c-h,c],d_{||\cdot||})$. Moreover, $(\sqrt{n}(d_t^{(n)})^2)_t = (\sqrt{n}d_t^{(n)}(\hat{\mu}_{1,\mathrm{loc},t}-\hat{\mu}_{1,\mathrm{loc},t}^{\hat{c}}))_t$ vanishes as also the second factor in the latter display converges to zero which can be easily seen using equation (4.13).

Thus, applying Slutsky's theorem we have shown (3.15), i.e. $\hat{\Gamma}^{(n)}-\Gamma^{(n)} \xrightarrow{\mathbb{P}} (0)_t$, for the locally estimated means $\hat{\mu}_{1,\mathrm{loc},t}^{\hat{c}},\hat{\mu}_{2,\mathrm{loc},t}^{\hat{c}}$. The substitution of these locally estimated means by the global means $\hat{\mu}_1^{\hat{c}} := N_{n\hat{c}}^{-1}\sum_{i=1}^{N_{n\hat{c}}}\xi_i, \hat{\mu}_2^{\hat{c}} := (N_{nT}-N_{n\hat{c}}-1)^{-1}\sum_{i=N_{n\hat{c}}+2}^{N_{nT}}\xi_i$ can be done with a decomposition argument similiar to the one in the proof of Theorem 3.4 as we show next for $\hat{\mu}_1^{\hat{c}}$. We derive

$$\begin{aligned}
\sum_{i=N_{nt}+2}^{N_{n\hat{c}}}(\xi_i-\hat{\mu}_1^{\hat{c}})^2 &= \sum_{i=N_{nt}+2}^{N_{n\hat{c}}}\xi_i^2 - 2\hat{\mu}_1^{\hat{c}}\sum_{i=N_{nt}+2}^{N_{n\hat{c}}}\xi_i + (N_{n\hat{c}}-N_{nt}-1)\hat{\mu}_1^{\hat{c}\,2}\\
&= \sum_{i=N_{nt}+2}^{N_{n\hat{c}}}(\xi_i-\hat{\mu}_{1,\mathrm{loc},t}^{\hat{c}})^2 + 2(\hat{\mu}_{1,\mathrm{loc},t}^{\hat{c}}-\hat{\mu}_1^{\hat{c}})\sum_{i=N_{nt}+2}^{N_{n\hat{c}}}\xi_i\\
&\quad + (N_{n\hat{c}}-N_{nt}-1)(\hat{\mu}_1^{\hat{c}\,2}-\hat{\mu}_{1,\mathrm{loc},t}^{\hat{c}\,2})\\
&= \sum_{i=N_{nt}+2}^{N_{n\hat{c}}}(\xi_i-\hat{\mu}_{1,\mathrm{loc},t}^{\hat{c}})^2 + (N_{n\hat{c}}-N_{nt}-1)(\mu_1^{\hat{c}}-\hat{\mu}_{1,\mathrm{loc},t}^{\hat{c}})^2.
\end{aligned}$$

Using the further decomposition $(\mu_1^{\hat{c}}-\hat{\mu}_{1,\mathrm{loc},t}^{\hat{c}}) = (\mu_1^{\hat{c}}-\mu_1)-(\hat{\mu}_{1,\mathrm{loc},t}^{\hat{c}}-\mu_1)$ identical arguments as for $R_t^{(n)}$ on page 25 together with assumption (3.10) show that $\left((N_{n\hat{c}}-N_{nt}-1)/\sqrt{n}(\mu_1^{\hat{c}}-\hat{\mu}_{1,\mathrm{loc},t}^{\hat{c}})^2\right)_t$ uniformly vanishes in probability as $n\to\infty$. Recalling the summands in (3.15) we observe

$$\begin{aligned}
&\frac{1}{(N_{n(t+h)}-N_{nt}-1)s_t^{(n)}}\left(\sum_{i=N_{nt}+2}^{N_{n\hat{c}}}(\xi_i-\mu_1^{\hat{c}})^2\right)\\
&\quad= \frac{1}{(N_{n(t+h)}-N_{nt}-1)s_t^{(n)}}\left(\sum_{i=N_{nt}+2}^{N_{n\hat{c}}}(\xi_i-\hat{\mu}_{1,\mathrm{loc},t}^{\hat{c}})^2\right) + \frac{(N_{n\hat{c}}-N_{nt}-1)(\mu_1^{\hat{c}}-\hat{\mu}_{1,\mathrm{loc},t}^{\hat{c}})^2}{(N_{n(t+h)}-N_{nt}-1)s_t^{(n)}}
\end{aligned}$$

where $s_t^{(n)}$ is asymptotically of order $\Theta(1/\sqrt{n})$ (recall eq. (3.13)) and thus the last term uniformly vanishes in probability as $n\to\infty$ as explained above. Hence, an application of Slutsky's theorem allows us to finally show (3.15).

In the last part of the proof we substitute the interpolated variance $(s_t^{(n)})^2$ by the estimated variance $\hat{s}^2_{nh,nt}$. With Lemma 4.6 below and weak convergence of $\hat{\Gamma} \to \widetilde{L}$, the assertion follows. □

Next, we show two technical lemmata. Using μ_{le} and μ_{ri} we obtain a convergence result for the scaled counting process $(N_t)_{t\geq 0}$.

Lemma 4.5. *Let Ξ be a renewal process like in Theorem 3.6 with mean functions $\mu_{le,h,t}$, $\mu_{ri,h,t}$ as in (3.12). Let $T > 0$, $h \in (0, T/2]$. Then we have in $(D[\tau_h], d_{||\cdot||})$ as $n \to \infty$ almost surely*

$$\left(\frac{N_{n(t+h)} - N_{nt}}{nh/\mu_{ri,h,t}}\right)_{t\in\tau_h} \longrightarrow (1)_{t\in\tau_h} \quad \textit{and} \quad \left(\frac{N_{nt} - N_{n(t-h)}}{nh/\mu_{le,h,t}}\right)_{t\in\tau_h} \longrightarrow (1)_{t\in\tau_h}.$$

Proof: This is Lemma 4.1 in Messer and Schneider (2017). □

The next result shows the convergence of the denominator of G. For a known rate the estimator $\hat{\nu}^2_{\text{le}}$ (3.5) may be written as

$$\hat{\nu}^2_{\text{le}} := \frac{1}{N_{nt} - N_{n(t-h)} - 1}\left(\sum_{i=N_{n(t-h)}+2}^{N_{nc}} ((\xi_i - \mu_1)^2 - \hat{\sigma}^2_{\text{le}})^2 + \sum_{i=N_{nc}+2}^{N_{nt}} ((\xi_i - \mu_2)^2 - \hat{\sigma}^2_{\text{le}})^2\right) \tag{4.15}$$

and analogous for $\hat{\nu}^2_{\text{ri}}$ where c denotes the rate change point. Note that the life time $\xi_{N_{nc}+1}$ is not considered in the terms above as its distribution is a mixture of two distributions.

Lemma 4.6. *Let $\Xi_1(\mu_1, \sigma^2)$ and $\Xi_2(\mu_2, \sigma^2)$ be independent elements of $\mathscr{R}$ with $\mu_1 \neq \mu_2$. Let $c \in (0, T]$ be a rate change point, so that the sequence $\Xi^{(n)}$ results from Ξ_1 and Ξ_2 according to model (3.9). Let $\hat{s}_{nh,nt}$ and $s_t^{(n)}$ be defined as in (3.4) and (3.13) and $\hat{c}$ be an estimator of c fulfilling assumption (3.10). Then it holds in $(D[\tau_h], d_{||\cdot||})$ for $n \to \infty$ in probability*

$$(\hat{s}_{nh,nt})_{t\in\tau_h} \longrightarrow \left(s_t^{(1)}\right)_{t\in\tau_h}.$$

Proof: We show that the limit behavior of $\hat{s}_{nh,nt}$ is given by

$$\frac{\nu^2_{\text{ri}}}{h/\mu_{\text{ri}}} + \frac{\nu^2_{\text{le}}}{h/\mu_{\text{le}}} \quad \forall t \in \tau_h,$$

where μ_{ri} and μ_{le} are the window means defined in (3.12).
$\nu^2_{\text{ri}} := \nu^2_{\text{ri}}(h,t)$ is given by ${\nu_1}^2$ for $t \leq c - h$, by ${\nu_2}^2$ for $t > c$ and by

$$\nu^2_{\text{ri}}(h,t) := \frac{(c-t)/\mu_1 \cdot {\nu_1}^2 + (t+h-c)/\mu_2 \cdot {\nu_2}^2}{h/\mu_{\text{ri}}} \tag{4.16}$$

otherwise. ν^2_{le} is defined analogously.
The uniform a.s. convergence of the estimators $\hat{\mu}_{\text{ri}}$ and $\hat{\mu}_{\text{le}}$ to μ_{ri} and μ_{le} is shown in Lemma 4.2 in Messer and Schneider (2017). The uniform convergence in probability of the estimators $\hat{\nu}^2_{\text{ri}}$ and $\hat{\nu}^2_{\text{ri}}$ (as in (3.5)) to ν^2_{ri} and ν^2_{le} (defined in (4.16)) can be shown using the consistency

result for ν^2 (Lemma 4.3). We show this for $\hat{\nu}^2_{\text{le}}$ with the argumentation for $\hat{\nu}^2_{\text{ri}}$ being similar and assume first a known mean profile. By Lemma 4.3 it holds for $n \to \infty$ that

$$\left(\frac{\sum_{i=N_{n(t-h)}+2}^{N_{nc}} ((\xi_i - \mu_1)^2 - \hat{\sigma}^2_{\text{le}})^2}{N_{nc} - N_{n(t-h)} - 1} \right)_{t \in \tau_h} \xrightarrow{a.s.} (\nu_1^2)_{t \in \tau_h}.$$

Lemma 4.5 and Slutsky's theorem imply for the first summand of (4.15)

$$\left(\frac{\sum_{i=N_{n(t-h)}+2}^{N_{nc}} ((\xi_i - \mu_1)^2 - \hat{\sigma}^2_{\text{le}})^2}{N_{nt} - N_{n(t-h)} - 1} \right)_{t \in \tau_h} \xrightarrow{a.s.} \left(\frac{(c - (t-h))/\mu_1}{h/\mu_{\text{ri}}} \nu_1^2 \right)_{t \in \tau_h}.$$

Similar calculations for the second summand yield

$$\left(\frac{\sum_{i=N_{nc}+2}^{N_{nt}} ((\xi_i - \mu_2)^2 - \hat{\sigma}^2_{\text{le}})^2}{N_{nt} - N_{n(t-h)} - 1} \right)_{t \in \tau_h} \xrightarrow{a.s.} \left(\frac{(t-c)/\mu_2}{h/\mu_{\text{ri}}} \nu_2^2 \right)_{t \in \tau_h}.$$

The exchange of the true means by their estimators results from Slutsky's theorem using assumption (3.10) of consistency (in probability) of the change point estimator, which yields $(\hat{\nu}^2_{\text{le}})_{t \in \tau_h} \longrightarrow (\nu^2_{\text{le}})_{t \in \tau_h}$ in probability. As all four functions $(\mu_{\text{ri}})_{t \in \tau_h}, (\mu_{\text{le}})_{t \in \tau_h}, (\nu^2_{\text{ri}})_{t \in \tau_h}$ and $(\nu^2_{\text{le}})_{t \in \tau_h}$ are continuous, $\hat{s} \to s^{(1)}$ holds in probability for $n \to \infty$ by the form of the estimator $\hat{s}$ in (3.4). □

Note that Theorem 3.6 holds not only for renewal processes but for all point processes for which (4.6) holds and s_t is consistently estimated, for example also for a subclass of renewal processes with varying variance (RPVVs, see Messer et al. (2014)).

Chapter 5

Change point detection and evaluation in simulations

In this chapter, we investigate the practical applicability of the MFT. First, we briefly discuss the window choice. Then, we investigate the empirical significance level of the MFT – which is an asymptotic method – in simulations. Section 5.1 assumes a constant rate, and Section 5.2 investigates the behavior for an unknown number of unknown change points in the rate thereby also explaining the multiple filter algorithm. In Section 5.3, we evaluate the detection probability of variance change points in different simulation settings thereby showing the importance of including estimated rate change points and the dependence of the detection probability on the magnitude of changes and on the regularity of processes.
We have already outlined in the introduction that the MFT uses multiple windows to combine the advantages of small and large windows and to avoid the problem of choosing the most appropriate single window. As discussed in Messer et al. (2014), adding more windows in the window set H only slightly increases the rejection threshold Q. Therefore, we recommend the following guidelines for choosing the window set H. The smallest window h_1 should be chosen such that the asymptotic significance level is kept. $T/2$ limits the choice of the largest window $h_{\max}$. A narrow grid between the smallest and largest window facilitates change-point detection in various time scales but increases Q (thereby reducing the probability to detect change points) and the computational effort.

5.1 Global rate

Figure 5.1 A shows the empirical significance level of the MFT applied to processes with independent and Gamma-distributed life times with mean μ and standard deviation σ. The global empirical mean of the life times is used as an estimator for μ. As discussed in Messer et al. (2014), the minimal window should be large enough such that a sufficiently high number of events can be observed. For change points in the rate, the minimal window should contain at least about 100-150 events (see Messer et al., 2014). For variance change points, the minimal window should be slightly larger. We use here the window set $H = \{150, 250, 500, 750, 1000, 1250\} \cdot \mu$, where the minimal window size increases linearly with the mean life time. As indicated in the figure, the test keeps the asymptotic significance level of 5% for a wide range of parameter combinations if $\sigma < 4\mu$ (roughly), i.e., if the process is not too irregular.

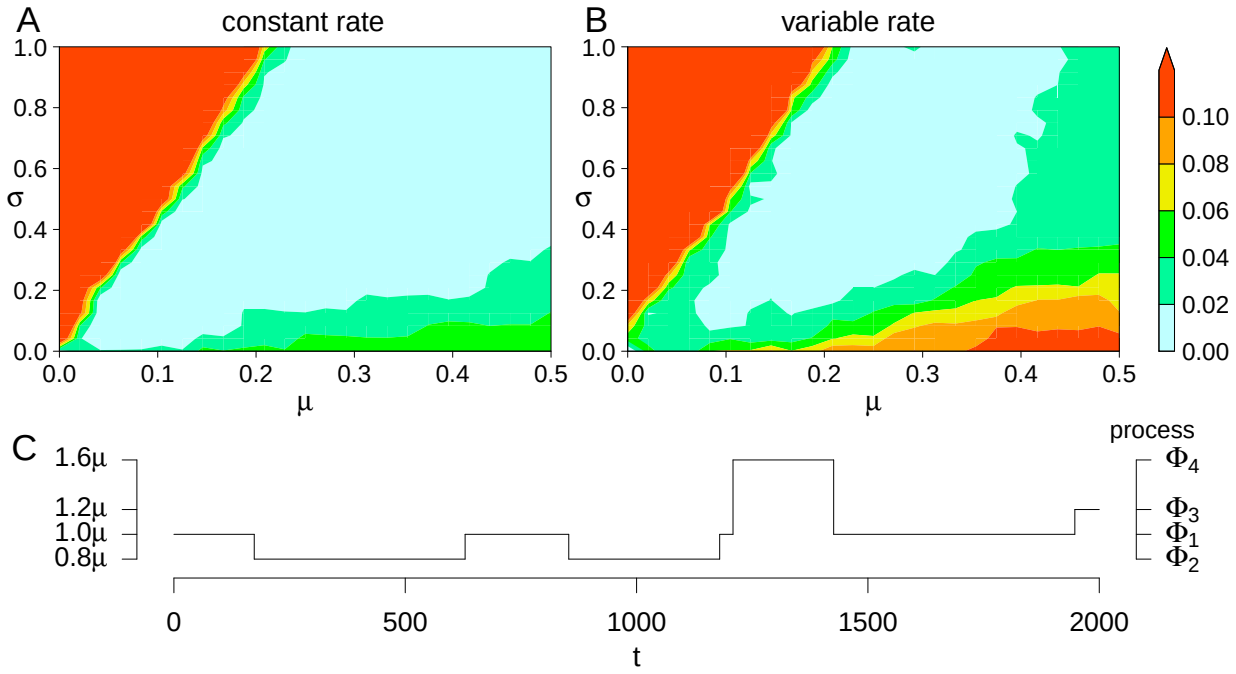

Figure 5.1: Simulated rejection probability of the MFT for processes with i.i.d. Gamma-distributed life times *($T = 2000$, $H = \{150, 250, 500, 750, 1000, 1250\} \cdot \mu$, 5000 simulations). (A) Constant unknown mean estimated by the global empirical mean. (B) The rate profile is given by a random change point model. For each simulation, a new rate profile is realized as exemplarily depicted in (C). The means and all change points are estimated using the MFA from Messer et al. (2014). (C) Process Ξ used in the simulations in (B) is a piecewise composition of four renewal processes $\Xi_1, \ldots, \Xi_4$ with Gamma-distributed life times with parameters $(\mu_1, \mu_2, \mu_3, \mu_4) = (\mu, 0.8\mu, 1.2\mu, 1.6\mu)$. Waiting times between rate change points are uniformly distributed on $[0, 800]$. At odd valued change points Ξ jumps from Ξ_1 to a randomly drawn other process, jumping back at even valued change points.*

In the following section, the significance level of the MFT is investigated for a set of multiple unknown rate change points, implying also an unknown rate profile.

5.2 Inhomogeneous rate

For the investigation of the significance level of the MFT in the case of multiple unknown rate change points, we first need to estimate the number and location of the rate change points. To this end, we apply here the multiple filter algorithm (MFA) for the rate proposed in Messer et al. (2014). After estimation of the rate change points, we include the estimated rates into the variance estimation in order to test the null hypothesis of variance homogeneity. When this null hypothesis is rejected, the MFA procedure can be extended to estimate the variance change points. In Section 5.2.1, we summarize the idea of the MFA and its two-step application for the detection of rate and variance change points. Section 5.2.2 will be concerned with investigating its significance level in simulations with multiple change points in the rate.

5.2.1 The two-step MFA for the detection of rate and variance change points

In a nutshell, the MFA works as follows. In case of rejection of the null hypothesis, change points are detected using the individual windows (compare Figure 5.2 A). For each window, we check whether the maximum of its $|G_{h,t}|$-process exceeds the rejection threshold Q and if so, its argument $\hat{c}_{h,1}$ is a change point candidate. As this maximum affects it h-neighborhood, we delete this h-neighborhood from the observation region τ_h and continue searching for the next maximizer. We repeat this procedure as long as the remaining process has points above Q. Thus, for each window $h \in H$ we obtain a set of change point candidates (diamonds in Figure 5.2 B, where we have two candidates for the smallest and largest window, respectively, and one candidat for the second window).
The second step of the MFA combines the change point candidates into the final set of estimates $\hat{C}$ by preferring change points detected by smaller windows (as change points being close together might affect the estimation precision of larger windows). First, all change points candidates of the smallest window h_1 are included in $\hat{C}$ (two blue triangles in Figure 5.2 B). Then, only those change points detected by the second smallest window h_2 are included in $\hat{C}$ whose h_2-neighborhood does not contain an already accepted change point. The procedure is continued successively for all larger windows. In Figure 5.2 B the change point estimated by h_3 is added to $\hat{C}$ (magenta triangle). Then, the quantity of interest (i.e., the rate or the variance) is estimated between the change points or – if the null hypothesis was not rejected – in the interval $[h, T-h]$. For more details on the MFA compare Messer et al. (2014).
We suggest to apply the MFA first for the estimation of rate change points. Second, we include the estimated rates into the variance estimation (eq. (3.3)). This sequential MFA is illustrated in the following line, where $\hat{c}^R$ and $\hat{c}^V$ denote the estimated sets of rate and variance change points, respectively, and $\hat{\mu}_t$ and $\hat{\sigma}_t^2$ are the estimated means and variances at time $t \in [h, T-h]$, respectively.

$$\begin{matrix}\text{MFT}\\ \text{Rate}\end{matrix} \xrightarrow[H_0?]{\text{Rej.}} \begin{cases}\text{Yes: MFA} : \hat{c}^R = (\hat{c}_1^R, \ldots), \hat{\mu}_t \\ \text{No: } \hat{c}^R = \{\}, \hat{\mu}_t\end{cases} \xrightarrow[\hat{\mu}_t]{\hat{c}^R} \begin{matrix}\text{MFT}\\ \text{Variance}\end{matrix} \xrightarrow[H_0?]{\text{Rej.}} \begin{cases}\text{Yes: MFA} : \hat{c}^V = (\hat{c}_1^V, \ldots), \hat{\sigma}_t^2 \\ \text{No: } \hat{c}^V = \{\}, \hat{\sigma}_t^2\end{cases}$$

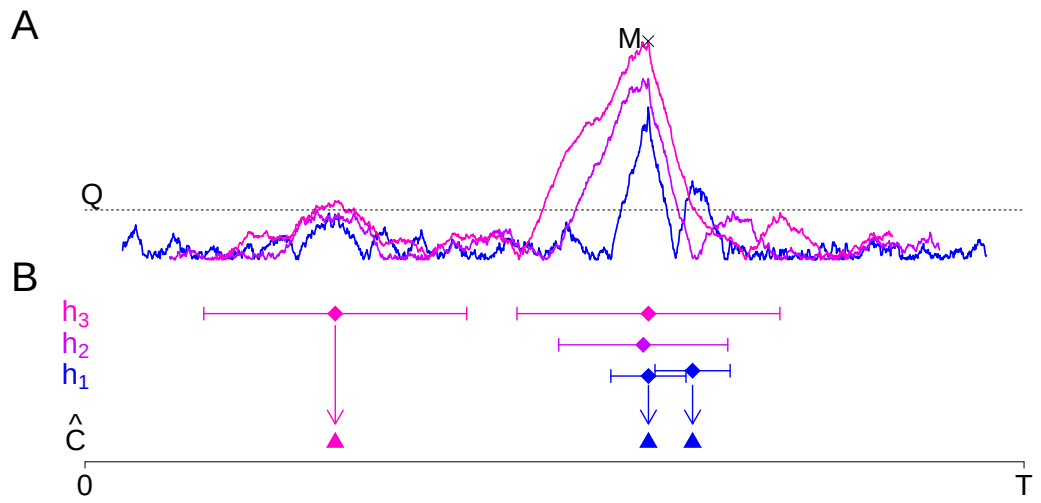

Figure 5.2: Visualization of the MFA for a window set $H = \{h_1, h_2, h_3\}$. *(A) Exemplary $|G_{h,t}|$-processes. (B) Change point candidates detected by single windows are shown as diamonds and their h-neighborhoods as horizontal lines. $\hat{C}$ contains all finally accepted change points. The MFA for rate and variance change points work identically. The figure is adopted from Figure 3 in Messer et al. (2018).*

The functions `MFT.rate()` and `MFT.variance()` in the `R`-package `MFT` (Messer et al., 2017) perform the MFT and the MFA for the rates and the variances, respectively.
Figure 5.3 shows the application of the sequential MFA to a simulated point process with two rate and two variance change points. In panels B and D-H the estimated variance fits well if the inhomogeneous rates are included in the estimation. Panels A and C also indicate that neglecting the rate change points and thus estimating a constant rate results in erroneous estimation of the rate and the variance profile. This is because the applied test statistic uses the wrong global mean (eq. (3.2)).
Note that this procedure requires consistency of the estimated rate (Theorem 3.6). Although this has not been shown for the MFA, our simulation results suggest good performance (see Section 5.2.2). In addition, note that in the second step of the sequential procedure, i.e., the detection of variance changes, the limit process $\widetilde{L}$ required to set the rejection threshold Q differs from L. However, as $\widetilde{L}$ depends on unknown process parameters, we argue here that one can replace $\widetilde{L}$ by L because the mean and variance of the two Gaussian processes are identical. Differences occur only in the covariance function $\Sigma^h_{u,v} := \mathrm{Cov}(L_{h,u}, L_{h,u+v})$ in the $3h$-neighborhood of a change point and are typically small (Figure 5.4 A, C), particularly for small σ/μ and small rate changes. For higher changes in the mean and higher σ/μ, larger differences can be observed between L and $\widetilde{L}$ (panel B, D), but their 95%-quantiles Q and $\widetilde{Q}$ remain close together. Also in larger simulation studies with different rate changes up to a factor of six, Q ranged between the 94.5%- and the 95.1%-quantile of $\max_{h,t} |\widetilde{L}_{h,t}|$ (data not shown).

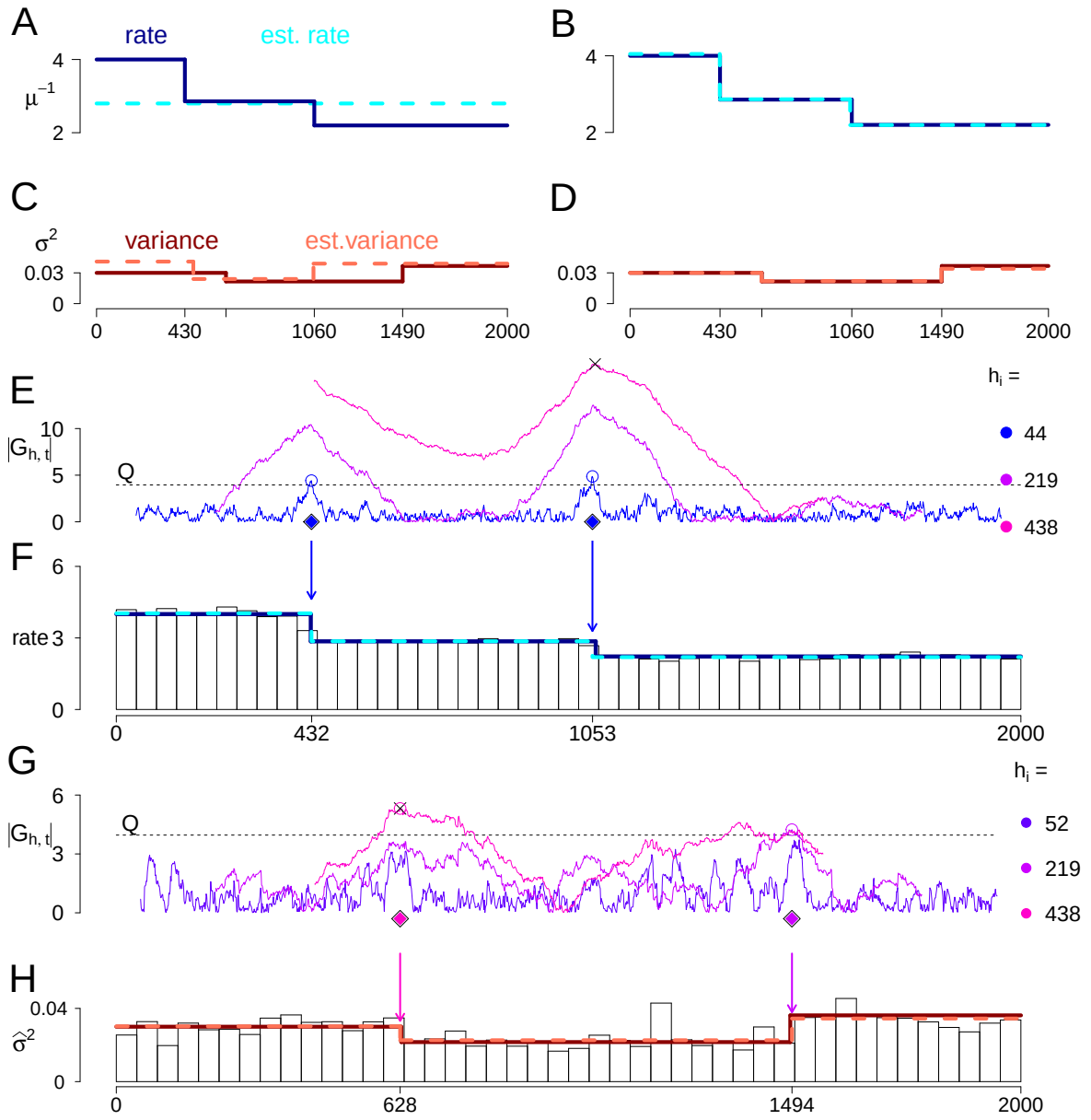

Figure 5.3: Application of the sequential MFA for estimation of rate and variance change points in a simulated point process. *The analyzed interval is* $(0, 2000]$ *with rate change points* $c_1 = 430, c_3 = 1060$ *and variance change points* $c_2 = 630, c_4 = 1490$. *All life times were Gamma-distributed with* (μ, σ^2) *equalling* $(0.25, 0.03)$ *in* $(0, c_1]$,$(0.35, 0.03)$ *in* $(c_1, c_2]$, $(0.35, 0.0216)$ *in* $(c_2, c_3]$, $(0.45, 0.0216)$ *in* $(c_3, c_4]$ *and* $(0.45, 0.0357)$ *in* $(c_4, 2000]$. *(A, C) Neglecting rate inhomogeneity in the variance estimation yields erroneous results. Estimated rate (blue) and variance (red), and true profiles (darkblue, darkred). (B, D) The rate change points are estimated and included in the variance estimation. (E, F) Rate MFA. (G, H) Variance MFA. Colored curves show the* $(|G_{h,t}|)$*-processes colored by window size indicated on the right. Dashed line indicates simulated threshold* Q*, estimated change points are marked by diamonds. Dashed blue and red lines show the estimated rate and variance profiles, solid lines indicate the true parameter values.*

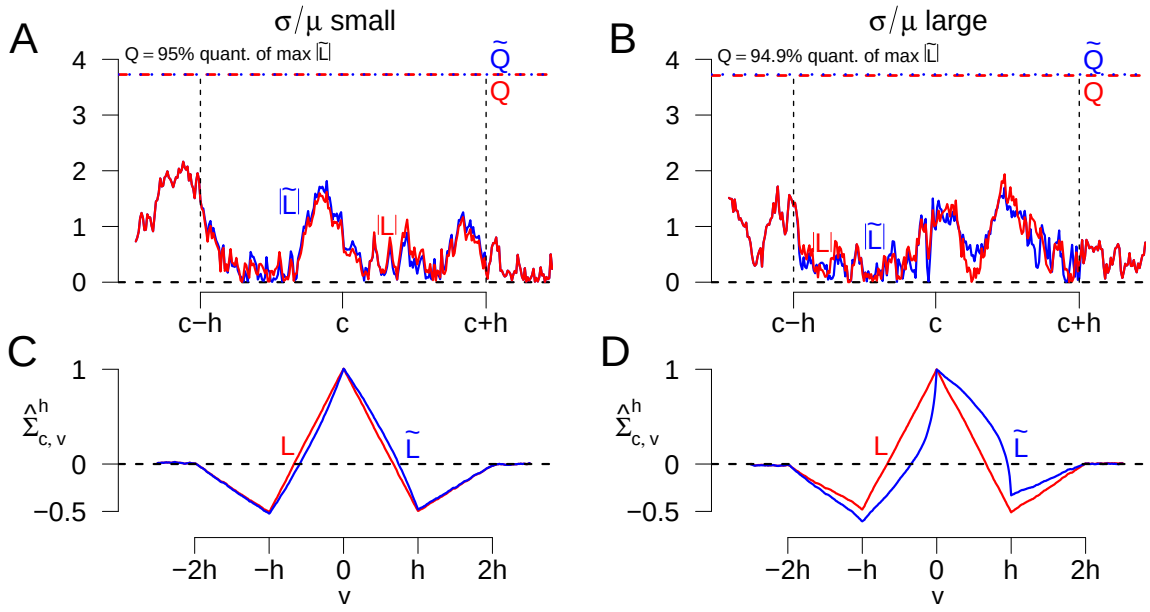

Figure 5.4: Comparison of the processes L and $\widetilde{L}$. *The processes are compared in the neighborhood of a rate change point at $c = T/2$ ($T = 2000$) where processes with small σ/μ and small rate change (A,C) and larger σ/μ and larger rate change (B,D) are used. (A, B) Realizations of $|L|$ (red) and $|\widetilde{L}|$ (blue), derived from the same Brownian motion. Outside the h-neighborhood of the change point, the marginals coincide. The 95%-quantiles Q and $\widetilde{Q}$ of the absolute maxima of L and $\widetilde{L}$ (estimated in 10000 simulations) are indicated by dashed and dotted lines. (C, D) The estimated empirical covariance functions $\hat{\Sigma}^h_{c,v}$ of L (red) and $\widetilde{L}$ (blue) at the change point c for one window size $h = 100$ estimated in 10000 simulations for the parameters given in A, B, respectively. Parameters for A, C: $\mu = \mu_1 = 0.1, \mu_2 = 0.15, \sigma = \sigma_1 = \sigma_2 = 0.1$. Parameters for B, D: $\mu = \mu_1 = 0.1, \mu_2 = 0.5, \sigma = \sigma_1 = \sigma_2 = 0.5$.*

5.2.2 Significance level under rate inhomogeneity

In order to investigate the empirical significance level of the MFT for variance changes under an unknown set of unknown change points estimated with the rate MFA, we use a random rate change point model with rate changes of different height and at different time scales (Figure 5.1 C). The empirical significance level of the resulting MFT derived in 5000 simulations is plotted in Figure 5.1 B as a function of the mean μ_1 of the process Ξ_1 and the standard deviation σ.
Compared to the situation with constant rate (Figure 5.1 A), a higher type I error is observed as the rate MFA can usually not correctly estimate all rate change points, which affects the MFT for variance changes (Figure 5.3 C). The parameter region with empirical significance level $> 5\%$ is larger than under rate homogeneity, including also parameter combinations with high mean and small variance. This suggests that if the average variance is not too large or too small compared to the mean, the smallest window in the MFT for variance changes should contain at least about 150 events.

5.3 Detection probability of variance change points

In this section, we investigate the empirical detection probability of variance change points in simulations, considering cases with homogeneous and with inhomogeneous rate. First, we recommend to always perform the two-step procedure of estimating rate change points first and then using these for the analysis of variance homogeneity and estimation of variance change points. This is because in practice, information about rate homogeneity is usually not given, and falsely assuming rate homogeneity can largely affect the analysis of variance homogeneity. As shown in Figure 5.5 B, rate change points can be falsely identified as variance changes points, while the detection probability of true variance change points can dramatically decrease.
Using this two-step procedure raises the question of whether the rate-MFT in the first step is applicable in the presence of variance change points. Indeed, one can show that the impact of variance change points on the performance of the rate-MFT is practically negligible (for details see Messer and Schneider, 2017, Corollary 3.4). The reason is that if only the variance changes but not the rate, the associated filtered derivative process for the rate still converges to a zero-mean unit-variance $2h$-dependent Gaussian process, and the change in the variance affects only the local covariance structure of the limit process.
Second, the MFT for variance changes shows a considerably high detection probability (Figure 5.5 D). In accordance with common neurophysiological models, we simulated Gamma-distributed life times and call processes with life time distributions with a coefficient of variation ($\mathrm{CV} = \sqrt{\mathbb{V}ar(\xi)}/\mathbb{E}(\xi)$) of up to 0.5 regular, while processes with $\mathrm{CV} = 1$ (e.g., a Poisson process) are called irregular, and processes with $\mathrm{CV} > 1$ very irregular. In regular and mildly irregular cases, a variance change factor of only 1.5 already had a considerable detection probability of 50% in the worst case, increasing quickly to detection probabilities close to 100% for a change factor of 2 (compare. e.g., Eckley et al., 2010; Killick et al., 2010). Only for extremely irregular cases, detection probability increased more slowly, reaching a detection probability of about 75% at a change factor of 3.

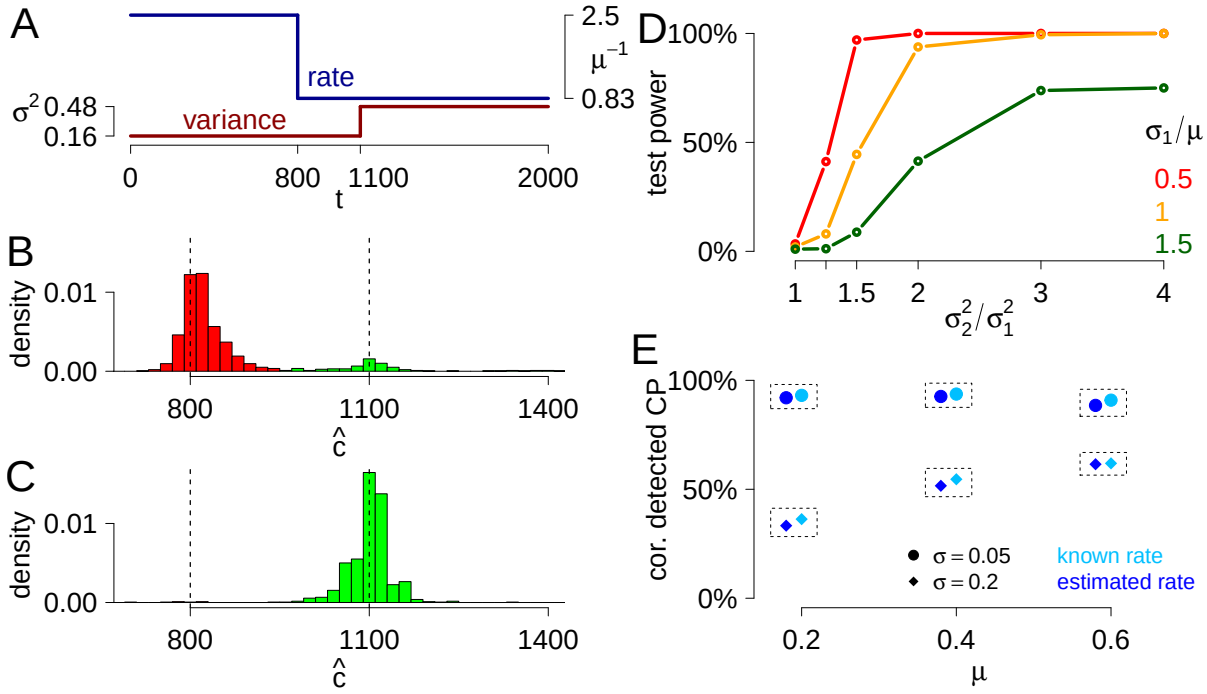

Figure 5.5: Detection probability of variance change points. *In all cases* $T = 2000$, $\alpha = 5\%$ *and* $H = \{150, 250, 500, 750, 1000, 1250\} \cdot \mu$ *were used. (A): Rate and variance profile of the Gamma processes used in B and C. (B): Locations of estimated variance change points when the rate is assumed constant and estimated globally. For illustration, estimated change points closer to the (falsely detected) rate change point are colored in red, change point estimates closer to the variance change point are colored in green. (C): Locations of estimated variance change points when the MFA for rate change detection is included as a first step. Colors as in B. (D): Test power of the MFT for variance homogeneity for Gamma processes with constant mean* $\mu = 0.4$ *and one variance change point at* $c = 1000$ *where the variance changes from* $\sigma_1^2 \in \{0.2^2, 0.4^2, 0.6^2\}$ *(compare colors) to* σ_2^2*. (E): Relative frequency of correctly detected variance change points in a random change point model for known inhomogeneous rates (light blue) and estimated inhomogeneous rates (dark blue). Rate and variance changes occur randomly with distances uniformly distributed on* $[90, 770]$*. At odd valued change points, the rate, the variance or both parameters change, each with probability one third. The variance changes uniformly from* σ^2 *to one of* $(3\sigma^2, 4\sigma^2, 5\sigma^2)$*, and the rate changes uniformly to one of* $(0.4\mu, 0.8\mu, 1.2\mu, 1.6\mu)$*, switching back to the original parameters* (μ, σ^2) *at even valued change points.* 5000 *simulations per data point.*

Finally the proposed two-step procedure showed high performance in random change point models with multiple rate and variance changes. Figure 5.5 E shows the percentage of correctly detected variance change points for different parameter combinations, where a change point is called *correctly detected* if it is contained in a neighborhood of at most 15 time units of an estimated change point. Figure 5.5 E also shows that the detection probability of variance change points was not strongly affected by the necessity to estimate inhomogeneous rate profiles if estimated rate change points were included in the procedure. The percentage of correctly detected change points in simulations with unknown (dark blue) and known (light blue) inhomogeneous rate profiles were highly comparable. This is because rate changes that fail to be detected are typically too small to considerably affect the second step of estimating variance change points. All simulations were based on i.i.d. Gamma-distributed life times, and similar results were also obtained with lognormally distributed life times (Table 5.1).

	Lognormal		Gamma	
μ/σ	0.05	0.2	0.05	0.2
0.2	88.9%	9.0%	92.0%	33.3%
0.4	90.2%	32.2%	92.6%	51.6%
0.6	87.6%	45.4%	88.5%	61.5%

Table 5.1: Detection probability of variance change points with various life time distributions. *5000 simulations with the random change point model explained in the figure caption of Figure 5.5 E were performed assuming unknown rates. In the first two columns lognormally distributed life times were used and in the last two columns Gamma-distributed life times were used (for the Gamma case numbers are visualized by the dark blue points in Figure 5.5 E).*

In summary, our simulations suggest good performance and practical applicability of the proposed two-step procedure of first detecting rate changes and then incorporating these estimates in the detection of variance change points. The significance level was kept for typical parameter constellations, and the detection probability of variance change points was high even in the presence of multiple rate changes, as often observed in empirical data sets. This allows the analysis of empirical point processes with multiple rate and variance changes as illustrated in Section 6.

Chapter 6

Application to spike train recordings

To illustrate practical application of the proposed method, we analyze 72 empirical spike train recordings of durations between 540 and 900 seconds which were reported partly in Schiemann et al. (2012) and analyzed for rate homogeneity in Messer et al. (2014). As the mean firing rate was about 6 Hz, the window set $H_R := \{25, 50, 75, 100, 125, 150\}$ was used there, and rate change points were estimated with the MFA. Here, we use these estimates of rate change points to analyze changes in the variance of inter spike intervals. In order to ensure about 150 events in the smallest window (see Section 5.2), we chose a window set $H_V = H_R$. The significance level was set to $\alpha = 5\%$.

In 36 out of all 72 spike trains the null hypothesis of variance homogeneity was rejected, and in 22 spike trains more than one variance change point was detected. In 11 cases, different change points were detected by different window sizes. In the mean over all spike trains 0.1 variance change points per minute were detected. To measure the strength of a detected variance change we used the absolute difference of the estimated variances $|\hat{\sigma}_1^2 - \hat{\sigma}_2^2|$ normed with their mean $0.5(\hat{\sigma}_1^2 + \hat{\sigma}_2^2)$. This strength ranged between $0.02 - 1.96$. The detected variance ratios of changes ranged between $1.02 - 94$, where 53.6% were below 2 and even 82.9% below 3. Thus, a majority of detected variance changes showed variance ratios smaller than 3 or even 2, which indicates a high sensitivity of the proposed method also to comparably small variance changes.

Combined with the results of the rate change point detection, both null hypotheses of rate and variance homogeneity were rejected in about 50% of all spike trains (35 out of 72). For 27 spike trains, only rate homogeneity was rejected, in one spike train only variance homogeneity was rejected, and for 9 spike trains, neither null hypothesis was rejected.

Figure 6.1 illustrates two spike train analyses with multiple rate and variance change points in which visual impression corresponds closely with the rate and variance profiles estimated by the algorithm. In the first example the rate only changes slightly while the variance shows six strong changes. In the second example, estimated rate and variance change points occur interestingly close to each other.

These findings stress that spike trains can show highly variable firing patterns, including a number of changes not only in the firing rate but also in the variability of inter spike intervals. Therefore, their detection prior to further analysis is strongly recommended when statistical analyses are sensitive to parameter changes.

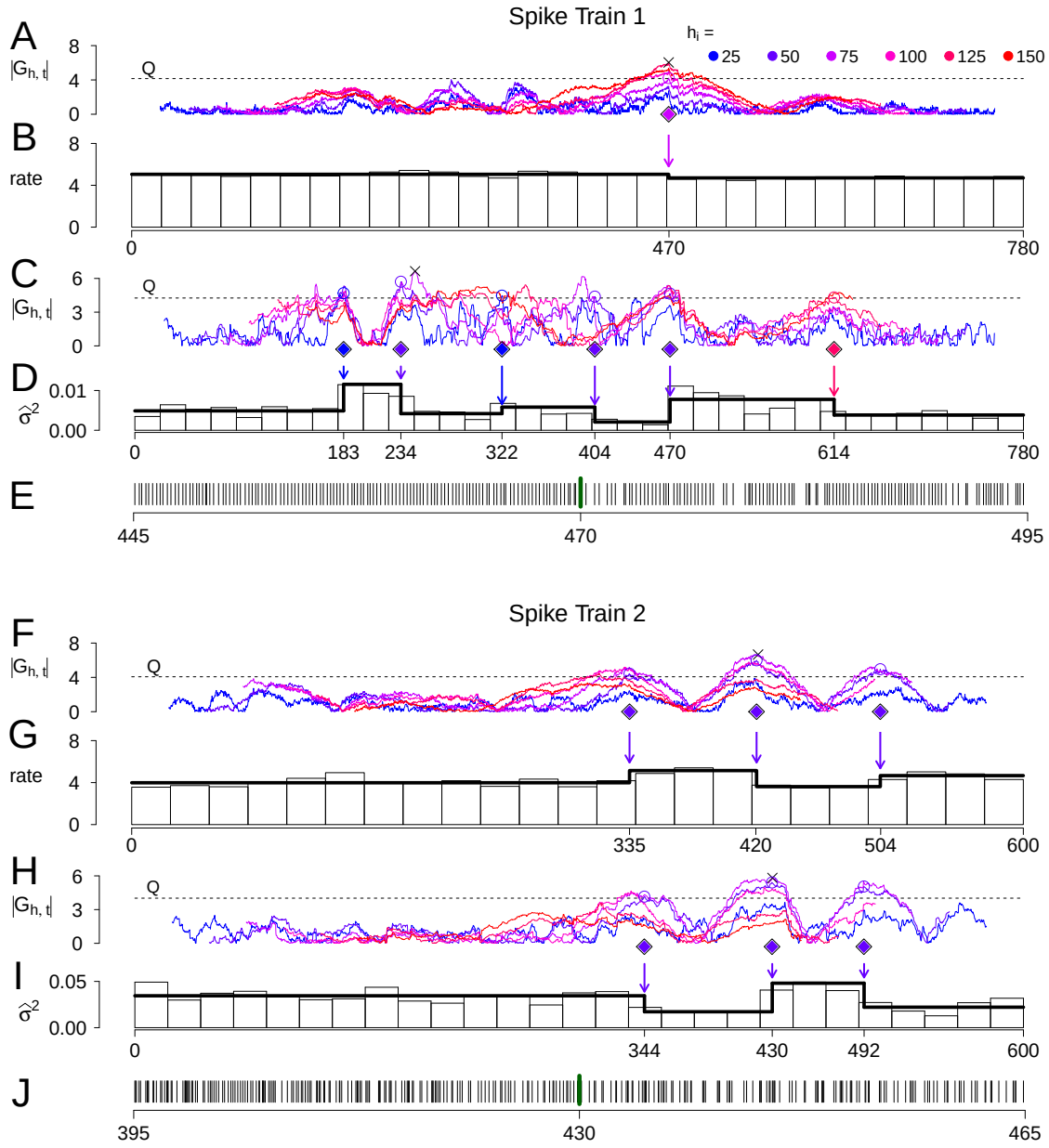

Figure 6.1: Application of the rate and variance MFT to two spike train recordings. *$H_R = H_V = \{25, 50, 75, 100, 125, 150\}$, $\alpha = 5\%$ were used. (A), (C), (F) and (H) The processes $|G|$. The window sizes are color coded (legend on the upper right), and the dashed line indicates the asymptotic rejection threshold Q. Diamonds mark the detected change points. In the first spike train (A-E) one rate and six variance change points are detected with four different windows. In the second spike train (F-J) one window detected three rate and three variance change points. (B) and (G) Rate histograms of the spike trains with estimated rates (black). (D) and (I) Variance histograms with estimated variances. (E) and (J) Parts of the spike trains with marked variance change points (green).*

Chapter 7

Summary and Discussion

This part of the thesis was concerned with our first main goal: the detection of non-stationarities in the rate and the variance of point processes like neuronal spike trains. Therefore, we have extended a multiple filter test (MFT) that has been proposed in Messer et al. (2014) and that aims at testing the null hypothesis of rate stationarity in renewal processes and to detect rate change points on multiple time scales. The rejection threshold of the test is derived from a Gaussian process L, which emerges as the limit of the filtered derivative process G under stationarity and is independent of the point process parameters.
By replacing the number of events in G by the variance of life times, homogeneity of the variance of the life times can be analyzed. When the rate is constant, the MFT extends directly to the null hypothesis of constant variance. In the presence of rate change points, the process G deviates from zero in expectation in the neighborhood of the rate change point if G is not adjusted for the rate change. This may lead to false interpretation of a rate change point as a variance change point. Therefore, we propose an adaptation of the process G that corrects for this deviation by taking into account the rate change. The resulting limit process $\widetilde{L}$ of G vanishes in expectation in the neighborhood of a change point, but its covariance shows slightly different properties from L, and these differences depend on unknown process parameters. The test can be extended to the null hypothesis of constant k-th order moments under the assumption of homogeneity of lower order moments.
In practice, we propose to estimate the rate change points first by procedures that allow for potential variance changes (e.g., the MFT for renewal processes with varying variance, Messer et al., 2014). One can then incorporate these estimates in the statistical test for variance homogeneity. This is important in order to prevent false detection of rate change points as variance change points. As $\widetilde{L}$ depends on unknown process parameters, we use the process L instead to compute asymptotic rejection thresholds. Our simulations suggest that the deviations between the limit processes tend to be small for a wide range of parameter values and that the use of L does in these cases not considerably change the properties of the statistical test. In simulations of point processes with constant variance and random rate change points the asymptotic significance level was kept if the smallest window was chosen sufficiently large. In addition, the simulations suggest that the detection of simulated variance change points – for which the multiple filter algorithm (MFA, Messer et al., 2014) is applied – is hardly affected by the necessity to estimate potential rate change points. For practical applicability, the `R`-package `MFT` (Messer et al. (2017)) contains the procedure for the rates as well as for the variances.

Interestingly, it is conceivable to modify the MFT such that changes in the variances in sequences of independent random variables can be detected. In this case a moving sum type statistic (MOSUM) should compare the scaled variances in two adjacent windows. Under the assumption of constant expectation we suppose the corresponding limit process to be L again (as it has recently been shown for the extension of the rate MFT to the detection of changes in the expectation in sequences of random variables that the limit process is L (Messer et al., 2018), and as variances can be interpreted as means of quadratic deviations from the expectation). Future work may study how the limit process is influenced by change points in the expectation.
Another possible issue for future work is the extension of the multiple filter framework to point process models that capture gradual changes of the rate and/or the variance. In its current form only step functions are estimated by the MFA. Moreover, consistency results for the number and the location of estimated change points would be desirable. Note, however, that proving consistency of argmax type estimators is a challenging task where not many results are known.

In summary, we have extended a statistical test for the null hypothesis of rate homogeneity to the analysis of variance homogeneity in renewal processes with a wide range of life time distributions where the rate is allowed to follow a step function. In addition, an algorithm is described that aims at detecting an unknown number of rate and variance change points that may occur at multiple time scales. When applying the procedure to empirical spike trains, both null hypotheses of constant rate and constant variance were rejected in the majority of cases, and multiple rate and variance change points were estimated. This suggests that the proposed method can be helpful for change point estimation and segmentation of empirical processes such as neuronal spike trains. It can thus be used as a means for signal detection or as a preprocessing step to statistical analyses that are sensitive to rate or variance changes.

As outlined in the introduction, the following second part of the thesis deals with another kind of variability changes arising in point processes in neuroscience. The variability in response patterns to stimulation by an ambiguous stimulus in general and the variability change between response patterns to continuous and intermittent presentation in particular shall be described in one model framework. Therefore, an appropriate model is developed that is fittable to typically short experimental data and that also allows for neuronal correlates.

Part II

A hierarchical stochastic model for bistable perception

Chapter 8

Introduction

Motivation

The phenomenon of bistable perception has fascinated researchers for a long time (Necker, 1832; von Helmholtz, 1866; Levelt, 1965). Recently, the description of response patterns to bistable stimuli such as the Necker Cube, Rubin's vase or rotating spheres with switching rotation direction gained increasing interest in computational neuroscience (Leopold and Logothetis, 1999; Hohwy et al., 2008; Sterzer et al., 2009; Braun and Mattia, 2010; Weilnhammer et al., 2017). By modeling dynamic changes of perception during viewing of one and the same stimulus, one aims at providing potential explanations for neuronal mechanisms underlying perception and perceptual changes and to identify related brain areas as well as potential dysfunctions, e.g. in schizophrenia (Schmack et al., 2013, 2015).

Interestingly, the response patterns to continuously shown bistable stimuli often share common properties (Braun and Mattia, 2010; Brascamp et al., 2015). Typically, the distribution of intervals of constant perception (termed dominance times) is unimodal and right-skewed, and extremely short dominance times, i.e., rapidly fluctuating precepts, are rare (Levelt, 1967; Moreno-Bote et al., 2007; Brascamp et al., 2009). The dominance times under continuous stimulation are therefore often modeled as Gamma-distributed (Leopold et al., 2002; Murata et al., 2003; Wilson, 2007; Gigante et al., 2009; Gershman et al., 2012; Pastukhov et al., 2013). The mean of dominance times can be highly variable across subjects (Brascamp et al., 2009; Pastukhov et al., 2013), whereas the coefficient of variation (CV) is often comparable (Cao et al., 2016). Very long dominance times of more than 100 seconds are rare in this situation. The great majority of dominance times is shorter than half a minute.

In comparison to a continuous presentation, intermittent presentation of a bistable stimulus, i.e., by repetitive interruption of stimulation for short time periods, has been observed to stabilize the percept if the interruption period is long enough, typically longer than 0.7 seconds (Orbach et al., 1963; Leopold et al., 2002; Maier et al., 2003; Kornmeier and Bach, 2004; Gigante et al., 2009; Pastukhov and Braun, 2013). In this case, dominance times get longer and can also show a certain degree of periodicity (Brascamp et al., 2009). In addition, such stable phases with long dominance times during intermittent presentation can also interchange with unstable phases of rapid percept changes. Figure 8.1 shows examples of response patterns to continuous and intermittent presentation of a bistable stimulus from the data set reported in Schmack et al. (2015).

Modeling studies with elaborated mathematical models have been proposed that can explain a number of properties of bistable perception like the distribution of dominance times under

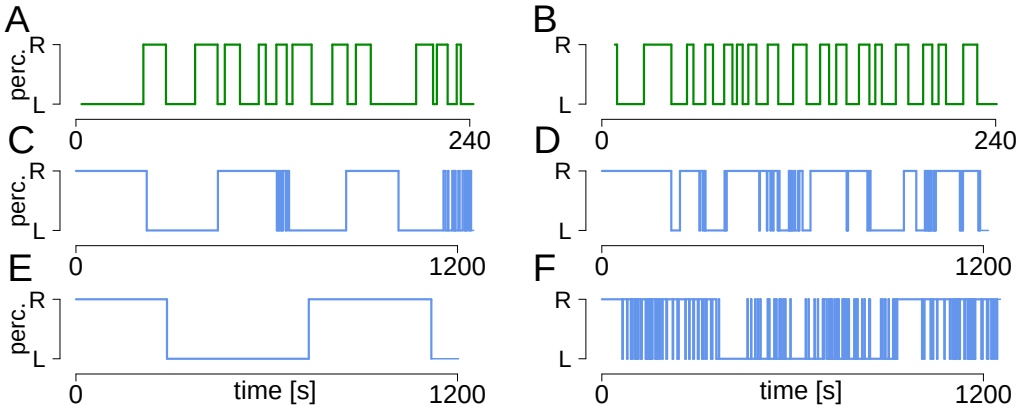

Figure 8.1: Examples of response patterns to a bistable stimulus. Response patterns to continuous (green, A,B) and intermittent (blue, C-F) presentation from the data set reported in Schmack et al. (2015). *While the distribution of dominance times tends to be unimodal in the continuous case, stable and unstable phases seem to interchange in intermittent stimulation. In addition, response patterns can be highly variable across subjects. This is a reprint of Figure 1.3.*

continuous stimulation (Wilson, 2007; Gershman et al., 2012; Pastukhov et al., 2013; Cao et al., 2014, 2016; Weilnhammer et al., 2017) or cyclic behavior and the impact of the duration of the stimulus presentation on the dominance times in intermittent stimulation (Brascamp et al., 2009; Gigante et al., 2009). One key ingredient of these models of bistable perception is typically a competition between neuronal populations that correspond to the different percepts (Laing and Chow, 2002; Wilson, 2007; Brascamp et al., 2009; Gigante et al., 2009; Pastukhov et al., 2013). In order to account for stabilized perception in intermittent viewing, the use of multiple timescales for memory traces of past perception has been proposed by Brascamp et al. (2009) and Gigante et al. (2009).

Many such models require a high number of parameters in order to describe the variety of response patterns. As a consequence, they can often hardly be fitted to experimental data, in particular in the typical cases when only a few dozen dominance times are observed. In addition, the majority of models focus either on continuous or on intermittent viewing. Interesting models that are applicable to both cases have been proposed by Wilson (2007); Brascamp et al. (2009); Gigante et al. (2009).

The relevance of a joint description of continuous and intermittent viewing is illustrated here on a data set including responses of patients with schizophrenia and of healthy controls to continuous and intermittent presentation of a rotating sphere with ambiguous perceived rotation direction reported earlier in Schmack et al. (2013, 2015). In Schmack et al. (2015), an enhanced alternation rate for the group of patients with schizophrenia during intermittent presentation was reported. Interestingly, when we analyzed data recorded in the same participants during continuous presentation, the opposite could be observed (Figure 8.2). Due to the differences in patterns and time scales between continuous and intermittent presentation, the potential neuronal mechanisms underlying the transitions between the different response properties remain unclear.

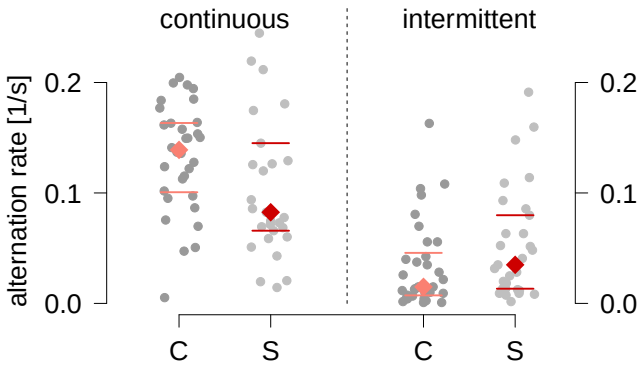

Figure 8.2: Alternation rates in control subjects and subjects with schizophrenia. *During continuous presentation healthy controls (C) in Schmack et al. (2015) showed higher alternation rates compared to patients with schizophrenia (S) (left), while the opposite could be observed for intermittent presentation (right). Each gray dot indicates the perceptual alternation rate from one individual participant, colored diamonds and lines indicate group medians with 25%/75% quantiles. Two-sided Wilcoxon tests yielded $p < .1$ for both continuous and intermittent stimulation.*

Note that strictly speaking, the term "dominance time" refers to slightly different objects in continuous and intermittent viewing. While during continuous presentation, switches occur from a dominant to a suppressed percept (percept-switch), dominance times during intermittent presentation consist of multiple continuous presentation periods, and switches typically occur because of different perceptual choices at the onset of the presentation (percept-choice, Noest et al., 2007). In the present model, the observed sequences of dominance times are treated as conceptually similar. This simplification allows for a parsimonious model description in both continuous and intermittent viewing but may not fully capture the relation between the perceptual processes in the two regimes.

Main goals of Part II

We propose in Part II a new model for the description of response patterns to bistable perception. The main goals of this model and the second part of the thesis are: First, the model should be able to describe the high variety of the response patterns to both continuous and intermittent stimulation within one model framework thereby grasping the change in variability between the presentation types. Second, the observed behavior in continuous and intermittent stimulation should be linked to potential underlying neuronal processes. Third, a minimal number of parameters should be used in order to allow parameter estimation and model fitting to the typically short experimental data. This can then allow the statistical investigation of differences between clinical groups. Especially the increased alternation rate of the control group during continuous presentation in contrast to the schizophrenia group having more perceptual reversals during intermittent presentation should be analyzed (Figure 8.2).

Outline of Part II and mathematical motivation

Part II is organized as follows. In the next section 8.1 the experiment conducted by Schmack et al. (2013, 2015) is illustrated briefly; Section 8.2 then lays out the basic definitions and propositions relevant for this part. To describe the data, we first use a simple Hidden Markov Model (HMM) that describes the observed perceptual processes with a few parameters (Chapter 9) and assumes Gamma or inverse Gaussian (IG) distributed emissions. For continuous presentation, one state produces independent and identically distributed dominance times with a two-parametric distribution (mean μ and standard deviation σ). Parameters can be estimated, for example, via maximum likelihood (Section 9.3). As an original result in this work we derive the exact sampling distribution for small sample sizes of the ML estimator $\hat{\sigma}$ of the inverse Gaussian distribution (Proposition 9.5). For intermittent presentation, switching between stable and unstable phases requires two hidden states with short and long dominance times, respectively. The two-state HMM allows straightforward model fitting by the Baum-Welch algorithm (BWA) (Section 9.4) and data description with a minimal number of parameters (Section 14.1). A Hidden Markov Model with inverse Gaussian distributed emissions has not been described in literature yet. Thus, a mathematical aim of this part is to derive the estimators of the parameters of the inverse Gaussian distribution in the framework of the BWA. The precision of parameter estimates is evaluated in Section 9.6. Theoretical properties of the point process of perceptual reversals generated by the HMM are discussed in Chapter 10 with a focus on the continuous case in Section 10.1 and on the intermittent case in Section 10.2. We investigate the number of changes, first passage times and stationarity properties. In particular, we are interested in the asymptotic probability that the hidden process $\tilde{Y}$ is in the stable state $\lim_{t\to\infty} \mathbb{P}(\tilde{Y}_t = S)$ (which corresponds to the relative time spent in the stable state). A drawback of the HMM is that it remains descriptive and lacks relations to potential underlying mechanisms. Moreover, the empirically observed property that stable dominance times before a state change to the unstable state are shorter than other stable dominance times cannot be explained within the HMM framework (Figure 14.11). Therefore, in Section 11, we link the HMM to a hypothetical underlying stochastic model. This model is termed here Hierarchical Brownian Model (HBM) and intends to describe aggregated underlying neuronal activity, producing the observed behavioral responses.
The HBM is based on two main ideas: First, it assumes that switching between percepts results from two conflicting neuronal populations (compare.,e.g., Gigante et al., 2009). In order to minimize the number of parameters, this process is reduced to a simple Brownian motion P with drift ν_0 that fluctuates between two thresholds $\pm b$, where the first passage times indicate perceptual changes (similar to Cao et al., 2016). With a standard Brownian motion W and the sign of drift S_t the process P can be defined as follows

$$dP_t = S_t \nu_0 dt + dW_t, \quad \text{where} \quad P_0 = -b.$$

For continuous presentation, one therefore requires only two parameters, i.e., the drift of the Brownian motion and the threshold (Chapter 11.1). The distribution of the resulting first passage times – i.e., dominance times – is then the same as in the HMM with IG distributed emissions, with a simple relation between the two HBM and the two HMM parameters. Second, in order to describe intermittent presentation in the same model framework, we use a hierarchical model (Chapter 11.2). The idea is to describe the switching between stable and unstable phases that is typical for intermittent presentation by using an analogous threshold crossing mechanism of conflicting neuronal populations. Specifically, we assume a

second pair of neuronal populations whose corresponding Brownian motion modulates the drift and threshold of the first population pair and thus causes switching between stable and unstable phases. We give a set of model assumptions under which the HBM parameters are comparable to HMM parameters, thus allowing both model fitting to experimental data sets and potential relation to underlying mechanisms. The transition probabilities between the hidden states depend as intended on the length of the current dominance time, which we investigate mathematically in Section 11.2. As shown in Sections 12.1 and 12.2, the parameter estimation is for the dominance times $d_1, \ldots, d_n$ straightforward using maximum likelihood. For continuous presentation we derive the exact sampling distributions of the estimators as original result (Section 12.1.1). For the intermittent presentation the likelihood L is approximately given by $L(d_1, \ldots, d_n) \approx \alpha_S(n) + \alpha_U(n)$, with the forward variable $\alpha_j(i)$ denoting the probability of observing $(d_1, \ldots, d_i)$ and being in state j at time i. The estimation procedure is evaluated in Section 12.4. Another mathematically interesting point is analyzed in Section 12.5: we prove that the well-known Viterbi algorithm (Viterbi, 1967) can be used for classification of dominance times as stable or unstable given the parameter estimates. Again, we investigate theoretical properties of the resulting point process like the number of changes, steady-state distributions or marginal distributions of the involved processes (Chapter 13.1 for the continuous presentation and Chapter 13.2 for the intermittent presentation). Therefore, we are also interested in linking the processes $(Y_i)_i$ and $(\tilde{Y}_t)_t$ (state of the i-th dominance time and state at time t, respectively) to other stochastic processes like semi-Markov processes. As shown in Chapter 14.2, the HBM can reproduce both, the unimodal distribution in the continuous presentation and the bimodal distribution of dominance times in the intermittent presentation, including also various different response patterns. Moreover, it allows the identification of specific differences between the clinical groups in Schmack et al. (2015) and relates these to the hypothesized underlying processes. An outlook about possible model adjustments with a conclusion of Part II is given in Chapter 15.

8.1 Experimental setup

The experimental protocol is presented in detail in Schmack et al. (2013), Schmack et al. (2015), where both studies essentially used the same stimuli. In Schmack et al. (2015) a group of 29 patients with schizophrenia and a group of 32 controls took part and in Schmack et al. (2013) 105 healthy subjects participated in an experiment examinating the perceptual inference of a continuously and intermittently presented ambiguous stimulus.
The stimulus was programed using Matlab (MathWorks Inc.) and the Cogent2000 toolbox (http://www.vislab.ucl.ac.uk/cogent.php) and then shown on a CRT monitor (1024×768 pixels resolution, 60 Hz frame rate). 450 yellow square dots moving coherently on a black background formed the ambiguous stimulus (Figure 8.3), where additionally a white frame square and a central white fixation cross were shown. The structure-from-motion phenomenon causes us to perceive the stimulus as a sphere rotating in depth around a vertical axis (diameter 4.1° of visual angle, rotation speed 1/6 revolutions/s). As the rotation direction is ambiguous, the perception changes every few seconds spontaneously between a left rotating sphere and a right rotating sphere.

During a training session of four minutes, the stimulus was presented continuously (mainly to make participants familiar with the experimental conditions), and each time their perception changed the subjects should indicate that by pressing the button according to their perceived perception ("Left" or "Right"). The data of Schmack et al. (2013) contain for each subject two sessions of continuous presentation.

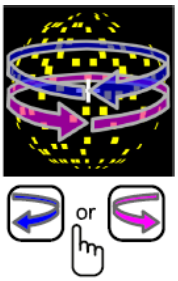

Figure 8.3: Continuous presentation used in Schmack et al. (2013, 2015). *The stimulus was presented continuously, and the subjects should indicate perceptual changes by pressing the corresponding button on a computer keyboard. This figure is taken from Schmack et al. (2015), Figure 1A (Creative Commons license).*

The main experimental session with a duration of about 20 minutes consisted of an intermittent presentation of the ambiguous sphere. The stimulus only was shown for short intervals of 0.6 seconds interleaved by blank screens of 0.8 seconds duration (Figure 8.4). In each presentation phase the participants should indicate their perceived rotation direction by presses on a computer keyboard.

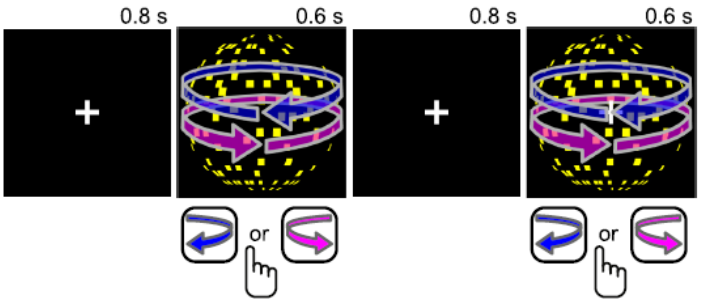

Figure 8.4: Intermittent presentation used in Schmack et al. (2013, 2015). *The stimulus was shown for periods of* 0.6*s followed by blank displays with a length of* 0.8*s. In each presentation period the subjects should press the button on a computer keyboard corresponding to their current perception. This figure is taken from Schmack et al. (2015), Figure 1A (Creative Commons License).*

An important issue one has to consider before analyzing the data are the so-called missings during intermittent presentation: At some stimulus reappearances subjects may not be sure about their perception or may just have missed to press the button. Here, we propose to substitute the missing response by the previous response (compare Schmack et al. (2015)) which is justified by the vast majority of trials where the perceived stimulus configuration

survived from one trial to the next trial. Moreover, it happened that subjects pressed two different buttons during the stimulus reappearance. We treated these cases as additional missing data and substituted them as explained above. The effects of including these responses and not treating them as missing responses are negligible.

8.2 Key concepts and results used throughout Part II

The following section should serve as a "reference work" for Part II of the thesis. We introduce (or recall) different definitions and results which are of major importance in Part II. As many of these definitions and results are used throughout the whole part, we state these concepts in this own section at the beginning of Part II and not as usual before the first occurrence of the corresponding term. We do not claim originality for the results. In Section 8.2.1, we focus on the Brownian motion with drift and related probability distributions thereby also summarizing properties and relations of these distributions. In Section 8.2.2, we discuss properties of point and renewal processes and introduce in Section 8.2.3 alternating renewal processes, regenerative processes and semi-Markov processes which all are related to processes occurring in this work.
First, we recall the convolution of two (probability density) functions f and g which is defined as

$$(f * g)(x) := \int_{-\infty}^{\infty} f(y)g(x-y)dy,$$

and understand for $k > 0$ the k-th convolution of a function f with itself as
$f^{*(k)} := (f * f * \ldots * f)$ with k convolution symbols $*$. Moreover, $f^{*(0)} := f$. Using a sum instead of an integral, the convolution of two discrete probability distributions is defined analogously.
Second, we recall vocabulary about estimators. Given a random sample $X = (X_1, \ldots, X_n)$ depending on a parameter θ and an estimator $\hat{\theta}$ of θ the **bias** of the estimator is defined as $\mathbb{B}\text{ias}(\hat{\theta}) := \mathbb{E}[\hat{\theta}] - \theta$. The estimator θ is called unbiased if its bias is zero. The estimator $\hat{\theta}$ is called **consistent** if

$$\forall \varepsilon > 0 : \mathbb{P}(|\hat{\theta} - \theta| > \varepsilon) \xrightarrow[n\to\infty]{} 0.$$

A sufficient condition for $\hat{\theta}$ to be consistent is that both the bias and the variance of $\hat{\theta}$ vanish asymptotically for $n \to \infty$ (e.g., Theorem 2.1.5 in Lehmann, 1999).
Next, we define the Geometric distribution (to clarify which of its parametrizations is used in this work). Assuming an experiment with independent trials each with success probability p, this distribution describes here the probability that the first success occurs in the k-th trial.

Definition 8.1. ***Geometric distribution***
For $p \in (0, 1)$ and $k \in \{1, 2, 3, \ldots\}$, the Geometric distribution is defined by the probability weights $(1-p)^{k-1}p$.

8.2.1 Brownian motion and some related probability distributions

A key ingredient of the Hierarchical Brownian Model is a Brownian motion with drift.

Definition 8.2. ***Brownian motion with drift***
A real-valued stochastic process $W = (W_t)_{t\in[0,\infty)}$ is called Brownian motion with drift $\nu \in \mathbb{R}$ if it holds

- $W_0 = 0$,
- *W has independent, stationary increments,*
- *W has Gaussian increments $W_{t+u} - W_t \sim N(\nu \cdot u, u)$ and*
- *W has continuous sample paths: $t \to W_t$ is continuous almost surely.*

W is a standard Brownian motion if $\nu = 0$.

The first passage time distribution of a positive border by a Brownian motion with positive drift has been studied since more than 100 years – it was first reported by Schrödinger (1915) – and been given the name **inverse Gaussian distribution** due to its similarity to the Gaussian distribution (Tweedie, 1945). For a historical survey about research related to this distribution, we refer to Chapter 1 in Seshadri (1993) and for a broad overview about application areas to Part II in Seshadri (1999). Here, we first state the definition of the inverse Gaussian distribution and recall results about the first moments. As assumed distribution of dominance times this distribution will be of major importance for the Hidden Markov as well as for the Hierarchical Brownian Model.

Definition 8.3. ***Inverse Gaussian distribution***
The inverse Gaussian (IG) distribution is for the mean parameter $\mu > 0$ and the shape parameter $\lambda > 0$ given by the density

$$f(x) = \begin{cases} \left(\frac{\lambda}{2\pi x^3}\right)^{1/2} \exp\left(\frac{-\lambda(x-\mu)^2}{2\mu^2 x}\right), & \text{if } x > 0, \\ 0, & \text{else.} \end{cases}$$

Proposition 8.4. ***Moments of the IG distribution***
Let X be IG distributed with parameters $\mu, \lambda > 0$. Then it holds

$$\mathbb{E}[X] = \mu, \qquad \mathbb{V}ar(X) = \mu^3/\lambda.$$

Proof: These results are, for example, given by Seshadri (1993). □

Remark 8.5. ***Reparametrization of the IG distribution used in this thesis***
To get a direct overview of the moments of the IG distribution, we use the standard deviation $\sigma = \sqrt{\mu^3/\lambda}$ instead of λ as second parameter when parametrizing the IG distribution in the rest of the thesis: we denote an IG distribution with mean μ and standard deviation σ by $IG(\mu, \sigma)$ with the density $f^{IG}_{\mu,\sigma}$.

Figure 8.5 gives an impression of the behavior of the inverse Gaussian distribution for different values of μ and σ. With μ increasing the peak of the distribution naturally shifts to the right and the density curve gets more and more bell shaped as the variance can be distributed around both sides of μ and not only to the right side as for small μ. This fact also explains why for a large σ the width of the distribution increases with μ.

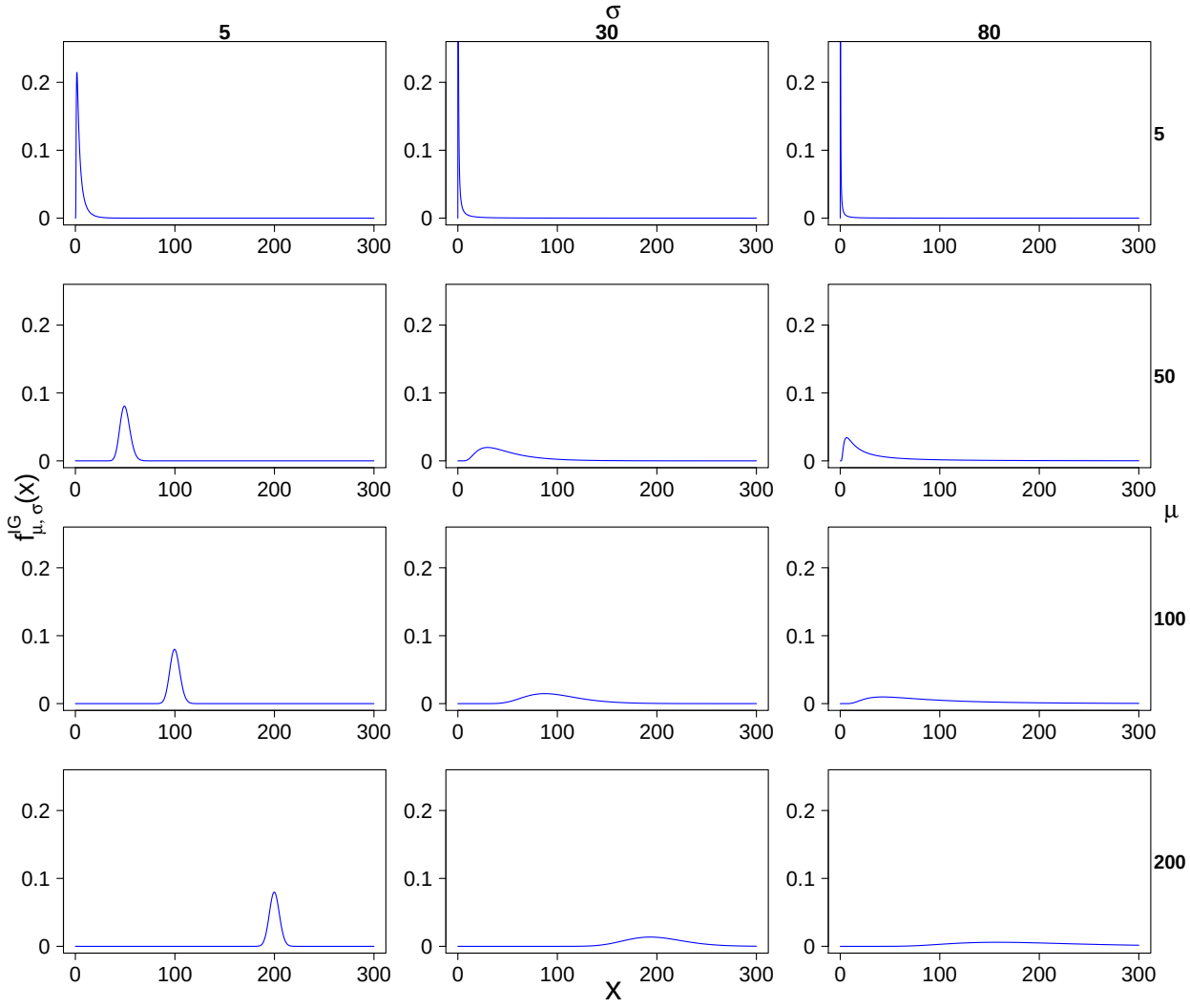

Figure 8.5: Density of the inverse Gaussian distribution $f^{IG}_{\mu,\sigma}(x)$ for different mean μ (rows) and standard deviation σ (columns).

Now we state the relation of the inverse Gaussian distribution to the Brownian motion.

Proposition 8.6. ***Relation of the IG distribution to the Brownian motion***
Let $a > 0$ be a fixed level and $W := (W_t)_{t\geq 0}$ be a Brownian motion with drift $\nu > 0$. Then, the first passage time of a by W is distributed according to an inverse Gaussian random variable T_a:

$$T_a := \inf\{t > 0 : X_t = a\} \sim IG(a/\nu, \sqrt{a/\nu^3}).$$

Proof: Compare, e.g., Seshadri (1993) or Mörters and Peres (2010). □

Further, the inverse Gaussian distribution can be expressed as a member of the exponential family, which we will need to state results about asymptotic normality of estimators later on. Note that the density of members of the exponential family with parameters Θ can be written as

$$f(x|\Theta) = h(x) \exp\left(\eta(\Theta)t(x) - A(\Theta)\right), \tag{8.1}$$

where $h(x), t(x), \eta(\Theta)$ and $A(\Theta)$ are known functions (e.g., Lehmann and Casella, 1998).

Corollary 8.7. ***IG distribution as member of the exponential family***
The $IG(\mu, \sigma)$ distribution is a representative of the exponential family with $\Theta = (\mu, \sigma)$ and

$$h(x) = \frac{1}{\sqrt{2\pi x^3}}, \qquad A(\Theta) = -\frac{1}{2}\log\left(\frac{\mu^3}{\sigma^2}\right) - \frac{\mu^2}{\sigma^2},$$
$$t(x) = \left(x, \frac{1}{x}\right)^T, \qquad \eta(\Theta) = \left(-\frac{\mu}{2\sigma^2}, -\frac{\mu^3}{2\sigma^2}\right).$$

Proof: Follows by rearranging the density of the inverse Gaussian distribution. □

Connection of the IG distribution to the Gamma distribution As we use both – the Gamma and the IG distribution – to model dominance times, we are interested in properties these two probability distributions share. The IG and the Gamma distribution are both special cases of the generalized inverse Gaussian distribution (Johnson et al., 1994) which cannot be converted into each other. However, in particular for a small CV$= \sigma/\mu$ the densities of the Gamma and the IG distributions are difficult to distinguish per eye (panels A and D in Figure 8.6). With an increasing CV the differences between the two densities tend to be more obvious, where the behavior for a small and large μ is comparable (compare A-C with D-F).

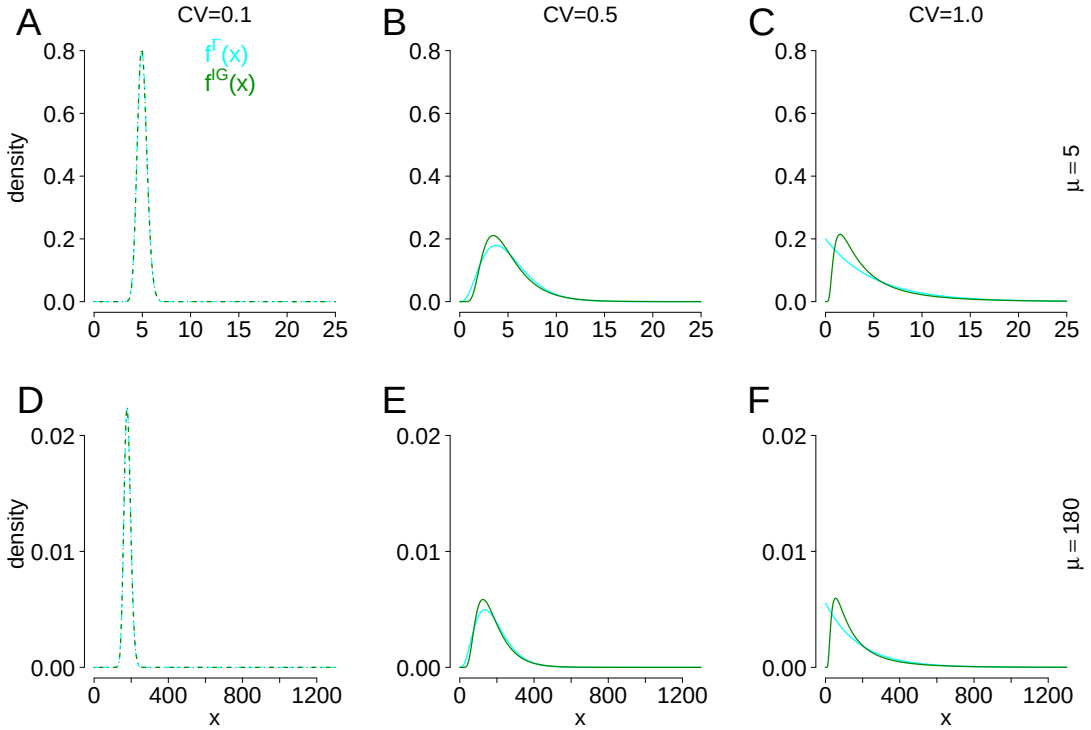

Figure 8.6: Comparison between the densities of the IG (green) and the Gamma (cyan) distribution. *The mean is $\mu = 5$ (A-C) and $\mu = 180$ (D-F). The CV is 0.1 (A,D), 0.5 (B,E) and 1 (C,F). In A and D the lines are not drawn continuously as otherwise only one density would be visible.*

Reciprocal inverse Gaussian distribution To derive results about the exact and asymptotic distribution of estimators of parameters of the IG distribution, we require the reciprocal of the IG distribution. If X is $\text{IG}(\mu, \sigma)$ distributed, the distribution of $1/X$ is called **reciprocal inverse Gaussian** (RIG) with parameters μ and σ (Seshadri, 1993). We state its density and expectation in the next proposition. These are given in Proposition 2.18 and Table 2.4 of Seshadri (1993), respectively.

Proposition 8.8. ***Density and expectation of the RIG distribution***
Let X be IG(μ, σ)-distributed. The density of $1/X$ is given by

$$f(x) = f^{IG}_{1/\mu, \mu/\sigma^2} * f^{\Gamma}_{\mu^3/(4\sigma^2), \mu^6/(8\sigma^4)}(x), \text{ if } x > 0,$$

and 0 otherwise. The sign $*$ denotes the convolution of the inverse Gaussian and the Gamma density. The expected value of $1/X$ is

$$\mathbb{E}\left[\frac{1}{X}\right] = \frac{1}{\mu} + \frac{\sigma^2}{\mu^3}.$$

Normal-inverse Gaussian distribution In the context of the HBM, the position of a Brownian motion with drift at a point in time determined by a normal distributed random variable is important to derive transition probabilities between hidden states. The distribution of this position is given by the **normal-inverse Gaussian distribution** (NIG) as is stated in Corollary 8.10. First, we introduce this distribution, which is a special case of the generalized hyperbolic distributions (Barndorff-Nielsen, 1978). The NIG distribution has four parameters and is fittable to a wide range of data including fat tails and skewness. Its application area mainly is in finance, e.g., for stochastic volatility modeling (Barndorff-Nielsen, 1997). Second, Corollary 8.10 is shown.

Definition 8.9. ***Normal-inverse Gaussian distribution***
Let Y be an IG$\left(\frac{\delta}{\sqrt{\alpha^2-\beta^2}}, \frac{\sqrt{\delta}}{(\alpha^2-\beta^2)^{3/4}}\right)$-distributed random variable. A random variable X follows the normal-inverse Gaussian (NIG) distribution with parameters $\xi, \alpha, \beta, \delta$ if

$$X|Y = y \sim N(\xi + \beta y, y),$$

where the parameters satisfy the conditions $\alpha \geq |\beta|$ and $\delta \geq 0$.
The density of a NIG($\xi, \alpha, \beta, \delta$)-distributed random variable is given by

$$f(x) = \frac{\alpha\delta}{\pi} \exp\left(\delta\sqrt{\alpha^2-\beta^2} + \beta(x-\xi)\right) \frac{K_1\left(\alpha\sqrt{\delta^2+(x-\xi)^2}\right)}{\sqrt{\delta^2+(x-\xi)^2}},$$

with $K_1(x) := \frac{1}{2}\int_0^\infty \exp\left(-\frac{1}{2}x\left(t+t^{-1}\right)\right) dt$ as the modified Bessel function of the third kind and order 1 (e.g., Watson, 1995). We term the density in this thesis as $\Psi_{\xi,\alpha,\beta,\delta}(x)$.

Corollary 8.10. ***Relation of the NIG distribution to the Brownian motion***
Let $(Y_t)_{t\geq 0}$ be a Brownian motion with drift $\nu_Y > 0$ and starting position $Y_0 = 0$. Moreover, $b_Y > 0$ is a border. Let $(X_t)_{t\geq 0}$ be another Brownian motion independent of $(Y_t)_{t\geq 0}$ with drift $\nu_X > 0$ and $X_0 = 0$. Define $T := \inf\{t \geq 0 : Y_t = b_Y\}$. It holds

$$X_T \sim NIG(0, \sqrt{\nu_X^2 + \nu_Y^2}, \nu_X, b_Y).$$

Proof: Due to Proposition 8.6, T is IG distributed with parameters b_Y/ν_Y and $\sqrt{b_Y/\nu_Y^3}$. Reparameterizing this in terms of $\xi, \alpha, \beta, \delta$ of Definition 8.9 yields the following equations

(I) $\delta/(\alpha^2 - \beta^2)^{1/2} = b_Y/\nu_Y$,
(II) $\delta/(\alpha^2 - \beta^2)^{3/2} = b_Y/\nu_Y^3$,
(III) $\beta = \nu_X$.

As X starts in 0, it holds $\xi = 0$. By (III) we directly have $\beta = \nu_X$. Dividing (I) by (II) yields $\nu_Y^2 = \alpha^2 - \beta^2$ (IV). Plugging this in (I) we obtain $\delta = b_Y$. Plugging (III) in (IV) we moreover obtain $\alpha = \sqrt{\nu_X^2 + \nu_Y^2}$. □

In the thesis the normal-inverse Gaussian distribution generally emerges from its relation to the Brownian motion. Hence, the parameter ξ vanishes, and for simplification we term for each $x \in \mathbb{R}$: $\Psi_{\alpha,\beta,\delta}(x) := \Psi_{0,\alpha,\beta,\delta}(x)$ unless stated otherwise.

8.2.2 More about point/renewal processes

The times of perceptual reversals $(t_1, t_2, \ldots, t_n)$ may be interpreted as a sequence of occurrence times of events being recorded over a finite interval $[0, T], T \in (0, \infty)$ and not happening at the same time. Therefore, a response pattern can be described by a realization of a point process on the real line and in certain cases also as renewal process. This allows, for example, the derivation of the expected relative time spent in the stable state which is very important when analyzing group differences. Note that we term the life times in this second part of the thesis D_i (or d_i for their realizations) instead of ξ_i due to the interpretation as dominance time. As we analyze residual times as well as stationarity properties in Chapters 10 and 13, we state the corresponding definitions and properties in the following.
Ross (1996) gives the following important results (Prop. 3.4.5, 3.4.6) for renewal processes (recall Definition 2.5).

Definition 8.11. ***Age and residual time of a renewal process***
*The **age** A_t of a renewal process at time $t > 0$ is defined as $A_t := t - S_{N_t}$ and the remaining or **residual** time R_t at $t > 0$ as $R_t := S_{N_{t+1}} - t$.*

Proposition 8.12. ***Asymptotic distribution of A_t and R_t***
For a renewal process with non-lattice distribution F of the life times D (i.e., $\nexists m : \sum_{n=0}^{\infty} \mathbb{P}(D = nm) = 1$) with mean $\mu < \infty$, the distribution of the random variable H_∞^D describing the asymptotic distribution of A_t and R_t is given by

$$\mathbb{P}(H_\infty^D < x) := \lim_{t\to\infty} \mathbb{P}(A_t \leq x) = \lim_{t\to\infty} \mathbb{P}(R_t \leq x) = \frac{1}{\mu} \int_0^t (1 - F(y))dy.$$

For the density it follows

$$f_{H_\infty^D}(x) = \frac{1}{\mu}(1 - F(x)).$$

Moreover, if $\mathbb{E}[D^2] < \infty$,

$$\mathbb{E}[H_\infty^D] = \lim_{t\to\infty} \mathbb{E}[A_t] = \lim_{t\to\infty} \mathbb{E}[R_t] = \frac{\mathbb{E}[D^2]}{2\mu}.$$

In this thesis, we let $R \sim H_\infty^D$ be the random variable describing the asymptotic residual time for the random variable D. Note that we skip the index t for convenience.
Now, we define renewal equations, which describe many quantities of interest when studying renewal processes (as, e.g., in Chapters 10 and 13). For the following compare, e.g, Serfozo (2009).

Definition 8.13. ***Renewal equation***
The renewal equation for a real-valued function $h(t)$ on $\mathbb{R}$, which is bounded on finite intervals and equals 0 for $t < 0$, and a distribution function F is given by

$$H(t) = h(t) + \int_{[0,t]} H(t - s)dF(s), t \geq 0,$$

with $H(t)$ as real-valued function. In short, $H = h + F * H$. A function $H(t)$ is a ***solution*** *of this equation if it is bounded on finite intervals, equals 0 for $t < 0$ and satisfies the equation.*

Renewal equations have a unique solution albeit this solution is only in special cases simple enough for computations.

We state the definition of a weaker form of stationarity (Daley and Vere-Jones, 1988) which is used to describe stationarity properties of the process of perceptual changes.

Definition 8.14. ***Crude stationarity***
A point process Ξ is crudely stationary when

$$\mathbb{P}(\textit{number of events of } \Xi \textit{ in } (t,t+h) = k), \quad h > 0, k = 0, 1, \ldots$$

depends only on the length h and not the location $t \in \mathbb{R}$.

8.2.3 Three types of stochastic processes

As we aim to embed different processes evolving in this work into the world of stochastic processes, we introduce here three important examples of stochastic processes without defining them in detail.

8.2.3.1 Alternating renewal process

Alternating renewal processes typically model systems which alternate between two states A and B, e.g., working and failure times of technical components (e.g., Medhi, 2009). Another interpretation is that the system switches between the ON and the OFF state. Mathematically, we assume $D_A := (D_{A,1}, D_{A,2}, \ldots)$ as the random variables describing the successive durations of state A and $D_B := (D_{B,1}, D_{B,2}, \ldots)$ as the (random) successive lengths of time the system is in state B. Thus starting in A, the system remains there for a duration of $D_{A,1}$ followed by a period of state B with length $D_{B,1}$, followed by a period of state A with length $D_{A,2}$ and so on. The key assumption is that D_A and D_B are two independent sequences of i.i.d. random variables. Then, $((D_{A,1}, D_{B,1}), (D_{A,2}, D_{B,2}), \ldots)$ is called alternating renewal process (e.g., Beichelt and Fatti, 2001). Figure 8.7 illustrates an alternating renewal process where state A produces long intervals (light blue) and state B produces short intervals (blue). The return times to state A can be interpreted as a renewal process with life times $D_{A,i} + D_{B,i}$ for $i \geq 1$.

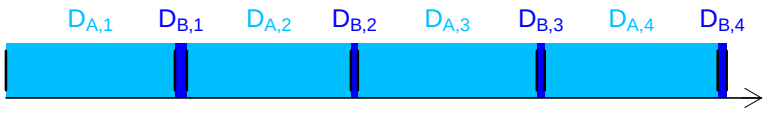

Figure 8.7: Illustration of the intervals $(D_{A,i}, D_{B,i})_{i\geq 1}$ of an alternating renewal process. *Long intervals of state A (light blue) interchange with short intervals of state B (blue). Given the state the intervals are independent and identically distributed.*

8.2.3.2 Regenerative process

Alternating renewal processes are an example of regenerative processes. A stochastic process $(X_t)_{t\geq 0}$ with a discrete state space is called regenerative if there exist points in time where the process probabilistically starts anew with the same probability distribution (compare, e.g., Chapter 3.7 in Ross, 1996). Thus, there exist times $\tilde{T}_1, \tilde{T}_2, \ldots$ where the continuation of the process beyond these points is a probabilistic replication of the whole process started at 0. The sequence $(\tilde{T}_i)_{i\geq 1}$ then describes a renewal process with life times $(\tilde{D}_i)_{i\geq 1}$. In an alternating renewal process the $(\tilde{T}_i)_{i\geq 1}$ are simply the points in time where a new interval of state A is drawn.
For any state j of a regenerative process it can be shown (Theorem 3.7.1 in Ross, 1996) that

$$\lim_{t\to\infty} \mathbb{P}(X_t = j) = \frac{\mathbb{E}[\text{amount of time in state j during } \tilde{D}_1]}{\mathbb{E}[\tilde{D}_1]}. \tag{8.2}$$

Moreover, Ross (1996) shows in Theorem 3.7.2 that it holds almost surely

$$\lim_{t\to\infty} \frac{\text{amount of time in state j during } (0,t)}{t} = \frac{\mathbb{E}[\text{amount of time in state j during } \tilde{D}_1]}{\mathbb{E}[\tilde{D}_1]}. \tag{8.3}$$

As can be seen directly from equations (8.2) and (8.3), the asymptotic probability that the process is in state j equals almost surely the long term relative time spent in this state.

8.2.3.3 Semi-Markov process

A stochastic process with discrete state space where state changes are caused by a Markov chain (i.e., depend only on the current state) and the time interval between two successive transitions is a random variable with an arbitrary distribution which may depend on the state before as well as on the state after the transition is called semi-Markov process (Lévy, 1954; Smith, 1955). In case of exponentially distributed inter transition times the process is a Markov process. The tuple of state and transition time is known as Markov renewal process (Pyke, 1961). Our formal definition of a Markov renewal process and a semi-Markov process follows Medhi (2009).

Definition 8.15. ***Markov renewal process and semi-Markov process***
Let $0 = t_1 < t_2 < t_3 < \dots$ denote the transition times of a stochastic process with discrete state space (where transitions between the same state are allowed) and Z_i be the i-th state. If

$$\mathbb{P}(Z_{i+1} = k, t_{i+1} - t_i \leq t | Z_i = z_i, \dots, Z_1 = z_1, t_i, \dots, t_1) = \mathbb{P}(Z_{i+1} = k, t_{i+1} - t_i \leq t | Z_i = z_i),$$

for all states k and all $i \geq 1$, then the tuple $(Z_i, t_i)_{i \geq 1}$ constitutes a ***Markov renewal process****. In case of time homogeneity the* ***semi-Markov kernel*** *of the Markov renewal process is the matrix $Q(t) = (Q_{jk}(t))$ where*

$$Q_{jk}(t) := \mathbb{P}(Z_{i+1} = k, t_{i+1} - t_i \leq t | Z_i = j).$$

for the states j and k and $t \geq 0$.
The continuous parameter process

$$(\tilde{Z}_t)_{t \geq 0} = Z_i \text{ on } t_i \leq t < t_{i+1}$$

is called ***semi-Markov process*** *with the embedded Markov chain $(Z_i)_{i \geq 1}$. The* ***conditional sojourn time*** *in state j given the next transition is to state k has the distribution function*

$$S_{jk}(t) := \mathbb{P}(t_{i+1} - t_i \leq t | Z_{i+1} = k, Z_i = j).$$

Chapter 9

A Hidden Markov Model

In the introduction (Chapter 8), we explained that a key characteristic of the dominance times resulting from continuous presentation of the ambiguous stimulus is the unimodal distribution, whereas dominance times in response to intermittent presentation are often better described by a bimodal distribution (with long stable and short unstable dominance times). In Figure 9.1 we present again six examples. Figure 9.2 shows the corresponding dominance time histograms pointing out the uni- or bimodality of the distributions, depending on the mode of stimulus presentation. All response patterns recorded in Schmack et al. (2015) can be found in Appendix A showing a high inter-individual variability. Our first main goal in this part is to develop one model for both – continuous and intermittent presentation – that captures these observations. Recall also that another main goal of Part II is that the model should only have a small number of parameters such that it is fittable to short pieces of data allowing, e.g., to refine the group differences between the patients and control group (Figure 8.2). Therefore, a simple descriptive approach to model the dominance time data is a Hidden Markov Model (HMM) with one state for the continuous presentation and two states (stable and unstable) for intermittent presentation of the stimulus. This is the first time that a HMM is applied to describe dominance times resulting from bistable perception experiments.

In the following we first establish fundamentals about Markov Chains (Section 9.1), then introduce Hidden Markov Models (Section 9.2) before focusing on the parameter estimation. We discuss two different distributions widely used in literature to describe the dominance times during bistable perception: the Gamma distribution (Fox and Herman, 1967; Levelt, 1967; Murata et al., 2003; Brascamp et al., 2005; Gershman et al., 2012) and the inverse Gaussian distribution (Cao et al., 2016). For both, we discuss the fitting for the data of continuous presentation (Section 9.3), where we examine extensively properties of the maximum likelihood (ML) estimators for the IG distribution and also present newly derived UMVU estimators (uniformly minimum-variance unbiased estimators, Section 9.3.1). To fit the HMM to the data recorded during intermittent presentation we explain the Baum-Welch algorithm (BWA) focusing in particular on its fitting to the inverse Gaussian and the Gamma distribution (Section 9.4). The estimated HMM parameters of the six example response patterns from Figure 9.1 are given in Section 9.5. A section about empirical results concerning the estimation precision of our ML estimators completes the chapter (Section 9.6).

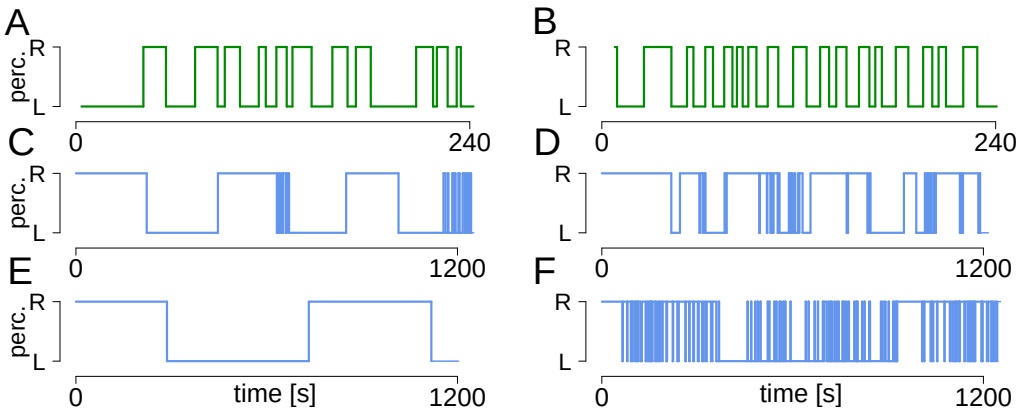

Figure 9.1: Examples of response patterns to a bistable stimulus. Response patterns to continuous (green, A,B) and intermittent (blue, C-F) presentation from the data set reported in Schmack et al. (2015). *While the distribution of dominance times tends to be unimodal in the continuous case, stable and unstable phases seem to interchange in intermittent stimulation. In addition, response patterns can be highly variable across subjects. This is reprint of Figure 1.3.*

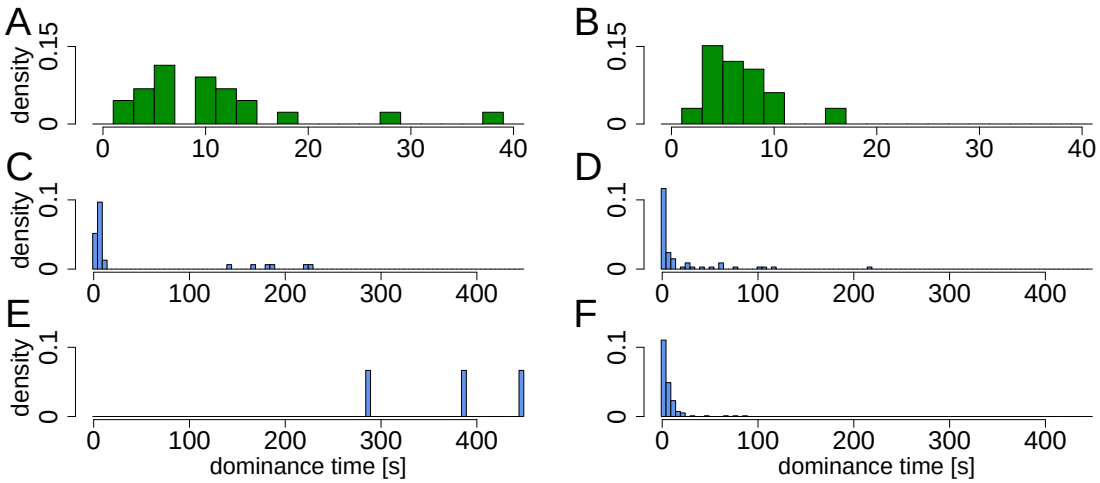

Figure 9.2: Histograms of dominance times during continuous (green, A,B) and intermittent (blue, C-F) presentation from the data set reported in Schmack et al. (2015). *The corresponding response patterns are printed above in Figure 9.1. The number of long dominance times in panels C, D and F is small compared to the number of short dominance times such that the long dominance times are difficult to identify in these histograms.*

9.1 Fundamentals: Markov chains

Here, we give a rough overview about the theory of Markov chains focusing on the properties that are essential for the construction of the Hidden Markov Models used in this thesis. For a detailed description of Markov chains see, e.g., Norris (1998); Grimmett and Stirzaker (2001). Assume a (discrete) state space S and a (discrete-time) stochastic process Y taking values in this space. The process Y is called **Markov chain** if given the current state of the process Y_i , the future Y_{i+1} is independent of the past $Y_{i-1}, Y_{i-2}, \dots Y_1$. This so-called **Markov property** is for a sequence of observations $y_1, y_2, \dots, y_n$ formalized as follows: for all $i \in \{1, 2, \dots\}$ it holds

$$\mathbb{P}(Y_{i+1} = y_{i+1}|Y_i = y_i, Y_{i-1} = y_{i-1}, \dots, Y_1 = y_1) = \mathbb{P}(Y_{i+1} = y_{i+1}|Y_i = y_i). \tag{9.1}$$

An important class of Markov chains are the homogeneous Markov chains with time-independent stationary transition probabilities $p_{jk} := \mathbb{P}(Y_{i+1} = k|Y_i = j) \forall j, k \in S$. In case of a homogeneous K-state Markov chain the transition probabilities are summarized in the $K \times K$ transition probability matrix P with

$$P := \begin{pmatrix} p_{11} & \dots & \dots & p_{1K} \\ \vdots & \ddots & & \vdots \\ \vdots & & \ddots & \vdots \\ p_{K1} & \dots & \dots & p_{KK} \end{pmatrix}$$

and $\sum_{k=1}^{K} p_{jk} = 1$ for all $j \in \{1, \dots, K\}$.
The long-term behavior of a homogeneous Markov chain is determined by the m-step transition probabilities $p_{jk}(m) := \mathbb{P}(Y_{i+m} = k|Y_i = j)$ (in contrast to the one-step transition probabilities given by P). The matrix $P(m)$ which contains the m-step transition probabilities can be calculated as the m-th power of P (e.g., Grimmett and Stirzaker, 2001).
π_{start} describes the probability distribution of the initial state. Using this initial distribution, the distribution of the state at time m may be computed as

$$(\mathbb{P}(Y_m = 1), \mathbb{P}(Y_m = 2), \dots, \mathbb{P}(Y_m = K)) = \pi_{\text{start}} P^{m-1}.$$

$\pi_{\text{start}} P^{m-1}$ converges to a fixed vector (which we term π) if the Markov chain is homogeneous and irreducible, i.e., all states are accessible from each other state (e.g., Norris, 1998). This so-called **stationary distribution** π can be determined by solving

$$\pi = \pi P \text{ subject to } \pi \mathbb{1}^T = 1.$$

A proof can be found in Seneta (1981).

9.2 The model

In this section, we give a brief introduction to HMMs and their basic properties. In a HMM the hidden state of an underlying Markov chain determines the distribution that generates an observation. This framework provides flexible models for univariate and multivariate time series such as discrete or continuous valued series or categorical series. Hidden Markov Models

are widely used, e.g, for temporal pattern recognition such as speech, gesture or handwriting recognition (e.g., Rabiner, 1989; Wilson and Bobick, 1999). Other fields of application involve computational linguistics (Och and Ney, 2003), bioinformatics (Yoon, 2009), finance (Rydén et al., 1998) or robotics (Fox et al., 2005). For further reading, see, e.g., Elliott et al. (1995); MacDonald and Zucchini (1997) or Ephraim and Merhav (2002). In the following, we also discuss parameter interpretation.

9.2.1 Definition

We define the HMM formally. The sequence of observations is denoted by $d := (d_i)_{i\in\{1,2,\dots,n\}}$ modeled as realizations of random variables $D := (D_i)_{i\in\{1,2,\dots,n\}}$. Furthermore, $y := (y_i)_{i\in\{1,2,\dots,n\}}$ describes the realization of a Markov chain $Y := (Y_i)_{i\in\{1,2,\dots,n\}}$ on the state space $\{1,\dots,K\}$ with initial distribution $\pi_{\text{start}} = (\pi_{\text{start},1}, \pi_{\text{start},2}, \dots, \pi_{\text{start},K})$. To ease notation, we write $d_{i_0}^{i_1} := \{d_{i_0},\dots,d_{i_1}\}$ where $i_0 < i_1$ and similarly for $D_{i_0}^{i_1}, y_{i_0}^{i_1}, Y_{i_0}^{i_1}$.

Definition 9.1. ***Hidden Markov Model***
Let Y be an underlying discrete-time hidden process fulfilling the Markov property (9.1) and D be a state-dependent observation process for which the conditional independence property

$$\mathbb{P}(D_i = d_i | D_1^{i-1} = d_1^{i-1}, Y_1^i = y_1^i) = \mathbb{P}(D_i = d_i | Y_i = y_i) \tag{9.2}$$

holds for all $1 \le i \le n$.
The pair of stochastic processes $(Y_i, D_i)_{1\le i\le n}$ is called Hidden Markov Model.

Equation (9.2) means that, if Y_i is known, D_i depends only on this current state and not on any previous states or observations. The probabilities for the state Y_{i+1} depend only on the previous state Y_i. A visualization of a HMM is given in Figure 9.3.

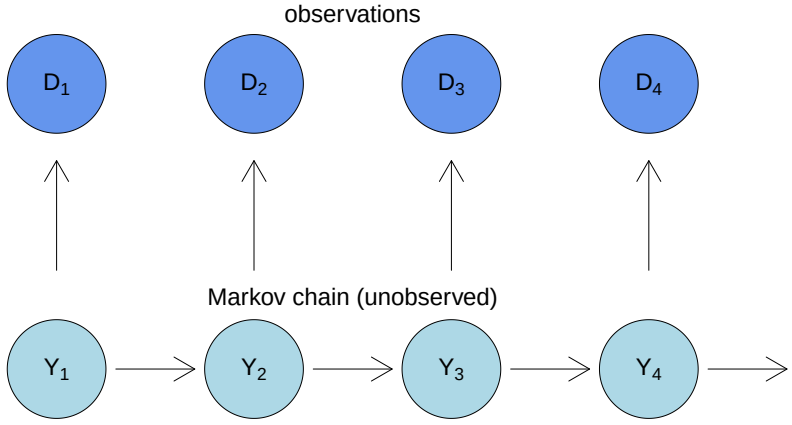

Figure 9.3: Basic structure of a Hidden Markov Model. *The unobserved/hidden Markov chain Y determines the density of the visible observation D_i at time $i \in \mathbb{N}$.*

Here, we intend to model response data from bistable perception experiments. We reduce data analysis to the dominance times $(d_i)_{i\in1,2,\dots,n}$, i.e., the times between reported changes of a percept. In the unimodal continuous case, we assume the d_i to be the realizations of i.i.d. distributed random variables $(D_i)_{i\in1,2,\dots,n}$(Figure 9.4 A), where the Gamma or the inverse Gaussian distribution are suitable two-parametric distributions (Wilson, 2007; Gigante et al., 2009; Gershman et al., 2012; Cao et al., 2016). This framework may also be interpreted as one-state HMM. For the intermittent case, the observed dominance times are modeled as the outcomes of a two-state Hidden Markov Model with a Markov chain Y on $\{S, U\}$ and continuous observations. In the stable state S long dominance times are emitted, and in the unstable state U perception changes quickly. To describe the dominance time distribution in S, we use an inverse Gaussian or a Gamma distribution which allows us to fit the mean μ_S of the dominance duration as well as its standard deviation σ_S. The unstable states are modeled either by another inverse Gaussian distribution with mean μ_U and standard deviation σ_U or – in the case of Gamma-distributed dominance times in S – by an Exponential distribution with parameter $1/\mu_U$. Furthermore, we denote the transition probabilities between S and U by $p_{SU} = 1 - p_{SS}$ and between U and S by $p_{US} = 1 - p_{UU}$, respectively (see Figure 9.4). We assume that not both of p_{SS} and p_{UU} equal one.

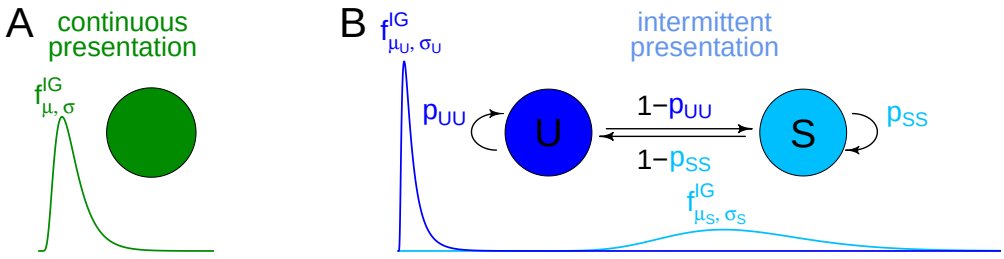

Figure 9.4: A simple HMM for bistable perception producing inverse Gaussian distributed dominance times. *(A) One state describes a unimodal distribution of dominance times under continuous presentation. (B) Two states (stable, S, and unstable, U) produce long and short dominance times under intermittent presentation.*

Note that independence of dominance times is assumed here in continuous presentation. This assumption enables straightforward parameter estimation (Section 9.3) and is in agreement with the observation that serial correlations of dominance times are typically not reported (e.g., Walker, 1975; Lehky, 1995). However, weak long-term dependencies of dominance times reported under continuous presentation (Pastukhov and Braun, 2011) cannot be reproduced in the HMM. As such long-term dependence was not observed in the majority of cases in the present data set, also showing no group differences (Section 14), we use here the simple assumption of independence.

9.2.2 Discussion of model parameters

We discuss how the different parameters of the HMM influence the visible response pattern. The interpretations are trivial for the one-state HMM describing the response patterns to continuous presentation: A larger mean μ increases stability, and a larger standard deviation σ increases irregularity.

We turn to the two-state HMM for intermittent stimulation. It is obvious that increasing μ_S increases the length of stable dominance times and increasing σ_S increases the variance of stable dominance times. Similar arguments hold for increasing μ_U, σ_U. Increasing the probabilities p_{SS} or p_{UU} implies that a state transition gets less likely. In case of a rather small difference between μ_S and μ_U or a large variance of at least one of the two distributions the stable and unstable distributions of dominance times are not separated clearly. This is visualized in Figure 9.5.

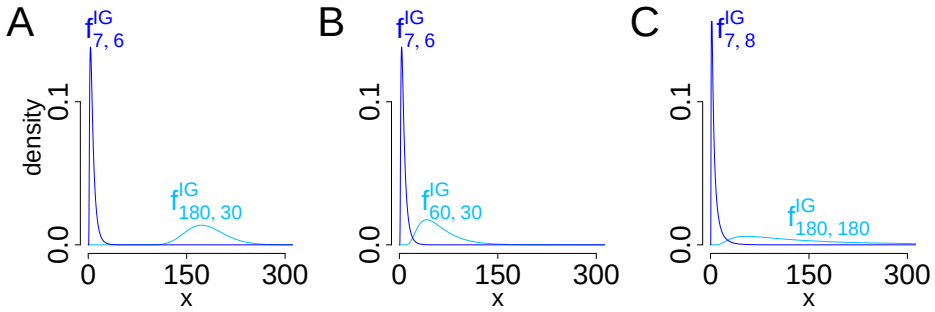

Figure 9.5: Comparison of densities in the stable (light blue) and the unstable (blue) state. *The parameters are indicated in the graph. In panel A the stable and unstable distribution are strictly separated, whereas in B a small μ_S and in C a large σ_S and large σ_U cause a stronger mixing of the distributions.*

Visually one may use criteria like regularity (Are the lengths of stable dominance times widespread?) and stability (Which types of dominance times occur? Long and/or short ones?) to distinguish between different response patterns. In the HMM the parameters p_{SS} and μ_S answer the question how stable the response pattern is. $p_{SS} = 1$ (together with $\pi_{\text{start},S} = 1$) indicates that only stable dominance times occur. In contrast, a small p_{SS} or a small mean of stable dominance times μ_S are an indicator of a response pattern with rather short dominance times. The regularity is judged by the coefficient of variation $\text{CV}_S = \sigma_S/\mu_S$ of the stable dominance times. A large CV_S implies irregular distributed stable dominance times (which are mainly responsible for the visual impression of regularity), whereas a small CV_S is typical for more regular response patterns.
Figure 9.6 illustrates the impact of different two-state HMM parameters on the response patterns. In panel E a stable response pattern with $p_{SS} = 1$ is shown. In contrast, panel B presents a rather unstable HMM with a small μ_S. The CV of the stable dominance times in panel D is large ($\text{CV}_S = 1$) leading to an irregular response pattern. Panel C shows the impact of increasing μ_U, and in panel F an example of a HMM with a large p_{UU} is printed.

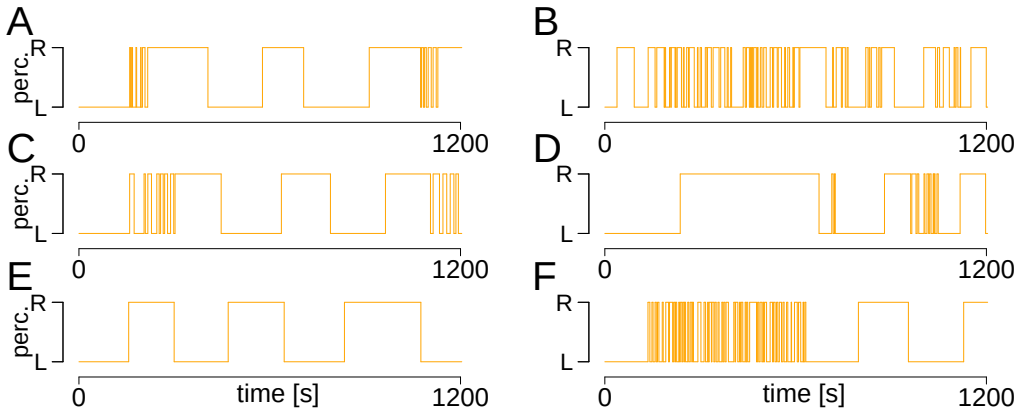

Figure 9.6: Impact of the two-state HMM parameter values on the response patterns. *Examples of simulated response patterns are shown for different values of the HMM parameters. In panel A we use* $\mu_S = 180$, $\sigma_S = 30$, $\mu_U = 7$, $\sigma_U = 6$, $p_{SS} = 0.67$, $p_{UU} = 0.95$. *In panels B-F one of these parameters is changed as follows where all others remain unchanged to panel A:* $\mu_S = 60$ *(B),* $\mu_U = 10$ *(C),* $\sigma_S = 180$ *(D),* $p_{SS} = 1$ *(E) and* $p_{UU} = 0.98$ *(F). Changing* σ_U *does not have clearly visible effects.*

9.3 Parameter estimation: Continuous presentation

To estimate the parameters of the HMM for continuous presentation, we distinguish between the inverse Gaussian and the Gamma distribution (Sections 9.3.1 and 9.3.2, respectively). For both distributions, we present maximum likelihood and moment estimators, where for the IG distribution we additionally derive UMVU estimators. In case the reader is just interested in a brief description of the parameter estimation used in practice (e.g., when analyzing the data set Schmack et al. (2015)), we suggest reading only the first paragraph of Subsection 9.3.1.1 and then jumping ahead to Section 9.4.

9.3.1 Inverse Gaussian distribution

First we derive ML estimators, followed by UMVU and moment estimators. In the last part the estimators are compared.

9.3.1.1 Maximum likelihood estimation

We first state the ML estimators of μ, σ. Then we discuss how to include the censored last dominance time in the ML estimation. The largest part of this subsection deals with the exact sampling distributions of the ML estimators.
Assuming inverse Gaussian distributed random variables D_i the log-likelihood-function ℓ derives for the data d and the parameters μ, σ as

$$\ell(d|\mu,\sigma) = \frac{1}{2}\sum_{i=1}^{n}\left(\log\left(\frac{\mu^3}{2\pi\sigma^2 d_i^3}\right) - \frac{\mu}{2\sigma^2}\frac{(d_i-\mu)^2}{d_i}\right).$$

Derivating partially and setting the derivatives to zero yields the following ML estimators (Seshadri, 1993)

$$\hat{\mu} := \hat{\mu}^{\mathrm{ML}} := \frac{1}{n}\sum_{i=1}^{n} d_i \qquad \text{and} \qquad \hat{\sigma} := \hat{\sigma}^{\mathrm{ML}} := \sqrt{\frac{\hat{\mu}^3}{n}\sum_{i=1}^{n}\left(\frac{1}{d_i} - \frac{1}{\hat{\mu}}\right)}. \tag{9.3}$$

Censored dominance times

Until now we have only incorporated the complete dominance times, i.e., the dominance times whose beginning and end is marked by a button press of the subject, in the estimation. However, there also exists a last dominance time that is the difference d_{n+1} between the last button press and the end of the experiment. Thus, we only know that the dominance time is at least d_{n+1} and not its exact value. In such a situation one speaks of **censored** data (e.g., Cox and Oakes, 1984). The log-likelihood of the data $d_{\mathrm{cens}} = (d_1, d_2, \ldots, d_n, d_{n+1})$ is then given by

$$\ell(d_{\mathrm{cens}}|\mu,\sigma) = \frac{1}{2}\sum_{i=1}^{n}\left(\log\left(\frac{\mu^3}{2\pi\sigma^2 d_i^3}\right) - \frac{\mu}{2\sigma^2}\frac{(d_i-\mu)^2}{d_i}\right) + \log(1 - F^{\mathrm{IG}}_{\mu,\sigma}(d_{n+1})),$$

where $F^{\mathrm{IG}}_{\mu,\sigma}$ denotes the distribution function of the $\mathrm{IG}(\mu,\sigma)$-distribution. Analytical approaches for the derivation of ML estimators in this situation are challenging (Cohen and Whitten, 1988). Therefore, we propose a numerical maximization of $\ell(d_{\mathrm{cens}}|\mu,\sigma)$ that can be performed by the `R`-routine `nlm()` using the moment estimates of μ and σ (based only on the not-censored dominance times, see page 83) as initial values.

Sampling distribution of the ML estimators $\hat{\mu}$ and $\hat{\sigma}$

Here, we focus on the exact sampling distributions of $\hat{\mu}$ and $\hat{\sigma}$. The result for $\hat{\sigma}$ is derived for the first time. For four different sample sizes, we compare in Figure 9.7 the simulated empirical distribution of $\hat{\sigma}$ with the exact theoretical distribution of $\hat{\sigma}$ given in Proposition 9.5 and the asymptotic normal distribution derived later in Section 9.3.3.1. For $n = 5, n = 10$ and $n = 20$ there is a remarkable difference between the asymptotic and the exact distribution that describes the empirical distribution very well. As comparable sample sizes occur also in the data, this underlines the importance of deriving the exact sampling distributions (for, e.g., computing confidence intervals in a following study). For the large $n = 100$, all three distributions closely resemble each other.
The exact sampling distributions of the sample mean $\hat{\mu} = \bar{d}$ and of the ML estimator $\hat{\lambda} = \hat{\mu}^3/\hat{\sigma}^2$ (compare the original parametrization of the IG distribution given in Definition 8.3) of a random sample of $\mathrm{IG}(\mu,\sigma)$-distributed random variables are well known in the literature and given in the next proposition.

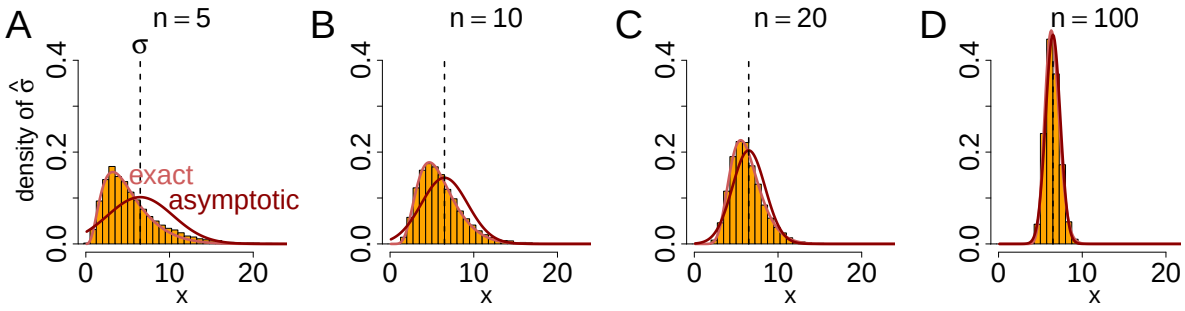

Figure 9.7: Comparison of exact (light red) and asymptotic (dark red) distribution of $\hat{\sigma}$. *The histograms show the empirical distribution of $\hat{\sigma}$ in 10000 simulations with $IG(8.5, 6.5)$-distributed random variables for the four sample sizes $n \in \{5, 10, 20, 100\}$ (corresponding to the panels A-D). The true value σ is indicated by a dashed line.*

Proposition 9.2. ***Sampling distributions of $\hat{\mu}$ and $\hat{\lambda}$***
Let $n \geq 2$ and $d = (d_1, d_2, \ldots, d_n)$ be the realization of a random sample of $IG(\mu, \sigma)$-distributed random variables. The sample mean $\hat{\mu} = \bar{d}$ is IG distributed with parameters μ and $\sigma/\sqrt{n}$. Moreover,

$$\frac{1}{n}\sum_{i=1}^{n}\frac{1}{d_i} - \frac{1}{\bar{d}}$$

is the ML estimator $1/\hat{\lambda}$ of $1/\lambda = \sigma^2/\mu^3$, and it holds

$$\frac{n\lambda}{\hat{\lambda}} \sim \chi^2_{n-1}.$$

$\frac{n\lambda}{\hat{\lambda}}$ and $\bar{d}$ are independent.

Proof: Compare Proposition 1.1 and 1.2 in Seshadri (1999). □

It follows directly that $\hat{\mu}$ as the sample mean is a consistent estimator. Moreover, we observe due to the expectation of a chi-squared distributed random variable $\mathbb{E}[1/\hat{\lambda}] = (n-1)/n \cdot 1/\lambda$ such that $1/\hat{\lambda}$ is asymptotically unbiased. Moreover, with the variance $2n$ of a χ^2_n distributed random variable, we have $\mathbb{V}\mathrm{ar}(1/\hat{\lambda}) = (2n-2)/n^2 \cdot 1/\lambda^2$, i.e., the variance tends to zero as $n \to \infty$. Together, this implies the consistency of $1/\hat{\lambda}$.

Now, we derive the sampling distribution of the ML estimator for the standard deviation $\hat{\sigma}$ given in equation (9.3). Moreover, the expectation $\mathbb{E}[\hat{\sigma}]$ and thereby the bias $\mathbb{E}[\hat{\sigma}] - \sigma$ are derived, and the consistency of $\hat{\sigma}$ is shown. Therefore, we require the χ-distribution. Its definition and expectation are given by, e.g., Forbes et al. (2011, page 73).

Definition 9.3. ***χ-distribution***
A random variable X is χ_k distributed (with $k > 0$ as the degrees of freedom) if X^2 is χ_k^2-distributed. The density of X is given by

$$f_k^{\chi}(x) = \frac{2^{1-k/2}x^{k-1}\exp(-x^2/2)}{\Gamma(k/2)}, \text{ if } x \geq 0$$

and $f_k^{\chi}(x) = 0$ else.

Proposition 9.4. ***Expectation of the χ-distribution***
The expectation of a χ_k-distributed random variable X derives as

$$\mathbb{E}[X] = \sqrt{2}\frac{\Gamma((k+1)/2)}{\Gamma(k/2)}.$$

Proposition 9.5. ***Sampling distribution and expectation of $\hat{\sigma}$***
Let $\hat{\sigma}$ be the ML estimator of the standard deviation σ derived using the realizations of a random sample of $n \geq 2$ $IG(\mu, \sigma)$-distributed random variables. The density of $\hat{\sigma}$ is given by

$$f(x) = \frac{\sqrt{\mu^3 n}}{\sigma}\int_0^{\infty}\frac{2x}{3y^{5/3}}f_{\mu,\sigma/\sqrt{n}}^{IG}\left(y^{1/3}\right)f_{n-1}^{\chi^2}\left(\frac{x^2\mu^3 n}{y\sigma^2}\right)dy$$

for $x > 0$ and 0 otherwise, where $f_{n-1}^{\chi^2}(x)$ is the chi-square density with $n-1$ degrees of freedom. The expectation of $\hat{\sigma}$ is

$$\mathbb{E}\left[\hat{\sigma}\right] = \frac{2\mu}{\sqrt{\pi}}\frac{\Gamma(n/2)}{\Gamma((n-1)/2)}\exp\left(\frac{n\mu^2}{\sigma^2}\right)K_1\left(\frac{n\mu^2}{\sigma^2}\right)$$

with $K_1(x)$ as the modified Bessel function of the third kind and order 1 (e.g., Watson, 1995). The estimator $\hat{\sigma}$ is asymptotically unbiased, i.e., $\lim_{n\to\infty}\mathbb{E}[\hat{\sigma}] = \sigma$ and consistent.

Proof: To derive the density we first use the random variable $\tilde{X} := \hat{\sigma}\sqrt{n\mu^3}/\sigma$ and derive the density of $\tilde{X}$. Then, we use this density to conclude the density of $\hat{\sigma}$.
We decompose $\hat{\sigma}\sqrt{n\mu^3}/\sigma$ as follows $\hat{\sigma}\sqrt{n\mu^3}\sigma = \hat{\mu}^{3/2}\sqrt{n\lambda/\hat{\lambda}}$ with $\lambda = \mu^3/\sigma^2$ and $\hat{\lambda}$ as its ML estimator (using the original parametrization of the IG distribution given in Definition 8.3). Letting $Y := \hat{\mu}^3$ and $Z := n\lambda/\hat{\lambda}$, we derive the density of the product $\tilde{X} = \sqrt{YZ}$. The density of Y depends as follows on the IG distribution

$$f_Y(y) = \frac{1}{3y^{2/3}}f_{\mu,\sigma/\sqrt{n}}^{IG}(y^{1/3})$$

as the variable $Y^{1/3}$ is $\text{IG}(\mu, \sigma)$-distributed. Z is chi-square distributed with $n-1$ degrees of freedom (Proposition 9.2).
Now, we use the variable transformation $T(y, z) = (\sqrt{yz}, y) = (x, y)$ with the inverse $T^{-1}(x, y) = (y, x^2/y) = (y, z)$. The determinant of the corresponding Jacobian matrix derives as $2x/y$. Thus, the density of $\tilde{X} = \sqrt{YZ}$ is $f_{\tilde{X}}(x) = \int_{-\infty}^{\infty} f_Y(y)f_Z(x^2/y)2x/|y|dy$ (e.g., Grimmett and Stirzaker, 2001) yielding

$$f_{\tilde{X}}(x) = \int_0^{\infty}\frac{1}{3y^{2/3}}f_{\mu,\sigma/\sqrt{n}}^{\text{IG}}(y^{1/3})f_{n-1}^{\chi^2}\left(\frac{x^2}{y}\right)\frac{2x}{y}dy$$

for $x > 0$ and 0 otherwise. To obtain the density f of the estimator $\hat{\sigma} = g(\tilde{X})$ itself with $g(x) = (\sigma/\sqrt{\mu^3 n})x$, note that due to the chain rule and $g(x)$ strictly increasing on $[0, \infty)$ we use the method of transformations (e.g., Klenke, 2008) as follows

$$f(x) = F'(x) = \frac{d}{dx}(F_{\tilde{X}}(g^{-1}(x))) = f_{\tilde{X}}(g^{-1}(x))\frac{d}{dx}g^{-1}(x).$$

With $g^{-1}(x) = (\sqrt{\mu^3 n}/\sigma)x$ it follows

$$f(x) = \int_0^\infty \frac{\sqrt{\mu^3 n}}{\sigma}\frac{2x}{3y^{5/3}} f^{\text{IG}}_{\mu,\sigma/\sqrt{n}}(y^{1/3}) f^{\chi^2}_{n-1}\left(\frac{x^2\mu^3 n}{y\sigma^2}\right) dy$$

for $x > 0$ and 0 otherwise. This is the assertion.
Next, we derive the expected value. Therefore, the independence of $\hat{\mu}$ and $\hat{\lambda}$ (Proposition 9.2) is used as follows

$$\mathbb{E}[\hat{\sigma}\sqrt{n\lambda}] = \mathbb{E}\left[\hat{\mu}^{3/2}\sqrt{\frac{n\lambda}{\hat{\lambda}}}\right] = \mathbb{E}\left[\hat{\mu}^{3/2}\right]\mathbb{E}\left[\sqrt{\frac{n\lambda}{\hat{\lambda}}}\right].$$

By Proposition 9.2 we know that $\sqrt{Z} = \sqrt{\frac{n\lambda}{\hat{\lambda}}}$ is χ_{n-1} distributed. Hence, its expectation is given by $\mathbb{E}[\sqrt{Z}] = \sqrt{2}\frac{\Gamma(n/2)}{\Gamma((n-1)/2)}$ (Proposition 9.4). The expected value of $\sqrt{Y} = \hat{\mu}^{3/2}$ is more difficult to derive. We need the following Sublemma 9.6, which is proven later.

Sublemma 9.6. *Let X be IG(μ, σ)-distributed. Then, the expected value of $X^{3/2}$ is given by*

$$\mathbb{E}\left[X^{3/2}\right] = \sqrt{\frac{2\mu}{\pi}}\frac{\mu^2}{\sigma}\exp\left(\frac{\mu^2}{\sigma^2}\right)K_1\left(\frac{\mu^2}{\sigma^2}\right).$$

As we know that $\hat{\mu}$ is IG($\mu, \sigma/\sqrt{n}$) distributed (Proposition 9.2), we use Sublemma 9.6 to derive

$$\mathbb{E}[\sqrt{Y}] = \mathbb{E}[\hat{\mu}^{3/2}] = \sqrt{\frac{2\mu}{\pi}}\frac{\sqrt{n}\mu^2}{\sigma}\exp\left(\frac{n\mu^2}{\sigma^2}\right)K_1\left(\frac{n\mu^2}{\sigma^2}\right).$$

Multiplying $\mathbb{E}[\sqrt{Y}]$ with $\mathbb{E}[\sqrt{Z}]$ and dividing by $\sqrt{n\lambda} = \sqrt{n\mu^3/\sigma^2}$ yields the assertion.
We obtain for the bias of the ML estimator $\hat{\sigma}$

$$\mathbb{B}\text{ias}\,(\hat{\sigma}) = \mathbb{E}[\hat{\sigma}] - \sigma = \frac{2\mu}{\sqrt{\pi}}\frac{\Gamma(n/2)}{\Gamma((n-1)/2)}\exp\left(\frac{n\mu^2}{\sigma^2}\right)K_1\left(\frac{n\mu^2}{\sigma^2}\right) - \sigma. \tag{9.4}$$

To show the asymptotic bias of zero of $\hat{\sigma}$ we apply formulas 6.1.39 and 9.7.2 from Abramowitz and Stegun (1972) leading to

$$\frac{\Gamma(n/2)}{\Gamma(n/2-1/2)} \propto \sqrt{\frac{n}{2}} \quad \text{and} \quad K_1\left(\frac{n\mu^2}{\sigma^2}\right) \propto \exp\left(-\frac{n\mu^2}{\sigma^2}\right)\sqrt{\frac{\sigma^2\pi}{2n\mu^2}},$$

where $\propto$ indicates "proportional to" for $n \to \infty$. Thus,

$$\mathbb{B}\text{ias}\left(\hat{\sigma}\right) = \frac{2\mu}{\sqrt{\pi}} \frac{\Gamma(n/2)}{\Gamma((n-1)/2)} \exp\left(\frac{n\mu^2}{\sigma^2}\right) K_1\left(\frac{n\mu^2}{\sigma^2}\right) - \sigma \propto \frac{2\mu}{\sqrt{\pi}} \sqrt{\frac{n}{2}} \frac{\sigma}{\mu} \sqrt{\frac{\pi}{2n}} - \sigma,$$

and the bias vanishes asymptotically for $n \to \infty$, i.e., $\hat{\sigma}$ is a asymptotically unbiased.
Using Remark 8.5, it follows $\hat{\sigma} = \sqrt{\hat{\mu}^3/\hat{\lambda}}$. We know by the explanations following Proposition 9.2 that $\hat{\mu}$ and $1/\hat{\lambda}$ are consistent, i.e., converge in probability toward μ and $1/\lambda$, respectively. Thus, by continuous mapping also $\sqrt{\hat{\mu}^3}$ and $1/\sqrt{\hat{\lambda}}$ are consistent such that the consistency of $\hat{\sigma}$ follows directly by Slutsky's theorem. □

Proof of Sublemma 9.6: To derive the expected value several identities about hyperbolic functions are required. We therefore always refer to Section 4.5 in Abramowitz and Stegun (1972) (via 4.5.x for equation 4.5.x therein) and use $\lambda = \mu^3/\sigma^2$ for the sake of simplicity.

$$\begin{aligned}
\mathbb{E}\left[X^{3/2}\right] &= \int_0^\infty \sqrt{\frac{\lambda}{2\pi}} \exp\left(\frac{-\lambda(x-\mu)^2}{2\mu^2 x}\right) dx \\
&= \sqrt{\frac{\lambda}{2\pi}} \int_0^\infty \exp\left(\frac{-\lambda}{2\mu^2}\left[\sqrt{x} - \frac{\mu}{\sqrt{x}}\right]^2\right) dx \\
&\overset{e^\theta := \sqrt{\frac{x}{\mu}}}{=} \sqrt{\frac{\lambda}{2\pi}} \int_{-\infty}^\infty \exp\left(\frac{-2\lambda}{\mu}\left[\frac{1}{2}\exp(\theta) - \exp(-\theta)\right]^2\right) 2\mu \exp(2\theta) d\theta \\
&\overset{4.5.1}{=} \sqrt{\frac{2\lambda}{\pi}}\mu \int_{-\infty}^\infty \exp\left(\frac{-2\lambda}{\mu}\sinh(\theta)^2\right) \exp(2\theta) d\theta \\
&\overset{\substack{4.5.16 \\ 4.5.32}}{=} \sqrt{\frac{2\lambda}{\pi}}\mu \int_{-\infty}^\infty \exp\left(\frac{-2\lambda}{\mu}\frac{\cosh(2\theta)-1}{2}\right) (\sinh(2\theta) + \cosh(2\theta) d\theta \\
&\overset{\omega := \theta/2}{=} \sqrt{\frac{2\lambda}{\pi}}\frac{\mu}{2} \exp\left(\frac{\lambda}{\mu}\right) \int_{-\infty}^\infty \exp\left(\frac{-\lambda}{\mu}\cosh(\omega)\right) (\sinh(\omega) + \cosh(\omega)) d\omega \\
&\overset{\substack{4.5.21 \\ 4.5.22}}{=} \sqrt{\frac{2\lambda}{\pi}}\mu \exp\left(\frac{\lambda}{\mu}\right) \int_0^\infty \exp\left(\frac{-\lambda}{\mu}\cosh(\omega)\right) (\cosh(\omega)) d\omega \\
&= -\sqrt{\frac{2\lambda}{\pi}}\mu \exp\left(\frac{\lambda}{\mu}\right) \frac{\partial}{\partial z} \int_0^\infty \exp\left(-z\cosh(\omega)\right) d\omega \Big|_{z=\lambda/\mu} \\
&\overset{*}{=} -\sqrt{\frac{2\lambda}{\pi}}\mu \exp\left(\frac{\lambda}{\mu}\right) K_0'\left(\frac{\lambda}{\mu}\right) \\
&\overset{**}{=} \sqrt{\frac{2\lambda}{\pi}}\mu \exp\left(\frac{\lambda}{\mu}\right) K_1\left(\frac{\lambda}{\mu}\right) = \sqrt{\frac{2\mu}{\pi}}\frac{\mu^2}{\sigma} \exp\left(\frac{\mu^2}{\sigma^2}\right) K_1\left(\frac{\mu^2}{\sigma^2}\right),
\end{aligned}$$

where in $*$ and $**$ we made use of an integral representation of the modified Bessel function of the third kind and order a: $K_a(x) = \int_0^\infty \exp(-x\cosh(t))\cosh(at)dt$ (p.181 in Watson, 1995). □

Figure 9.8 shows the relative bias (defined as $\mathbb{B}\text{ias}(\hat{\sigma})/\sigma$) of the ML estimator $\hat{\sigma}$ for different values of μ and $\sigma = 6.5$. Interestingly, the (absolute) relative bias of the ML estimator $\hat{\sigma}$ shown in Figure 9.8 decreases with an increasing CV$=\sigma/\mu$. In all three cases a sample size $n \geq 8$ implies a relative bias smaller than ten percent.

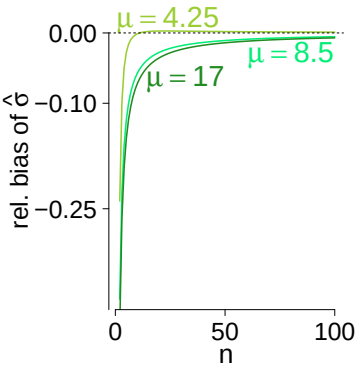

Figure 9.8: Relative bias of the ML estimator $\hat{\sigma}$ *for $\sigma = 6.5$ and $\mu \in \{4.25, 8.5, 17\}$ as indicated by the different colors. The bias is given by* (9.4).

In the next subsection, we introduce an unbiased estimator of σ.

9.3.1.2 UMVU estimators

As we have shown in Proposition 9.5, the ML estimator of σ is biased. One idea to handle the bias of the ML estimator for σ is the derivation of the so-called **UMVU estimator** (uniformly minimum-variance unbiased estimator), which is the goal of this subsection. As its name indicates, an UMVU estimator is unbiased and moreover has the smallest variance for all possible values of the parameter in the set of all other unbiased estimators (e.g., Lehmann and Casella, 1998). Note, however, that the UMVU estimator is not always the "best" solution to a specific estimation problem. An important result for the derivation of UMVU estimators is the Lehmann-Scheffé-Theorem. Recall that for random data X a statistic $S(X)$ is called **sufficient** for an underlying parameter θ if the conditioned distribution of X given $S(X)$ does not depend on θ. The statistic $S(X)$ is **complete** if for any measurable function g we have

$$\mathbb{E}_\theta[g(S(X))] = 0 \text{ for all } \theta \Rightarrow \mathbb{P}_\theta(g(S(X)) = 0) = 1 \text{ for all } \theta.$$

For more details about sufficiency and completeness we refer to, e.g., Young and Smith (2005), Chapter 6.

Proposition 9.7. ***Lehmann-Scheffé-Theorem***
Let $X := (X_1, X_2, \ldots, X_n)$ be random variables with distribution depending on a parameter θ. Let further $S = h(X_1, \ldots, X_n)$ be a complete and sufficient statistic for θ. If $f(S)$ is an unbiased estimate of θ, then $f(S)$ has the minimum variance among all unbiased estimates of θ, i.e., $f(S)$ is the UMVU estimator of θ.

Proof: Can be found in, e.g., Casella and Berger (2002). □

In the context of UMVU estimators for the inverse Gaussian distribution, the statistic $(\bar{d}, v)$ using the sample mean $\bar{d}$ and

$$v := \sum_{i=1}^{n} \left(\frac{1}{d_i} - \frac{1}{\bar{d}} \right) \tag{9.5}$$

is minimal sufficient (i.e., can be represented as a function of any other sufficient statistic) and complete (Prop. 6.1 in Seshadri, 1993).
Iwase and Seto (1983) showed the following Lemma 9.9 enabling us to derive UMVU estimators for different parametrizations of the inverse Gaussian distribution based on the quantities $\bar{d}$ and v. An important ingredient of these UMVU estimators is the hypergeometric function, which we define following Abramowitz and Stegun (1972). Note that several other identities exist.

Definition 9.8. ***Hypergeometric function***
The hypergeometric function $F(a, b; c; z)$ is for $a, b \in \mathbb{R}$, $c > 0$ and $z \in \mathbb{R}$ with $|z| < 1$ defined as

$$F(a, b; c; z) := \sum_{n=0}^{\infty} \frac{(a)_n (b)_n}{(c)_n} \frac{z^n}{n!}$$

with $(a)_n = \Gamma(a + n)/\Gamma(a)$ as the Pochhammer symbol and $(b)_n, (c)_n$ analogously. For $|z| \geq 1$ an integral representation is given by

$$F(a, b; c; z) := \frac{\Gamma(c)}{\Gamma(b)\Gamma(c - b)} \int_0^1 t^{b-1} (1 - t)^{c-b-1} (1 - tz)^{-a} dt.$$

Lemma 9.9. ***Unbiased estimation of the parameters of the IG distribution***
Let $d = (d_1, d_2, \ldots, d_n)$ be the realization of a random sample of size $n \geq 2$ from the $IG(\mu, \sigma)$-distribution and α, β and τ be real numbers with $(n - 1)/2 + \tau > 0$. Then, with v as in (9.5),

$$\begin{aligned} &\mathbb{E}\left[\bar{d}^{\alpha+\beta+1/2} v^{\tau} F\left(\alpha, \beta; \frac{n-1}{2} + \tau; -\frac{\bar{d}v}{n} \right) \right] \\ &= \frac{\Gamma(n/2 - 1/2 + \tau)}{\Gamma(n/2 - 1/2)} \mu^{\alpha+\beta+1/2} \left(\frac{2\sigma^2}{\mu^3} \right)^{\tau} \left(\frac{2n\mu^2}{\sigma^2 \pi} \right)^{1/2} \exp\left(\frac{n\mu^2}{\sigma^2} \right) K_{\alpha-\beta}\left(\frac{n\mu^2}{\sigma^2} \right), \end{aligned} \tag{9.6}$$

where $F()$ is the hypergeometric function (Definition 9.8) and
$K_\alpha(x) := \int_0^\infty \exp(-x \cosh t) \cosh(\alpha t) dt$ the modified Bessel function of the third kind of order α (e.g., Watson, 1995).

Proof: See Iwase and Seto (1983). □

The following result about the UMVU estimators of of μ and σ is also given in Table 6.1 of Seshadri (1993). To understand the application of Lemma 9.9, we show the proof.

Corollary 9.10. ***UMVU estimators of μ and σ***
Let $d = (d_1, d_2, \ldots, d_n)$ be the realization of a random sample of $n \geq 2$ $IG(\mu, \sigma)$-distributed random variables. The UMVU estimator of μ is the sample mean $\bar{d}$, and the UMVU estimator of σ is given by

$$\hat{\sigma}^{UMVU} = \frac{\Gamma(n-1)/2}{\sqrt{2}\Gamma(n/2)}(\bar{d}^3 v)^{1/2} \times F\left(\frac{1}{4}, \frac{3}{4}; \frac{n}{2}; -\frac{\bar{d}v}{n}\right).$$

Proof: The assertion for μ follows by setting $\alpha = 0, \beta = \frac{1}{2}$ and $\tau = 0$ in Lemma 9.9. For σ we set $\alpha = \frac{1}{4}, \beta = \frac{3}{4}$ and $\tau = \frac{1}{2}$ in the same Lemma. In both cases, we multiply in equation (9.6) with the reciprocal of the terms involving the Gamma function and exploit the relationship $\left(\frac{2n\mu^2}{\sigma^2\pi}\right)^{1/2} \exp\left(\frac{n\mu^2}{\sigma^2}\right) K_{1/2}\left(\frac{n\mu^2}{\sigma^2}\right) = 1$ (Iwase and Seto, 1983) as well as $K_\alpha(x) = K_{-\alpha}(x)$ for $x \in \mathbb{R}$ and $\alpha \in \mathbb{R}$. The UMVU property follows by the Lehmann-Scheffé-Theorem (Proposition 9.7) as the only random inputs of both estimators are $\bar{d}$ and v being a complete and sufficient statistic for (μ, σ). □

9.3.1.3 Moment estimators

The fitting of moment estimators to the inverse Gaussian distribution with parameters μ and σ is straightforward by regarding the sample mean $\hat{\mu}^{\text{mom}} := \bar{d} = 1/n \sum_{i=1}^n d_i$ and sample standard deviation $\hat{\sigma}^{\text{mom}} := \sqrt{1/n \sum_{i=1}^n (d_i - \hat{\mu}^{\text{mom}})^2}$, where $d = (d_1, d_2, \ldots, d_n)$ denotes a realization of IG distributed random variables ($n \geq 2$).

9.3.1.4 Comparison of different estimators

Figure 9.9 compares for random samples of inverse Gaussian distributions with different parameter combinations (μ, σ) the ML, the moment and the UMVU estimator of σ dependent on the sample size n. Recall that the estimator of μ is identical for all three estimation techniques.
Figure 9.9 A depicts the bias of the ML and moment estimator for σ clearly. For all three values of σ the (simulated) bias of the ML estimator is almost always smaller than the bias of the moment estimator. The relative bias of the ML estimator is in all cases for $n \geq 8$ smaller than ten percent of the true σ, which justifies to use the ML estimators if the sample is large enough. The UMVU estimator is per construction unbiased. The median absolute relative error ($\text{RE}(\hat{\sigma}) = |\hat{\sigma} - \sigma|/\sigma$) of the estimators is shown for different values of σ in panels B-D. We note that the relative error (RE) of the UMVU estimator is in most of the cases slightly smaller than the RE of the ML estimator. The RE of the moment estimator is larger than the relative error of the two other estimators. We therefore conclude that moment estimators are not recommendable to estimate σ. Comparing the mean squared error yields similar results (data not shown). Note that using a denominator $n - 1$ instead of n in the moment estimator yields only slightly better results (as we estimate the standard deviation and not the variance). Hence, if one aims at using moment estimators, research about unbiased transformations of moment estimators for the IG distribution would be interesting.

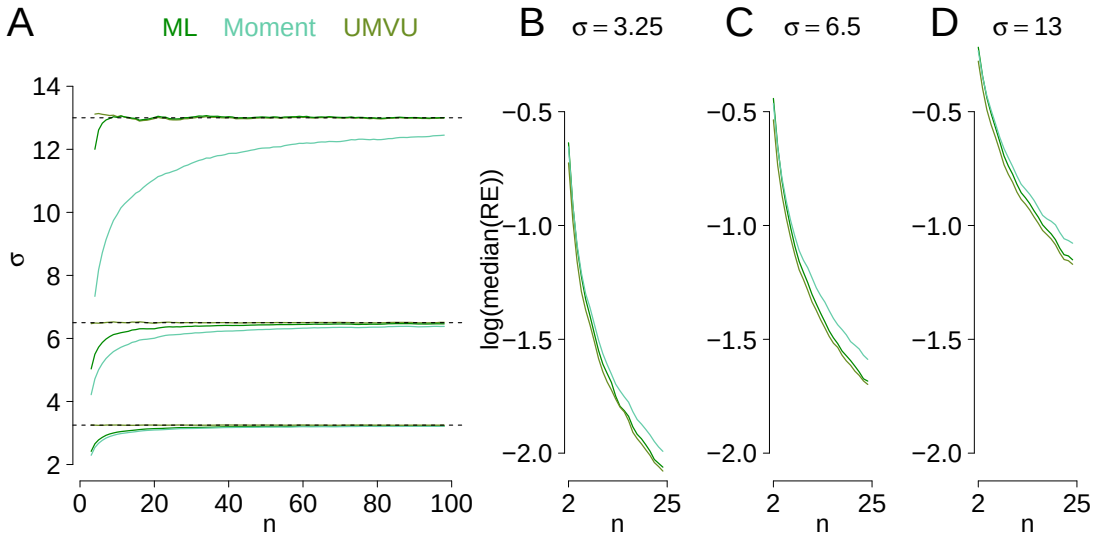

Figure 9.9: IG distribution: Comparison of different estimators for σ. *(A) Simulated mean $\hat{\sigma}_M^x := (1/m)\sum_{j=1}^m \hat{\sigma}^x$ in $m = 10000$ simulations of the ML ($x = ML$), the moment ($x = mom$) and the UMVU ($x = UMVU$) estimator of σ for a sample of $n \in \{2, \ldots, 100\}$ random variables (estimators visualized in different green tones). The mean parameter of the IG distribution is $\mu = 8.5$, and three different values of σ were used $\sigma \in \{3.25, 6.5, 13\}$. The true values are indicated by dashed lines. (B-D) log (median) of the absolute relative error ($RE = |\hat{\sigma}^x - \sigma|/\sigma$) of the estimator $\hat{\sigma}^x$ with $x \in \{ML, mom, UMVU\}$ where the colors printed in panel A are used (10000 simulations were used). The true σ differs from B-D and is printed at the top.*

In addition to the ML, moment and UMVU approaches, Bayesian inference for the inverse Gaussian distribution is possible. The literature lists several results for different parametrizations (reviews can be found in Seshadri (1993, 1999), no results are known for the (μ, σ)-parametrization). However, the methods highly depend on numerical integration routines and Markov-Chain-Monte-Carlo methods as well as their performance is comparable to UMVU estimators (Pandey and Bandyopadhyay, 2012) such that we do not investigate them further in this thesis.

9.3.2 Gamma distribution

The Gamma distribution offers a second possibility to describe the dominance times resulting from bistable stimulation. We introduce ML and moment estimators for the mean μ and the standard deviation σ of the Gamma distribution. In the last part of the subsection the two estimators are compared in simulations.

9.3.2.1 Maximum likelihood estimators

To derive the ML estimators, we first focus on the traditional parametrization $p = \mu^2/\sigma^2$, $\theta = \mu/\sigma^2$ (Remark 2.3) and then use the invariance property of ML estimators. The log-likelihood ℓ of n data $d = (d_1, d_2, \ldots, d_n)$ realized from a Gamma distribution with parameters p and θ is given by

$$\begin{aligned}\ell(d|p,\theta) &= (p-1)\sum_{i=1}^{n}\log d_i - n\log\Gamma(p) - np\log(1/\theta) - \theta\sum_{i=1}^{n} d_i \\ &= n(p-1)\overline{\log d} - n\log\Gamma(p) - np\log(1/\theta) - n\theta\overline{d} \qquad (9.7)\end{aligned}$$

with $\overline{\log d} = 1/n\sum_{i=1}^{n}\log d_i$ and $\overline{d} = 1/n\sum_{i=1}^{n} d_i$. The ML estimate for θ can be directly derived as $\hat{\theta}^{ML} := p/\overline{d}$. Plugging this estimate in (9.7) yields

$$\ell(D|p,\theta) = n(p-1)\overline{\log d} - n\log\Gamma(p) - np\log\overline{d} + np\log p - np.$$

Note that maximization of the latter display w.r.t. p is analytically not possible (due to the Gamma function in the density). Hence, we refer to an algorithm applying the "generalized Newton" principle introduced by Minka (2002) to maximize the latter equation. We choose a starting value $\hat{p}$ as follows

$$\hat{p} = \frac{1}{2(\log\overline{d} - \overline{\log d})}$$

and update then the estimator $\hat{p}_{\text{new}}$ iteratively

$$\frac{1}{\hat{p}_{\text{new}}} = \frac{1}{\hat{p}} + \frac{\overline{\log d} - \log\overline{d} + \log\hat{p} - \psi(\hat{p})}{\hat{p}^2(1/\hat{p} - \psi'(\hat{p}))}; \qquad \hat{p} = \hat{p}_{\text{new}}$$

until a desired level of convergence has been reached. $\psi(x)$ and $\psi'(x)$ denote the values of the diGamma and the triGamma function evaluated at x. The diGamma function is known as the logarithmic derivative of the Gamma function $\psi(x) = \frac{d}{dx}\log(\Gamma(x))$, and the triGamma function is the derivative of the diGamma function (e.g., Lawless, 1982).

The ML estimators for μ and σ are then due to Proposition 2.2 and the invariance property of ML estimators

$$\hat{\mu} := \hat{\mu}^{ML} = \hat{p}^{ML}/\hat{\theta}^{ML} = \bar{d} \text{ and } \hat{\sigma} := \hat{\sigma}^{ML} = \sqrt{\hat{p}^{ML}}/\hat{\theta}^{ML}.$$

Note especially that the ML estimator of μ is the sample mean. Be aware that the ML estimator for σ is biased (Figure 9.10 A). As during continuous presentation there are mostly more than ten dominance times, the effect of the bias is small. Moreover, we are mainly interested in the inverse Gaussian distribution to describe the dominance times. Therefore, we do not derive an UMVU estimator for σ in the case of the Gamma distribution.

Censored dominance times

As with the IG distribution, censored dominance times may be included using a numerical maximization procedure of the log-likelihood

$$\begin{aligned}\ell(d_{\text{cens}}|\mu,\sigma) = n(\mu^2/\sigma^2 - 1)\overline{\log d} - n\log\Gamma(\mu^2/\sigma^2) - n\mu^2\log(\sigma^2/\mu)/\sigma^2 - n\mu\bar{d}/\sigma^2 \\ + \log(1 - F^{\Gamma}_{\mu,\sigma}(d_{n+1})),\end{aligned}$$

where $F^{\Gamma}_{\mu,\sigma}$ denotes the distribution function of the Gamma distribution with mean μ and standard deviation σ. The `nlm()`-approach using the moment estimates of μ and σ (derived only from the complete dominance times, see below) is a simple way to perform that in `R`.

9.3.2.2 Moment estimators

The fitting of moment estimators to the Gamma distribution is straightforward by regarding the sample mean $\hat{\mu}^{\text{mom}} := \bar{d} = 1/n\sum_{i=1}^{n} d_i$ and sample standard deviation $\hat{\sigma}^{\text{mom}} := \sqrt{1/n\sum_{i=1}^{n}(d_i - \hat{\mu}^{\text{mom}})^2}$.

9.3.2.3 Comparison of different estimators

Figure 9.10 contrasts for random samples of Gamma distributions with different parameter combinations (μ, σ) the ML and the moment estimator of σ dependent on the sample size n. Recall that the estimator of μ is identical using the two estimation methods.
Figure 9.10 A depicts the (simulated) bias of the ML and moment estimator for σ clearly. For all three values of σ the bias of the ML estimator is always smaller than the bias of the moment estimator. The median absolute relative error ($\text{RE}(\hat{\sigma}) = |\hat{\sigma} - \sigma|/\sigma$) of the estimators is printed depending on σ in panels B-D. We note that the RE of the moment estimator is larger than the relative error of the ML estimator. We therefore recommend not to estimate σ via moment estimators. Results for the mean squared error are comparable (data not shown). Again, using a denominator $n - 1$ instead of n in the moment estimator yields only slightly better results (data not shown).

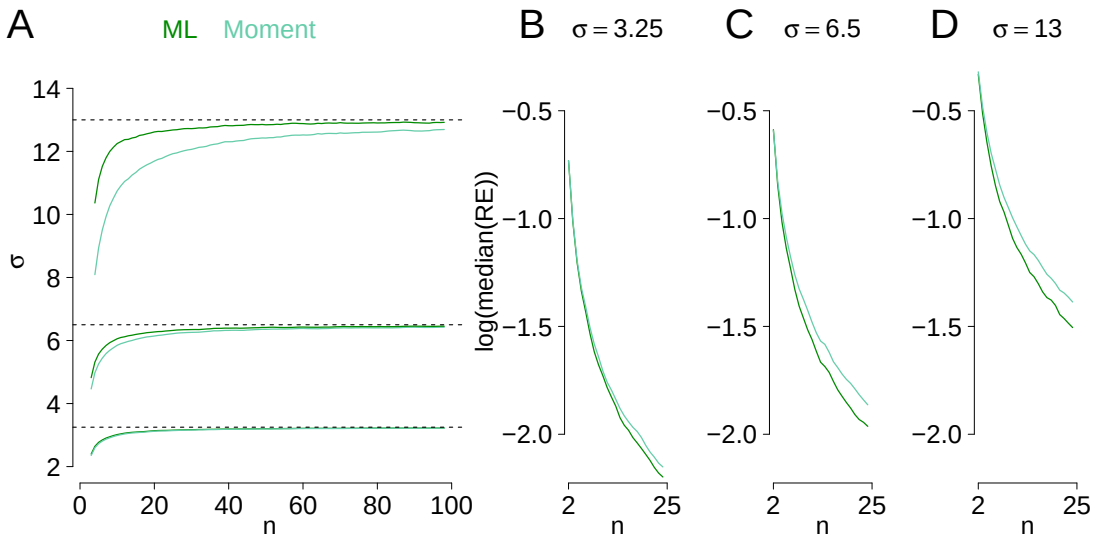

Figure 9.10: Gamma distribution: Comparison of the ML and the moment estimator for σ. *(A) Simulated mean $\hat{\sigma}^x_M := (1/m)\sum_{j=1}^m \hat{\sigma}^x$ in $m = 10000$ simulations of the ML ($x = ML$) and the moment ($x = mom$) estimator of σ for $n \in \{2, \ldots, 100\}$ (estimators visualized in different green tones). The mean parameter of the Gamma distribution is $\mu = 8.5$, and three different values of σ were used $\sigma \in \{3.25, 6.5, 13\}$. The true values are indicated by dashed lines. (B-D) log (median) of the absolute relative error (RE= $|\hat{\sigma}^x - \sigma|/\sigma$) of the estimator $\hat{\sigma}^x$ with $x \in \{ML, mom\}$ where the colors printed in panel A are used (10000 simulations were used). The true σ differs from B-D and is printed at the top.*

9.3.3 ML estimators: Asymptotic distribution

Next, we derive additionally the asymptotic distributions of the ML estimators for the parameters of the IG and the Gamma distribution (as the exact distributions are complicated or unknown). We can make use of the intensively investigated nature of the ML estimators and derive for a sample D of random variables with density $f_\Theta(d)$ depending on the parameter set Θ the Fisher-information matrix $I(\Theta)$ with entries

$$[I(\Theta)]_{i,j} := \mathbb{E}\left[\left(\frac{\partial}{\partial\Theta_i}\log f_\Theta(D)\right)\left(\frac{\partial}{\partial\Theta_j}\log f_\Theta(D)\right)\middle|\,\Theta\right],$$

which is directly connected to the precision of parameter estimates (Lehmann and Casella, 1998). For members of the exponential family (recall equation (8.1)) with open parameter space, injective and continuously differentiable η (with nonsingular derivatives) as well as a nonsingular covariance matrix of $t(D)$ (i.e., with nonzero determinant), it holds

$$\sqrt{n}(\hat{\Theta}^{ML} - \Theta) \sim N\left(0, I(\Theta)^{-1}\right) \tag{9.8}$$

as is shown in Theorem 4.6. of van der Vaart (1998). Moreover, if the parameter space is open and the first and second partial derivatives of $f_\Theta(d)$ exist, are finite and continuous (such that integration and differentiation can be interchanged by the Leibniz integral rule (e.g., Lang, 1997)) the Fisher-information matrix can be rewritten (Lemma 5.3 (p. 116) in Lehmann and Casella, 1998) as

$$[I(\Theta)]_{i,j} = -\mathbb{E}\left[\frac{\partial^2}{\partial\Theta_i\,\partial\Theta_j}\log f_\Theta(D)\middle|\,\Theta\right]. \tag{9.9}$$

The conditions required for equation (9.9) are fulfilled by the inverse Gaussian and the Gamma distribution as can be checked easily. In the next paragraphs, we use (9.9) to derive the Fisher information and thereby the asymptotic variances of the ML estimators for the IG and the Gamma distribution using equation (9.8). These variances can be used to derive asymptotic confidence intervals.

9.3.3.1 Inverse Gaussian distribution

Recall that the inverse Gaussian distribution with parameters $\Theta = (\mu, \sigma)$ belongs to the exponential family (Corollary 8.7) with $t(D) = (D, 1/D)^T, \eta(\Theta) = (-\mu, -\mu^3)/(2\sigma^2)$. One can check easily that for $\mu > 0, \sigma > 0$ η is injective and continuously differentiable with nonsingular derivatives. The determinant of the covariance matrix of $t(D)$ is given by

$$\begin{aligned}
&\mathbb{V}\mathrm{ar}(D)\mathbb{V}\mathrm{ar}(1/D) - \mathrm{Cov}(D, 1/D)^2 \\
&= \sigma^2(\mathbb{E}[1/D^2] - \mathbb{E}[1/D]^2) - 1 + 2\mathbb{E}[D]\mathbb{E}[1/D] - \mathbb{E}[D]^2\mathbb{E}[1/D]^2 \\
&= \sigma^2\left(\frac{1}{\mu^2} + 3\frac{\sigma^4}{\mu^6} + 3\frac{\sigma^2}{\mu^4} - \frac{1}{\mu^2} - 2\frac{\sigma^2}{\mu^4} - \frac{\sigma^4}{\mu^6}\right) - 1 + 2 + 2\frac{\mu^2}{\sigma^2} - \mu^2\left(\frac{1}{\mu^2} + 2\frac{\sigma^2}{\mu^4} + \frac{\sigma^4}{\mu^6}\right) \\
&= 2\frac{\sigma^6}{\mu^6} \neq 0,
\end{aligned}$$

where we used the expected values of $1/D$ and $1/D^2$ as given in Proposition 8.8 and Seshadri (1993), Table 2.3.

Hence, the regularity conditions for the derivation of the asymptotic variance by the Fisher information are fulfilled (eq. (9.8)). Using equation (9.9), we derive for an $\mathrm{IG}(\mu, \sigma)$-distributed random variable D

$$\begin{aligned} I(\mu,\sigma) &:= -\mathbb{E}\begin{bmatrix} \frac{\partial^2}{\partial\mu^2}\log f^{\mathrm{IG}}_{\mu,\sigma}(D) & \frac{\partial^2}{\partial\mu\partial\sigma}\log f^{\mathrm{IG}}_{\mu,\sigma}(D) \\ \frac{\partial^2}{\partial\sigma\partial\mu}\log f^{\mathrm{IG}}_{\mu,\sigma}(D) & \frac{\partial^2}{\partial\sigma^2}\log f^{\mathrm{IG}}_{\mu,\sigma}(D) \end{bmatrix} \\ &= -\mathbb{E}\begin{bmatrix} \frac{2-3\mu/D}{\sigma^2} - \frac{3}{2\mu^2} & \frac{3\mu^2-4\mu D+D^2}{\sigma^3 D} \\ \frac{3\mu^2-4\mu D+D^2}{\sigma^3 D} & \frac{1}{\sigma^2} - \frac{3\mu(D-\mu)^2}{\sigma^4 D} \end{bmatrix} \\ &= \begin{bmatrix} \frac{9}{2}\frac{1}{\mu^2} + \frac{1}{\sigma^2} & -\frac{3}{\mu\sigma} \\ -\frac{3}{\mu\sigma} & \frac{2}{\sigma^2} \end{bmatrix}, \end{aligned}$$

where we used for the last equal sign that $\mathbb{E}[1/D] = 1/\mu + \sigma^2/\mu^3$ (Proposition 8.8).
By using equation (9.8), inverting $I(\mu, \sigma)$ and dividing by n, we obtain for the asymptotic variances of the asymptotic normal distributions with means μ and σ, respectively,

$$\begin{aligned} \mathbb{V}\mathrm{ar}\left(\hat{\mu}^{\mathrm{ML}}\right) &\approx \frac{I_{11}^{-1}(\mu,\sigma)}{n} = \frac{2}{n\sigma^2(2/\sigma^4)} = \frac{\sigma^2}{n} \\ \mathbb{V}\mathrm{ar}\left(\hat{\sigma}^{\mathrm{ML}}\right) &\approx \frac{I_{22}^{-1}(\mu,\sigma)}{n} = \frac{1/\sigma^2 + 9/2\cdot 1/\mu^2}{2n/\sigma^4} = \frac{\sigma^2}{2n} + \frac{9}{4n}\frac{\sigma^4}{\mu^2} = \frac{1}{2n}\sigma^2 + \frac{9}{4n}\sigma^2\mathrm{CV}^2. \end{aligned}$$

Note that as $\hat{\mu}^{\mathrm{ML}}$ is the sample mean even its exact variance is given by σ^2/n.

9.3.3.2 Gamma distribution

We aim to derive the asymptotic variance of the estimators $\hat{\mu}$ and $\hat{\sigma}$ of the Gamma distribution. Therefore, we need the density of a Gamma-distributed random variable D with the corresponding parametrization

$$\log f^{\Gamma}_{\mu,\sigma}(d) = (\mu^2/\sigma^2 - 1)\log d - \log\Gamma(\mu^2/\sigma^2) - \mu^2\log(\sigma^2/\mu)/\sigma^2 - \mu d/\sigma^2.$$

Recall that the Gamma distribution is a representative of the exponential family (e.g., Lehmann and Casella, 1998). For $\Theta = (\mu, \sigma)$ the existence and continuity of the derivatives of $\eta(\Theta) = (-\mu/\sigma^2, \mu^2/\sigma^2 - 1)$ and its injectivity follow easily as well as the nonsingularity of the covariance matrix of $t(D) = (D, \log(D))$ (not shown here). Moreover, the parameter space is open. Thus, the regularity conditions for equation (9.8) to hold are fulfilled, and we derive

$$I(\mu,\sigma) = -\mathbb{E}\begin{bmatrix} \frac{\partial^2}{\partial\mu^2}\log f^{\Gamma}_{\mu,\sigma}(D) & \frac{\partial^2}{\partial\mu\partial\sigma}\log f^{\Gamma}_{\mu,\sigma}(D) \\ \frac{\partial^2}{\partial\sigma\partial\mu}\log f^{\Gamma}_{\mu,\sigma}(D) & \frac{\partial^2}{\partial\sigma^2}\log f^{\Gamma}_{\mu,\sigma}(D) \end{bmatrix}$$

as also the regularity conditions required for equation (9.9) are fulfilled. For notational reasons we write the entries of the matrix $I := I(\mu, \sigma)$ separately

$$
\begin{aligned}
I_{11} &= -\mathbb{E}\left[\frac{1}{\sigma^2}\left(-2\log(\sigma^2/\mu) - 2\psi(\mu^2/\sigma^2) + 2\log(D) + 3 - 4\mu^2\psi^{'}(\mu^2/\sigma^2)/\sigma^2\right)\right] \\
&= \frac{1}{\sigma^2}\left(2\log(\sigma^2/\mu) + 2\psi(\mu^2/\sigma^2) + 2\psi(\mu^2/\sigma^2) - 2\log(\mu/\sigma^2) - 3 + 4\mu^2\psi^{'}(\mu^2/\sigma^2)/\sigma^2\right) \\
I_{12} = I_{21} &= -\mathbb{E}\left[\frac{1}{\sigma^3}\left(4\mu^3\psi^{'}(\mu^2/\sigma^2)/\sigma^2 + 4\mu\psi(\mu^2/\sigma^2) - 4\mu\log(D) + 4\mu\log(\sigma^2/\mu) - 6\mu + 2D\right)\right] \\
&= \frac{1}{\sigma^3}\left(-4\mu^3\psi^{'}(\mu^2/\sigma^2)/\sigma^2 - 4\mu\log(\mu/\sigma^2) - 4\mu\log(\sigma^2/\mu) + 4\mu\right) \\
I_{22} &= -\mathbb{E}\left[\frac{1}{\sigma^4}\left(6\mu^2\log(D) - 6\mu^2\log(\sigma^2/\mu) + 10\mu^2 - 6\mu^2\psi(\mu^2/\sigma^2) - 4\mu^4\psi^{'}(\mu^2/\sigma^2)/\sigma^2 - 6\mu D\right)\right] \\
&= \frac{1}{\sigma^4} \times \left(-6\mu^2(\psi(\mu^2/\sigma^2) - \log(\mu/\sigma^2)) + 6\mu^2\log(\sigma^2/\mu) - 10\mu^2\right. \\
&\qquad \left. +6\mu^2\psi(\mu^2/\sigma^2) + 4\mu^4\psi^{'}(\mu^2/\sigma^2)/\sigma^2 + 6\mu^2\right).
\end{aligned}
$$

We plugged in $\mathbb{E}[\log(D)] = \psi(\mu^2/\sigma^2) - \log(\mu/\sigma^2)$, which can be obtained via elementary integral calculations.
We invert the Fisher-information matrix and divide by n to obtain for the asymptotic variances of the asymptotic normal distributions of the estimators $\hat{\mu}^{\mathrm{ML}}$ and $\hat{\sigma}^{\mathrm{ML}}$ the values

$$
\mathbb{V}\mathrm{ar}\left(\hat{\mu}^{\mathrm{ML}}\right) \approx \frac{I_{11}^{-1}(\mu,\sigma)}{n} = \frac{1}{n}\frac{I_{22}(\mu,\sigma^2)}{I_{11}(\mu,\sigma^2)I_{22}(\mu,\sigma^2) - I_{12}(\mu,\sigma^2)^2} = \frac{\sigma^2}{n},
$$

where we do not show the last equal sign in detail and

$$
\mathbb{V}\mathrm{ar}\left(\hat{\sigma}^{\mathrm{ML}}\right) \approx \frac{I_{22}^{-1}(\mu,\sigma)}{n} = \frac{1}{n}\frac{I_{11}(\mu,\sigma^2)}{I_{11}(\mu,\sigma^2)I_{22}(\mu,\sigma^2) - I_{12}(\mu,\sigma^2)^2}.
$$

Note that as $\hat{\mu}^{\mathrm{ML}}$ is the sample mean even its exact variance is given by σ^2/n.

9.4 Parameter estimation: Intermittent presentation

The parameters of Hidden Markov Models are typically estimated via maximum likelihood. Prominent approaches carried out are the expectation maximization (EM) algorithm (Baum et al., 1970; Dempster et al., 1977) and direct numerical maximization (MacDonald and Zucchini, 1997). In this study, we focus on the EM algorithm, which is in the case of HMMs called Baum-Welch algorithm (BWA). In Section 9.4.1 we discuss the BWA and refer for more details to Baum et al. (1970); Dempster et al. (1977); Rabiner (1989); Bilmes (1998). Section 9.4.2 contains a short introduction to the direct numerical maximization idea.

9.4.1 Baum-Welch algorithm

For the HMM with inverse Gaussian dominance times we aim at estimating the parameter set $\Theta_{\mathrm{HMM}} := (\mu_S, \sigma_S, \mu_U, \sigma_U, p_{SS}, p_{UU}, \pi_{\mathrm{start},S})$ and for the HMM with Gamma distributions the

parameter set $\Theta_{\text{HMM}} := (\mu_S, \sigma_S, \mu_U, p_{SS}, p_{UU}, \pi_{\text{start},S})$ should be estimated. In both cases the likelihood $L(d|\Theta_{\text{HMM}})$ given by

$$L(d|\Theta_{\text{HMM}}) = \mathbb{P}\left(D_1^n = d_1^n|\Theta_{\text{HMM}}\right) = \pi_{\text{start}} E(d_1) P E(d_2) P \dots P E(d_n)(1,1)^T \tag{9.10}$$

is maximized with P as the transition matrix of the hidden Markov chain with diagonal entries p_{SS} and p_{UU} and $E(d_i)$ as diagonal matrices with the conditional densities $f_{\mu_S,\sigma_S}(d_i)$, $f_{\mu_U,\sigma_U}(d_i)$ on the diagonal (compare, e.g., Bulla (2006)).
The parameter set is estimated with the Baum-Welch algorithm (Baum et al., 1970) which is an iteratively working instance of the EM-Algorithm maximizing the model likelihood locally. Here, we explain its most important steps (for details see, e.g., Rabiner, 1989) and distinguish between IG and Gamma distributions when updating the emission parameters. A graphical summary of the algorithm can be found in Figure 9.11. In order to avoid computational problems when using very small numbers, we additionally present a scaling technique for the BWA. Moreover, we discuss starting values as well as constraints necessary to obtain reasonable estimates also for subjects with less clear distinction between stable and unstable dominance times.
In the first step of the BWA one applies the so-called forward- and backward-Algorithm. The forward-variable $\alpha_j(i) := \alpha_j(i|\Theta_{\text{HMM}}) := \mathbb{P}(D_1^i = d_1^i, Y_i = j|\Theta_{\text{HMM}})$ is defined as the probability of being in state j at time i and observing the sequence $d_1, d_2, \dots, d_i$ given the model parameters. The backward-variable $\beta_j(i) := \beta_j(i|\Theta_{\text{HMM}}) := \mathbb{P}(D_{i+1}^n = d_{i+1}^n|Y_i = j, \Theta_{\text{HMM}})$ denotes the probability of observing the ending partial sequence $d_{i+1}, d_{i+2}, \dots, d_n$ given state j at time i. Both variables can be derived iteratively as follows (Lemma 9.12 a) + b))

$$\alpha_j(1) = \pi_{\text{start},j} f_{\mu_j,\sigma_j}(d_1) \text{ and } \alpha_j(i+1) = f_{\mu_j,\sigma_j}(d_{i+1}) \sum_{k\in\{S,U\}} \alpha_k(i) p_{kj} \text{ for } i = 1, \dots, n-1$$

$$\beta_j(n) = 1 \text{ and } \beta_j(i) = \sum_{k\in\{S,U\}} p_{jk} f_{\mu_k,\sigma_k}(d_{i+1}) \beta_k(i+1) \text{ for } i = n-1, \dots, 1,$$

where $p_{SU} = 1 - p_{SS}$, $p_{US} = 1 - p_{UU}$, and $f_{\mu,\sigma}(x)$ denotes the density of the IG or the Gamma distribution with expectation μ and standard deviation σ evaluated at x. Note that we suppress the dependence of $\alpha_j(i)$ and $\beta_j(i)$ on the parameter set Θ_{HMM} for convenience.
The forward and backward variables are used to derive the probability
$\gamma_j(i) := \gamma_j(i|\Theta_{\text{HMM}}) := \mathbb{P}(Y_i = j|D_1^n = d_1^n, \Theta_{\text{HMM}})$ of being in state j at time i, given the whole sequence $d := (d_1, \dots, d_n)$ and the parameters Θ_{HMM} (Lemma 9.12 c))

$$\gamma_j(i|\Theta_{\text{HMM}}) = \frac{\alpha_j(i)\beta_j(i)}{\alpha_S(i)\beta_S(i) + \alpha_U(i)\beta_U(i)}.$$

Moreover, we need the probability
$\xi_{j,k}(i) := \xi_{j,k}(i|\Theta_{\text{HMM}}) := \mathbb{P}(Y_i = j, Y_{i+1} = k|D_1^n = d_1^n, \Theta_{\text{HMM}})$ of being in state j at time i and in state k at time $i+1$, given the whole data d and the parameters Θ_{HMM},

$$\xi_{j,k}(i|\Theta_{\text{HMM}}) = \frac{\alpha_j(i) p_{jk} \beta_k(i+1) f^{\text{IG}}_{\mu_k,\sigma_k}(d_{i+1})}{\sum_j \sum_k \alpha_j(i) p_{jk} \beta_k(i+1) f^{\text{IG}}_{\mu_k,\sigma_k}(d_{i+1})}$$

which is proven in Lemma 9.12 d).
To iteratively derive the parameter estimates, the BWA applies expectation maximization as follows. Let $\Theta^{(m)}_{\text{HMM}}$ denote the parameter estimates after the m-th iteration step, and let $\mathfrak{Y}$

denote the set of all possible state sequences of the hidden Markov chain. Let $Y = (Y_1, \ldots, Y_n)$ denote a $\mathfrak{Y}$-valued random variable and $y = (y_1, \ldots, y_n)$ a realization of Y. In the E-step (Figure 9.11) the *Q-function* (e.g., Ephraim and Merhav, 2002) over Y,

$$\begin{aligned} Q := Q(\Theta_{\text{HMM}}|\Theta_{\text{HMM}}^{(m)}) &:= \mathbb{E}\left[\log L\left(d, y|\Theta_{\text{HMM}}\right)|D = d, \Theta_{\text{HMM}}^{(m)}\right] \\ &= \sum_{y\in\mathfrak{Y}} \log L(d, y|\Theta_{\text{HMM}})\mathbb{P}(Y = y|d, \Theta_{\text{HMM}}^{(m)}), \end{aligned}$$

i.e., the expectation of the complete-data log-likelihood L across all possible paths $y \in \mathfrak{Y}$ is derived. In the M-step the updated parameter set $\Theta_{\text{HMM}}^{(m+1)}$ is chosen such that it maximizes Q. These iterative steps are repeated until a desired level of convergence is reached. Here, we stop the algorithm if the improvement in the log-likelihood from the last iteration to the present one is smaller than $\delta_{\text{stop}} = 0.005$ or if 1000 iterations were computed (compare also page 98).

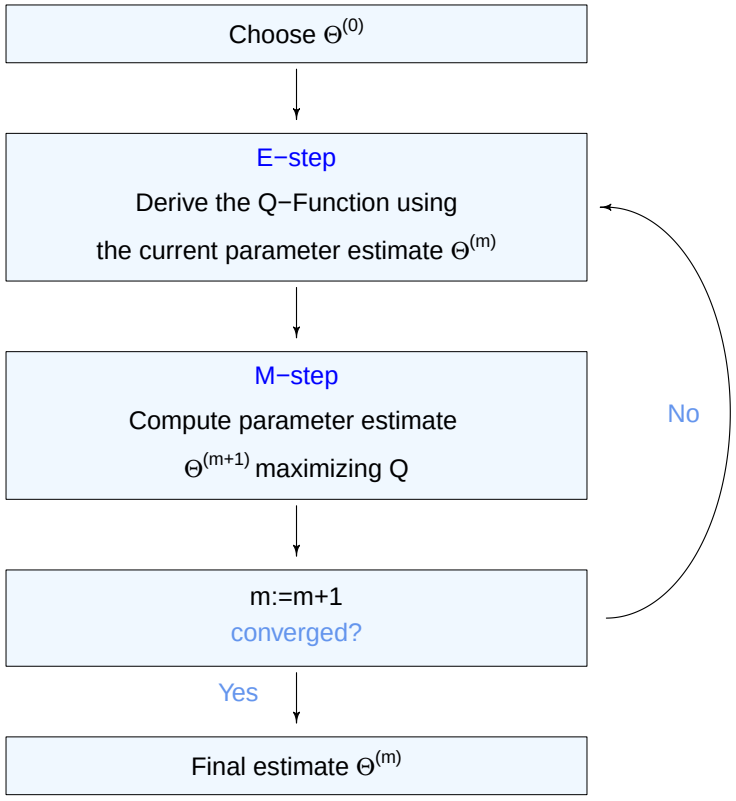

Figure 9.11: The Baum-Welch algorithm as Expectation-Maximization-Algorithm. *The steps are explained in detail in the main text. Note that we set* $\Theta := \Theta_{HMM}$ *in the graph.*

The following Lemma 9.11 – which shows that maximizing the Q-function is equivalent to maximizing the likelihood-function – is essential for the correctness of the Baum-Welch algorithm.

Lemma 9.11. ***Maximization of the Q-function***
It holds $Q\left(\Theta_{HMM}|\Theta_{HMM}^{(m)}\right) \geq Q\left(\Theta_{HMM}^{(m)}|\Theta_{HMM}^{(m)}\right) \Rightarrow L\left(D_1^n = d_1^n|\Theta_{HMM}\right) \geq L\left(D_1^n = d_1^n|\Theta_{HMM}^{(m)}\right)$.
Moreover,

$$Q\left(\Theta_{HMM}|\Theta_{HMM}^{(m)}\right) = Q\left(\Theta_{HMM}^{(m)}|\Theta_{HMM}^{(m)}\right) \Leftrightarrow L\left(D_1^n = d_1^n|\Theta_{HMM}^{(m)}\right) = L\left(D_1^n = d_1^n|\Theta_{HMM}\right).$$

Proof: See Ephraim and Merhav (2002). □

Next, we show in detail how to update the parameters in the $m+1$-st step. For a fixed state sequence $y = (y_1, \ldots, y_n)$ the log-likelihood of the data is

$$\log L(d, y|\Theta_{\text{HMM}}) = \log \pi_{\text{start},y_1} + \log f_{\mu_{y_1}\sigma_{y_1}}(d_1) + \sum_{i=2}^{n} \left(\log(p_{y_{i-1}y_i}) + \log(f_{\mu_{y_i},\sigma_{y_i}}(d_i))\right).$$

Insertion into Q yields (e.g., Ephraim and Merhav, 2002)

$$\begin{aligned} Q\left(\Theta_{\text{HMM}}|\Theta_{\text{HMM}}^{(m)}\right) = & \sum_{y_1\in\{S,U\}} \log \pi_{\text{start},y_1} \mathbb{P}(Y_1 = y_1|d, \Theta_{\text{HMM}}^{(m)}) \\ & + \sum_{i=2}^{n} \sum_{y_{i-1}\in\{S,U\}} \sum_{y_i\in\{S,U\}} \log p_{y_{i-1}y_i} \mathbb{P}(Y_{i-1} = y_{i-1}, Y_i = y_i|d, \Theta_{\text{HMM}}^{(m)}) \\ & + \sum_{i=1}^{n} \sum_{y_i\in\{S,U\}} \log f_{\mu_{y_i},\sigma_{y_i}}(d_i) \mathbb{P}(Y_i = y_i|d, \Theta_{\text{HMM}}^{(m}). \end{aligned} \tag{9.11}$$

Note that the first line depends only on the initial distribution π_{start}, the second line depends on the transition probabilities and the third line depends on the parameters of the IG or the Gamma distributions. Therefore, iterative parameter estimation separately maximizes these terms. Note further that we can rewrite $\mathbb{P}(Y_i = y_i|d, \Theta_{\text{HMM}}^{(m)}) = \gamma_{y_i}(i|\Theta_{\text{HMM}}^{(m)})$ and $\mathbb{P}(Y_{i-1} = y_{i-1}, Y_i = y_i|d, \Theta_{\text{HMM}}^{(m)}) = \xi_{y_{i-1}y_i}(i-1|\Theta_{\text{HMM}}^{(m)})$, which yields the following estimates in the $m+1$-st iteration step.
Using the Lagrangian multiplier Γ with the constraint $\sum_j \pi_{\text{start},j} = 1$ and setting the derivative with respect to $\pi_{\text{start},j}$ to zero, we obtain

$$\frac{\mathbb{P}(Y_1 = j|d, \Theta_{\text{HMM}}^{(m)})}{\pi_{\text{start},j}} + \Gamma = 0.$$

Multiplying with $\pi_{\text{start},j}$, summing over j to get Γ and solving for $\pi_{\text{start},j}$ we arrive at

$$\hat{\pi}_{\text{start},j}^{(m+1)} = \mathbb{P}(Y_1 = j|d, \Theta_{\text{HMM}}^{(m)}) = \gamma_j(1).$$

Alternatively to this procedure and in order to reduce the number of parameters we assume that the HMM starts in its stationary distribution $(\pi_S, 1-\pi_S) = (p_{UU}-1, p_{SS}-1)/(p_{SS}+p_{UU}-2)$ (Corollary 10.8). Under this assumption the initial distribution for the stable state is updated in the $m+1$-th step of the BWA by

$$\hat{\pi}_{\text{start},S}^{(m+1)} = \frac{\hat{p}_{UU}^{(m+1)} - 1}{\hat{p}_{SS}^{(m+1)} + \hat{p}_{UU}^{(m+1)} - 2} \tag{9.12}$$

and for the unstable state we obtain $\hat{\pi}^{(m+1)}_{\text{start},U} = 1 - \hat{\pi}^{(m+1)}_{\text{start},S}$.
For the entries of the transition matrix, Lagrange maximization of the second line of $Q\left(\Theta_{\text{HMM}}|\Theta^{(m)}_{\text{HMM}}\right)$ under the constraints $p_{SS} + p_{SU} = p_{UU} + p_{US} = 1$ yields the estimate

$$\hat{p}^{(m+1)}_{jk} = \frac{\sum_{i=2}^{n} \mathbb{P}(Y_{i-1} = j, Y_i = k|d, \Theta^{(m)}_{\text{HMM}})}{\sum_{i=2}^{n} \mathbb{P}(Y_{i-1} = j|d, \Theta^{(m)}_{\text{HMM}})} = \frac{\sum_{i=1}^{n-1} \xi_{j,k}(i|\Theta^{(m)}_{\text{HMM}})}{\sum_{i=1}^{n-1} \gamma_j(i|\Theta^{(m)}_{\text{HMM}})},$$

in the $(m+1)$-st step of the BWA (e.g., Rabiner, 1989).
Now, we investigate the term in the last line (9.11) of the Q-function (which we term $Q^*(\Theta_{\text{HMM}}|\Theta^{(m)}_{\text{HMM}})$) and distinguish between the assumption of inverse Gaussian and Gamma-distributed dominance times.

Parameter estimation for IG distributions

In the case of inverse Gaussian distributed observations we obtain

$$\begin{aligned} Q^*\left(\Theta_{\text{HMM}}|\Theta^{(m)}_{\text{HMM}}\right) =& \sum_{i=1}^{n} \mathbb{P}(Y_i = S|d, \Theta^{(m)}_{\text{HMM}}) \frac{1}{2} \log\left(\frac{\mu_S^3}{2\sigma_S^2 \pi d_i^3}\right) \\ &- \sum_{i=1}^{n} \mathbb{P}(Y_i = S|d, \Theta^{(m)}_{\text{HMM}}) \frac{\mu_S}{2\sigma_S^2} \frac{(d_i - \mu_S)^2}{d_i} \\ &+ \sum_{i=1}^{n} \mathbb{P}(Y_i = U|d, \Theta^{(m)}_{\text{HMM}}) \frac{1}{2} \log\left(\frac{\mu_U^3}{2\sigma_U^2 \pi d_i^3}\right) \\ &- \sum_{i=1}^{n} \mathbb{P}(Y_i = U|d, \Theta^{(m)}_{\text{HMM}}) \frac{\mu_U}{2\sigma_U^2} \frac{(d_i - \mu_U)^2}{d_i}. \end{aligned}$$

We maximize the first and the second line (for the third and fourth line all calculations can be done similarly). Derivating partially gives

$$\begin{aligned} \frac{\partial Q^*}{\partial \mu_S} =& \frac{3}{2\mu_S} \sum_{i=1}^{n} \mathbb{P}(Y_i = S|d, \Theta^{(m)}_{\text{HMM}}) - \frac{1}{2\sigma_S^2} \sum_{i=1}^{n} \mathbb{P}(Y_i = S|d, \Theta^{(m)}_{\text{HMM}}) \frac{(d_i - \mu_S)^2}{d_i} \\ &+ \frac{\mu_S}{\sigma_S^2} \sum_{i=1}^{n} \mathbb{P}(Y_i = S|d, \Theta^{(m)}_{\text{HMM}}) - \frac{\mu_S^2}{\sigma_S^2} \sum_{i=1}^{n} \mathbb{P}(Y_i = S|d, \Theta^{(m)}_{\text{HMM}}) \frac{1}{d_i} \end{aligned} \tag{9.13}$$

and

$$\frac{\partial Q^*}{\partial \sigma_S} = -\frac{1}{\sigma_S} \sum_{i=1}^{n} \mathbb{P}(Y_i = S|d, \Theta^{(m)}_{\text{HMM}}) + \frac{\mu_S}{\sigma_S^3} \sum_{i=1}^{n} \mathbb{P}(Y_i = S|d, \Theta^{(m)}_{\text{HMM}}) \frac{(d_i - \mu_S)^2}{d_i}.$$

Setting $\frac{\partial Q^*}{\partial \sigma_S} = 0$ and solving for σ_S we obtain

$$\sigma_S = \sqrt{\frac{\mu_S}{\sum_{i=1}^{n} \mathbb{P}(Y_i = S|d, \Theta^{(m)}_{\text{HMM}})} \sum_{i=1}^{n} \mathbb{P}(Y_i = S|d, \Theta^{(m)}_{\text{HMM}}) \frac{(d_i - \mu_S)^2}{d_i}}. \tag{9.14}$$

Plugging this in (9.13) and setting to zero yields

$$
\begin{aligned}
0 &= \frac{1}{\mu_S}\sum_{i=1}^{n}\mathbb{P}(Y_i = S|d,\Theta_{\text{HMM}}^{(m)}) + \frac{\left(\sum_{i=1}^{n}\mathbb{P}(Y_i = S|d,\Theta_{\text{HMM}}^{(m)})\right)^2}{\sum_{i=1}^{n}\mathbb{P}(Y_i = S|d,\Theta_{\text{HMM}}^{(m)})(d_i-\mu_S)^2/d_i} \\
&\quad - \frac{\mu_S\sum_{i=1}^{n}\mathbb{P}(Y_i = S|d,\Theta_{\text{HMM}}^{(m)})\sum_{i=1}^{n}\mathbb{P}(Y_i = S|d,\Theta_{\text{HMM}}^{(m)})\frac{1}{d_i}}{\sum_{i=1}^{n}\mathbb{P}(Y_i = S|d,\Theta_{\text{HMM}}^{(m)})(d_i-\mu_S)^2/d_i} \\
\Rightarrow 0 &= \sum_{i=1}^{n}\mathbb{P}(Y_i = S|d,\Theta_{\text{HMM}}^{(m)})(d_i-\mu_S)^2/d_i + \mu_S\sum_{i=1}^{n}\mathbb{P}(Y_i = S|d,\Theta_{\text{HMM}}^{(m)}) \\
&\quad - \mu_S^2\sum_{i=1}^{n}\mathbb{P}(Y_i = S|d,\Theta_{\text{HMM}}^{(m)})\frac{1}{d_i} \\
\Rightarrow \sum_{i=1}^{n}\mathbb{P}(Y_i = S|d_i,\Theta_{\text{HMM}}^{(m)})d_i &= \mu_S\sum_{i=1}^{n}\mathbb{P}(Y_i = S|d,\Theta_{\text{HMM}}^{(m)}) \\
\Rightarrow \hat{\mu}_S^{(m+1)} &= \frac{\sum_{i=1}^{n}\mathbb{P}(Y_i = S|d,\Theta_{\text{HMM}}^{(m)})d_i}{\sum_{i=1}^{n}\mathbb{P}(Y_i = S|d,\Theta_{\text{HMM}}^{(m)})} = \frac{\sum_{i=1}^{n}\gamma_S(i|\Theta_{\text{HMM}}^{(m)})d_i}{\sum_{i=1}^{n}\gamma_S(i|\Theta_{\text{HMM}}^{(m)})}.
\end{aligned}
$$

We plug this estimator in (9.14)

$$
\begin{aligned}
\hat{\sigma}_S^{(m+1)} &= \sqrt{\frac{\hat{\mu}_S^{(m+1)^3}}{\sum_{i=1}^{n}\mathbb{P}(Y_i = S|d,\Theta_{\text{HMM}}^{(m)})}\sum_{i=1}^{n}\mathbb{P}(Y_i = S|d,\Theta_{\text{HMM}}^{(m)})\frac{(d_i-\hat{\mu}_S^{(m+1)})^2}{\hat{\mu}_S^{(m+1)^2}d_i}} \\
&= \sqrt{\frac{\hat{\mu}_S^{(m+1)^3}}{\sum_{i=1}^{n}\mathbb{P}(Y_i = S|d,\Theta_{\text{HMM}}^{(m)})}\sum_{i=1}^{n}\mathbb{P}(Y_i = S|d,\Theta_{\text{HMM}}^{(m)})\left(\frac{1}{d_i}-\frac{1}{\hat{\mu}_S^{(m+1)}}\right)} \\
&= \sqrt{\frac{\hat{\mu}_S^{(m+1)^3}}{\sum_{i=1}^{n}\gamma_S(i,\Theta_{\text{HMM}}^{(m)})}\sum_{i=1}^{n}\gamma_S(i|\Theta_{\text{HMM}}^{(m)})\left(\frac{1}{d_i}-\frac{1}{\hat{\mu}_S^{(m+1)}}\right)}. \qquad (9.15)
\end{aligned}
$$

For the unstable dominance times we obtain similar results

$$
\begin{aligned}
\hat{\mu}_U^{(m+1)} &= \frac{\sum_{i=1}^{n}\gamma_U(i|\Theta_{\text{HMM}}^{(m)})d_i}{\sum_{i=1}^{n}\gamma_U(i|\Theta_{\text{HMM}}^{(m)})} \\
\hat{\sigma}_U^{(m+1)} &= \sqrt{\frac{\hat{\mu}_U^3}{\sum_{i=1}^{n}\gamma_U(i|\Theta_{\text{HMM}}^{(m)})}\sum_{i=1}^{n}\gamma_U(i|\Theta_{\text{HMM}}^{(m)})\left(\frac{1}{d_i}-\frac{1}{\hat{\mu}_U}\right)}. \qquad (9.16)
\end{aligned}
$$

Parameter estimation for Gamma distributions

Assuming Gamma-distributed stable dominance times and exponentially distributed dominance times in the unstable state and substituting $p_S = \mu_S^2/\sigma_S^2, \theta_S = \mu_S/\sigma_S^2$ (compare Remark 2.3) equation (9.11) becomes

$$\begin{aligned}
&Q^*\left(\Theta_{\text{HMM}}|\Theta_{\text{HMM}}^{(m)}\right) \\
&\quad= (p_S-1)\sum_{i=1}^{n}\mathbb{P}(Y_i=S|d,\Theta_{\text{HMM}}^{(m)})\log d_i - \log(\Gamma(p_S))\sum_{i=1}^{n}\mathbb{P}(Y_i=S|d,\Theta_{\text{HMM}}^{(m)}) \\
&\qquad- p_S\log\left(\frac{1}{\theta_S}\right)\sum_{i=1}^{n}\mathbb{P}(Y_i=S|d,\Theta_{\text{HMM}}^{(m)}) - \theta_S\sum_{i=1}^{n}\mathbb{P}(Y_i=S|d,\Theta_{\text{HMM}}^{(m)})d_i \\
&\qquad- \frac{1}{\mu_U}\sum_{i=1}^{n}\mathbb{P}(Y_i=U|d,\Theta_{\text{HMM}}^{(m)})d_i + \log\left(\frac{1}{\mu_U}\right)\sum_{i=1}^{n}\mathbb{P}(Y_i=U|D_i=d_i,\Theta_{\text{HMM}}^{(m)}) \\
&\quad= (p_S-1)\sum_{i=1}^{n}\mathbb{P}(Y_i=S|d,\Theta_{\text{HMM}}^{(m)})\overline{\log d_{w_S}} - \log(\Gamma(p_S))\sum_{i=1}^{n}\mathbb{P}(Y_i=S|d,\Theta_{\text{HMM}}^{(m)}) \\
&\qquad- p_S\log\left(\frac{1}{\theta_S}\right)\sum_{i=1}^{n}\mathbb{P}(Y_i=S|d,\Theta_{\text{HMM}}^{(m)}) - \theta_S\sum_{i=1}^{n}\mathbb{P}(Y_i=S|d,\Theta_{\text{HMM}}^{(m)})\overline{d_{w_S}} \\
&\qquad- \frac{1}{\mu_U}\sum_{i=1}^{n}\mathbb{P}(Y_i=U|d,\Theta_{\text{HMM}}^{(m)})d_i + \log\left(\frac{1}{\mu_U}\right)\sum_{i=1}^{n}\mathbb{P}(Y_i=U|d,\Theta_{\text{HMM}}^{(m)}).
\end{aligned}$$

In the latter display we made use of the weighted means

$$\overline{d_{w_S}} := \frac{\sum_{i=1}^{n}\mathbb{P}(Y_i=S|d,\Theta_{\text{HMM}}^{(m)})d_i}{\sum_{i=1}^{n}\mathbb{P}(Y_i=S|d,\Theta_{\text{HMM}}^{(m)})} \quad\text{and}\quad \overline{\log d_{w_S}} := \frac{\sum_{i=1}^{n}\mathbb{P}(Y_i=S|d,\Theta_{\text{HMM}}^{(m)})\log d_i}{\sum_{i=1}^{n}\mathbb{P}(Y_i=S|d,\Theta_{\text{HMM}}^{(m)})}.$$

Derivating $Q^*(\Theta_{\text{HMM}}|\Theta_{\text{HMM}}^{(m)})$ partially with respect to μ_U and setting the derivative to zero yields the well-known ML estimator for the Exponential distribution

$$\hat{\mu}_U^{(m+1)} = \frac{\sum_{i=1}^{n}\mathbb{P}(Y_i=U|d,\Theta_{\text{HMM}}^{(m)})d_i}{\sum_{i=1}^{n}\mathbb{P}(Y_i=U|d,\Theta_{\text{HMM}}^{(m)})} = \frac{\sum_{i=1}^{n}\gamma_U(i|\Theta_{\text{HMM}}^{(m)})d_i}{\sum_{i=1}^{n}\gamma_U(i|\Theta_{\text{HMM}}^{(m)})}.$$

Partially derivating $Q^*(\Theta_{\text{HMM}}|\Theta_{\text{HMM}}^{(m)})$ with respect to θ_S and setting the derivative to zero gives

$$\hat{\theta}_S = p_S/\overline{d_{w_S}}.$$

Finding an approximate ML estimate of p_S is more tricky. Again following Minka (2002) (compare Section 9.3.2) and applying a "generalized Newton" principle, we update $\hat{p}_{S_{\text{new}}}$ iteratively

$$\frac{1}{\hat{p}_{S_{\text{new}}}} = \frac{1}{\hat{p}_S} + \frac{\overline{\log d_{w_S}} - \log\overline{d_{w_S}} + \log\hat{p}_S - \psi(\hat{p}_S)}{\hat{p}_S^2\,(1/\hat{p}_S - \psi'(\hat{p}_S))}; \qquad \hat{p}_S = \hat{p}_{S_{\text{new}}}$$

until the change in p_S gets sufficiently small. As starting value

$$\hat{p}_S = \frac{1}{2(\log \overline{d_{w_S}} - \overline{\log d_{w_S}})}$$

is used (Minka, 2002).
The ML estimators for μ_S and σ_S are obtained by reparametrization

$$\hat{\mu}_S^{(m+1)} = \frac{\hat{p}_S}{\hat{\theta}_S} = \overline{d_{w_S}}$$
$$\hat{\sigma}_S^{(m+1)} = \frac{\hat{p}_S}{\hat{\theta}_S^2}.$$

The next lemma states that the derivations of the forward and backward variables as well as of $\gamma_j(i)$ and $\xi_{jk}(i)$ are correct (recall page 91).

Lemma 9.12. ***Correctness of the BWA***
It holds for $j \in \{S, U\}$

a)

$$\alpha_j(1) = \pi_{start,j} f_{\mu_j,\sigma_j}(d_1) \text{ and}$$
$$\alpha_j(i+1) = f_{\mu_j,\sigma_j}(d_{i+1}) \sum_{k\in\{S,U\}} \alpha_k(i) p_{kj} \text{ for } i = 1, \ldots, n-1,$$

b) $\beta_j(n) = 1$ *and* $\beta_j(i) = \sum_{k\in\{S,U\}} p_{jk} f_{\mu_k,\sigma_k}(d_{i+1})\beta_k(i+1)$ *for* $i = n-1, \ldots, 1$,

c) $\gamma_j(i) = \frac{\alpha_j(i)\beta_j(i)}{\alpha_S(i)\beta_S(i)+\alpha_U(i)\beta_U(i)}$,

d) $\xi_{j,k}(i) = \frac{\alpha_j(i)p_{jk}\beta_k(d_{i+1})f_k(d_{i+1})}{\sum_{j\in\{S,U\}}\sum_{k\in\{S,U\}}\alpha_j(i)p_{jk}\beta_j(d_{i+1})f_k(d_{i+1})}$.

Proof: a) The claim is shown inductively with the case $i = 1$ being trivial. For $i \to i+1$ it holds

$$\begin{aligned}
\alpha_j(i+1) &= \mathbb{P}(D_1^{i+1} = d_1^{i+1}, Y_{i+1} = j|\Theta_{\text{HMM}}) \\
&= \mathbb{P}(D_{i+1} = d_{i+1}|D_1^i = d_1^i, Y_{i+1} = j, \Theta_{\text{HMM}})\mathbb{P}(D_1^i = d_1^i, Y_{i+1} = j|\Theta_{\text{HMM}}) \\
&= f_{\mu_j,\sigma_j}(d_{i+1}) \sum_{k\in\{S,U\}} \mathbb{P}(D_1^i = d_1^i, Y_i = k|\Theta_{\text{HMM}})\mathbb{P}(Y_{i+1} = j|Y_i = k, \Theta_{\text{HMM}}) \\
&= f_{\mu_j,\sigma_j}(d_{i+1}) \sum_{k\in\{S,U\}} \alpha_k(i) p_{kj},
\end{aligned}$$

where in the third line the conditional independence and Markov property have been applied. In the fourth line, the definitions of $\alpha_k(i)$ and p_{jk} have been plugged in.
b), c) and d) follow by similar elementary calculations using the Markov and independence properties of the HMM. □

Computational issues of the BWA: Scaling

Note that $\alpha_j(i)$ essentially is the sum of terms each being a product

$$\left(\prod_{k=1}^{i-1} p_{y_k,y_{k+1}} \prod_{k=1}^{i-1} f_{\mu_{y_k},\sigma_{y_k}}(d_k)\right).$$

All terms with p are smaller than one and are often even close to zero. Moreover, the terms with f are typically close to zero. Thus, with increasing i the forward variable $\alpha_j(i)$ heads to zero which leads to computational problems. Similar problems are observable for the backward variable $\beta_j(i)$. Scaling offers a solution here. We need to find a scaling coefficient $c(i)$ depending only on i (and not on j) that is multiplied with $\alpha_j(i)$ and $\beta_j(i)$ in each step and cancels out at the end of computation.
We follow the ideas of Rabiner (1989); Turner (2008) and set $c(i) := \alpha_S(i) + \alpha_U(i)$ and divide the unscaled values of $\alpha_j(i)$ and $\beta_j(i)$ in each step of the forward- and backward-algorithm by $c(i)$ to obtain normalized values $\tilde{\alpha}_j(i), \tilde{\beta}_j(i)$. Formally,

$$\begin{aligned}
&\alpha_j^*(1) := \pi_{\text{start},j} f_{\mu_j,\sigma_j}(d_1), \qquad c(i) := \alpha_S^*(i) + \alpha_U^*(i), \qquad \tilde{\alpha}_j(i) := \alpha_j^*(i)/c(i),\\
&\alpha_j^*(i) := f_{\mu_j,\sigma_j}(d_i) \sum_{k\in\{S,U\}} \tilde{\alpha}_k(i-1)\tilde{p}_{kj} \text{ for } i = 2,\dots,n,\\
&\tilde{\beta}_j(n) = 1/c_n \text{ and } \tilde{\beta}_j(i) = \sum_{k\in\{S,U\}} p_{jk} f_{\mu_k,\sigma_k}(d_{i+1})\tilde{\beta}_k(i+1)/c(i) \text{ for } i = n-1,\dots,1.
\end{aligned}$$

To derive $\gamma_j(i)$ and $\xi_{j,k}(i)$ and consequently to update parameters, we always use the normalized values $\tilde{\alpha}_j(i), \tilde{\beta}_j(i)$ in the practical implementation (instead of $\alpha_j(i), \beta_j(i)$). Note, however, that – as it was intended – the scaling cancels out in the derivation of $\gamma_j(i)$ and $\xi_{j,k}(i)$, and therefore the resulting estimates in each iteration step are identical for the unscaled and the scaled version of the BWA. We show this for $\gamma_j(i)$ and refer for more details to Rabiner (1989). It holds

$$\begin{aligned}
\gamma_j(i) &= \frac{\tilde{\alpha}_j(i)\tilde{\beta}_j(i)}{\tilde{\alpha}_S(i)\tilde{\beta}_S(i) + \tilde{\alpha}_U(i)\tilde{\beta}_U(i)}\\
&= \frac{\prod_{k=1}^{i}(1/c_k)\alpha_j(i)\prod_{k=i+1}^{n}(1/c_k)\beta_j(i)}{\prod_{k=1}^{i}(1/c_k)\alpha_S(i)\prod_{k=i+1}^{n}(1/c_k)\beta_S(i) + \prod_{k=1}^{i}(1/c_k)\alpha_U(i)\prod_{k=i+1}^{n}(1/c_k)\beta_U(i)}\\
&= \frac{\left(\prod_{k=1}^{n}(1/c_k)\right)\alpha_j(i)\beta_j(i)}{\left(\prod_{k=1}^{n}(1/c_k)\right)\left(\alpha_S(i)\beta_S(i) + \alpha_U(i)\beta_U(i)\right)} = \frac{\alpha_j(i)\beta_j(i)}{\alpha_S(i)\beta_S(i) + \alpha_U(i)\beta_U(i)}.
\end{aligned}$$

The likelihood then derives as (Turner, 2008)

$$L(d|\Theta_{\text{HMM}}) = \alpha_S(n) + \alpha_U(n) = \prod_{i=1}^{n} c(i)(\tilde{\alpha}_S(n) + \tilde{\alpha}_U(n)) = \prod_{i=1}^{n} c(i),$$

yielding

$$\ell(d|\Theta_{\text{HMM}}) = \log L(d|\Theta_{\text{HMM}}) = \sum_{i=1}^{n} \log(c(i)).$$

Recall that the stopping rule for the BWA we use here is defined as: Stop the BWA if the improvement in the log-likelihood from the last iteration to the present one is smaller than $\delta_{\text{stop}} = 0.005$ or if 1000 iterations were computed.

Starting values and constraints

As starting values $\mu_S^{(s)}, \sigma_S^{(s)}, \mu_U^{(s)}, \sigma_U^{(s)}, p_{SS}^{(s)}, p_{UU}^{(s)}$ for the Baum-Welch algorithm we chose, in correspondence with the data set, $p_{SS}^{(s)} = p_{UU}^{(s)} = 0.5$; $\mu_U^{(s)} = 4$; $\sigma_U^{(s)} = 5$ (assuming inverse Gaussian distributed dominance times). In order to reduce the probability that the Baum-Welch algorithm will be captured in a local extremum, we chose ten equidistant values for $\mu_S^{(s)}$ ranging between 60 and $0.95 \max_i d_i$, and for each value of $\mu_S^{(s)}$ we choose ten equidistant values for $\sigma_S^{(s)}$ between 10 and $1.1\mu_S^{(s)}$. Very irregular stable distributions with a CV larger than 1.1 are not reasonable as consequently the stable and unstable dominance times are not separated clearly. Moreover, a mean of stable dominance times larger than the maximum length of dominance times is not reasonable. Out of the resulting one hundred sets of parameter estimates we chose the parameter set with the highest log-likelihood (satisfying also the constraints A)-C) below).

If the response pattern shows only dominance times larger than 30 seconds we reduce the model to the stable phase. The parameters μ_S and σ_S are derived by ML as described in Section 9.3.1.1, and we set $p_{SS} := 1$. If the dominance time are only smaller than 30 seconds, we only estimate μ_U and σ_U by ML and use $p_{UU} := 1$.

For subjects with relatively clear distinction between long and short dominance times this procedure yields reasonable estimates. For subjects with less clear distinction, we added the following constraints based on the idea that short dominance times should not affect estimation of the stable parameters and long dominance times should not affect estimation of unstable parameters. Note that in continuous presentation where only one state exists, about 90% of the dominance times are shorter than 15 seconds, while only about two percent are larger than 30 seconds. Therefore, we require the following conditions

$$\text{A) } \hat{\sigma}_S > 1 \qquad \text{B) } \hat{\mu}_S \geq 0.98\hat{\mu}_{15} \qquad \text{C) } \hat{\mu}_S < 1.02\hat{\mu}_{75}$$

with $\hat{\mu}_k := (1/\sum_{i=1}^n \mathbb{1}_{d_i>k}) \sum_{i=1}^n d_i \mathbb{1}_{d_i>k}$ if any dominance time is larger than k seconds and $\hat{\mu}_k = k$ else. A) prevents that not just the largest dominance time is estimated as stable and all others are categorized as unstable (which may increase the likelihood). B) prevents dominance times smaller than 15 seconds to be considered for the estimation of μ_S. Third, we require C) such that rather stable dominance times longer than 75 seconds are not classified as unstable.

Instead of rejecting the result of the BWA for a given set of starting values when the conditions A)-C) are not fulfilled one may also stop the updating procedure immediately when parameters not satisfying the constraints are estimated and then take the last parameters that are not outside the parameter range as result of the BWA. This is slightly less robust but leads for the great majority of cases to the same results and has also comparable estimation precision properties.

For the HMM with Gamma-distributed dominance times, we use as starting value for the Exponential distribution $\mu_U^{(s)} = 5$. All other starting values and the constraints are identical to the inverse Gaussian-HMM.

To derive confidence intervals for the HMM parameters (block) bootstrap approaches are thinkable (e.g., Efron and Tibshirani, 1994; Scholz, 2007).

IG distribution: UMVU inspired estimators

As explained in Section 9.3.1, the ML estimator of σ for the IG distribution is biased. Hence, the BWA estimates of the standard deviations in the stable and the unstable state are also biased as they are based on the ML principle. Applying UMVU estimators would lead to unbiased estimators of σ_S and σ_U. However, note that the corresponding ML estimators are a kind of weighted means (equations (9.15) and (9.16)) as

$$\hat{\sigma}_j^{(m+1)} = \sqrt{\frac{\hat{\mu}_j^3}{\sum_{i=1}^n \gamma_j(i)} \sum_{i=1}^n \gamma_j(i) \left(\frac{1}{d_i} - \frac{1}{\hat{\mu}_j} \right)}$$

for $j \in \{S, U\}$ and with $\gamma_j(i)$ as the probability of being in state j at time i given the estimated parameters and all observations (resulting from the BWA). The derivation of UMVU estimators for $\hat{\sigma}_S$ and $\hat{\sigma}_U$ being weighted means is an open question. Here, we give a first idea how UMVU inspired estimators may be included in the BWA without claiming theoretical correctness. We just apply an intuitive idea.
The usual BWA estimators $\hat{\Theta}_{\text{HMM}}$ are used as initial points for the UMVU inspired estimation. Define $v_j := \sum_{i=1}^n \gamma_j(i)(1/d_i - 1/\hat{\mu}_j)$ and $\tilde{n}_j := (\sum_{i=1}^n \gamma_j(i))^2 / \sum_{i=1}^n \gamma_j(i)^2$. v_j plays the role of v in the traditional UMVU estimation (compare equation (9.5)). The weighting factor $\tilde{n}_j$ is motivated by the variance of a random variable $Z := \sum w_i X_i / \sum w_i$ where $w_i \geq 0$ are weights and X_i i.i.d. with variance σ^2. It holds $\mathbb{V}\text{ar}(Z) = \sum w_i^2 \sigma^2 / (\sum w_i)^2$ as can be shown by a short derivation. In our case the X_i are the $\frac{1}{d_i} - \frac{1}{\hat{\mu}_j}$ and w_i is $\gamma_j(i)$. Inspired by the UMVU estimator for σ (Corollary 9.10) we define the UMVU inspired estimator for $\sigma_j, j \in \{S, U\}$ as

$$\hat{\sigma}_j^{\text{UMVU}} := \frac{\Gamma(\tilde{n}_j - 1)/2}{\sqrt{2}\Gamma(\tilde{n}_j/2)} (\hat{\mu}_j^3 v_j)^{1/2} \times F\left(\frac{1}{4}, \frac{3}{4}; \frac{\tilde{n}_j}{2}; -\frac{\hat{\mu}_j v_j}{\tilde{n}_j} \right). \tag{9.17}$$

The estimates of $\mu_S, \mu_U, p_{SS}, p_{UU}$ remain unchanged. Thus, the only difference compared to the traditional Baum-Welch algorithm is that we re-estimate the estimators for the standard deviations in the end of the estimation procedure using equation (9.17). In case of only stable or only unstable dominance times, we use the usual UMVU estimator of σ (given in Corollary 9.10). In Section 9.6.3.2, we compare the bias of the traditional BWA and the UMVU inspired estimates of σ_S and σ_U empirically.

Remark on the estimation implementation

The estimation of model parameters speeds up remarkably when outsourcing parts of the code from the statistical package `R` to the widely used programming language `C++`. When estimating the Hidden Markov Model the forward- and backward algorithm are typically performed in loops, which are not recommended to use in `R`. Therefore, we suggest to perform these algorithms in `C++` using the weights of the inverse Gaussian or the Gamma distribution for each data point as input.

9.4.2 Direct numerical maximization of the log-likelihood

Besides the traditional approach of estimating Hidden Markov Models by the Baum-Welch algorithm direct numerical maximization (DNM) of the log-likelihood was introduced by several authors (e.g., MacDonald and Zucchini, 1997; Turner, 2008). The (scaled) forward

variables $\tilde{\alpha}_j(i)$ are used to compute the likelihood of the complete model given the parameter set Θ_{HMM}

$$L(d_1, \ldots, d_n|\Theta_{\text{HMM}}) = \prod_{i=1}^{n} c(i)(\tilde{\alpha}_S(n) + \tilde{\alpha}_U(n)) = \prod_{i=1}^{n} c(i),$$

where $(c(i))_{i=1,\ldots,n}$ are the normalizing constants defined on page 98. The corresponding log-likelihood $\sum_i \log(c(i))$ is maximized subject to the constraints

A) $\hat{\mu}_S > 0.98\hat{\mu}_{15}$ B) $\hat{\mu}_S < 1.02\hat{\mu}_{75}$ C) $\hat{\sigma}_S < 1.2\hat{\sigma}_{15}$ D) $\hat{p}_{SS} \in [0,1]$ E) $\hat{p}_{UU} \in [0,1]$

applying the Newton-type algorithm implemented in the `R`-function `nlm()`. In the latter display we use $\hat{\sigma}_k := (1/\sum_{i=1}^{n} \mathbb{1}_{d_i>k}) \sum_{i=1}^{n} (d_i - \hat{\mu}_k)^2 \mathbb{1}_{d_i>k}$ if any dominance time is larger than k seconds and 0 else. We only accept estimates where all constraints are fulfilled. Constraints A) and B) are also used for the BWA and constraints D) and E) are due to the model formulation. Constraint C) prevents the distribution of the stable dominance times to be implausibly irregular.
This approach can be used for the HMM with IG as well as for the HMM with Gamma-distributed dominance times.

Censored dominance times

Like in the continuous viewing experiment we did not consider the censored last dominance time d_{n+1} until now. Using the direct likelihood maximization approach, it is straightforward how to include this censored dominance time. For $\tilde{\alpha}_j(1), \ldots, \tilde{\alpha}_j(n)$ with $j \in \{S, U\}$ the estimates remain changed, but we define $\alpha_j^*(n+1)$ as follows

$$\alpha_j^*(n+1) = (1 - F_{\mu_j,\sigma_j}(d_{n+1})) \sum_{i \in \{S,U\}} p_{ij}\tilde{\alpha}_i(n)$$

and norm it to obtain $\tilde{\alpha}_j(n+1)$. Depending on the model F_{μ_j,σ_j} is the distribution function of either the inverse Gaussian or the Gamma distribution (for $j = U$ F_{μ_j,σ_j} is in the second case the distribution function of the $\exp(1/\mu_U)$-distribution). Thereby, $c(n+1) = \alpha_S^*(n+1) + \alpha_U^*(n+1)$. Then, the resulting log-likelihood $\sum_i \log(c(i))$ is maximized subject to the constraints A)-E) given above.

9.4.3 ML estimators: Asymptotic distribution

As with the ML estimators for the IG or the Gamma distribution asymptotic properties of the ML estimators for the two-state HMM are of principal interest. The consistency and asymptotic normality of maximum likelihood estimators for HMMs was shown first by Baum and Petrie (1966) assuming a finite state space, stationarity and some more technical conditions. Bickel et al. (1998) generalized these results assuming regularity conditions on the conditional distributions. Moreover, it is to assure that the log-likelihood of the HMM is twice continuously differentiable and that the score function and the observed information have finite first two moments. A detailed treatise of the statistical properties of the ML estimator for Hidden Markov Models can be found in Cappé et al. (2005). We leave it for future work to check in detail if the conditions for consistency and asymptotic normality are fulfilled by

the HMM used in this chapter. Note, however, that the sample sizes given in the data sets of Schmack et al. (2013, 2015) are small and therefore asymptotic results are not necessarily of major practical importance for this thesis.

9.5 Parameters of example response patterns

In Figure 9.1 response patterns typical for continuous and intermittent presentation are shown. For intermittent presentation, we chose examples of a stable response pattern with only three perceptual reversals (panel E), a rather unstable response pattern with many changes (F) and two examples of response patterns with long stable as well as short unstable dominance times with different degrees of regularity (C and D). In terms of visual inspection, all other response patterns in the data sets Schmack et al. (2013, 2015) are similar to panel A or B for continuous presentation and C, D, E or F for intermittent presentation (compare Figures A.1 and A.2 in the appendix). Here, we fit Hidden Markov Models with inverse Gaussian distributed dominance times to the response patterns from Figure 9.1 and show the estimated parameters.

9.5.1 Continuous presentation

Table 9.1 gives the estimated parameter combinations for the two original response patterns visualized in Figure 9.1 (page 70, panels A and B). The histograms of the dominance times are plotted in Figure 9.2 A and B.

panel	μ	σ
A	10.50	8.18
B	6.69	3.58

Table 9.1: Estimated exemplary HMM parameter combinations for continuous presentation *assuming IG distributed dominance times. The original data response patterns are shown in Figure 9.1 A and B (page 70).*

9.5.2 Intermittent presentation

In Table 9.2 we show the estimated parameter constellations for the four realizations shown in Figure 9.1 C-F. The corresponding dominance time histograms are printed in Figure 9.2 C-F.

panel	μ_S	σ_S	μ_U	σ_U	p_{SS}	p_{UU}	$\pi_{\text{start},S}$
C	186.45	30.50	5.01	3.06	0.67	0.96	0.11
D	67.12	50.81	3.25	2.76	0.33	0.82	0.21
E	372.28	68.30	NA	NA	1.00	NA	1.00
F	77.13	9.99	5.37	6.26	0.00	0.99	0.01

Table 9.2: Estimated exemplary HMM parameter combinations for intermittent presentation *assuming IG distributed dominance times. The corresponding data response patterns are shown in Figure 9.1 C-F (page 70). The entry NA implies that only the parameters of the stable state were estimated as only long dominance times larger than 30 seconds occur (compare page 99).*

9.6 Precision of parameter estimates

Basic error measures are defined in the first part of this section (Section 9.6.1). Simulations to quantify the quality of the fitting procedure for the continuous HMM follow where also censored dominance times are included (Section 9.6.2). In the last part, the estimation precision of the HMM for intermittent presentation is investigated including short paragraphs about the estimation precision of the UMVU inspired approach and the DNM approach (Section 9.6.3). Note that we focus on the HMM with inverse Gaussian distributed observations here as the inverse Gaussian distribution first provides a better fit to the data (compare Section 14.1.3), and second inverse Gaussian distributed dominance times are directly comparable to the dominance times of the later on introduced Hierarchical Brownian Model.

9.6.1 Error measures

Let $\hat{\theta}$ be an estimator of the true parameter $\theta \in \mathbb{R}$ and $(\hat{\theta}_i)_{i=1,\dots,n}$ be a sample of realizations of $\hat{\theta}$. To quantify the estimation precision, we introduce (or recall) two error measures. The *absolute error* (AE) is defined as

$$\mathrm{AE}(\hat{\theta}_i) := \mathrm{AE}_\theta(\hat{\theta}_i) := |\hat{\theta}_i - \theta|,$$

and the *absolute relative error* (RE) is given by

$$\mathrm{RE}(\hat{\theta}_i) := \mathrm{RE}_\theta(\hat{\theta}_i) := \frac{\mathrm{AE}(\hat{\theta}_i)}{\theta}.$$

9.6.2 Continuous presentation

In order to investigate the estimation precision for small data sets, we applied parametric bootstrap. For each parameter combination $(\mu_i, \sigma_i)_{i=1,\dots,61}$ estimated from the data set Schmack et al. (2015) we simulated 1000 response patterns with length $T = 240s$ as in the original data. We then compared the estimators $(\hat{\mu}_i, \hat{\sigma}_i)_{i=1,\dots,61}$ with the true parameter values using the RE. The median relative errors for the 61 parameter constellations are shown in Figure 9.12 A. Out of these, 54 (89%) showed estimation errors with median REs less than 0.25 (across the two parameters μ and σ, black). The remaining simulations (dark orange) showed only few percept changes, $n < 20$, as well as large coefficient of variation (σ/μ, Figure 9.12 B).
Simulation results for the Gamma distribution are comparable (data not shown).

Precision of parameter estimates including censored dominance times

The estimation precision of the ML estimators including the censored last dominance times can be evaluated using the same parametric bootstrap method as described above. The results are comparable, i.e., the effect of including the censored last dominance time is negligible. This is due to the relatively large number of dominance times during continuous presentation (the median number of dominance times in Schmack et al. (2015) is 27) such that the effect of including an additional (censored) dominance time is small.

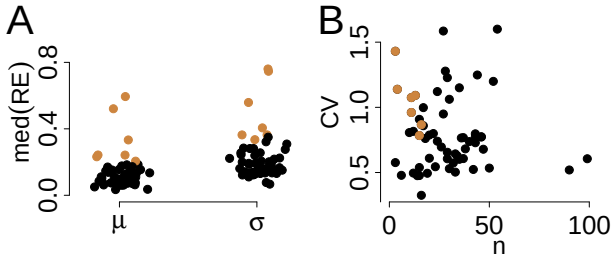

Figure 9.12: Precision of parameter estimates in the one-state HMM. *For each of 61 parameter constellations in continuous presentation, 1000 simulations were performed with sample sizes as in Schmack et al. (2015). (A) Median of the relative error (RE) for each parameter and (B) a scatterplot of CV and n for the parameter estimates. Black points indicate constellations with mean RE across the parameters smaller than* 0.25*.*

9.6.3 Intermittent presentation

9.6.3.1 Precision of parameter estimates using the BWA

In order to investigate the estimation precision of the Baum-Welch algorithm, we again apply parametric bootstrap to the 61 parameter combinations estimated from the response patterns to intermittent presentation in the sample data set. Figure 9.13 shows the median errors obtained in 1000 simulations for every parameter constellation for $T_1 = 1200$ s (like in Schmack et al. (2013, 2015)) and $T_2 = 3600$ s where $\pi_{\text{start},S}$ is not analyzed as it is estimated as function of p_{SS} and p_{UU} (9.12). For p_{SS} and p_{UU} the absolute errors are presented due to the small values of the two parameters. For the time horizon of the data, T_1 (panel A), 50 of the 61 parameter combinations yielded average errors (i.e., mean median errors across all parameters) smaller than 0.25 (black). The remaining cases (dark orange) showed a large $\text{CV}_U = \sigma_U/\mu_U$, i.e., less distinguishable stable and unstable distributions, or small sample size $n \approx 10$ (panel C). For the larger time horizon T_2 (panel B), almost all parameter combinations showed errors smaller than 0.25.
The HMM with Gamma-distributed dominance times yields comparable results concerning the precision of parameter estimation. Moreover, subjects yielding large estimation errors for the IG-model often also yield comparatively large errors for the model with Gamma-distributed dominance times (data not shown).

9.6.3.2 Precision of parameter estimates using UMVU inspired estimates

We discussed in Section 9.4.1 (page 100) that UMVU inspired estimators could improve the estimation results of the estimators of the standard deviations, especially concerning bias. Figure 9.14 now shows the simulated median bias (defined as the difference between the empirical median of the estimator and the true value) of $\hat{\sigma}_S$ (panel A) and $\hat{\sigma}_U$ (B) depending on the estimation procedure (ML or UMVU inspired) for the 61 subjects of Schmack et al. (2015) and using $T_1 = 1200$ s.

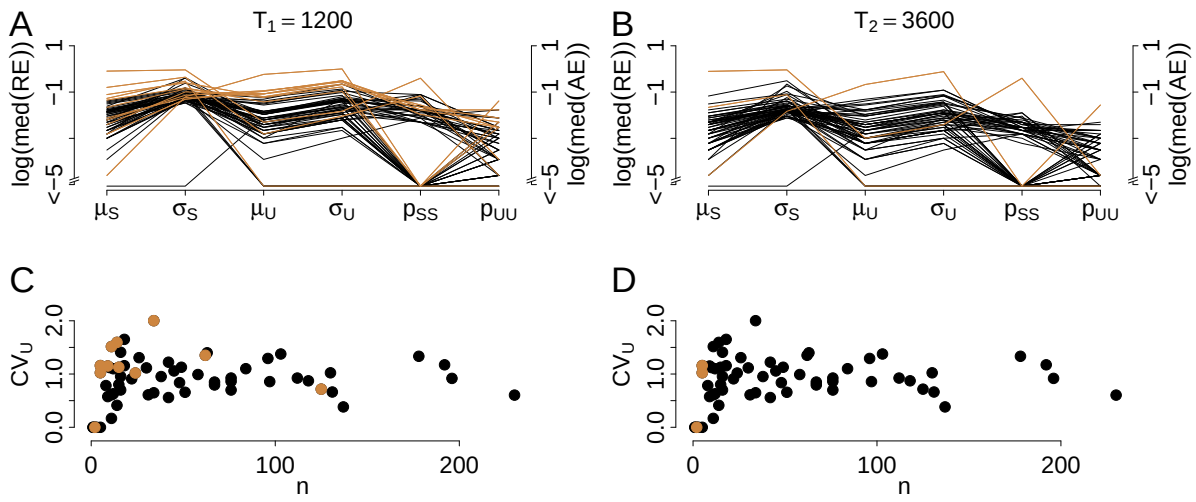

Figure 9.13: Precision of parameter estimates in the two-state HMM. *For each of 61 parameter constellations in intermittent presentation 1000 simulations were performed. Log(median) of RE (for $\mu_S, \sigma_S, \mu_U, \sigma_U$) or of AE (for p_{SS}, p_{UU}) for $T_1 = 1200$ (A) and $T_2 = 3600$ (B). Black lines indicate constellations with mean error across the parameters < 0.25. (C) and (D): Scatterplot of CV_U and the sample size n where parameter combinations yielding large mean errors ≥ 0.25 are printed dark orange for $T_1 = 1200$ (C) and $T_2 = 3600$ (D).*

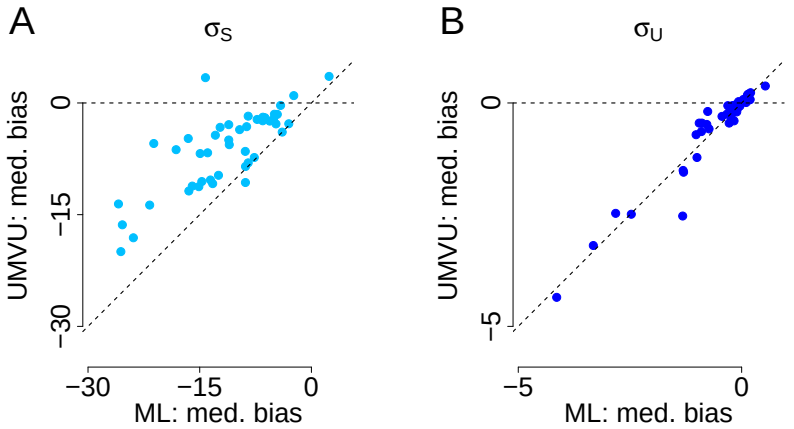

Figure 9.14: Comparison of ML and UMVU inspired estimators. *The simulated median bias (defined as the difference between the empirical median of the estimator and the true value) is shown for ML and UMVU inspired estimators for σ_S (A) and σ_U (B). Each point represents the median bias of the ML estimator (x-axis) and the UMVU inspired estimator (y-axis) for the response pattern of one subject in Schmack et al. (2015). To derive the median bias 1000 simulations were performed. Additionally, the main diagonal is drawn.*

For almost all subjects shown in Figure 9.14 A the median bias of the UMVU inspired estimator of σ_S is smaller than the median bias of the ML estimator. For σ_U this effect is visible much less clearly (panel B) as there are more unstable dominance times which decrease the bias of the ML estimator and make it comparable to the UMVU inspired estimator in terms of bias. The relative errors for the two types of estimators are comparable (data not shown). However, recall that the UMVU inspired estimators are just intuitive estimators which lack further detailed mathematical considerations.

9.6.3.3 Fitting the HMM to the data set Schmack et al. (2015) via Direct Numerical Maximization

We now estimate the HMM parameters of the 61 response patterns in the data set Schmack et al. (2015) via direct numerical maximization (DNM) explained in Section 9.4.2. Moreover, we contrast the results with the estimation results obtained by the Baum-Welch algorithm.
For 37 of the 61 subjects in Schmack et al. (2015) the estimated likelihoods of BWA and DNM are identical, for ten the DNM likelihood is less than one percent worse and for another ten subjects the likelihood of the DNM is even more than one percent smaller than the BWA likelihood. For four subjects the DNM approach yields slightly larger likelihoods than the BWA. In addition, simulations with the DNM estimated parameters in some cases with smaller likelihoods do not yield such convincing results as simulations with the parameters estimated using the BWA. Therefore, we recommend to apply the BWA to estimate the HMM parameters.

Precision of parameter estimates using the DNM approach

Comparing the estimation precision of the DNM approach with the BWA approach using the response patterns of the 61 subjects in Schmack et al. (2015) yields better results for the BWA. For the recording length $T = 1200$ s the DNM yields 27 subjects with a mean median relative error larger than 0.25, where the BWA only yields eleven subjects. For $T = 3600$ s there are for the BWA three subjects with a mean median relative error larger than 0.25 and for the DNM twelve subjects.

Precision of parameter estimates including censored dominance times

The estimation precision when including the censored dominance times via the DNM method can be evaluated using the data set of (Schmack et al., 2015). It should be compared to the DNM method in the paragraph above. The results are comparable, i.e., the effect of including the censored last dominance time is small.

Chapter 10

The HMM: Theoretical properties

In this chapter we aim to investigate the mathematical properties of the sequences of dominance times generated by the Hidden Markov Model more in detail thereby also deriving quantities important for the comparison of clinical groups. There are several possibilities to interpret these sequences. First, the points in time where the perception changes can be understood as point process on the (non-negative) real line. Second, the perceptual reversals may be interpreted as renewal points and the whole process in the case of continuous stimulation as renewal process. When incorporating the stable and unstable phases occurring in intermittent presentation, the process can be connected to an alternating renewal process (e.g., Medhi, 2009) introduced in Chapter 8.2.3.1.
In this chapter we always assume HMMs with inverse Gaussian distributed emissions. In Section 10.1 we derive results on the distribution and expectation of the number of perceptual reversals during continuous presentation. The central theme of Section 10.2 is the theoretical investigation of the point process induced by the HMM for intermittent presentation (HMMi). First, we explain the connection to semi-Markov processes. Then, the number of changes is discussed as well as first passage times, stationary distributions and renewal equations. Note that first passage times are required for the derivation of the steady-state distribution, which is very important to analyze differences between clinical groups as an increased time spent in the unstable state is an indicator for a less stable perception. Thus, Corollary 10.8 about the steady-state distribution is the result in this chapter being most important for application. Moreover, we investigate the expectation and distribution of the residual time. A knowledge about the residual time enables us to make a prognosis about the next perceptual reversal.
We understand Ξ_{HMMc} and Ξ_{HMMi} as the point processes on the non-negative line generated by the points in time $(t_0, t_1, t_2, \ldots, t_n)$ of the perceptual reversals of the HMM for continuous (HMMc) and for intermittent presentation, respectively. There, we use $t_0 = 0$. Formally, for the set of realized dominance times $(d_1, d_2, \ldots, d_n)$ of a HMMc

$$\Xi_{\text{HMMc}} := \{0\} \cup \{t \in \mathbb{R} | \sum_{i=1}^{k} d_i = t, k = 1, 2, \ldots, n\} = \{t_0, t_1, t_2, \ldots, t_n\}$$

and equivalently for the set of dominance times $(d_1, d_2, \ldots, d_n)$ of a HMMi

$$\Xi_{\text{HMMi}} := \{0\} \cup \{t \in \mathbb{R} | \sum_{i=1}^{k} d_i = t, k = 1, 2, \ldots, n\} = \{t_0, t_1, t_2, \ldots, t_n\}.$$

We define $\tilde{Y}_t := (\tilde{Y}_t)_{t\geq 0}$ as the hidden state at time t governing the point process Ξ_{HMMi} (in contrast to Y_i which is the hidden state of the i-th dominance time). In precise terms,

$$\begin{aligned}\tilde{Y}_t &:= j \in \{S,U\} | \sum_{i=1}^{k} d_i \leq t < \sum_{i=1}^{k+1} d_i, Y_{k+1} = j, \quad k = 0,1,2,\ldots,n-1 \\ &= Y_i \text{ on } t_{i-1} \leq t < t_i,\end{aligned}$$

with $\sum_{i=1}^{0} d_i := 0$. The difference between Y_i and $\tilde{Y}_t$ is illustrated in Figure 10.1 for a simulated example of a HMMi. Panel C shows $\tilde{Y}_t$ as variable defined on a continuous time space, and panel D shows Y_i as variable defined on a discrete time space. $\tilde{Y}_t$ may be described using an alternating renewal process with states S and U or a regenerative process (compare Sections 8.2.3.1 and 8.2.3.2).

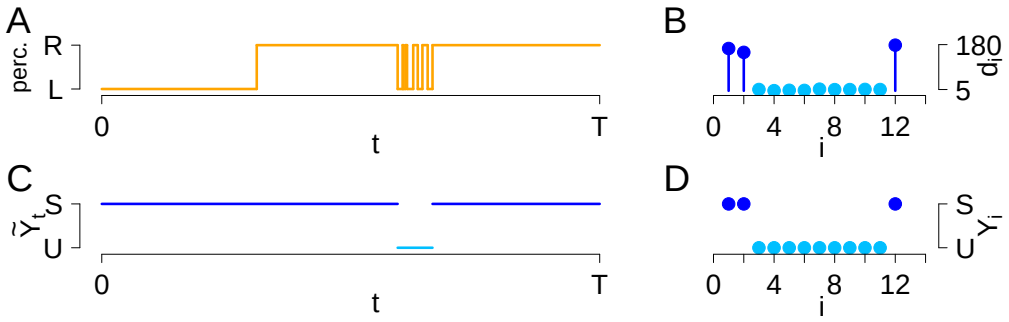

Figure 10.1: Overview of different variables in the HMM. *(A) The perception at time $t \in [0,T]$. (B) The resulting dominance times $(d_i)_{i\geq 1}$. (C) The hidden state $\tilde{Y}_t$ on the continuous axis $[0,T]$. (D) The hidden state Y_i of each dominance time d_i.*

Note that Ξ_{HMMi} is not a continuous time Markov chain as the probabilities $\mathbb{P}(\tilde{Y}_t = S|\tilde{Y}_s = S), 0 \leq s < t$ depend on how long the current state is S and thus also depend on the state of the chain at points in time $s_1, s_2, \ldots < s$. As a simple example, imagine that the hidden state changes at time $t = 100$ from unstable to stable. Then, we observe that $\mathbb{P}(\tilde{Y}_{200} = S|\tilde{Y}_{150} = S) \neq \mathbb{P}(\tilde{Y}_{200} = S|\tilde{Y}_{150} = S, \tilde{Y}_{101} = S)$ as the inverse Gaussian distribution is not memoryless.
Often we speak of "phases": A stable phase comprises all stable dominance times between a change from the unstable to the stable state and the change back to the unstable state. An unstable phase is defined analogously.

10.1 Continuous presentation

In this section the number of changes in the HMM as well as the residual time are analyzed.

10.1.1 Number of changes

We derive the distribution and (asymptotic) expectation of the number of perceptual changes in a given interval of length $\Delta \geq 0$ starting with a perceptual change. There, we use that the distribution function $\tilde{F}_{M_\nu(t)}$ of the maximum $M_\nu(t)$ of a Brownian motion with drift $\nu > 0$ is

given by (Corollary 7.2.2 in Shreve, 2004)

$$\tilde{F}_{M_\nu(t)}(m) = \Phi\left(\frac{m-\nu t}{\sqrt{t}}\right) - \exp(2\nu m)\,\Phi\left(\frac{-m-\nu t}{\sqrt{t}}\right) \tag{10.1}$$

for $m \geq 0$ and by 0 else, where Φ is the distribution function of the standard normal distribution.

Proposition 10.1. ***Number of changes in the HMMc***
Let (μ, σ) be the parameter set of a HMM for continuous presentation and $I(\Delta)$ be a right-open interval of length $\Delta \geq 0$ starting with a perceptual change. Let $b := \sqrt{\mu^3/\sigma^2}$ and $\nu := \sqrt{\mu/\sigma^2}$. The number of perceptual changes in this interval $N(\Delta)$ has the following probability distribution

$$w_\Delta(j) := \mathbb{P}(N(\Delta) = j) = \tilde{F}_{M_\nu(\Delta)}(jb) - \tilde{F}_{M_\nu(\Delta)}((j-1)b),$$

for $j \geq 1$ and 0 else with $\tilde{F}_{M_\nu(t)}(m)$ as in (10.1). For $\Delta \to \infty$ it holds for the expected number of changes in the interval $I(\Delta)$: $\frac{\mathbb{E}[N(\Delta)]}{\Delta} \to \frac{1}{\mu}$.

Note that $w_\Delta(1)$ also writes as $w_\Delta(1) = \tilde{F}_{M_\nu(\Delta)}(b)$ as $\tilde{F}_{M_\nu(\Delta)}(0) = 0$.

Proof: By transferring the parameters μ and σ to b and ν we interpret the inverse Gaussian distributed dominance times as hitting times of a border $b > 0$ by a Brownian motion $W := (W_t)_{t\geq 0}$ with drift $\nu > 0$ starting in 0 (Proposition 8.6). Having hit jb for $j \geq 0$ the border is instantaneously set to $(j+1)b$ (Figure 10.2). Note that the first change occurs at the beginning of the interval. Thus, j changes in the interval $I(\Delta)$ correspond to the Brownian motion having crossed $(j-1)b$ but not jb in the interval $I(\Delta)$. This means that in the interval $I(\Delta)$ the maximum distance covered was in $[(j-1)b, jb)$. As for a Brownian motion with drift $\nu > 0$ this distance has the distribution function $\tilde{F}_{M_\nu(\Delta)}(m)$ (10.1), the assertion follows.

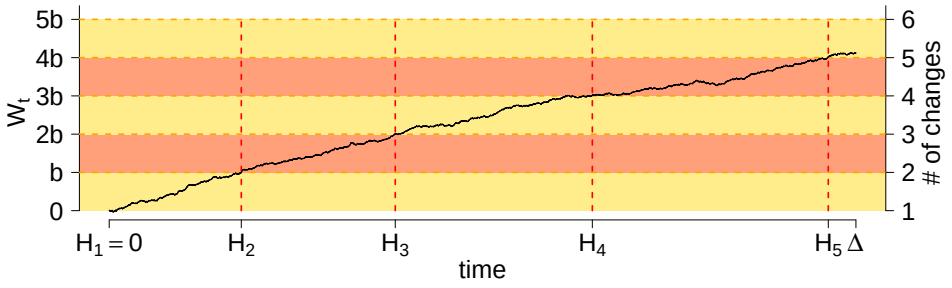

Figure 10.2: Interpretation of the inverse Gaussian distribution as hitting time of a border by a Brownian motion W with drift. *Hitting a border jb ($j \geq 0$, shown on the left axis) corresponds to a perceptual change (right axis). There is one change in the interval $I(\Delta)$ if the dominance time is larger than Δ which implies that the related Brownian motion has not crossed the border b and thus has not left the yellow stripe at the bottom upwards during $I(\Delta)$. There are two perceptual changes in the interval if the maximum of W has crossed the border b but not the next border $2b$ and so on. The $(H_i)_{i\geq 1}$ denote the times of percept changes (with $H_1 = 0$). In the graph five changes occur.*

Concerning the expected value $\mathbb{E}[N(\Delta)]$ note that the process of perceptual changes may be interpreted as renewal process (Definition 2.5) with life times following the IG(μ, σ)-distribution. The assertion $\frac{\mathbb{E}[N(\Delta)]}{\Delta} \xrightarrow[\Delta\to\infty]{} \frac{1}{\mu}$ follows directly by the Elementary Renewal Theorem (e.g., Ross, 1996). □

Next, we relax the assumption that the interval $I(\Delta)$ starts with a perceptual change and state an asymptotic result. Thereby, we prove that the point process Ξ_{HMMc} induced by the HMMc is (in the limit) crudely stationary. Recalling Definition 8.14 crude stationarity in the limit means that

$$\mathbb{P}(\text{number of events of } \Xi_{\text{HMMc}} \text{ in } (t, t+h) = k), \quad h > 0, k = 0, 1, \ldots$$

depends for $t \to \infty$ only on the length h.

Corollary 10.2. ***Crude stationarity of the HMMc***
Contrary to Proposition 10.1 it is now assumed that the start t of the right-open interval $I(\Delta)$ with length $\Delta \geq 0$ does not coincide with a perceptual change. Then, it holds

$$\lim_{t\to\infty} \mathbb{P}(N(\Delta) = j) = \begin{cases} \mathbb{P}(R^c > \Delta), & \text{if } j = 0, \\ \int_0^\Delta w_{\Delta-\Delta_r}(j) f_{R^c}(\Delta_r) d\Delta_r, & \text{if } j \geq 1, \end{cases}$$

with R^c as the asymptotic residual time with density $f_{R^c} = 1/\mu(1 - F^{IG}_{\mu,\sigma})$ as given in the next Corollary 10.3 and w_Δ as given in Proposition 10.1.
For the expected number of changes it again holds asymptotically

$$\frac{\mathbb{E}[N(\Delta)]}{\Delta} \xrightarrow[\Delta\to\infty]{} \frac{1}{\mu}.$$

Ξ_{HMMc} is in the limit crudely stationary.

Proof: The interval $I(\Delta)$ has to be divided into the residual time Δ_r until the first perceptual change and the remaining interval $I_r(\Delta - \Delta_r)$ of length $\Delta - \Delta_r$. If the residual time is larger than Δ, no changes occur in the interval $I(\Delta)$. Hence, for $t \to \infty$: $\mathbb{P}(N(\Delta) = 0) = \mathbb{P}(R^c > \Delta)$. For $j > 0$ we require the distribution of changes in the interval $I_r(\Delta - \Delta_r)$ (now starting with a perceptual change) given that the residual time is Δ_r. The assertion follows directly by noting that j changes in the interval $I_r(\Delta - \Delta_r)$ imply j changes in the whole interval $I(\Delta)$ (such that the weights of j have to be used) and by the law of total probability.
Asymptotically the difference between the interval $I(\Delta)$ starting with a perceptual change or not is negligible such that the assertion

$$\frac{\mathbb{E}[N(\Delta)]}{\Delta} \xrightarrow[\Delta\to\infty]{} \frac{1}{\mu}$$

directly follows from Proposition 10.1. As the distribution of $N(\Delta)$ is (asymptotically) independent of t and depends only on the interval length Δ, the resulting point process Ξ_{HMMc} is in the limit crudely stationary. □

10.1.2 Residual time

Now, we derive results for the density and the expectation of the residual time, i.e., the time span until the next perceptual change.

Corollary 10.3. ***Residual time in the HMMc***
Let Ξ_{HMMc} be the point process of a HMMc with parameters (μ, σ) and R^c be the asymptotic residual time. Its expectation is given by

$$\mathbb{E}[R^c] = \frac{\sigma^2}{2\mu} + \frac{\mu}{2},$$

and the distribution has the density $f_{R^c}(x) = 1/\mu \left(1 - F^{IG}_{\mu,\sigma}(x)\right)$.

Proof: It holds for the second moment of an $\mathrm{IG}(\mu, \sigma)$ distributed random variable D: $\mathbb{E}[D^2] = \mathbb{V}\mathrm{ar}(D) + \mathbb{E}[D]^2 = \sigma^2 + \mu^2$. With this relation and Proposition 8.12 the assertion concerning the mean and the density of R^c can be concluded easily. □

10.2 Intermittent presentation

We derive results on the point process induced by the two-state HMM for intermittent presentation. Note that for technical reasons the structure of this chapter differs from the structure of Chapter 10.1, i.e., results on the number of perceptual reversals and residual times are not derived at the beginning. Instead, we first discuss the relation to semi-Markov processes (Section 10.2.1). Second, first passage times as well as stationarity properties are derived (Section 10.2.2). Then, the number of perceptual reversals is investigated as well as the residual time (Sections 10.2.3 and 10.2.4). The most important result is the steady-state distribution discussed in Corollary 10.8. Another important result (Proposition 10.14) concerns the theoretical rate of changes.

10.2.1 HMM as semi-Markov process

We link the HMM to the concept of semi-Markov processes (recall the introduction in Section 8.2.3.3), which is widely used in the theory of stochastic processes. We conclude easily that in our HMM with $(t_i)_{i\geq 1}$ as the perceptual reversal times the process $(Y_i, (0, t_i))_{i\geq 1}$ is a Markov renewal process and that $(\tilde{Y}_t)_{t\geq 0}$ is a semi-Markov process (assuming known hidden states). Moreover, we directly observe for the semi-Markov kernel Q that $Q_{jk}(t) = p_{jk} F^{\mathrm{IG}}_{\mu_j,\sigma_j}(t)$ (i.e., the duration of a dominance time is independent of the next state) and for the conditional sojourn time $S_{jk}(t) = F^{\mathrm{IG}}_{\mu_j,\sigma_j}(t)$, which again is independent of the next state. The theory of semi-Markov processes is widely developed (compare, e.g., Medhi, 2009, and the references therein), and different renewal equations (recall Definition 8.13) are well known. Here, we focus only on the aspects relevant for this thesis and derive, if possible, even exact results for properties like first hitting times instead of renewal equations.

10.2.2 First passage times, steady-state distributions and renewal equations

We introduce the terminology of first passage and first recurrence times for Hidden Markov Models for both the discrete number of dominance times until a state change and the continuously defined time until a state change of the point process Ξ_{HMMi}. We need the first passage times later on to derive the steady-state distribution, i.e., the asymptotic probability that a subject is in a given state which is of practical interest, e.g., when comparing the two groups in the data set of Schmack et al. (2015).

Definition 10.4. ***First passage and first recurrence times of the HMMi***
Let $(Y_i)_{i\geq 1}$ be the underlying Markov chain of a HMM and $(\tilde{Y}_t)_{t\geq 0}$ be the state at time t of the associated point process Ξ_{HMMi}. Assuming a start in state i (and a start of the dominance time at 0) the first passage times T_{ij} and $\tilde{T}_{ij}$ of a state $j \neq i$ are defined as

$$T_{ij} := \inf\{m \geq 2 : Y_m = j | Y_1 = i\} - 1, \qquad \tilde{T}_{ij} := \inf\{t > 0 : \tilde{Y}_t = j | \tilde{Y}_0 = i\}.$$

The first recurrence times T_{ii} and $\tilde{T}_{ii}$ are defined as

$$T_{ii} := \inf\{m \geq 3 : Y_m = i | \exists\, 2 \leq l < m : Y_l \neq i, Y_1 = i\} - 1,$$
$$\tilde{T}_{ii} := \inf\{t > 0 : \tilde{Y}_t = i | \exists\, 0 < s < t : \tilde{Y}_s \neq i, \tilde{Y}_0 = i\}.$$

Note that we understand the first recurrence time here as the sum of the time spent in state i and outside of state i before returning for the first time to state i. Now, we derive the expected first passage times which are the key ingredient for the steady-state distributions discussed later on.

Proposition 10.5. ***First passage and first recurrence times of the HMMi: Expectation***
Let $\Theta_{HMM} = (\mu_S, \sigma_S, \mu_U, \sigma_U, p_{SS}, p_{UU}, \pi_{start,S})$ be the parameter set of a HMM for intermittent presentation.
Assume the HMM starts with a perceptual change in the stable state S and $p_{SS} < 1$. The expected first passage times of the unstable state U are given by

$$\mathbb{E}[T_{SU}] = \frac{1}{1 - p_{SS}} \text{ and } \mathbb{E}[\tilde{T}_{SU}] = \frac{1}{1 - p_{SS}}\mu_S.$$

A similar result holds for the first passage time of the stable state when starting with a perceptual change in the unstable state and $p_{UU} < 1$.
If $p_{SS} = 1$ or $p_{UU} = 1$, the corresponding expected first passage times are ∞.

The expected first recurrence time to the initial state is independent of the starting state given by $\mathbb{E}[T_{SS}] = \mathbb{E}[T_{UU}] = \frac{1}{1-p_{SS}} + \frac{1}{1-p_{UU}}$ and $\mathbb{E}[\tilde{T}_{SS}] = \mathbb{E}[\tilde{T}_{UU}] = \frac{1}{1-p_{SS}}\mu_S + \frac{1}{1-p_{UU}}\mu_U$ if $\max(p_{SS}, p_{UU}) < 1$ and by $\mathbb{E}[T_{SS}] = \mathbb{E}[T_{UU}] = \mathbb{E}[\tilde{T}_{SS}] = \mathbb{E}[\tilde{T}_{UU}] = \infty$ else.

Proof: Assume $p_{SS} < 1$ and a start in the stable state. The success probability of a change to U is $1 - p_{SS}$ when a new percept emerges. Therefore, the number of percepts in the stable state until the change to U is a geometrically distributed random variable with parameter $1 - p_{SS}$. The expected value is well known as the inverse of the parameter. Thus, $\mathbb{E}[T_{SU}] = 1/(1 - p_{SS})$.

$\tilde{T}_{SU}$ is a random variable distributed like $\sum_{i=1}^{T_{SU}} D_i^S$, where $D_1^S, \ldots, D_{T_{SU}}^S$ are $\mathrm{IG}(\mu_S, \sigma_S)$-distributed and independent from each other and also independent of T_{SU}. Therefore, we have (Wald, 1944)

$$E\left[\tilde{T}_{SU}\right] = \mathbb{E}\left[\sum_{i=1}^{T_{SU}} D_i^S\right] = \mathbb{E}\left[T_{SU}\right]\mathbb{E}\left[D_i^S\right] = \frac{\mu_S}{1 - p_{SS}}.$$

Now, let $p_{SS} = 1$. The process therefore always remains in the stable state and never reaches the unstable state. This causes non-finite first passage times of the unstable state.
The assertions for the first passage time of the stable state when starting in U follow by similar arguments.
The first recurrence time is the first time the process reaches the stable state again having started in the stable state plus the time spent in the stable state. Hence, we can due to the linearity of the expectation add the expected number of dominance times in the stable and the unstable state before a change as well as the corresponding time spans in the stable and unstable state. □

As an additional result we prove a representation for the distribution of the first passage times. Applying the law of total probability, we therefore sum for a given $x > 0$ about all state sequences $S, SS, SSS, \ldots$ consisting only of stable dominance times and having length x until the first entry in the unstable state (see Figure 10.3). This yields the density of the first passage time of U by the point process Ξ_{HMMi} for this x.

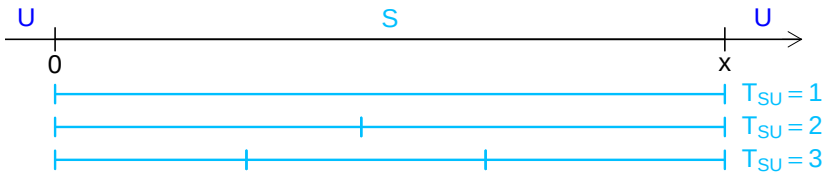

Figure 10.3: Different numbers of dominance times in a stable phase T_{SU} leading to the same length x of the stable phase. *In the graph, examples for $T_{SU} = 1$, $T_{SU} = 2$ and $T_{SU} = 3$ are shown. Perceptual changes are marked by vertical bars.*

Proposition 10.6. ***First passage and first recurrence times of the HMMi: Distribution***
a) Assume the HMM starts with a perceptual change in the stable state S and $p_{SS} < 1$. The weights $w_{T_{SU}}$ of the first passage time of U are the weights of a Geometric distribution with parameter $p = 1 - p_{SS}$. The density $f_{\tilde{T}_{SU}}$ can be expressed using convolutions

$$f_{\tilde{T}_{SU}}(x) = \sum_{i=1}^{\infty} f^i_{\tilde{T}_{SU}}(x) = \sum_{i=1}^{\infty} (1 - p_{SS}) p_{SS}^{i-1} {f^{IG}_{\mu_S,\sigma_S}}^{*(i-1)}(x),$$

if $x \geq 0$ and 0 otherwise.
Similar results hold for the first passage time of the stable state when starting with a perceptual change in the unstable state and $p_{UU} < 1$.
If $\max(p_{SS}, p_{UU}) = 1$, all finite weights vanish.

b) If $\max(p_{SS}*, p_{UU}) < 1$, the weights $w_r(i)$ of the first recurrence time T_{SS} are $w_r(i) = 0$ if $i \leq 1$ and

$$w_r(i) = \sum_{j=1}^{i-1} w_{T_{US}}(j) w_{T_{SU}}(i - j),$$

else. The density $f_r(x)$ of the first recurrence time $\tilde{T}_{SS}$ is $f_r(x) = 0$ if $x < 0$ and

$$f_r(x) = \int_0^x f_{\tilde{T}_{US}}(y) f_{\tilde{T}_{SU}}(x - y) dy,$$

else.
If $\max(p_{SS}, p_{UU}) = 1$, the first recurrence times are ∞.

Proof: First, we show a). As discussed in the proof of Proposition 10.5, T_{SU} is for $p_{SS} < 1$ a geometrically distributed random variable with parameter $1 - p_{SS}$. The density of $\tilde{T}_{SU}$ follows by similar arguments as in the proof of Proposition 13.9 later in this thesis (page 183).
Now, let $p_{SS} = 1$. The process therefore always remains in the stable state and never reaches the unstable state. This causes non-finite first passage times of the unstable state.
The assertions for the first passage time of the stable state when starting in U follow by similar arguments.
We turn to b). The first recurrence time is the first time the process reaches the stable state again having started in the stable state with a perceptual reversal plus the time spent in the stable state. Thus, for $\max(p_{SS}, p_{UU}) < 1$ the weights and the density are given by convolutions. The assertion for $\max(p_{SS}, p_{UU}) = 1$ follows directly. □

There also exists a renewal equation (recall Definition 8.13) for the distribution function of the first passage time of the process $\tilde{Y}_t$ (whose solution in terms of the density is given in Proposition 10.6).

Proposition 10.7. ***Renewal equation for the first passage time of the HMMi***
Let $G_{jk}(t) := \mathbb{P}(\tilde{T}_{jk} \leq t | \tilde{Y}_0 = j)$ describe the distribution function of the first passage time of state k starting in j of the process $\tilde{Y}_t$ and $Q(t)$ be the semi-Markov kernel (Section 10.2.1). It holds for $j, k \in \{S, U\}$ and $t \geq 0$

$$G_{jk}(t) = Q_{jk}(t) + \int_0^t G_{jk}(t-x) dQ_{jj}(x).$$

Proof: This is Theorem 7.5 in Medhi (2009) (where we do not need the summation as we only have two states). □

The stationary distribution of the underlying Markov chain and the steady-state distribution of the point process Ξ_{HMMi} are derived in the following corollary which is the most important result for application in this chapter. Recall that the steady-state distribution $\tilde{\pi} = (\tilde{\pi}_S, \tilde{\pi}_U)$ denotes the probabilities of being in a given state at time t for $t \to \infty$, i.e., $\tilde{\pi}_S := \lim_{t\to\infty} \tilde{Y}_t = S$. $\tilde{\pi}_S$ moreover denotes the long term relative time spent in state S (equation (8.3)).

Corollary 10.8. ***Stationary/steady-state distributions of the HMMi***
Let $\Theta_{HMM} = (\mu_S, \sigma_S, \mu_U, \sigma_U, p_{SS}, p_{UU}, \pi_{start,S})$ be the parameter set of a HMM for intermittent presentation. Assume $\max(p_{SS}, p_{UU}) < 1$. The stationary distribution $\pi = (\pi_S, \pi_U)$ of the underlying Markov chain is given by

$$\pi = \left(\frac{p_{UU} - 1}{p_{SS} + p_{UU} - 2}, \frac{p_{SS} - 1}{p_{SS} + p_{UU} - 2} \right).$$

The steady-state distribution $\tilde{\pi} = (\tilde{\pi}_S, \tilde{\pi}_U)$ of the resulting point process Ξ_{HMMi} derives as

$$\tilde{\pi} = \left(\frac{\frac{1}{1-p_{SS}}\mu_S}{\frac{1}{1-p_{SS}}\mu_S + \frac{1}{1-p_{UU}}\mu_U}, \frac{\frac{1}{1-p_{UU}}\mu_U}{\frac{1}{1-p_{SS}}\mu_S + \frac{1}{1-p_{UU}}\mu_U} \right). \tag{10.2}$$

If $p_{SS} = 1$, we have $\pi = \tilde{\pi} = (1, 0)$, and if $p_{UU} = 1$, it holds $\pi = \tilde{\pi} = (0, 1)$.

Proof: Assume $\max(p_{SS}, p_{UU}) < 1$. Let P be the transition matrix of the hidden Markov chain. The stationary distribution of a Markov chain is defined as the normalized vector π satisfying $\pi P = \pi$ (Section 9.1). Thus, π is a normalized multiple of the eigenvector of the transposed matrix P^T to the eigenvalue 1. It can be derived explicitly via standard derivation methods as $\pi = \left(\frac{p_{UU}-1}{p_{SS}+p_{UU}-2}, \frac{p_{SS}-1}{p_{SS}+p_{UU}-2} \right)$.
To derive the steady-state-distribution of Ξ_{HMMi}, we interpret Ξ_{HMMi} as regenerative process and use equation (8.2) on page 67. The life times $(\tilde{D}_i)_{i\geq 1}$ of the regenerative process are given by the first recurrence times in the HMM, and the expected amount of time spent in S during a life time is the expected first passage time of the state U when starting in S and by Proposition 10.5 given by $\frac{1}{1-p_{SS}}\mu_S$. Thus, it follows directly

$$\tilde{\pi}_S = \frac{\mathbb{E}[\text{amount of time in state j during } \tilde{D}_1]}{\mathbb{E}[\tilde{D}_1]} = \frac{\mathbb{E}[\tilde{T}_{SU}]}{\mathbb{E}[\tilde{T}_{SS}]} = \frac{\frac{1}{1-p_{SS}}\mu_S}{\frac{1}{1-p_{SS}}\mu_S + \frac{1}{1-p_{UU}}\mu_U}$$

and analogously for $\tilde{\pi}_U$.
The assertions for $p_{SS} = 1$ or $p_{UU} = 1$ are trivial. □

Next, we translate classical results of the theory of alternating renewal processes (compare Section 8.2.3.1) to our case of Hidden Markov Models (mainly for the sake of mathematical interest). We introduce the concept of a cycle which corresponds to a life time in a regenerative process: A cycle comprises all dominance times during a stable phase and all dominance times during the next unstable phase (or vice versa). The idea is illustrated in Figure 10.4.

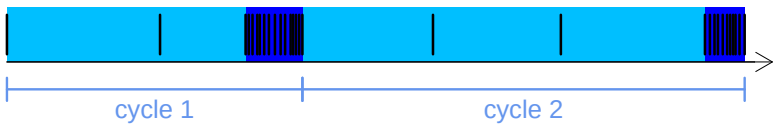

Figure 10.4: Visualization of a cycle. *A cycle comprises a stable (light blue) and an unstable phase (blue). The graph shows two complete cycles.*

We derive the expected number of cycles in an interval of length $\Delta > 0$ (Lemma 10.9) and renewal equations for the exact probabilities that the i-th dominance time is stable and that the HMMi is at time t in the stable state (Proposition 10.10, the steady-state distribution in contrast yields the corresponding asymptotic probability).

Lemma 10.9. ***Expected number of cycles in the HMMi***
Assume the HMM starts with a perceptual change in the stable state S, and let $F_S(t)$ and $F_U(t)$ be the distribution functions of the length of stable and unstable phases in the point process Ξ_{HMMi} (which derive from the densities given in Proposition 10.6). The expectation of the number of cycles $C_S(\Delta)$ in an interval $I(\Delta)$ of length $\Delta > 0$ is given by

$$\mathbb{E}[C_S(\Delta)] = \sum_{m=1}^{\infty} (F_S * F_U)^{*(m)}(\Delta),$$

where $*(m)$ denotes m-fold convolution.

Proof: See p.121 in Beichelt and Fatti (2001). □

Proposition 10.10. ***Renewal equations for the state of the HMMi***
The renewal equation for the hidden Markov chain of the HMMi is for $i \geq 1$ given by

$$\mathbb{P}(Y_i = S|Y_1 = S) = \mathbb{P}(T_{SU}^1 \geq i) + \sum_{m=1}^{i-1} \mathbb{P}(Y_{i-m} = S|Y_1 = S)c_A(m), \tag{10.3}$$

where T_{SU}^1 is the number of stable dominance times in the first stable phase and $c_A(m)$ is the probability that the first cycle has length m, i.e., the first new cycle occurs at the $m+1$-st dominance time.
For the renewal equation of the induced point process Ξ_{HMMi}, it holds for $t > 0$ with Q as the semi-Markov kernel and $F_S(t)$ and $F_U(t)$ as the distribution functions of the length of stable and unstable phases in the point process Ξ_{HMMi} (which derive from the densities given in Proposition 10.6)

$$\begin{aligned}\mathbb{P}(\tilde{Y}_t = S|\tilde{Y}_0 = S) &= (1 - F_S(t)) + \int_0^t (1 - F_S(t-s))d\mathbb{E}[C_S(s)] \\ &= (1 - F_S(t)) + \sum_{k\in\{S,U\}} \int_0^t \mathbb{P}(\tilde{Y}_{t-x} = S|\tilde{Y}_0 = k)dQ_{Sk}(x).\end{aligned}$$

Proof: The proof for the renewal equation of the Markov chain is given in (Barbu and Limnios, 2008, Example 2.8). Note that our first index is 1 and not 0 as in Barbu and Limnios (2008) such that our upper limit of summation is $i - 1$.
The first representation of the renewal equation for Ξ_{HMMi} can be found on p.122 in (Beichelt and Fatti, 2001), and the second one is given in Theorem 7.1 of Medhi (2009). □

Applying the renewal equation for the Markov chain, we obtain an exact result for the probability that the i-th state is stable given a start in the stable state.

Corollary 10.11. ***Exact probability of being in the stable state***
Assume a start in the stable state ($Y_1 = S$). The probability that the i-th hidden state of the HMM is also stable is for $i \geq 1$ given by

$$\mathbb{P}(Y_i = S|Y_1 = S) = \sum_{m=0}^{i-1} u_A(m)p_{SS}^{i-m-1}$$

with $u_A(m)$ as the probability that a renewal of the stable state occurs in the $m+1$-st dominance time.

Proof: Solving the renewal equation (10.3) yields (Barbu and Limnios, 2008, p.39)

$$\mathbb{P}(Y_i = S|Y_1 = S) = \sum_{m=0}^{i-1} u_A(m)\mathbb{P}(T_{SU}^1 \geq i - m) = \sum_{m=0}^{i-1} u_A(m)p_{SS}^{i-m-1},$$

where the $i - 1$ in the upper summation border again is due to our starting index 1. □

The probabilities $u_A(m)$ can be obtained by evaluating the m-th derivative of the probability generating function η_A at zero (given in Lemma 10.13):

$$u_A(m) = \frac{\eta_A^{(m)}(0)}{m!}$$

We require the probability generating function of the Geometric distribution.

Lemma 10.12. ***Probability generating function of a Geometric distribution***
The probability generating function (PGF) $\rho_X = \mathbb{E}[s^X]$ *of a Geometric distributed random variable* X *with success parameter* p *is given by* $\rho_X(s) = \frac{ps}{1-(1-p)s}$.

Proof: Follows by elementary calculations. □

Lemma 10.13. ***PGF of a HMM***
Let S_k *and* U_k *denote the number of dominance times in the* k*-th stable or* k*-th unstable phase, respectively. Then, the sequence of stable renewals* $A_k = S_k + U_k$ *has the probability generating function*

$$\rho_A(s) = s^2 \frac{(1-p_{SS})(1-p_{UU})}{(1-p_{SS}s)(1-p_{UU}s)},$$

and for the PGF η_A *of the sequence* $u_A(i)$ *that a renewal of the stable state occurs at time* $i \in \mathbb{N}$ *it holds*

$$\eta_A(s) = \frac{(1-p_{SS}s)(1-p_{UU}s)}{(s-1)(p_{SS}s + p_{UU}s - s - 1)}.$$

Proof: S_k and U_k are geometrically distributed with parameters $1-p_{SS}$ and $1-p_{UU}$. The PGF of the sum of two independent random variables is the product of the PGFs and thus, it holds by the PGF of the geometric distribution (Lemma 10.12)

$$\rho_A(s) = \rho_S(s) \cdot \rho_U(s) = s^2 \frac{(1-p_{SS})(1-p_{UU})}{(1-p_{SS}s)(1-p_{UU}s)}.$$

To derive the PGF η_A of $u_A(i)$, we use the relation $\eta_A(s) = 1/(1-\rho_A(s))$ (Barbu and Limnios, 2008, Proposition 2.1):

$$\eta_A(s) = \frac{1}{1 - s^2 \frac{(1-p_{SS})(1-p_{UU})}{(1-p_{SS}s)(1-p_{UU}s)}} = \frac{(1-p_{SS}s)(1-p_{UU}s)}{(s-1)(p_{SS}s + p_{UU}s - s - 1)}.$$

□

10.2.3 Number of changes

We focus on the theoretical (asymptotic) rate of perceptual changes in the HMMi which is one important result of this chapter. We also evaluate the result compared to the rate of changes observed in the original data.

Proposition 10.14. ***Rate of changes in the HMMi***
Let $\Theta_{HMM} = (\mu_S, \sigma_S, \mu_U, \sigma_U, p_{SS}, p_{UU}, \pi_{start,S})$ *be the parameter set of a HMMi. For the expected number of changes* $\mathbb{E}[N(\Delta)]$ *in an interval* $I(\Delta)$ *of length* $\Delta \geq 0$ *of the point process* Ξ_{HMMi}*, it holds for* $\max(p_{SS}, p_{UU}) < 1$

$$\frac{\mathbb{E}[N(\Delta)]}{\Delta} \xrightarrow[\Delta\to\infty]{} \frac{p_{SS} + p_{UU} - 2}{(p_{UU}-1)\mu_S + (p_{SS}-1)\mu_U}.$$

If $p_{SS} = 1$*, it holds*

$$\frac{\mathbb{E}[N(\Delta)]}{\Delta} \xrightarrow[\Delta\to\infty]{} \frac{1}{\mu_S}$$

and analogously for $p_{UU} = 1$.
We define $\rho^{HMMi} := \lim_{\Delta\to\infty} \frac{\mathbb{E}[N(\Delta)]}{\Delta}$ *as the (asymptotic) rate of changes.*

Proof: Assume $\max(p_{SS}, p_{UU}) < 1$. Let $N_S(\Delta)$ denote the number of perceptual changes during a stable phase in an interval of length $\Delta \geq 0$ and Δ_S be the amount of time spent in the stable state in an interval of length Δ. Regarding only the stable phases it holds by the Elementary Renewal Theorem (e.g., Ross, 1996)

$$\frac{\mathbb{E}[N_S(\Delta_S)]}{\Delta_S} = \frac{\mathbb{E}[N_S(\Delta_S)]}{\mathbb{E}[\Delta_S]} \xrightarrow[\Delta_S \to \infty]{} \frac{1}{\mu_S}$$

as in this setting Δ_S is deterministic. Turning back from the stable phases to the whole process, note that Δ_S is now random and $\Delta \to \infty$ also implies $\Delta_S \to \infty$. Moreover, the number of perceptual changes in the stable state during stable phases corresponds to the overall number of changes during stable phases $\mathbb{E}[N_S(\Delta_S)] = \mathbb{E}[N_S(\Delta)]$. Thus,

$$\frac{\mathbb{E}[N_S(\Delta)]}{\mathbb{E}[\Delta_S]} \xrightarrow[\Delta \to \infty]{} \frac{1}{\mu_S}.$$

Note that $\Delta = \Delta_S + \Delta_U$ where Δ_U is the time spent in the unstable state.
By interpreting Ξ_{HMMi} as alternating renewal process with states S and U and using Theorem 4.8 in Beichelt and Fatti (2001) we obtain $\mathbb{E}[\Delta_S]/\Delta \xrightarrow[\Delta \to \infty]{} \tilde{\pi}_S$. This yields

$$\frac{\mathbb{E}[N_S(\Delta)]}{\Delta} \xrightarrow[\Delta \to \infty]{} \frac{\tilde{\pi}_S}{\mu_S}.$$

An analogous result holds for the unstable state such that we obtain

$$\frac{\mathbb{E}[N_S(\Delta) + N_U(\Delta)]}{\Delta} = \frac{\mathbb{E}[N(\Delta)]}{\Delta} \xrightarrow[\Delta \to \infty]{} \frac{\tilde{\pi}_S}{\mu_S} + \frac{\tilde{\pi}_U}{\mu_U}.$$

Plugging in the expressions for $\tilde{\pi}_j$ (Corollary 10.8) gives

$$\begin{aligned}\frac{\mathbb{E}[N(\Delta)]}{\Delta} &\xrightarrow[\Delta \to \infty]{} \frac{\frac{1}{1-p_{SS}}}{\frac{1}{1-p_{SS}}\mu_S + \frac{1}{1-p_{UU}}\mu_U} + \frac{\frac{1}{1-p_{UU}}}{\frac{1}{1-p_{SS}}\mu_S + \frac{1}{1-p_{UU}}\mu_U} \\ &= \frac{p_{SS} + p_{UU} - 2}{(p_{UU} - 1)\mu_S + (p_{SS} - 1)\mu_U},\end{aligned}$$

where in the last line we used the common denominator $(1 - p_{UU})(1 - p_{SS})$.
For $p_{SS} = 1$ or $p_{UU} = 1$, we are in the situation of a renewal process. Thus, the Elementary Renewal Theorem yields the assertion. □

The theoretical (asymptotic) rate of changes in the HMM ρ^{HMMi} and the empirical rate of changes in the data set of Schmack et al. (2015) are compared in Figure 10.5 A for all 61 subjects. In the majority of cases, the rates are close together (mostly not more than 10% apart from each other). Deviations occur because in some cases there is a difference between the starting state in the data and the steady-state distribution. For example a large weight of the steady-state distribution in the unstable state but a first rather stable dominance time in the data may lead to differences between the asymptotic and the empirical rate of changes in an interval of length 1200 seconds. Note, moreover, that the model rate of changes is larger than the data rate of changes especially if there is a long unstable phase at the end of the recording due to a "censoring" problem. We explain that by using response pattern C from

Table 9.2 (page 102) as an example where this problem occurs. The corresponding most likely state path (estimated by the Viterbi algorithm explained in Section 12.5) is illustrated in Figure 12.7 A on page 167 (for the HBM, but the same is estimated for the HMM). Here, the first unstable phase consists of eight dominance times, and the second of (at least) 17 dominance times and is located at the end of the response pattern. This explains why the probability to remain in the unstable state is estimated as $\hat{p}_{UU} = 23/24$, and the estimated mean duration of an unstable phase has $1/(1 - \hat{p}_{UU}) = 24$ dominance times. Consequently, the model predicts in this example more changes than there are in the original data.
Panel B of Figure 10.5 shows the comparison of the mean simulated rate of changes in the HMM conditioned on starting in the same state than in the data set of Schmack et al. (2015) and recording for the same length T to the empirical rate of changes for all 61 subjects. The starting state is estimated using the Viterbi path. Now in the great majority of cases the model and the data rate fit perfectly (and the deviations are due to the censoring problem explained in the paragraph above).

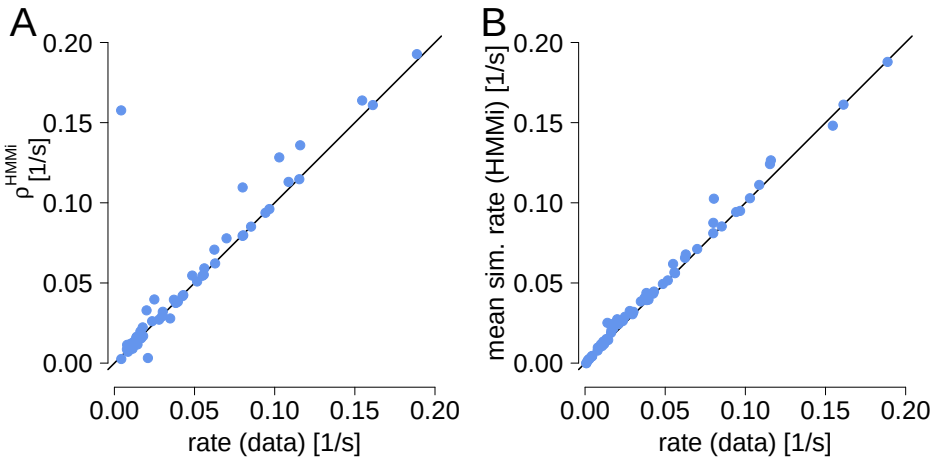

Figure 10.5: Comparison of the rate of changes in Schmack et al. (2015) and in the HMMi. *(A) The theoretical (asymptotic) rate ρ^{HMMi} (Proposition 10.14) is used. (B) The mean simulated rate in 1000 simulations starting with the same Viterbi-estimated state as in the original data is contrasted to the rate of perceptual changes in the data.*

As an additional result we investigate the distribution of the number of changes in an interval of length Δ. First, we claim that the interval starts with a perceptual change (Proposition 10.15). Second, we relax this assumption (Proposition 10.16). This split in two propositions simplifies the notation and argumentation.

Proposition 10.15. ***Number of changes in the HMMi: Distribution I***
Let $\Theta_{HMM} = (\mu_S, \sigma_S, \mu_U, \sigma_U, p_{SS}, p_{UU}, \pi_{start,S})$ be the parameter set of a HMMi, π its stationary distribution and $I(\Delta) := [t, t+\Delta)$ be an interval of length $\Delta \geq 0$ starting with a perceptual change. Moreover, let Y be a random sequence of hidden states. The probability of a realized state sequence y covering $I(\Delta)$ with $|y| \geq 2$ hidden states in $I(\Delta)$ is for $t \to \infty$ given by

$$\mathbb{P}(Y = y) = \pi_{y_1} \int_0^{\Delta} \left(1 - F^{IG}_{\mu_{y_{|y|}}, \sigma_{y_{|y|}}}(\Delta - s)\right) \begin{cases} g_{y_1}(s)ds, & \text{if } |y| = 2, \\ (g_{y_1} * \ldots * g_{y_{|y|-1}})(s)ds, & \text{if } |y| > 2, \end{cases}$$

where the following function is folded

$$g_{y_i}(s) := f^{IG}_{\mu_{y_i}, \sigma_{y_i}}(s) \cdot p_{y_i, y_{i+1}}.$$

If $|y| = 1$, we have

$$\mathbb{P}(Y = y) = \pi_{y_1} \left(1 - F^{IG}_{\mu_{y_1}, \sigma_{y_1}}(\Delta)\right).$$

The probability weights of the number of changes $N_c(\Delta)$ of Ξ_{HMMi} in the interval $I(\Delta)$ (starting with a perceptual change) are then given by

$$\mathbb{P}(N_c(\Delta) = j) = \sum_{y \in \mathfrak{Y}(\Delta) || y| = j} \mathbb{P}(Y = y), \tag{10.4}$$

where $\mathfrak{Y}(\Delta)$ denotes all hidden state sequences starting with a perceptual change whose resulting point processes cover the interval $I(\Delta)$.

Proof: The proof follows the same steps as the proof of Proposition 13.14 later on in this thesis (page 188). □
An example of a realized state sequence y covering the interval $I(\Delta)$ is given in Figure 10.6.

Figure 10.6: Example of a realized state sequence covering $I(\Delta)$. *Here, the state sequence y starting with a perceptual change at time t and covering the interval $I(\Delta) = [t, t+\Delta)$ consists of two unstable dominance times followed by two stable dominance times, i.e., $y = (U, U, S, S)$. Four perceptual changes marked by vertical bars occur in $I(\Delta)$.*

We extend Proposition 10.15 by allowing an arbitrary start of the interval $I(\Delta)$, i.e., the interval does not have to start with a perceptual change. Thereby, we show crude stationarity (Definition 8.14) of the process of perceptual changes.

Proposition 10.16. ***Number of changes in the HMMi: Distribution II***
Let $I(\Delta) := [t, t+\Delta)$ be an interval of length $\Delta \geq 0$. The probability weights of the number of changes $N(\Delta)$ of Ξ_{HMMi} in the interval $I(\Delta)$ are then for $j \geq 1$ and $t \to \infty$ given by

$$\mathbb{P}(N(\Delta) = j) =$$
$$\tilde{\pi}_S \left(\int_0^\Delta f_{R^S}(\Delta_S) p_{SS} \mathbb{P}(N_c^S(\Delta - \Delta_S) = j)/\pi_S + f_{R^S}(\Delta_S)\,(1 - p_{SS})\,\mathbb{P}(N_c^U(\Delta - \Delta_S) = j)/\pi_U d\Delta_S \right)$$
$$+ \tilde{\pi}_U \times$$
$$\left(\int_0^\Delta f_{R^U}(\Delta_U)\,(1 - p_{UU})\,\mathbb{P}(N_c^S(\Delta - \Delta_U) = j)/\pi_S + f_{R^U}(\Delta_U) p_{UU} \mathbb{P}(N_c^U(\Delta - \Delta_U) = j)/\pi_U d\Delta_U \right),$$

where $N_c^S(\Delta)$ and $N_c^U(\Delta)$ denote the number of changes in an interval of length Δ starting with a perceptual change and in the stable or the unstable state, respectively (equation (10.4)). Moreover, f_{R^S}, f_{R^U} are the densities of the asymptotic residual times given in Proposition 8.12 (where the life times are IG distributed with parameters μ_S, σ_S and μ_U, σ_U, respectively) and $\tilde{\pi}_S, \tilde{\pi}_U$ are the steady-state weights given in equation (10.2)*. For $j = 0$ we have*

$$\mathbb{P}(N(\Delta) = 0) = \tilde{\pi}_S \mathbb{P}(R^S > \Delta) + \tilde{\pi}_U \mathbb{P}(R^U > \Delta).$$

The induced point process Ξ_{HMMi} is in the limit crudely stationary.

Proof: Conditioning on the hidden state the probability of $N(\Delta) = j$ is given by

$$\mathbb{P}(N(\Delta) = j) = \lim_{t \to \infty} \left(\mathbb{P}(\tilde{Y}_t = S) \mathbb{P}(N(\Delta) = j | \tilde{Y}_t = S) + \mathbb{P}(\tilde{Y}_t = U) \mathbb{P}(N(\Delta) = j | \tilde{Y}_t = U) \right). \tag{10.5}$$

We use this equation and analyse the case $j = 0$. Moreover, we assume that the current state is the stable one. This event has for $t \to \infty$ the probability $\tilde{\pi}_S$ (Corollary 10.8). If the residual time R^S is larger than Δ, we do not observe any change. With similar observations for the current state being unstable the conclusion for $j = 0$ follows directly using (10.5).
Now, we consider the case $j \geq 1$. Assume the stable state as current one. Thus, we observe a perceptual change at $t + \Delta_S < t + \Delta$ with density $f_{R^S}(\Delta_S)$ (compare Figure 10.7). This is the first change in the interval $[t + \Delta_S, t + \Delta)$ such that in the whole interval j changes should occur. With probability p_{SS} the state remains stable and the distribution of the number of changes is therefore given by the distribution of $N_c^S(\Delta - \Delta_S)$ from equation (10.4). Note that the perceptual change at t in equation (10.4) corresponds to the change at $t + \Delta_S$ here. The S in the exponent implies that we consider only the hidden state sequences y starting with a stable state. We divide by π_S as we condition on a start in the stable state. With probability $1 - p_{SS}$ the state changes to unstable and we need the distribution of $N_c^U(\Delta - \Delta_S)$ from (10.4) where we consider only the paths y starting in the unstable state. Due to the different values Δ_S can take (compare the first two arrows in Figure 10.7), integration is required and the first summand of the assertion follows. Similar arguments hold if the current state is the unstable one, which happens with probability $\tilde{\pi}_U$. Plugging into (10.5) yields the assertion.
The weights $\mathbb{P}(N(\Delta) = j)$ in the limit only depend on the length of the interval. Thus, Ξ_{HMMi} is crudely stationary. □

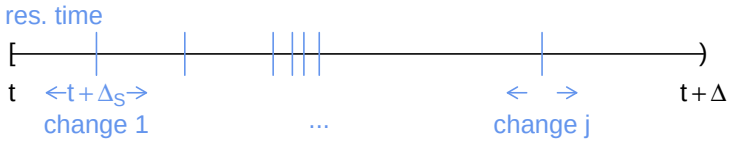

Figure 10.7: Visualization of the number of perceptual changes in the HMMi. *$j > 1$ changes (marked by vertical bars) occur in the interval $I(\Delta)$ which starts in the stable state. The first change occurs after the residual time at $t + \Delta_S$. The interval $[t + \Delta_S, t + \Delta)$ starts with a perceptual change such that the results of Proposition 10.15 can be applied. The positions of all j changes are variable as indicated by the exemplary arrows.*

10.2.4 Residual time

Here, we derive the density and the expected value of the residual time, i.e., the time until the next percept change in the HMMi.

Corollary 10.17. ***Residual time in the HMMi***
Let Ξ_{HMMi} be the point process of a HMMi with parameters $\Theta_{HMM} = (\mu_S, \sigma_S, \mu_U, \sigma_U, p_{SS}, p_{UU}, \pi_{start,S})$ and asymptotic residual time R^{in}. Its expectation is given by

$$\mathbb{E}[R^{in}] = \tilde{\pi}_U \left(\frac{\sigma_U^2}{2\mu_U} + \frac{\mu_U}{2} \right) + \tilde{\pi}_S \left(\frac{\sigma_S^2}{2\mu_S} + \frac{\mu_S}{2} \right),$$

and its distribution has the density

$$f_R^{in}(x) = \frac{\tilde{\pi}_U}{\mu_U} \left(1 - F^{IG}_{\mu_U,\sigma_U}(x)\right) + \frac{\tilde{\pi}_S}{\mu_S} \left(1 - F^{IG}_{\mu_S,\sigma_S}(x)\right).$$

Proof: We condition on the hidden state $\tilde{Y}_t$ and apply Corollary 10.8 about the steady-state distribution in the HMMi and Corollary 10.3 about the expected residual time in the HMMc as conditioning on a hidden state we are in the situation of the HMMc again. This yields

$$\begin{aligned}
\mathbb{E}[R^{\text{in}}] &= \lim_{t\to\infty} \mathbb{E}[R_t^{\text{in}}] \\
&= \lim_{t\to\infty} \left(\mathbb{P}(\tilde{Y}_t = U)\mathbb{E}[R_t^{\text{in}} | \tilde{Y}_t = U] + \mathbb{P}(\tilde{Y}_t = S)\mathbb{E}[R_t^{\text{in}} | \tilde{Y}_t = S] \right) \\
&= \tilde{\pi}_U \left(\frac{\sigma_U^2}{2\mu_U} + \frac{\mu_U}{2} \right) + \tilde{\pi}_S \left(\frac{\sigma_S^2}{2\mu_S} + \frac{\mu_S}{2} \right).
\end{aligned}$$

The density can be derived using the same split into states S and U. Then, an application of Corollary 10.8 and Corollary 10.3 yields the assertion. □

Chapter 11

A hierarchical Brownian motion model

With its small number of parameters, the HMM can be fitted also to short data sections available empirically. As shown later in Chapter 14.1, the HMM moreover can capture the high variety of response patterns both in continuous and intermittent viewing, including uni- and bimodal distributions of dominance times with alternations between stable and unstable states and a high variability across subjects.

However, the HMM description remains phenomenological and does not provide insight into potential neuronal processes. Also, it cannot provide explanations for potential effects that different lengths of blank displays could have on the response patterns, as discussed for example by Orbach et al. (1963); Kornmeier and Bach (2004); Brascamp et al. (2009); Pastukhov and Braun (2013). In addition, the HMM cannot represent the following interesting empirical observation: Before changing from stable to unstable state, the last dominance time tends to be shorter (see Figure 14.11). Therefore, we introduce here a new model, called Hierarchical Brownian Model (HBM), which provides a potential link between the phenomenological description of the response and potential underlying neuronal processes. The HBM assumptions can also provide hypotheses on the effects of different lengths of blank displays and naturally yield shorter dominance times before a state change to the unstable state.

The HBM assumes two competing neuronal populations which indicate perception of right and left rotation, respectively. As has been proposed by various authors (Brascamp et al., 2009; Gigante et al., 2009), we implicitly assume mechanisms of self-excitation, cross-inhibition and adaptation across these neuronal populations, without explicitly modeling them in order to reduce the number of parameters and to allow for model fitting to short trials. In order to obtain a parsimonious model description, we again assume independence of dominance times by neglecting potential mechanisms of week long-term adaptation (Pastukhov and Braun, 2011). For possible model extensions compare Section 15.2.

We use the simplified assumption that perception arises from the difference in the activity of the two populations, which is modeled here by a Brownian motion with drift (similar to Cao et al., 2016) that fluctuates between two thresholds, where the first passage times indicate perceptual reversals. This results in two parameters for the case of continuous presentation that are directly linked to the two parametric inverse Gaussian distribution of dominance times in the HMM (Section 9.2). Further, we describe switching between stable and unstable states

in intermittent presentation by applying an analogous mechanism, which leads to a hierarchical model. We assume another hierarchical layer of neuronal populations and a corresponding Brownian motion which modulates the drift and the threshold of the first population pair and thus causes switching between stable and unstable phases.
The HBM for continuous presentation is explained in detail in Section 11.1, and Section 11.2 elaborates on the HBM for intermittent presentation. There, we also extensively discuss model assumptions, the connection to the HMM and the distribution of dominance times conditioned on the next state.

11.1 Continuous presentation

First, we introduce the model (Section 11.1.1), then elaborate on the effects of single parameter changes (Section 11.1.2) and finally discuss its simulation (Section 11.1.3).

11.1.1 The model

The HBM in continuous presentation (HBMc) simply assumes a Brownian motion with drift $\pm\nu_0$ between two borders, $\pm b$, where the first hitting times of the borders indicate a percept change and lead to a sign change in the drift. As a potential neurophysiological interpretation, b could be considered the size of the activity difference between the L and R population required for a perception change and thereby be related to the respective population sizes. Roughly speaking, the speed of the drift ν_0 could be considered related to the inverse of the connection strengths within and across populations that engage in self excitation and cross inhibition.
Formally, let $b > 0$ be a fixed border, $\nu_0 > 0$ be a drift and $T > 0$ a time horizon, and let $(W_t)_{t\in[0,T]}$ be a standard Brownian motion. The perception process $P := (P_t)_{t\in[0,T]}$ is then defined by

$$dP_t = S_t\nu_0 dt + dW_t, \quad \text{where} \quad P_0 = -b,$$

and the process $S_t := S(P_t, t)$ takes the value -1 if P_t last hit b and 1 if P_t last hit $-b$, with $S_0 := 1$. Formally, for $t \in (0, T]$ let

$$t^* := t^*(t) := \sup\{x : x < t, |P_x| = b\}, \text{ where } t^*(0) = 0$$

be the last time before t that P_t hit either b or $-b$. Then

$$S_t := S(P_t, t) := -\text{sgn}(P_{t^*}).$$

The perception at time $t \geq 0$ takes the value L (*left*) if $S_t = 1$ and R (*right*) if $S_t = -1$ and switches at the first-hitting times $(H_i)_i$ of the borders $\pm b$ defined by $H_0 := 0$ and

$$H_i := \inf\{t \leq T : t > H_{i-1}, P_t = S_t b\} \qquad i = 1, 2, \ldots. \tag{11.1}$$

An example of such a process is shown in Figure 11.1. Panel A shows the process P, where the sign of the drift changes at each first hitting time of b or $-b$ indicated by the process $(H_i)_i$, which also marks switches in the percept (panel B). In panel A it is visible that P is allowed to overshoot the borders meaning that the process is not reflected there.

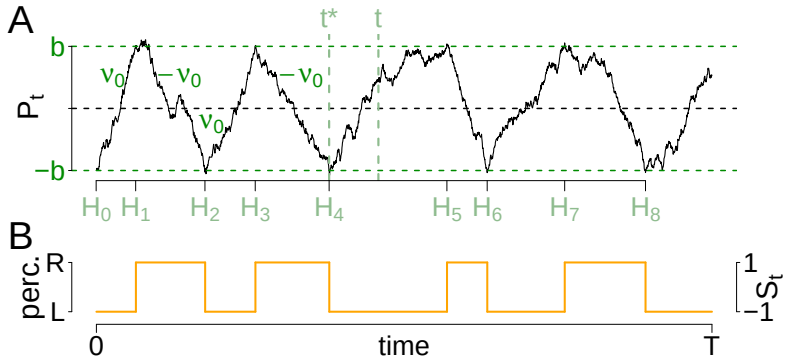

Figure 11.1: The HBMc. *The first passage times (H_i) (green) of a Brownian motion (black, panel A) with drift $\pm\nu_0$ at borders $\pm b$ indicate the times of the percept changes (orange, panel B). The Brownian motion is assumed to summarize the activity difference of two conflicting neuronal populations with only two parameters. Additionally, for a given t the value of t^* is visualized.*

11.1.2 Effect of single parameter changes

The influence of b and ν_0 on the mean dominance time μ and the CV is shown in Figure 11.2. Note that b has opposite effects on the mean ($2b/\nu_0$) and the CV$= 1/\sqrt{2b\nu_0}$ of the dominance times, whereas ν_0 has the same effect on mean and CV as it is in the denominator of both quantities (recall Proposition 8.6 for the transformation of b and ν_0 to μ and CV).

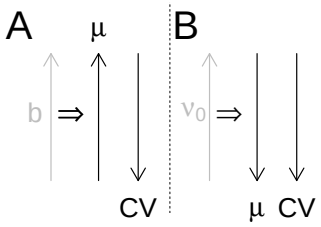

Figure 11.2: Influence of the HBMc parameters on mean and CV of the dominance times. *The influence of increasing the two parameters b (panel A) and ν_0 (panel B) while leaving the other one constant on μ and $CV = \sigma/\mu$ is shown.*

11.1.3 Remarks on the simulation

The simulation of the Hierarchical Brownian model (for continuous stimulation) on the interval $[0, T]$ mainly relies on the simulation of a Brownian motion on $[0, T]$. One way to generate such a stochastic process is to use the discrete skeleton $0 = t_0 < t_1 < \ldots < t_{T/\Delta} = T$ with step width $t_i - t_{i-1} =: \Delta > 0 \quad \forall i = 1, \ldots, T/\Delta$ by simulating i.i.d. random variables $I_1^\Delta, I_2^\Delta, \ldots, I_{T/\Delta}^\Delta$ with normal distribution with mean 0 and variance Δ (e.g., Asmussen and Glynn, 2007). To simulate the perception process $(P_t^\Delta)_{t=0,\Delta,2\Delta,\ldots}$ during continuous presentation on the discrete skeleton with step width Δ, we use for $i \geq 1$ the summing of the increments as follows

$$P_{t_i}^{\Delta} = P_{t_{i-1}}^{\Delta} + I_i^{\Delta} + \Delta \cdot \begin{cases} \nu_0, & \text{if } \operatorname{argmax}_{t_i}\{P_{t_i}^{\Delta} : P_{t_i}^{\Delta} \leq -b\} > \operatorname{argmax}_{t_i}\{P_{t_i}^{\Delta} : P_{t_i}^{\Delta} \geq b\}, \\ (-\nu_0), & \text{if } \operatorname{argmax}_{t_i}\{P_{t_i}^{\Delta} : P_{t_i}^{\Delta} \leq -b\} < \operatorname{argmax}_{t_i}\{P_{t_i}^{\Delta} : P_{t_i}^{\Delta} \geq b\}, \end{cases}$$

with $P_0^{\Delta} := -b$ and $\operatorname{argmax}\{\} := -1$.
Hence, in every simulation step we have to check whether the perception process is above b or below $-b$. Implementing this in a `for()`-loop is in the standard statistical programming package `R` time consuming in particular for small step widths Δ. Therefore, we propose to outsource the simulation to `C++` which is much more efficient while performing standard loops. Nevertheless, the normal distributed random variables are simulated in `R` and then transferred as function input to the `C++`-function. We compare the runtimes using the two different programming languages in Figure 11.3 for three different time horizons T and four different step widths Δ. The dependence of the computation time on the time horizon T and the programming language – `C++` (yellow points) leads to faster simulations – is clearly visible. The choice of the step width Δ is another crucial point in the simulation. Large Δ leads to inaccurate simulation, whereas a small Δ increases the computational effort (compare the different symbols in Figure 11.3). We recommend the step width $\Delta = 0.01$.

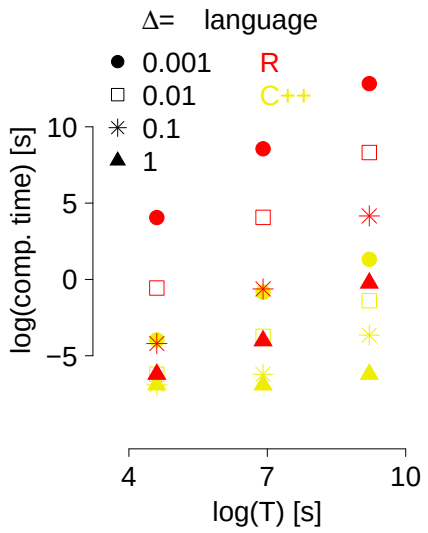

Figure 11.3: Comparison of the computation times for simulation of the HBMc. *Mean computation times (in ten trials) with `R` are printed red, whereas the `C++` results are printed yellow. The simulation of the HBMc is performed using different time horizons T and step widths Δ visualized by different symbols (see legend). Both axes are logarithmic due to the different magnitudes.*

11.2 Intermittent presentation

In this section we introduce the Hierarchical Brownian Motion model for intermittent presentation (Section 11.2.1), discuss its assumptions and its relation to the HMM (Sections

11.2.2 and 11.2.3) and elaborate on the effects of single parameter changes (Section 11.2.4). Moreover, in Sections 11.2.5 and 11.2.6, the dominance time distributions dependent on the following hidden state and Markov properties are examined. Finally, hints for simulation are given (Section 11.2.7).

11.2.1 The model

In the Hierarchical Brownian Motion model for intermittent presentation (HBMi), we require mechanisms for long dominance times in the stable state as well as for short dominance times in the unstable state. In order to describe the responses to intermittent and continuous presentation in one model framework, we assume the identical perceptual process as in the HBMc (Section 11.1) during phases of stimulus presentation. The periods of blank display represent the only difference in the experimental setup to continuous presentation. In these periods, we assume additional neuronal mechanisms. In particular, we assume that the perceptual process then takes on one of two mean drifts, ν_S in the stable state and $\nu_U \geq \nu_S$ in the unstable state, with potentially opposite signs of ν_0 and ν_S for increased stability (Figure 11.4). Note that the drifts ν_S and ν_U are not necessarily constant across the whole period of blank display, but they denote the mean drift of the process, which is sufficient to describe the distribution of dominance times. Interestingly, additional assumptions on the temporal behavior of the drift terms could also allow describing the impact of the lengths of blank displays (compare Section 15.2). Further, in the unstable state the border b_U at which perception and drift direction change is assumed smaller than the border b_S during stable perception. Switches between the stable and unstable state will be caused by a similar mechanism in a so-called background process B described later in this section.
Within a state (S or U), the fluctuation of the perception process between the borders is assumed analogous to the HBMc, except that the borders are dependent on the hidden state and that the drift is ν_0 during presentation and ν_S or ν_U during blank display. Formally, we denote by PR and BL the sets of all periods of stimulus presentation and blank display, respectively. Assuming that we start a trial with a presentation interval and then switch regularly between presentation intervals of length l_p and blank display of length l_b, PR and BL are given by

$$\mathrm{PR} = \bigcup_{i=1}^{T/(l_p+l_b)} [(i-1)(l_p+l_b); (i-1)(l_p+l_b)+l_p)$$
$$\mathrm{BL} = \bigcup_{i=1}^{T/(l_p+l_b)} [(i-1)(l_p+l_b)+l_p; i(l_p+l_b))$$

as shown in Figure 11.4.
The perception process $P := (P_t)_t$ is then given by

$$dP_t = \begin{cases} S_t\nu_0 dt + dW_t, & \text{if } t \in \mathrm{PR}, \\ S_t\nu_{\tilde{Y}_t} dt + dW_t, & \text{if } t \in \mathrm{BL}, \end{cases}$$

where $\tilde{Y}_t \in \{S, U\}$ denotes the hidden state at time $t \geq 0$ and $(W_t)_t$ denotes a standard Brownian motion. As a result, the mean drift per second is given by the weighted mean

$$\nu_S^* := \frac{l_b \cdot \nu_S + l_p \cdot \nu_0}{l_b + l_p} \quad \text{and} \quad \nu_U^* := \frac{l_b \cdot \nu_U + l_p \cdot \nu_0}{l_b + l_p} \tag{11.2}$$

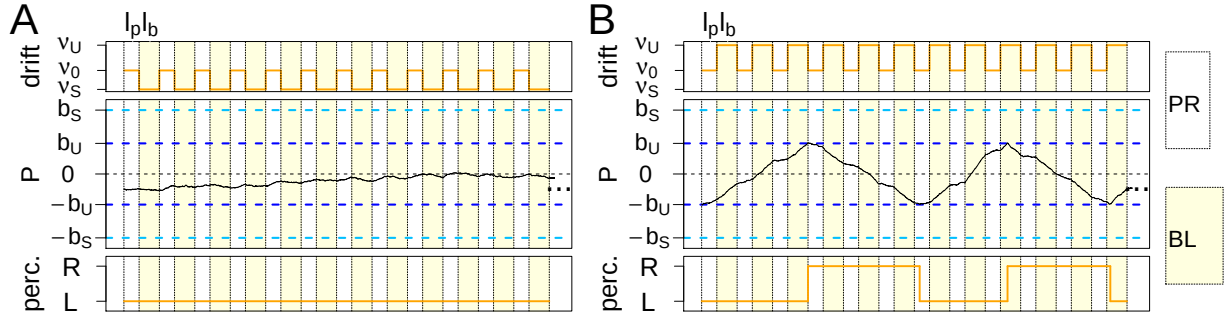

Figure 11.4: The perception process P in the HBMi during intermittent presentation. *During presentation, P has drift ν_0. During blank displays (yellow), P has drift ν_S in the stable phase (A), and drift ν_U in the unstable phase (B). Typically, we have $\nu_S \leq \nu_0$ and $\nu_U \geq \nu_0$. The borders are b_S (light blue horizontal line) in the stable state and b_U (blue horizontal line) in the unstable state.*

for states S and U, respectively. Because the periods l_b and l_p are typically short in relation to a dominance time, the behavior of P can be approximated by a Brownian motion with absolute drifts ν_S^* and ν_U^*, respectively. As in the HBMc, the sign of the drift $S_t := S(P_t, t)$ changes at every first hitting time of the respective border, i.e.,

$$S(P_t, t) := -\text{sgn}(P_{t^*}), \text{ where } t^* := t^*(t) := \sup\{x : x < t, |P_x| = b_{Y_x}\} \text{ with } t^*(0) = 0.$$

We initialize $P_0 = -b_{\tilde{Y}_0}$ for the initial state $\tilde{Y}_0$ which is the stable state with probability $\pi^*_{\text{start},S} := \mathbb{P}(\tilde{Y}_0 = S)$. The perception then takes the value L if $S_t = 1$ and R if $S_t = -1$ and switches at the first-hitting times $(H_i)_i$ of the borders $\pm b_i$ comparable to equation (11.1). Note that perception also changes during blank display. The dominance times are therefore again given by $d_i := H_i - H_{i-1}, i = 1, 2, \ldots$.
In order to describe the switching between the two states S and U, we use an analogous upper hierarchical level with another pair of conflicting neuronal populations. Their difference activity is described by a so-called background process $B := (B_t)_t$ (Figure 11.5 A, middle panel). B is also assumed to be a Brownian motion with drift. Its drift is assumed to vanish during presentation and to take the value $\pm\nu_B$ during blank display, where the sign of drift depends on the hidden state as follows

$$dB_t = \begin{cases} d\tilde{W}_t, & \text{if } t \in \text{PR}, \\ \nu_B dt + d\tilde{W}_t, & \text{if } t \in \text{BL}, \tilde{Y}_t = S, \\ -\nu_B dt + d\tilde{W}_t, & \text{if } t \in \text{BL}, \tilde{Y}_t = U, \end{cases} \tag{11.3}$$

where $(\tilde{W}_t)_t$ is a Brownian motion independent of $(W_t)_t$. Again, the mean drift across PR and BL intervals is $\nu_B^* := \frac{l_b \cdot \nu_B}{l_b + l_p}$.
The background process B evokes changes between the stable and the unstable state. Specifically, at the time of a percept change t^*, the question of whether the process stays in the former state (S or U) or switches to the other state depends only on the value of B. Two borders, $\tilde{b}_S$ and $\tilde{b}_U$, determine this switching as follows (see Figure 11.5). If the former state is S, the process remains stable if and only if $B_{t^*} \geq \tilde{b}_S$ (first light blue arrow in panel A), while switching to the unstable state if $B_{t^*} < \tilde{b}_S$ (blue arrow, panel A). Analogously, if the

former state is U, the process switches to S if and only if $B_{t^*} \geq \tilde{b}_U$ (right light blue arrow, panel A), while staying in U if $B_{t^*} < \tilde{b}_U$ (blue arrow, panel B). After the percept change, the background process B is reset to zero and then follows its usual dynamic (eq. (11.3)), i.e., the sign of its drift changes if and only if the state has changed. Finally, as the perception process P fluctuates between $\pm b_S$ in the stable state and between $\pm b_U$ in the unstable state, the value of P is reset when the state changes, to the value $\mathrm{sgn}(P)b_S$ when changing to the stable state and to $\mathrm{sgn}(P)b_U$ when changing to the unstable state.

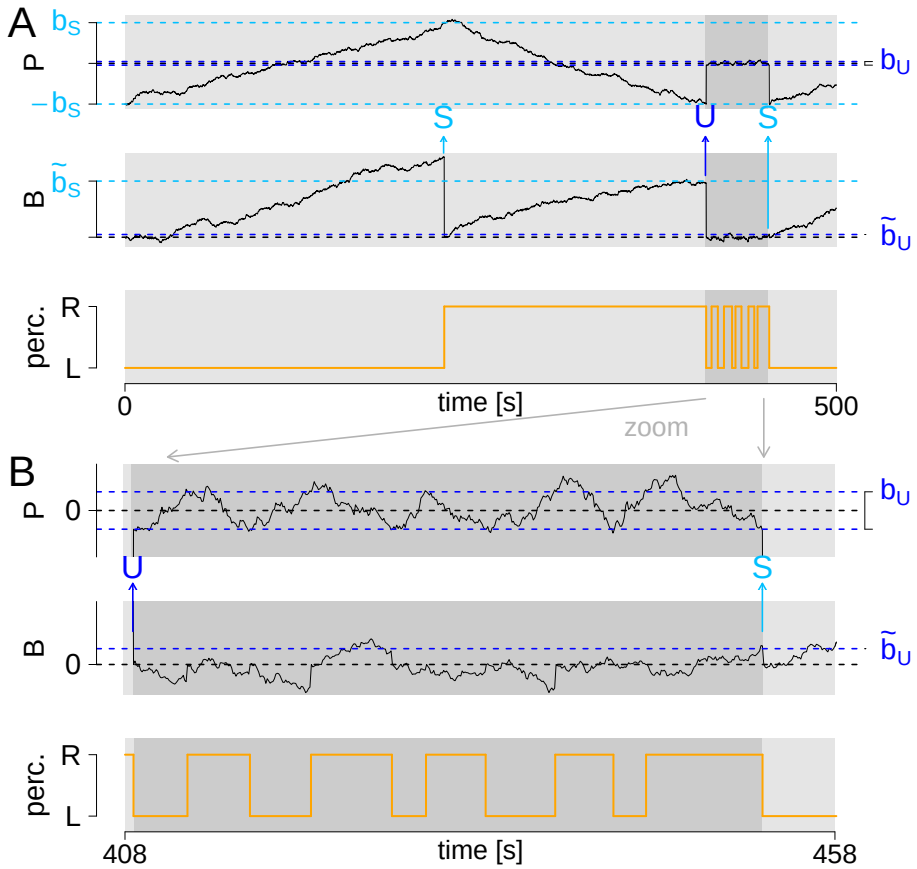

Figure 11.5: The HBMi. *The perception process P, the background process B and the resulting percept. (A): A simulation on $[0, 500]$. (B): The same realization, zoomed in on the time interval $[408, 458]$. Stable phases indicated by light gray background, unstable phases indicated by dark gray background. The beginnings of stable and unstable phases are marked with light blue and blue arrows, respectively.*

Detailed model definition

Here, we state a precise mathematical model definition of the HBMi (as supplement to the prose definition given above).

Model 11.1. ***Hierarchical Brownian model in intermittent presentation (HBMi)*** *Let $b_S > 0$, $b_U \in (0, b_S]$, $\tilde{b}_S > 0$ and $\tilde{b}_U \in \mathbb{R}$ be four borders, let $\nu_0 > 0, \nu_S \in \mathbb{R}, \nu_U \geq \nu_S, \nu_B > 0$ be drift parameters, $T > 0$ be a time horizon, $l_p > 0$ be the length of stimulus presentation and $l_b > 0$ be the length of blank display. Furthermore, $0 \leq \pi^*_{start,S} \leq 1$ is the initial weight of the stable state.*
Let $(W_t)_t$ and $(\tilde{W}_t)_t$ be independent standard Brownian motions and P_0^S be a Bernoulli($\pi^*_{start,S}$)-distributed random variable. Then, the dynamics of the perception process $P := (P_t)_{t\in[0,T]}$ and the background process $B := (B_t)_{t\in[0,T]}$ are assumed to be

$$dP_t = \begin{cases} S(P_t,t)\nu(P_t,B_t,t)dt + dW_t, & \text{if } db_t = 0, \\ |b_S - b_U|, & \text{if } db_t \neq 0 \wedge P_t \leq \min(sgn(P_t)b_S, sgn(P_t)b_U), \\ -|b_S - b_U|, & \text{if } db_t \neq 0 \wedge P_t > \min(sgn(P_t)b_S, sgn(P_t)b_U), \end{cases}$$

with $P_0 = -b_0$, (b_t) the border process defined below and the process (S_t) depending on the sign of the last hit border $\pm b_t$

$$S_t := S(P_t, b_t, t) := -sgn(P_{t^*}), \text{ where } t^* := t^*(t) := \sup\{x : x < t, |P_x| = b_x\} \text{ with } t^*(0) = 0.$$

The drift $\nu(P_t, B_t, t)$ depends on the background process (see below)

$$\nu(P_t, B_t, t) := \begin{cases} \nu_0, & \text{if } t \in PR, \\ \nu_t^{blank}, & \text{if } t \in BL, \end{cases}$$

where $\nu_t^{blank} := \nu^{blank}(P_t, B_t, t)$

$$\nu_t^{blank}(P_t, B_t, t) := \begin{cases} V_0, & \text{if } t^* = 0, \\ \nu_S, & \text{if } t^* > 0 \wedge ((B_{t^*} \geq \tilde{b}_S \wedge \nu_{t^*}^{blank} = \nu_S) \text{ or } (B_{t^*} \geq \tilde{b}_U \wedge \nu_{t^*}^{blank} = \nu_U)), \\ \nu_U, & \text{if } t^* > 0 \wedge ((B_{t^*} < \tilde{b}_S \wedge \nu_{t^*}^{blank} = \nu_S) \text{ or } (B_{t^*} < \tilde{b}_U \wedge \nu_{t^*}^{blank} = \nu_U)), \end{cases}$$

where V_0 is v_S if $P_0^S = 1$ and v_U otherwise, and the border process $(b_t) := b(\nu_t^{blank}, t)$ is assumed to be

$$b(\nu_t^{blank}, t) := \begin{cases} b_S, & \text{if } \nu_t^{blank} = \nu_S, \\ b_U, & \text{if } \nu_t^{blank} = \nu_U. \end{cases}$$

The perception at time $t \geq 0$ takes the value L if $S_t = 1$ and R if $S_t = -1$ and $(H_i)_{i=0,1,\ldots}$ denotes the process of first passage times as defined in (11.1) with b replaced by b_t.
For the background process $(B_t)_{t\in[0,T]}$ we assume $B_0 = 0$ and

$$dB_t = \begin{cases} \mathbb{1}_{t\in BL}\tilde{S}(B_t, P_t, t)\nu_B dt + d\tilde{W}_t, & \text{if } dS_t = 0, \\ -sgn(B_t)B_t, & \text{if } dS_t \neq 0, \end{cases}$$

with the sign of drift

$$\tilde{S}_t := \tilde{S}(\nu_t^{blank}, t) := \begin{cases} 1, & \text{if } \nu_t^{blank} = \nu_S, \\ -1, & \text{if } \nu_t^{blank} = \nu_U. \end{cases}$$

We say that the HBMi is in state S at time t if v_t^{blank} equals ν_S and in state U otherwise.

11.2.2 Discussion of assumptions and interpretation of model parameters

The technical advantage of the HBMi is that the resulting dominance times agree in most parts with the dominance times resulting from the inverse Gaussian HMM assumptions, which allows model fitting also to short data sections and comparison across clinical groups. In addition, the HBMi also provides a relation to potential underlying neuronal processes, as discussed in the following and illustrated in Figure 11.6.

Both HBMi-processes P and B are assumed Brownian motions with drift which may be interpreted as the activity difference between neuronal populations. Implicitly, this assumes mechanisms of self-excitation, cross-inhibition and adaptation across these neuronal populations, as proposed by various authors (Brascamp et al., 2009; Gigante et al., 2009). Without explicitly modeling such mechanisms in order to reduce the number of parameters and allow model fitting, the parameter sets are reduced to the mean drifts ν and the borders b. Analogously to the HBMc, the speed of the drifts could be considered related to the inverse of the connection strengths within and across populations that engage in self excitation and cross inhibition. The border b, in analogy to the HBMc, could be considered related to the size of the respective populations under consideration. The use of different borders allows fitting of highly various response patterns and can be motivated as follows.

In the HBMi, the perception process P has two borders, $b_S \geq b_U$ for the stable and the unstable state. This suggests different population sizes of neurons involved in the stable and unstable state. Typically $b_S > b > b_U$, suggesting that in the stable state, the activity of the dominant population is increased by joining additional neurons to the population, for example by positive feedback mediated by population S. Vice versa, in the unstable state, only a minimal population is involved in the respective percept, leading to fast changes. Thus, one could assume that the dominant percept population size is decreased by the population U (red arrows). The active population sizes are indicated by different circle sizes in the first line of Figure 11.6 and are assumed modulated by the background populations S and U.

The background process B models the activity difference between S and U and is also associated with two borders, $\tilde{b}_S$ and $\tilde{b}_U$. The assumption regarding resetting of B at percept change is technically necessary to generate independent dominance times and to thus allow straightforward model fitting (compare Section 12.2). In the picture of Figure 11.6 it can be motivated as follows. Population S is capable of offering positive feedback to the currently active population, L or R, which results in an increased population size as described above. S is also activated by the active population. Therefore, a percept change causes a resetting to zero. However, if S had shown high previous activation (above $\tilde{b}_S$), the activity of S can increase rapidly again, causing another stable dominance time. In contrast, in case of weak previous activation (below $\tilde{b}_S$), the unstable population U is taking over, marking the transition to an unstable state. With opposite signs, i.e., negative drift and a small new border $\tilde{b}_U$, the process proceeds analogously. Similar to the mean drift terms ν_S and ν_U, the drift ν_B is not necessarily constant but describes the mean drift of B during the period of blank display. During continuous presentation the background process is of no relevance as its drift vanishes during presentation phases and moreover the drift of P is generally given by ν_0.

In addition to the potential neurophysiological interpretations of the model parameters, we give here a relation of the parameters to the response patterns. Interestingly, the seven HBMi parameters allow the reproduction of highly variable response patterns as are also observed in the empirical data sets (e.g., Figure 1.3). The following quantities, which are easily derived from the parameters, offer a straightforward pattern interpretation.

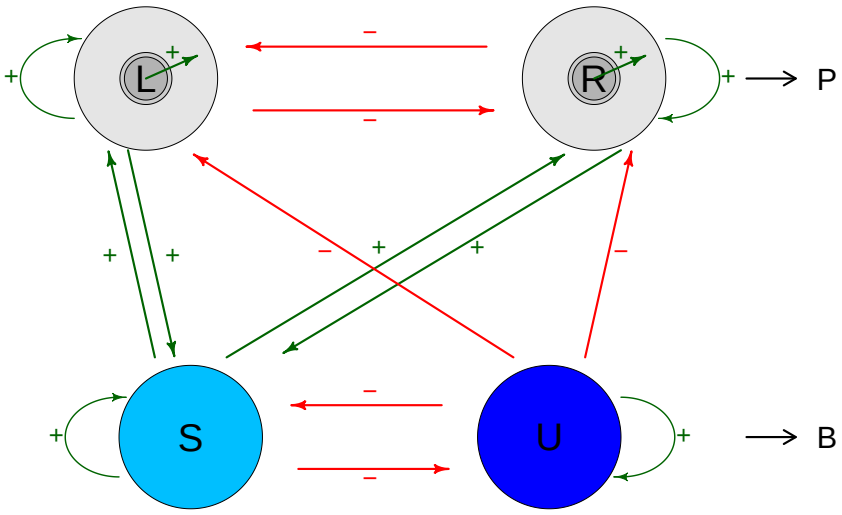

Figure 11.6: Motivation of HBMi assumptions. *The populations L and R being active during continuous presentation are visualized by the medium circles. During stable phases in intermittent presentation the population size is increased (large circles), whereas during unstable phases it is decreased (small circles). The populations S and U are responsible for the hidden state. Excitations are visualized by green arrows and inhibitions by red arrows.*

First, the parameter sets (b_S, ν_S^*) and (b_U, ν_U^*) can be interpreted analogously to the parameters (b, ν_0) in continuous stimulation (Section 11.1.2). That means, an increase in the border (b_S or b_U) increases the mean dominance time and decreases the CV in the respective state. An increase in the drift (ν_S^* or ν_U^*) decreases the mean dominance time, while also decreasing the CV. Recall that the CVs of dominance times during stable and unstable states are given by

$$\mathrm{CV}_S^* := 1/\sqrt{2b_S\nu_S^*} \quad \text{and} \quad \mathrm{CV}_U^* := 1/\sqrt{2b_U\nu_U^*}, \quad \text{respectively.}$$

Figure 11.7 illustrates examples with small CV_S^* (panels A-D) and large CV_S^* (panels E-H). Second, the parameters $\tilde{b}_S$ and ν_B^* can be interpreted best when compared to b_S and ν_S^* as follows. Consider the expected fraction of $\tilde{b}_S$ reached by the background process at the end of a stable dominance time,

$$\frac{\text{Expected duration of a stable dominance time}}{\text{Expected duration until } B \text{ reaches } \tilde{b}_S} = \frac{2b_S/\nu_S^*}{\tilde{b}_S/\nu_B^*} = \frac{2b_S\nu_B^*}{\tilde{b}_S\nu_S^*},$$

which is related to the transition probability from stable to unstable state. In case of a small background border $\tilde{b}_S < b_S$ and small ν_S^*, the probability of B crossing $\tilde{b}_S$ until percept change is high, such that the process remains stable. Figure 11.7 A, B, E and F show such parameter combinations. An analogous term can be derived in comparison to the parameters $\tilde{b}_U$ and ν_U^*. Third, the parameter $\tilde{b}_U$ is related to the number of dominance times in the unstable state observed before changing to the stable state. Recall that the drift of B is negative during unstable phases. Therefore, a large value of $\tilde{b}_U$ implies a low probability to reach $\tilde{b}_U$ until the percept change. This implies a high expected number of dominance times in the unstable state, or a low transition probability from the unstable to the stable state. Figure 11.7 B, D, F and H show examples with large values of $\tilde{b}_U$.

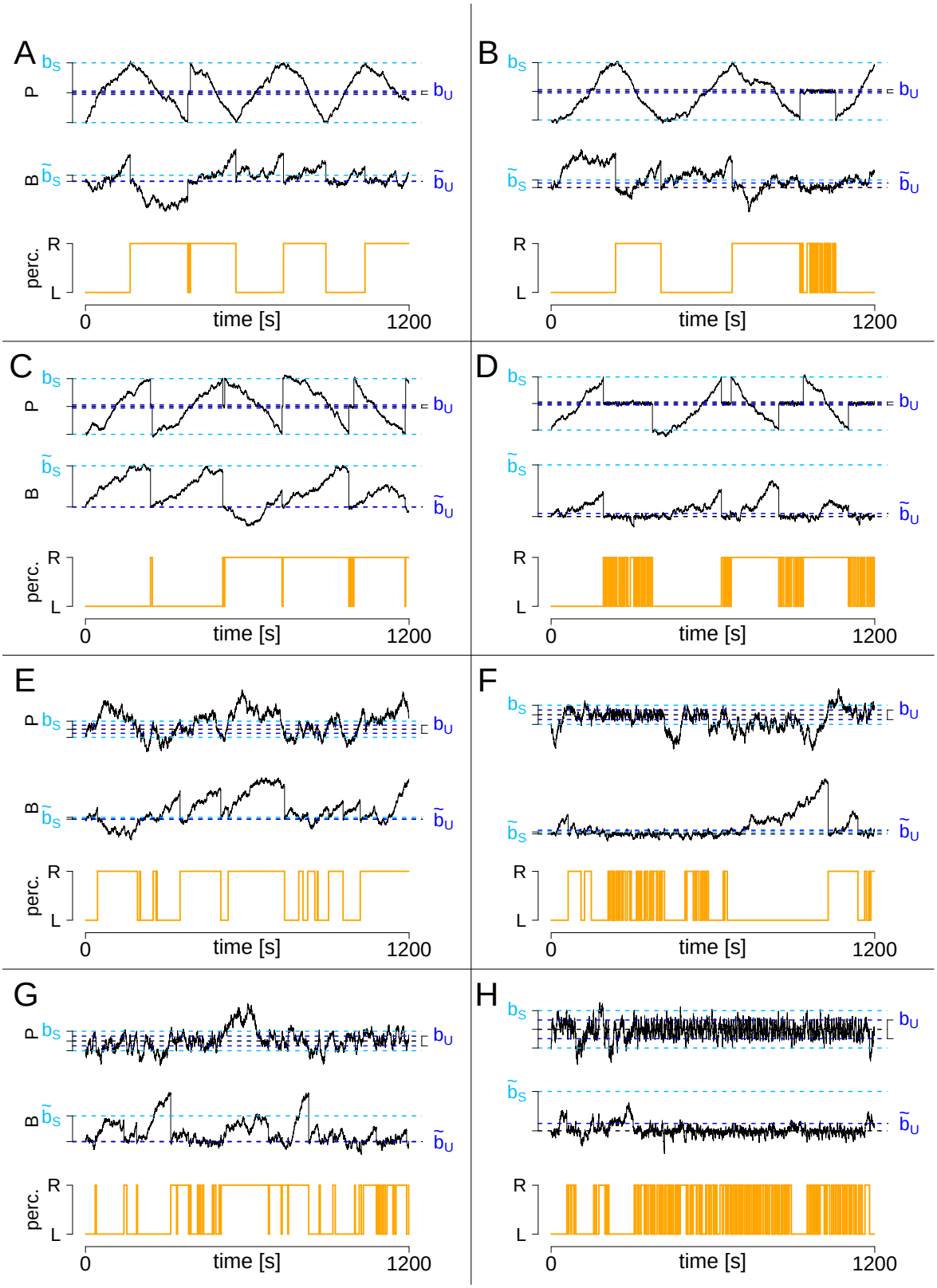
A
B
C
D
E
F
G
H
P
B
perc.
R
L
0
time [s]
1200

Figure 11.7: Impact of HBMi parameter values on the response patterns. *Examples of simulated response patterns are shown for different values of the three quantities* CV_S^*, $2b_S\nu_B^*/\tilde{b}_S\nu_S^*$ *and* $\tilde{b}_U$. *The quantities for panels A-H were* $CV_S^* = \{0.2, 0.2, 0.2, 0.2, 1, 1, 1, 1\}, 2b_S\nu_B^*/\tilde{b}_S\nu_S^* = \{4, 4, 0.4, 0.4, 4, 4, 0.4, 0.4\}$, $\tilde{b}_U = \{0, 3, 0, 3, 0, 3, 0, 3\}$.

Starting positions We discuss the starting positions P_0, which is $-b_S$ with probability $\pi^*_{\text{start},S}$ and $-b_U$ else, and $B_0 = 0$. Thus, the first dominance time is distributed like all other dominance times. Choosing P_0 as b_U or b_S does not change the distributions and as we are only interested in the alternation behavior it does not matter whether the starting perception is left or right. Choosing a starting point different from a border for the perception process leads to a different distribution of the first dominance time which we do not observe in the data. A nonzero starting value for the background process also imposes challenges as then the probability to remain in the current state would be different for the first dominance time which is not justified by the data or theoretical reflections.

11.2.3 Relation of the HBMi to the two state HMM

In the following we only consider the HMM with inverse Gaussian distributed dominance times. The relation of the HBMc to the one state HMM is simple as is represents only a reparametrization. Both the one state HMM and the HBMc yield independent and IG distributed dominance times.
For the intermittent case, the relation of the HBMi to the two state HMM is not as straightforward. The two models are highly similar in the sense that they use two parameters to describe long and short dominance times, respectively (e.g., (μ_S, σ_S) and (b_S, ν_S^*) for the stable state). In the HMM, the dominance times are IG distributed, given the state with the respective parameters. In the HBMi, the dominance times are approximately IG distributed, where the minor deviation from the IG distribution originates from the minor deviation of P from a Brownian motion with drift ν_S^* (or ν_U^*), instead of exactly assuming drift ν_0 during stimulation and ν_S (or ν_U) during blank display. However, the marginal distribution of P at multiples of such intervals $l_p + l_b$ is identical to the marginal distribution of a Brownian motion with drift ν_S^* (or ν_U^*) at these time points, and the differences can only be observed in the meantime. Because dominance times usually span multiple trials of duration $l_p + l_b$, the approximation is very close. To simplify comparison between the HMM and the HBMi we denote by (μ_S^*, σ_S^*) and (μ_U^*, σ_U^*) the mean and standard deviation of dominance times in the HBMi in the stable and unstable state, respectively. These have analogous interpretations as (μ_S, σ_S) and (μ_U, σ_U) in the HMM and are given by

$$\mu_S^* \approx 2b_S/\nu_S^* \quad \text{and} \quad \sigma_S^* \approx \sqrt{2b_S/{\nu_S^*}^3}, \tag{11.4}$$

and analogously for μ_U^* and σ_U^*, where the approximation is again due to the minimal difference between the mean drift ν_S^* and the changing drift $\nu_S + \nu_0$ during presentation and blank display. As another similarity, both models use additional parameters $((p_{SS}, p_{UU})$ and $(\tilde{b}_S, \tilde{b}_U, \nu_B))$ to describe the transition probabilities between the stable and the unstable state.
The main difference between the HBMi and the two state HMM concerns the dynamic of the state transitions between stable and unstable state. In the HMM, transition probabilities

are given by $(1 - p_{SS})$ and $(1 - p_{UU})$ and are independent of the duration of the previous dominance time. In contrast, in the HBMi, a transition from stable to unstable state requires that B has not reached $\tilde{b}_S$ at the end of the respective dominance time. Therefore, the transition probability $\tilde{p}_{SU}(d_i)$ depends on the duration d_i of the i-th dominance time, where shorter dominance times yield higher transition probabilities. Note that the position of B at the end of a dominance time d_i is given by an increment of a Brownian motion with drift ν_B^* in the fixed time interval d_i. Therefore the position is normally distributed with mean $d_i \cdot \nu_B^*$ and variance d_i, and the probability to remain in the stable state (which is the probability that the background process exceeds $\tilde{b}_S$) is given by

$$\tilde{p}_{SS}(d_i) := \mathbb{P}(Y_{i+1} = S | Y_i = S, d_i) \approx 1 - \Phi_{\nu_B^* d_i, d_i}\left(\tilde{b}_S\right), \tag{11.5}$$

where $\Phi_{\mu,\sigma^2}()$ denotes the distribution function of the normal distribution with mean μ and variance σ^2 and Y_i is the hidden state of the i-th dominance time. Similarly, the relation between the transition probability and the previous dominance time d_i is for the unstable state given by

$$\tilde{p}_{UU}(d_i) := \mathbb{P}(Y_{i+1} = U | Y_i = U, d_i) \approx \Phi_{-\nu_B^* d_i, d_i}\left(\tilde{b}_U\right). \tag{11.6}$$

Note that we use the approximate sign "$\approx$" because the drift of B is not exactly ν_B^* throughout, but is assumed to change between ν_0 and ν_B during stimulation and blank display, respectively, yielding a mean drift of ν_B^*. Analogously to the above explanation, differences caused by the approximation can be considered minimal.
In order to obtain quantities comparable to the transition probabilities p_{SS} and p_{UU} in the HMM, we can obtain the marginal transition probabilities in the HBMi as the expected value of $\tilde{p}_{SS}$ and $\tilde{p}_{UU}$ by integration across all dominance times. As shown in Corollary 8.10 the positions X_S and X_U of B at the end of an independent stable or unstable IG distributed dominance time follow the normal-inverse Gaussian (NIG) distribution. The resulting transition probabilities in the HBMi can then be calculated as

$$p_{SS}^* \approx \mathbb{P}(X_S \geq \tilde{b}_S) \quad \text{and} \quad p_{UU}^* \approx \mathbb{P}(X_U < b_U), \tag{11.7}$$

where X_S is NIG distributed with parameters $(0, \sqrt{{\nu_S^*}^2 + {\nu_B^*}^2}, \nu_B^*, 2b_S)$ and X_U is NIG distributed with parameters $(0, \sqrt{{\nu_U^*}^2 + {\nu_B^*}^2}, -\nu_B^*, 2b_U)$. For the parametrization, recall the proof of Corollary 8.10. In a reasonable model, not both of p_{SS}^* and p_{UU}^* equal one.
One should note that due to the difference in transition probabilities of the two models, the parameters (b_S, ν_S^*) are not direct reparametrization of (μ_S, σ_S) (and similarly for the unstable state). Furthermore, the dependence of the transition probability on the length of the previous dominance time is one important new aspect in the HBMi not described in the HMM, which will also be used in Section 14.2.1 for comparison of models and empirical observations.

Influence of the length of dominance times on the transition probabilities

As explained above (equation (11.5)), the transition probability from the stable to the unstable state $\tilde{p}_{SU}(d)$ decreases with the length of the stable dominance time. This is visualized in Figure 11.8 A.
Investigating the influence of the length d of an unstable dominance time (which depends on b_U and ν_U^*) on the transition probability $\tilde{p}_{US}(d)$ to the stable state, the model implication

is ambiguous which we illustrate in Figure 11.8 B and C. Non-positive borders $\tilde{b}_U$ (panel B) cause very large transition probabilities for short unstable dominance times as there is not enough time for the background process to reach $\tilde{b}_U$ (the state only remains unstable if the background process is below $\tilde{b}_U$ at the end of a dominance time, recall moreover the negative drift of the background process during unstable phases). The longer the dominance time, the more time the background process has to cross $\tilde{b}_U$.
Positive values of $\tilde{b}_U$ (panel C) imply generally smaller transition probabilities (due to the negative drift of the background process). Additionally, the curves have a maximum turning point as a minimum time is needed for a process with negative drift to reach a positive border with a small probability.

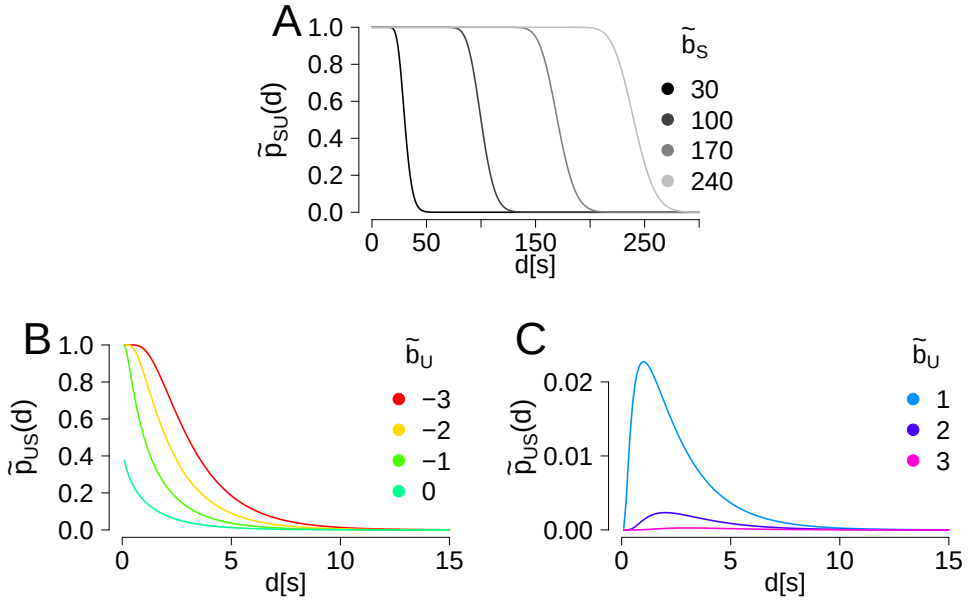

Figure 11.8: Transition probabilities $\tilde{p}_{SU}(d), \tilde{p}_{US}(d)$ depending on the length d of the dominance time for $\nu_B^* = 1$ and different values of $\tilde{b}_S, \tilde{b}_U$ as indicated in the legends. *(A) The transition probability in the unstable state $\tilde{p}_{SU}(d)$ decreases with the length of the stable dominance time. (B) $\tilde{b}_U \leq 0$ leads to monotonously decreasing transition probabilities $\tilde{p}_{US}(d)$. (C) $\tilde{b}_U > 0$ causes transition probability curves with a maximum which decreases with $\tilde{b}_U$ increasing. The transition probabilities are much smaller than the largest probabilities in panel B.*

11.2.4 Effect of single parameter changes

How does an increase in the size of the neuronal pool b_S or in the border $\tilde{b}_S$ of the background process influence the response pattern? These and other comparable questions are important for understanding the HBMi and its interpretation properly. Therefore, we discuss the influence of single HBMi parameters on the response patterns. As the response patterns are determined by the distribution of the stable and the unstable dominance times as well as by the transition probabilities we examine the impact of each HBMi parameter on $\mu_S^*, \mathrm{CV}_S^*, \mu_U^*, \mathrm{CV}_U^*, p_{SS}^*, p_{UU}^*$. The results are summarized in Table 11.1.

Parameter	Change	μ_S^*	CV_S^*	μ_U^*	CV_U^*	p_{SS}^*	p_{UU}^*
b_S	↑	↑	↓	→	→	↑	→
	↓	↓	↑	→	→	↓	→
ν_S^*	↑	↓	↓	→	→	↓	→
	↓	↑	↑	→	→	↑	→
b_U	↑	→	→	↑	↓	→	Fig. 11.9
	↓	→	→	↓	↑	→	Fig. 11.9
ν_U^*	↑	→	→	↓	↓	→	Fig. 11.9
	↓	→	→	↑	↑	→	Fig. 11.9
$\tilde{b}_S$	↑	→	→	→	→	↓	→
	↓	→	→	→	→	↑	→
$\tilde{b}_U$	↑	→	→	→	→	→	↑
	↓	→	→	→	→	→	↓
ν_B^*	↑	→	→	→	→	↑	↑
	↓	→	→	→	→	↓	↓

Table 11.1: Effect of single parameter changes in the HBMi. *The influence of changing one of the seven parameters $b_S, \nu_S^*, b_U, \nu_U^*, \tilde{b}_S, \tilde{b}_U, \nu_B^*$ while leaving the others constant on the target parameters $\mu_S^*, CV_S^*, \mu_U^*, CV_U^*, p_{SS}^*, p_{UU}^*$ is shown. An increase in a parameter is highlighted yellow, and a decrease is highlighted red where no influence is colored orange. The effect of b_U and ν_U^* on p_{UU}^* is more complex and shown in Figure 11.9.*

The explanations for the effects of b_S and ν_S^* on μ_S^* and CV_S^* as well as for the effects of b_U and ν_U^* on μ_U^* and CV_U^* are as already explained similar to the effects of drift and border parameter in the HBMc (compare Section 11.1.2). Increasing b_S moreover also increases the probability to remain in the stable state p_{SS}^* as the background process has more time to reach its border. Increasing the drift ν_S^* has the opposite effect as the background process has less time to exceed the border.
A larger drift ν_B^* of the background process also increases the probability to stay in the current state as the process gets faster above or below the borders $\tilde{b}_S$ and $\tilde{b}_U$, respectively. Increasing $\tilde{b}_S$ hinders the background process to pass the border and thus p_{SS}^* decreases. Increasing $\tilde{b}_U$ facilitates the background process to be below the border and thus p_{UU}^* increases.
The dependence of p_{UU}^* on b_U and ν_U^* depends on the sign of $\tilde{b}_U$ and is illustrated in Figure 11.9 and explained in the following. Panel A indicates for a positive $\tilde{b}_U$ (orange line) a negative correlation between b_U and p_{UU}^* for small b_U and a positive correlation for larger b_U. Increasing b_U implies longer unstable dominance times. The negative drift of B in unstable phases therefore causes for a long dominance time a large probability for B to be negative and thus below b_U. If the dominance time is short, there is not enough time for the background process to reach $\tilde{b}_U$ and thus increasing a short dominance time by increasing b_U increases the probability to reach the border and therefore has a negative impact on p_{UU}^*. With $\tilde{b}_U \leq 0$ (red line) there is a positive relation between b_U and $\tilde{p}_{UU}$ as longer dominance times enhance the probability of B to be below $\tilde{b}_U$.
The impact of ν_U^* on p_{UU}^* is visualized in panel B. Generally, increasing ν_U^* causes shorter unstable dominance times. Assuming a positive $\tilde{b}_U$ (orange line) only for rather long dominance times (small ν_U^*) the background process has some chance to hit $\tilde{b}_U$. For shorter dominance times the process does not have enough time and therefore remains below $\tilde{b}_U$ and in the

unstable state. In case of a non-positive $\tilde{b}_U$ (red line), shorter dominance times (i.e., larger ν_U^*) imply that B with negative drift has less time to reach the border and thus p_{UU}^* approaches zero.

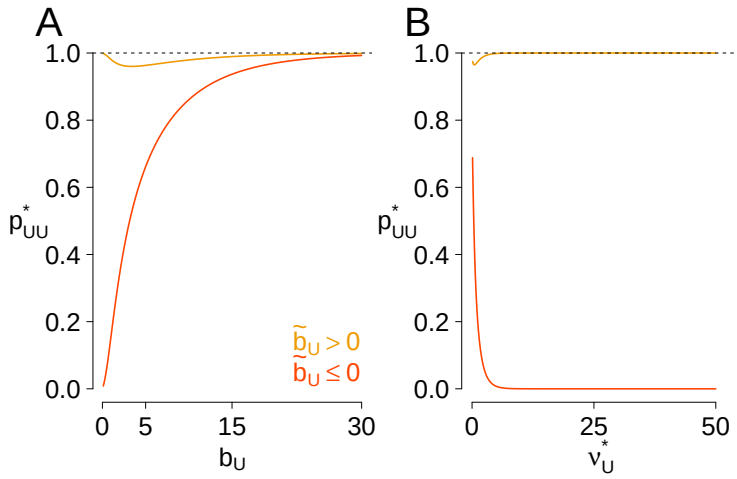

Figure 11.9: Dependence of p_{UU}^* on b_U and ν_U^*. *In panel A we let $\nu_U^* = 0.73$ and vary b_U, and in panel B ν_U^* varies and $b_U = 1.84$ is used. The orange lines code a positive $\tilde{b}_U = 2.39$, and the red lines code a negative $\tilde{b}_U = -2.39$. All other parameters can be found in Table 12.2, subject C (page 162).*

11.2.5 Dominance time distributions depending on the next state

As already discussed in Section 11.2.3 the definition of the HBMi implies shorter stable dominance times before a state change. Here, in Lemma 11.2 we derive the expected values of a stable dominance time before a state change (termed μ_S^-) and before another stable dominance time (termed μ_S^+). Moreover, the corresponding expected values μ_U^+ and μ_U^- for the unstable states are derived. Again, due to taking the mean of different drifts, this derivation is only a close approximation, but we omit approximation signs here for convenience. The distribution of the dominance times depending on the next state is computed in Lemma 11.3.

Lemma 11.2. ***Expected dominance times conditioned on the next state***
Let $\Theta_{HBMi} = (b_S, \nu_S, b_U, \nu_U, \tilde{b}_S, \tilde{b}_U, \nu_B, \nu_0, \pi^*_{start,S})$ be the parameter set of a HBMi and p_{SS}^*, p_{UU}^* be defined as in equation (11.7). Then it holds

$$\mu_S^+ := \mathbb{E}[D_1 | Y_1 = S, Y_2 = S] = \frac{\int_0^\infty f^{IG}_{2b_S/\nu_S^*, \sqrt{2b_S/\nu_S^{*3}}}(t)(1 - \Phi_{\nu_B^* t, \sqrt{t}}(\tilde{b}_S))tdt}{p_{SS}^*},$$

$$\mu_S^- := \mathbb{E}[D_1 | Y_1 = S, Y_2 = U] = \frac{\int_0^\infty f^{IG}_{2b_S/\nu_S^*, \sqrt{2b_S/\nu_S^{*3}}}(t)\Phi_{\nu_B^* t, \sqrt{t}}(\tilde{b}_S)tdt}{1 - p_{SS}^*},$$

$$\mu_U^+ := \mathbb{E}[D_1 | Y_1 = U, Y_2 = U] = \frac{\int_0^\infty f^{IG}_{2b_U/\nu_U^*, \sqrt{2b_U/\nu_U^{*3}}}(t)\Phi_{-\nu_B^* t, \sqrt{t}}(\tilde{b}_U)tdt}{p_{UU}^*},$$

$$\mu_U^- := \mathbb{E}[D_1 | Y_1 = U, Y_2 = S] = \frac{\int_0^\infty f^{IG}_{2b_U/\nu_U^*, \sqrt{2b_U/\nu_U^{*3}}}(t)(1 - \Phi_{-\nu_B^* t, \sqrt{t}}(\tilde{b}_U))tdt}{1 - p_{UU}^*}.$$

Proof: First, we focus on μ_S^+. It holds with D_1^S as $\text{IG}(2b_S/\nu_S^*, \sqrt{2b_S/\nu_S^{*3}})$-distributed dominance time emitted in the stable state

$$\begin{aligned}\mu_S^+ &= \mathbb{E}[D_1^S|Y_1 = S, Y_2 = S] = \mathbb{E}[D_1^S|Y_1 = S, B_{D_1^S} \geq \tilde{b}_S] \\ &= \frac{\int_0^\infty \mathbb{P}(D_1^S = t, B_{D_1^S} \geq \tilde{b}_S)tdt}{\mathbb{P}(B_{D_1} \geq \tilde{b}_S)} \\ &= \frac{\int_0^\infty f^{\text{IG}}_{2b_S/\nu_S^*, \sqrt{2b_S/\nu_S^{*3}}}(t)(1 - \Phi_{\nu_B^* t, \sqrt{t}}(\tilde{b}_S))tdt}{p_{SS}^*}.\end{aligned}$$

In the second line, we used the definition of conditional expected values. The independence of P and B during one dominance time was applied in the third line to derive the joint distribution in the numerator. The first hitting time of the border b_S (leading to the perceptual reversal) is inverse Gaussian distributed, and the position of the background process (which started from 0) given the fixed and known hitting time t is a normal distributed random variable. The expression in the denominator just is the term for p_{SS}^* as given in equation (11.7).
The derivation for μ_S^- follows similar ideas:

$$\begin{aligned}\mu_S^- &= \mathbb{E}[D_1^S|Y_1 = S, Y_2 = U] = \mathbb{E}[D_1^S|Y_1 = S, B_{D_1^S} < \tilde{b}_S] \\ &= \mathbb{E}[D_1|Y_1 = S, Y_2 = U] = \frac{\int_0^\infty f^{\text{IG}}_{2b_S/\nu_S^*, \sqrt{2b_S/\nu_S^{*3}}}(t)\Phi_{\nu_B^* t, \sqrt{t}}(\tilde{b}_S)tdt}{1 - p_{SS}^*}.\end{aligned}$$

Here, the background process should not reach the border $\tilde{b}_S$ at the time of perceptual reversal. Therefore, basically the $1 - \Phi()$- and p_{SS}^*-factors are substituted by $\Phi()$ and $1 - p_{SS}^*$, and the same explanation as above can be used.
The proofs for μ_U^+ and μ_U^- follow analogously. □

Figure 11.10 shows the values of $\mu_S^+, \mu_S^-, \mu_U^+$ and μ_U^- as well as μ_S^* and μ_U^* for the four response patterns printed in Figure 9.1 (page 70, parameter combinations given in Table 12.2). μ_S^- is (if it exists) per construction always smaller than μ_S^+. For the unstable state, there are two examples with $\mu_U^- > \mu_U^+$ and one with $\mu_U^- < \mu_U^+$ (for subject E the unstable state does not occur). This is due to the fact that the impact of longer unstable dominance times on the state change probability is not always monotone (recall Figure 11.8).
In case of large transition probabilities to the other state, the unconditioned expectations μ_j^* are close to μ_j^- as most of the dominance times are followed by a dominance time of the other state $i \neq j$. An analogous argument holds for small transition probabilities.

Analytical treatments of $\mu_S^+, \mu_S^-, \mu_U^+$ and μ_U^- are difficult due to the involved distribution functions. We therefore analyze the qualitative influence of the HBMi parameters using μ_S^+ as an example. We distinguish between the absolute value of μ_S^+ and its value relative to the mean $\mu_S^* \approx 2b_S/\nu_S^*$ of all stable dominance times.
An *increase* in μ_S^+ is caused by

$$b_S \uparrow, \quad \nu_S^* \downarrow, \quad \tilde{b}_S \uparrow, \quad \nu_B \downarrow .$$

A larger border b_S or a smaller drift ν_S^* in general causes longer stable dominance times (Table 11.1) and therefore also μ_S^+ increases. Increasing $\tilde{b}_S$ or decreasing ν_B implies that the

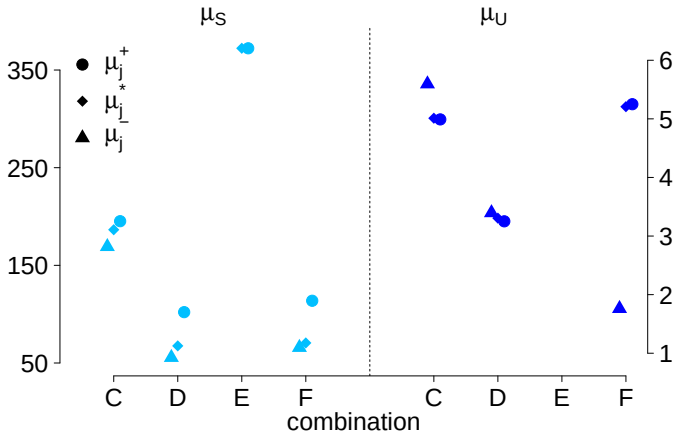

Figure 11.10: Example values of conditioned expectations. *The values of the conditioned expectations $\mu_S^+, \mu_S^-, \mu_U^+, \mu_U^-$ and the unconditioned expectations μ_S^*, μ_U^* for the four parameter combinations C, D, E, F whose response patterns are shown in Figure 9.1 C-F (page 70) and whose parameters are given in Table 12.2 (page 162). The left part of the graph shows the expectations for the stable state, whereas the right part shows the expectations for the unstable state. Note that for parameter combination E only stable phases occur such that only $\mu_S^+ = \mu_S^*$ exists.*

background process needs more time to cross $\tilde{b}_S$, and thereby only very long stable dominance times are followed by another stable dominance time. A *decrease* in μ_S^+ is caused by the opposite parameter changes.
An *increase* in μ_S^+/μ_S^* is caused by

$$b_S \downarrow, \quad \nu_S^* \uparrow, \quad \tilde{b}_S \uparrow, \quad \nu_B \downarrow .$$

Decreasing the border b_S or increasing the drift ν_S^* causes shorter stable dominance times (Table 11.1). Thus, only atypically long stable dominance times are followed by another stable dominance time. The same effect is caused by an increase in $\tilde{b}_S$ or a decrease in ν_B which complicate the crossing of the border $\tilde{b}_S$ by the background process. A *decrease* in μ_S^+/μ_S^* is caused by the opposite parameter changes.
Similar observations and arguments hold for the parameter influence on μ_S^-, μ_U^+ and μ_U^-.

Next, we derive in Lemma 11.3 the distribution of dominance times in the HBMi conditioned on the next state.

Lemma 11.3. ***Distribution of dominance times conditioned on the next state***
Let $\Theta_{HBMi} = (b_S, \nu_S^*, b_U, \nu_U^*, \tilde{b}_S, \tilde{b}_U, \nu_B^*, \pi_{start,S}^*)$ be the parameter set of a HBMi and p_{SS}^*, p_{UU}^* be defined as in equation (11.7). Then it holds for the densities of the dominance times given the state of the next dominance time

$$f_{D_S^+}(d) := f_{D_{SS}}(d) := f(d|Y_1 = S, Y_2 = S) = \frac{f^{IG}_{2b_S/\nu_S^*, \sqrt{2b_S/\nu_S^{*3}}}(d)(1 - \Phi_{\nu_B^* d, \sqrt{d}}(\tilde{b}_S))}{p_{SS}^*},$$

$$f_{D_S^-}(d) := f_{D_{SU}}(d) := f(d|Y_1 = S, Y_2 = U) = \frac{f^{IG}_{2b_S/\nu_S^*, \sqrt{2b_S/\nu_S^{*3}}}(d)\Phi_{\nu_B^* d, \sqrt{d}}(\tilde{b}_S)}{1 - p_{SS}^*},$$

$$f_{D_U^+}(d) := f_{D_{UU}}(d) := f(d|Y_1 = U, Y_2 = U) = \frac{f^{IG}_{2b_U/\nu_U^*, \sqrt{2b_U/\nu_U^{*3}}}(d)\Phi_{-\nu_B^* d, \sqrt{d}}(\tilde{b}_U)}{p_{UU}^*},$$

$$f_{D_U^-}(d) := f_{D_{US}}(d) := f(d|Y_1 = U, Y_2 = S) = \frac{f^{IG}_{2b_U/\nu_U^*, \sqrt{2b_U/\nu_U^{*3}}}(d)(1 - \Phi_{-\nu_B^* d, \sqrt{d}}(\tilde{b}_U))}{1 - p_{UU}^*}.$$

Proof: First, we focus on $f_{D_S^+}(d)$ and observe

$$\begin{aligned} f_{D_S^+}(d) &= f(d|Y_1 = S, Y_2 = S) = f(d|Y_1 = S, B_{D_1} \geq \tilde{b}_S) \\ &= \frac{\int_{\tilde{b}_S}^{\infty} \mathbb{P}(D_1^S = d, B_{D_1^S} = x)dx}{\mathbb{P}(B_{D_1^S} \geq \tilde{b}_S)} \\ &= \frac{f^{\text{IG}}_{2b_S/\nu_S^*, \sqrt{2b_S/\nu_S^{*3}}}(d)(1 - \Phi_{\nu_B^* d, \sqrt{d}}(\tilde{b}_S))}{p_{SS}^*}, \end{aligned}$$

where exactly the same ideas as in the proof of Lemma 11.2 were applied.
The derivation for the other three cases follows similar ideas. □

The next corollary connects the expectations μ_S^* and μ_U^* of stable and unstable dominance times to the corresponding conditioned expectations. Again, approximation signs are omitted.

Corollary 11.4. ***Connection of μ_j^* to μ_j^+ and μ_j^-***
Let μ_S^*, μ_U^* be defined as in equation (11.4), $\mu_S^+, \mu_S^-, \mu_U^+, \mu_U^-$ be as in Lemma 11.2 and p_{SS}^*, p_{UU}^* be as in equation (11.7). Then,

$$\mu_S^* = p_{SS}^*\mu_S^+ + (1 - p_{SS}^*)\mu_S^- \quad \text{and} \quad \mu_U^* = p_{UU}^*\mu_U^+ + (1 - p_{UU}^*)\mu_U^-.$$

Proof: We show the assertion for the stable state with similar arguments holding true for the unstable state. We have with D_1^S as a dominance time in the stable state and the law of total probability

$$\begin{aligned} \mu_S^* = \mathbb{E}[D_1^S] &= \mathbb{P}(Y_1 = S, Y_2 = S)\mathbb{E}[D_1^S|Y_1 = S, Y_2 = S] \\ &\quad + \mathbb{P}(Y_1 = S, Y_2 = U)\mathbb{E}[D_1^S|Y_1 = S, Y_2 = U] \\ &= p_{SS}^*\mu_S^+ + (1 - p_{SS}^*)\mu_S^-. \end{aligned}$$

□

11.2.6 Markov property of the HBMi

The underlying processes of Hidden Markov Models fulfill the conditional independence assumption (9.1) and the Markov property (9.2). Now, let Y_i be the hidden state of the i-th dominance time in the HBMi. The conditional independence property

$$\mathbb{P}(D_i = d_i | Y_i = y_i) = \mathbb{P}(D_i = d_i | Y_1^i = y_1^i, D_1^{i-1} = d_1^{i-1}), \quad 1 \leq i \leq n, \tag{11.8}$$

is also fulfilled for the HBMi $(Y_i, D_i)_{1 \leq i \leq n}$ as the drift ν_{y_i} and the border b_{y_i} being responsible for the distribution of the dominance times depend only on the current hidden state y_i and are independent of the history. Moreover, the HBMi constitutes a kind of Markov property

$$\mathbb{P}(Y_i = y_i | Y_{i-1} = y_{i-1}, D_{i-1} = d_{i-1}) = \mathbb{P}(Y_i = y_i | Y_1^{i-1} = y_1^{i-1}, D_1^{i-1} = d_1^{i-1}), \quad 2 \leq i \leq n, \tag{11.9}$$

where the only difference to the Markov property of the HMM is the additional condition $D_{i-1} = d_{i-1}$ on the left hand side of equation (11.9) due to the dependence of the state transition on the emission. Again, this property follows directly by the model construction as discussed in Section 11.2. Note that the mean probability $\mathbb{P}(Y_i = y_i | Y_{i-1} = y_{i-1})$ is given by $p^*_{y_{i-1} y_i}$ (equation (11.7)) and that $(Y_i)_{1 \leq i \leq n}$ can also be interpreted as embedded Markov chain (when the dominance times are unknown).
As with the HMM, the state $\tilde{Y}_t$ of the HBMi at a given time t can also be understood as a semi-Markov process (Definition 8.15). We will focus on that more in detail in Section 13.2.1.

11.2.7 Remarks on the simulation

The same remarks about outsourcing parts of the code to `C++` as for the simulation of the HBMc (Section 11.1.3) hold for the simulation of the HBMi, i.e., the simulation speeds up remarkably using `C++`. Additionally, the different drifts and borders during stable and unstable state as well as the different drifts during presentation of the stimulus and blank displays have to be considered.

Chapter 12

The HBM: Parameter estimation

This chapter explains and evaluates the parameter estimation of the Hierarchical Brownian Model for continuous presentation as well as for intermittent presentation of a bistable stimulus. In the case of continuous presentation, we apply maximum likelihood estimation to the dominance times (comparable to the estimation of the HMM for continuous stimulation, Section 9.3). Again, the exact sampling distributions for small sample sizes are derived. We also introduce UMVU and moment estimators for the border parameter b and the drift parameter ν_0 (Section 12.1).
In Section 12.2 the estimation procedure for the HBMi is discussed. Basically, we derive the log-likelihood of the model using forward variables and then maximize the log-likelihood numerically.
In Section 12.3 estimated HBM parameter sets of typical response patterns are shown. Section 12.4 uses parametric bootstrap to evaluate the precision of parameter estimation for the HBMc and the HBMi. Finally, in Section 12.5 we show why the Viterbi algorithm for the estimation of the most likely hidden state path can be transferred from the world of Hidden Markov Models to the HBMi.

12.1 Continuous presentation: Parameter estimation

Here, we present different approaches for the parameter estimation in the HBMc. In practice, we use the maximum likelihood approach (Section 12.1.1). As the ML estimators are biased, we moreover discuss an UMVU idea where, however, the drawbacks predominate (Section 12.1.2). Additionally, in Section 12.1.3 moment estimators are briefly introduced. In case the reader is just interested in a brief description of the parameter estimation used in practice (e.g., when analyzing the data set Schmack et al. (2015)), we suggest reading only the first paragraph of Section 12.1.1 and then jumping ahead to Section 12.2.

12.1.1 Maximum likelihood estimation

First, we derive the ML estimators of b and ν_0 in the HBMc. Then, we compute exact sampling distributions of these ML estimators. These results are original. Moreover, we also derive the asymptotic normal distribution of the estimators.

The ML estimation in the HBMc makes use of the fact that with $(H_i)_{i\geq 0}$ as the first hitting times of the borders (equation (11.1)) the resulting dominance times

$$d_i := H_i - H_{i-1}, \qquad i = 1, 2, \ldots$$

are independent and IG distributed, with a known relation between the HBMc parameters b and ν_0 and the parameters μ and σ of the IG distribution, given by $\mu = 2b/\nu_0$ and $\sigma = \sqrt{2b/\nu_0^3}$ (Proposition 8.6). Due to the invariance property of ML estimators, the ML estimators $\hat{b}$ and $\hat{\nu}_0$ can be derived via

$$\hat{b} := \hat{b}^{\mathrm{ML}} = (1/2) \cdot \sqrt{\hat{\mu}^3/\hat{\sigma}^2}, \qquad \hat{\nu}_0 := \hat{\nu}_0^{\mathrm{ML}} = \sqrt{\hat{\mu}/\hat{\sigma}^2},$$

where $\hat{\mu}$ and $\hat{\sigma}$ are derived from equation (9.3). Explicitly, we have

$$\hat{b} = \frac{1}{2}\sqrt{\frac{1}{1/n\sum_{i=1}^{n} 1/d_i - n/\sum_{i=1}^{n} d_i}} \qquad \hat{\nu}_0 = \frac{2n\hat{b}}{\sum_{i=1}^{n} d_i}. \tag{12.1}$$

Censored dominance times may be included as in the estimation of the HMM for continuous presentation (page 76).

12.1.1.1 Sampling distribution of the estimators $\hat{b}$ and $\hat{\nu}_0$

The sampling distributions of the ML estimators of b and ν_0 for n independent IG(b, ν_0)-distributed random variables are derived. In Figure 12.1 we compare for four different sample sizes the simulated empirical distributions with the exact theoretical distributions of $\hat{b}$ and $\hat{\nu}_0$ given in Propositions 12.2 and 12.3 and the asymptotic normal distributions derived in the next Section 12.1.1.2. For $n = 5, n = 10$ and $n = 20$ there is a notable difference between the asymptotic and the exact distributions which describe the empirical distributions very well. For the largest $n = 100$, the theoretical as well as the asymptotic distributions fit the simulated data closely. In a potential future work the theoretical distributions can be used to compute confidence intervals for parameters estimated from small sample sizes.

To derive the sampling distribution of $\hat{b}$ note that due to Proposition 8.4 and Proposition 8.6 $4b^2 = \mu^3/\sigma^2 = \lambda$ and thus $4\hat{b}^2 = \hat{\mu}^3/\hat{\sigma}^2 = \hat{\lambda}$ when using the ML estimators. Therefore, it follows by the sampling distributions of $\hat{\mu}$ and $\hat{\lambda}$ (Proposition 9.2)

$$\frac{nb^2}{\hat{b}^2} \sim \chi^2_{n-1}.$$

Extracting the root gives

$$\tilde{X} := \frac{\sqrt{n}b}{\hat{b}} \sim \chi_{n-1},$$

where χ_{n-1} denotes the chi-distribution (Definition 9.3) with $n-1$ degrees of freedom. To obtain the density f of the estimator $\hat{b} = g(\tilde{X})$ itself with $g(x) = b\sqrt{n}/x$ we apply for $x > 0$ the method of transformations as follows

$$f(x) = F'(x) = \frac{d}{dx}(F_{\tilde{X}}(g^{-1}(x))) = f_{\tilde{X}}(g^{-1}(x))\Big|\frac{d}{dx}g^{-1}(x)\Big|.$$

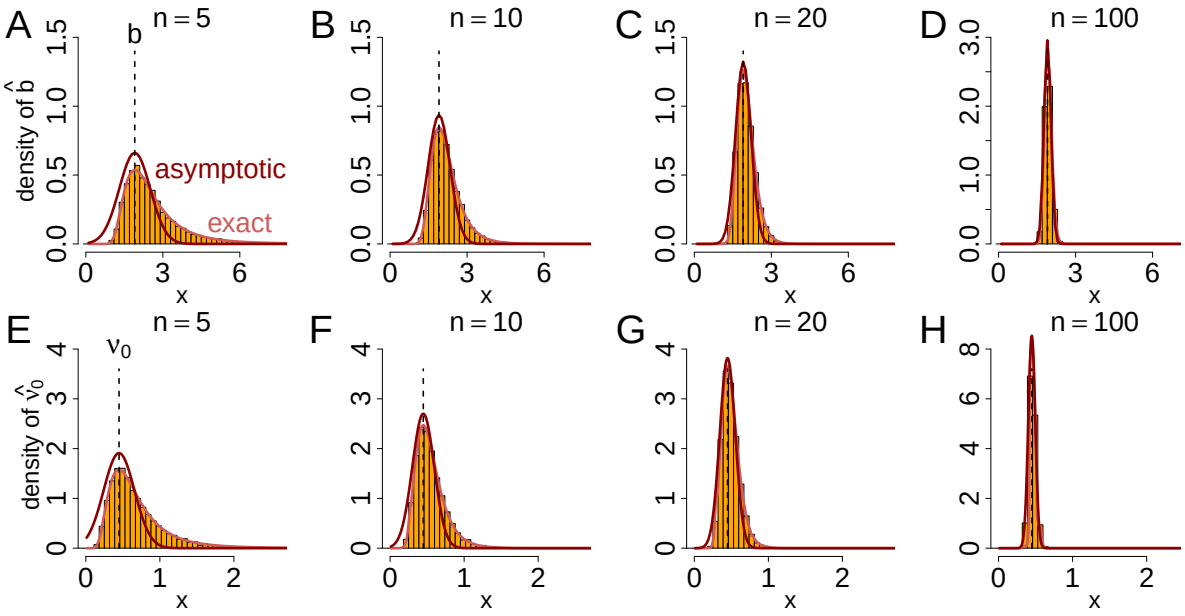

Figure 12.1: Comparison of exact (light red) and asymptotic (dark red) distribution of $\hat{b}$ (A-D) and $\hat{\nu}_0$ (E-H). *The histograms show the empirical distribution of $\hat{b}$ or $\hat{\nu}_0$ in 10000 simulations with $IG(8.5, 6.5)$-distributed random variables for the four sample sizes $n \in \{5, 10, 20, 100\}$, respectively. The true values are indicated by dashed lines. Consider the different scaling of the y-axes in panels D and H, respectively*

With $g^{-1}(x) = b\sqrt{n}/x$ we derive

$$f(x) = f_{n-1}^{\chi}\left(\frac{b\sqrt{n}}{x}\right)\frac{b\sqrt{n}}{x^2}$$

for $x > 0$ and 0 otherwise.
Now, the expectation of the estimator $\hat{b}$ is derived. Therefore, we need the expectation of the inverse of a χ_k-distributed random variable X. The distribution of $1/X$ is called **reciprocal chi-distribution**.

Lemma 12.1. ***Expectation of the reciprocal chi-distribution***
Let X be χ_k distributed. Then it holds

$$\mathbb{E}\left[\frac{1}{X}\right] = \frac{\Gamma(k/2 - 1/2)}{\sqrt{2}\Gamma(k/2)}.$$

Proof: We derive

$$\begin{aligned}\mathbb{E}\left[\frac{1}{X}\right] &= \int_0^\infty x^{k-2}\frac{2^{1-k/2}\exp(-x^2/2)}{\Gamma(k/2)}dx \\ &= \frac{2^{1-k/2}}{\Gamma(k/2)}\int_0^\infty x^{k-2}\exp(-x^2/2)dx. \qquad (12.2)\end{aligned}$$

Next, note that $\Gamma(k/2-1/2)/2 = \int_0^\infty (z^{k-2}\exp(-z^2)dz)$ (for the definition of $\Gamma(k)$ compare, e.g., Abramowitz and Stegun, 1972). Substituting $z/\sqrt{2} = x$ yields

$$\Gamma((k-1)/2)2^{k/2-3/2} = \int_0^\infty x^{k-2}\exp(-x^2/2)dx.$$

Plugging this in (12.2) we obtain

$$\mathbb{E}\left[\frac{1}{X}\right] = \frac{\Gamma(k/2-1/2)}{\sqrt{2}\Gamma(k/2)}.$$

□

Using Lemma 12.1, we derive with X now as χ_{n-1} distributed random variable

$$\mathbb{E}[\hat{b}] = b\sqrt{n}\mathbb{E}\left[\frac{1}{X}\right] = b\sqrt{n}\frac{\Gamma(n/2-1)}{\sqrt{2}\Gamma(n/2-1/2)}.$$

Hence, the bias of $\hat{b}$ is given by

$$\mathbb{B}\text{ias}(\hat{b}) = \left(\sqrt{n}\frac{\Gamma(n/2-1)}{\sqrt{2}\Gamma(n/2-1/2)} - 1\right) b. \tag{12.3}$$

Applying an asymptotic approximation for the Gamma function (eq. 6.1.39 in Abramowitz and Stegun, 1972), we observe for $n \to \infty$: $\Gamma(n/2-1)/\Gamma(n/2-1/2) \propto \sqrt{\frac{2}{n}}$. Thus, the bias of $\hat{b}$ vanishes asymptotically.
Moreover, we have $\hat{b} = \sqrt{\hat{\mu}^3/\hat{\sigma}^2}/2$. We know by Propositions 9.2 and 9.5 that $\hat{\mu}$ and $\hat{\sigma}$ are consistent, i.e., converge in probability toward μ and σ, respectively. Thus, by continuous mapping and Slutskys's theorem the consistency of $\hat{b}$ follows.

The results are summarized in the following Proposition.

Proposition 12.2. ***Sampling distribution and expectation of $\hat{b}$***
Let $\hat{b}$ be the ML estimator of b using a sample of $n \geq 2$ $IG(2b/\nu_0, \sqrt{2b/\nu_0^3})$-distributed random variables. The random variable $\sqrt{n}b/\hat{b}$ is χ_{n-1} distributed. $\hat{b}$ has the density

$$f(x) = f_{n-1}^{\chi}\left(\frac{b\sqrt{n}}{x}\right)\frac{b\sqrt{n}}{x^2},$$

if $x > 0$ and 0 otherwise, and the expectation of $\hat{b}$ is

$$\mathbb{E}[\hat{b}] = b\sqrt{n}\frac{\Gamma(n/2-1)}{\sqrt{2}\Gamma(n/2-1/2)}.$$

The estimator $\hat{b}$ is consistent.

Next, we investigate the distribution of the ML estimator $\hat{\nu}_0$.

Proposition 12.3. ***Sampling distribution and expectation of $\hat{\nu}_0$***
Let $\hat{\nu}_0$ be the ML estimator of ν_0 using a sample of $n \geq 2$ $IG(2b/\nu_0, \sqrt{2b/\nu_0^3})$-distributed random variables. The density of $\hat{\nu}_0$ is given by

$$f(x) = \frac{8b^2 n}{x^3} \int_0^\infty f^{IG}_{2b/\nu_0, \sqrt{2nb/\nu_0^3}}(y) f^{\chi^2}_{n-1}\left(\frac{4nb^2}{x^2 y^2}\right) \frac{1}{y^2} dy$$

for $x > 0$ and 0 otherwise. The expectation of $\hat{\nu}_0$ is

$$\mathbb{E}[\hat{\nu}_0] = \sqrt{2n}b \frac{\Gamma(n/2-1)}{\Gamma(n/2-1/2)} \left(\frac{\nu_0}{2b} + \frac{1}{4nb^2}\right).$$

The estimator $\hat{\nu}_0$ is consistent.

Proof: To derive the density we first define $\tilde{X} := (2b\sqrt{n})/\hat{\nu}_0$ and derive the density of $\tilde{X}$. Then, we use this density to conclude the density of $\hat{\nu}_0$.
With $\hat{\nu}_0 = 2\hat{b}/\hat{\mu}$, $\lambda = 4b^2$ (Proposition 8.4 and Proposition 8.6) and $\hat{\lambda} = 4\hat{b}^2$ we observe

$$\frac{2b\sqrt{n}}{\hat{\nu}_0} = \frac{2b\sqrt{n}\hat{\mu}}{2\hat{b}} = \frac{\sqrt{n\lambda}\hat{\mu}}{\sqrt{\hat{\lambda}}}.$$

By Proposition 9.2 we know that $\tilde{Y} := \hat{\mu}$ is IG distributed with parameters μ and $\sigma/\sqrt{n}$ (in the parametrization used here $2b/\nu_0$ and $\sqrt{2nb/\nu_0^3}$) and that $\tilde{Z} := n\lambda/\hat{\lambda}$ is χ^2_{n-1}-distributed. The density function of the product $\tilde{X} = \tilde{Y}\sqrt{\tilde{Z}}$ is given by $f_{\tilde{X}}(x) = \int_{-\infty}^{\infty} f_{\tilde{Y}}(y) f_{\tilde{Z}}(x^2/y^2) 2x/y^2 dy$ (e.g., Grimmett and Stirzaker, 2001). Thus,

$$f_{\tilde{X}}(x) = \int_0^\infty f^{\text{IG}}_{2b/\nu_0, \sqrt{2nb/\nu_0^3}}(y) f^{\chi^2}_{n-1}\left(\frac{x^2}{y^2}\right) \frac{2x}{y^2} dy$$

for $x > 0$ and 0 otherwise. The latter display is the density of $\tilde{X}$. To obtain the density f of the estimator $\hat{\nu}_0 = g(\tilde{X})$ itself with $g(x) = 2b\sqrt{n}/x$ for $x > 0$ and $g(x) = 0$ otherwise, we apply the method of transformations. With $g^{-1}(x) = 2b\sqrt{n}/x$ it follows

$$f(x) = \int_0^\infty f^{\text{IG}}_{2b/\nu_0, \sqrt{2nb/\nu_0^3}}(y) f^{\chi^2}_{n-1}\left(\frac{4nb^2}{x^2 y^2}\right) \frac{4b\sqrt{n}}{xy^2} \frac{2b\sqrt{n}}{x^2} dy$$

for $x > 0$ and 0 otherwise which is the assertion after rearranging terms.
To compute the expected value note that the distribution of

$$\frac{\hat{\nu}_0}{2b\sqrt{n}} = \frac{2\hat{b}}{2b\sqrt{n}\hat{\mu}} = \frac{\sqrt{\hat{\lambda}}}{\sqrt{n\lambda}\hat{\mu}}$$

is the product distribution of the random variables $1/\sqrt{\tilde{Z}} = \sqrt{\hat{\lambda}/n\lambda}$ and $1/\tilde{Y} = 1/\hat{\mu}$. By Propositions 9.2 and 8.8 $1/\tilde{Y}$ is RIG distributed with parameters $2b/\nu_0$ and $\sqrt{2nb/\nu_0^3}$ and expected value

$$\mathbb{E}\left[\frac{1}{\tilde{Y}}\right] = \frac{\nu_0}{2b} + \frac{1}{4nb^2},$$

and by Proposition 9.2 and the explanations on page 147 $1/\sqrt{\tilde{Z}}$ follows the reciprocal chi-distribution with $n-1$ degrees of freedom. Its expected value is known by Lemma 12.1

$$\mathbb{E}\left[\frac{1}{\sqrt{\tilde{Z}}}\right] = \frac{\Gamma(n/2-1)}{\sqrt{2}\Gamma(n/2-1/2)}.$$

Moreover, $1/\tilde{Y}$ and $1/\sqrt{\tilde{Z}}$ are independent due to Proposition 9.2. Thus, the assertion about the expected value follows directly by multiplying $1/\mathbb{E}[\tilde{Y}]$, $1/\mathbb{E}[\sqrt{\tilde{Z}}]$ and $2b\sqrt{n}$.
Hence, the bias of $\hat{\nu}_0$ derives as

$$\mathbb{B}\text{ias}(\hat{\nu}_0) = \left(1 - 2b\left(\frac{1}{2b} + \frac{1}{4nb^2\nu_0}\right)\sqrt{\frac{n}{2}}\frac{\Gamma(n/2-1)}{\Gamma(n/2-1/2)}\right)\nu_0. \tag{12.4}$$

Again, an application of the asymptotic approximation for the Gamma function shows that the bias vanishes asymptotically.
In addition, we observe $\hat{\nu}_0 = \sqrt{\hat{\mu}/\hat{\sigma}^2}$. We know by Propositions 9.2 and 9.5 that $\hat{\mu}$ and $\hat{\sigma}$ are consistent, i.e., converge in probability toward μ and σ, respectively. Thus, by continuous mapping and Slutskys's theorem the consistency of $\hat{\nu}_0$ follows. □

Figure 12.2 visualizes the relative bias $(\mathbb{B}\text{ias}(\hat{\theta})/\theta)$ for the parameters $\theta = b, \theta = \nu_0$ depending on the sample size n. The relative bias for ν_0 is slightly larger than that for b. Both are larger than 0.25 for $n \leq 5$, larger than 0.1 for $n \leq 13$ and larger than 0.01 for $n \leq 126$ (not shown in the graph).

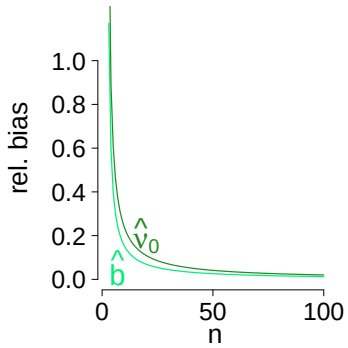

Figure 12.2: Relative bias of $\hat{b}$ and $\hat{\nu}_0$. *The true parameters are $b = 1.91, \nu_0 = 0.45$, and equations* (12.3) *and* (12.4) *are used.*

12.1.1.2 ML estimators: Asymptotic distribution

Recall from Section 9.3.3 that under certain regularity conditions the asymptotic distribution of ML estimators is normal with the variance determined by the inverse of the Fisher-information matrix. Here, we let D denote an inverse Gaussian distributed random variable and investigate the asymptotic variances of the ML estimators $\hat{b}$ and $\hat{\nu}_0$. Using this parametrization, we have $\eta(b, \nu_0) = (-\nu_0^2/2, -2b^2)$ in the exponential family representation of the IG distribution. The existence and continuity of the derivatives of η are easy to see as well as its injectivity. The nonsingularity of the covariance matrix of $t(D)$ was shown in Section 9.3.3. Therefore,

the regularity conditions are met, and the asymptotic variance of the asymptotic normal distribution of the estimators is given by the diagonal entries of the inverse Fisher-information matrix $I(b, \nu_0)$. The means of the asymptotic normal distribution are the true parameter values b and ν_0, respectively.
The density $\log f^{\text{IG}}_{2b/\nu_0, \sqrt{2b/\nu_0^3}}(d)$ of the inverse Gaussian distribution with parameters $2b/\nu_0$ and $\sqrt{2b/\nu_0^3}$ is given by

$$\log f^{\text{IG}}_{2b/\nu_0, \sqrt{2b/\nu_0^3}}(d) = \log(2b) - (1/2)\log(2\pi d) - \frac{\nu_0^2(d - 2b/\nu_0)^2}{2d}.$$

As for the IG distribution the regularity conditions for equation (9.9) to hold are fulfilled, the Fisher-information matrix for an IG$(2b/\nu_0, \sqrt{2b/\nu_0^3})$-distributed random variable D hence is given by

$$\begin{aligned} I(b, \nu_0) &:= -\mathbb{E}\begin{bmatrix} \frac{\partial^2}{\partial b^2}\log f^{\text{IG}}_{2b/\nu_0, \sqrt{2b/\nu_0^3}}(D) & \frac{\partial^2}{\partial b \partial \sigma}\log f^{\text{IG}}_{2b/\nu_0, \sqrt{2b/\nu_0^3}}(D) \\ \frac{\partial^2}{\partial \sigma \partial b}\log f^{\text{IG}}_{2b/\nu_0, \sqrt{2b/\nu_0^3}}(D) & \frac{\partial^2}{\partial \nu_0}\log f^{\text{IG}}_{2b/\nu_0, \sqrt{2b/\nu_0^3}}(D) \end{bmatrix} \\ &= -\mathbb{E}\begin{bmatrix} -\frac{1}{b^2} - \frac{4}{D} & 2 \\ 2 & -D \end{bmatrix} \\ &= \begin{bmatrix} \frac{2\nu_0}{b} + \frac{2}{b^2} & -2 \\ -2 & \frac{2b}{\nu_0} \end{bmatrix}. \end{aligned}$$

In the last line, we plugged in $\mathbb{E}[1/D] = \nu_0/2b + 1/4b^2$ (Prop. 8.8).
We invert the Fisher-information matrix $I(b, \nu_0)$, divide by n and obtain for the asymptotic variances of the estimators $\hat{b}^{\text{ML}}$ and $\hat{\nu}_0^{\text{ML}}$ the values

$$\mathbb{V}\text{ar}\left(\hat{b}^{\text{ML}}\right) \approx \frac{b^2}{2n} \qquad \mathbb{V}\text{ar}\left(\hat{\nu}_0^{\text{ML}}\right) \approx \frac{\nu_0^2 + \nu_0/b}{2n}.$$

12.1.2 UMVU estimators

As with the estimators $\hat{\mu}$ and $\hat{\sigma}$ in the HMM, we introduce here UMVU estimators to correct the bias of the ML estimators for the border and drift parameter applying Lemma 9.9 again. However, we do not recommend using these estimators in practice as the HBMc with the UMVU estimates of b and ν_0 produces a dominance time distribution with a bias in μ and σ (and our key aim is to reproduce the empirical behavior of the dominance times, where we "see" the expectation μ and the standard deviation σ and not the border and drift parameters). We explain that in detail. Recall that ML estimation of b and ν_0 leads to an unbiased estimate $\hat{\mu}$.

Corollary 12.4. ***UMVU estimators of b and ν_0***
Let d be a realization of $n \geq 3$ IG$(2b/\nu_0, \sqrt{2b/\nu_0^3})$-distributed random variables D. The UMVU estimators of b and ν_0 are given by

$$\hat{b}^{UMVU} = \frac{\Gamma(n/2 - 1/2)}{\sqrt{2}\Gamma(n/2 - 1)}\frac{1}{\sqrt{v}} \times F\left(-\frac{1}{2}, 0; \frac{n}{2} - 1; -\frac{\bar{d}v}{n}\right),$$

$$\hat{\nu_0}^{UMVU} = \sqrt{2}\frac{\Gamma(n/2 - 1/2)}{\Gamma(n/2 - 1)}\frac{1}{\bar{d}\sqrt{v}} \times F\left(-1, -\frac{1}{2}; \frac{n}{2} - 1; -\frac{\bar{d}v}{n}\right),$$

with $\bar{d}$ as the sample mean and v defined in equation (9.5). $F()$ is the hypergeometric function (Definition 9.8).

Proof: The assertion for b follows by the relation $b = \sqrt{\frac{\mu^3}{\sigma^2}}/2$ (Proposition 8.6) and by setting $\alpha = -\frac{1}{2}, \beta = 0$ and $\tau = -\frac{1}{2}$ in Lemma 9.9. For ν_0 note $\nu_0 = \sqrt{\frac{\mu}{\sigma^2}}$, and set $\alpha = 1, \beta = -\frac{1}{2}$ and $\tau = -\frac{1}{2}$ in the same Lemma. In both cases, we multiply in equation (9.6) with the reciprocal of the terms involving the Gamma function and exploit the relationship $\left(\frac{2n\mu^2}{\sigma^2\pi}\right)^{1/2} \exp\left(\frac{n\mu^2}{\sigma^2}\right) K_{1/2}\left(\frac{n\mu^2}{\sigma^2}\right) = 1$ (Iwase and Seto, 1983) as well as $K_\alpha(x) = K_{-\alpha}(x)$ for $x \in \mathbb{R}$ and $\alpha \in \mathbb{R}$. In detail, this means for b

$$\begin{aligned}
&\mathbb{E}\left[\frac{1}{\sqrt{v}} F\left(-\frac{1}{2}, 0; \frac{n}{2} - 1; -\frac{\bar{d}v}{n}\right)\right] = \frac{\Gamma(n/2 - 1/2 + \tau)}{\Gamma(n/2 - 1/2)}\sqrt{2}b \\
&\Rightarrow \mathbb{E}\left[\frac{\Gamma(n/2 - 1/2)}{\sqrt{2}\Gamma(n/2 - 1)} \frac{1}{\sqrt{v}} F\left(-\frac{1}{2}, 0; \frac{n}{2} - 1; -\frac{\bar{d}v}{n}\right)\right] = b,
\end{aligned}$$

where an analogous computation is necessary for ν_0. The UMVU property follows by the Lehmann-Scheffé-Theorem (Proposition 9.7) as the only random inputs of both estimators are $\bar{d}$ and v which build a complete and sufficient statistic for b and ν_0 (Seshadri, 1993). □

In the following, we explain why we propose not to use the UMVU estimators for b and ν_0 in practice. We perform the following step-wise simulation procedure with 10000 simulations in each simulation step.

- Simulate an $\mathrm{IG}(2b/\nu_0, \sqrt{2b/\nu_0^3})$ distributed random-variable, where $\mu = 2b/\nu_0, \quad \sigma = \sqrt{2b/\nu_0^3}$.
- Estimate the parameters $\hat{b}^{\mathrm{UMVU}}$ and $\hat{\nu}_0{}^{\mathrm{UMVU}}$.
- Simulate an $\mathrm{IG}\left(2\hat{b}^{\mathrm{UMVU}}/\hat{\nu}_0{}^{\mathrm{UMVU}}, \sqrt{2\hat{b}^{\mathrm{UMVU}}/\hat{\nu}_0^{\mathrm{UMVU}\,3}}\right)$ distributed random-variable.
- Estimate the parameters $\hat{\mu}^{\mathrm{UMVU}}$ and $\hat{\sigma}^{\mathrm{UMVU}}$.

The estimators $\hat{\mu}^{\mathrm{UMVU}}$ and $\hat{\sigma}^{\mathrm{UMVU}}$ should be close to μ and σ if the estimation procedure works well.
Figure 12.3 visualizes for a constant mean μ and three different values of σ the drawback of using the UMVU estimators for b and ν_0. Estimating the UMVU estimators for b and ν_0 and then resimulating the response pattern even for large n does not yield (when estimating) the original parameters $\mu = 2b/\nu_0$ and $\sigma = \sqrt{2b/\nu_0^3}$. This can be explained by the following observations

$$\begin{aligned}
\frac{2\hat{b}^{\mathrm{UMVU}}}{\hat{\nu}_0^{\mathrm{UMVU}}} &= \frac{F(-1/2, 0; n/2; -\bar{d}v/n)}{F(-1, -1/2; n/2; -\bar{d}v/n)}\bar{d} \neq \bar{d} = \hat{\mu}^{\mathrm{UMVU}} \\
\sqrt{\frac{2\hat{b}^{\mathrm{UMVU}}}{\hat{\nu}_0{}^{\mathrm{UMVU}\,3}}} &= \sqrt{\frac{\Gamma(n/2 - 1)^2 F(-1/2, 0; n/2; -\bar{d}v/n)}{2\Gamma(n/2 - 1/2)^2 F(-1, -1/2; n/2; -\bar{d}v/n)^3}\bar{d}^3 v} \neq \hat{\sigma}^{\mathrm{UMVU}}.
\end{aligned}$$

Thus, when using the UMVU estimators the visible response patterns cannot be reproduced precisely. Therefore, we recommend using the ML estimators for b and ν_0, which yield an unbiased mean μ even though the estimators $\hat{b}^{ML}$ and $\hat{\nu}_0^{ML}$ themselves are biased.

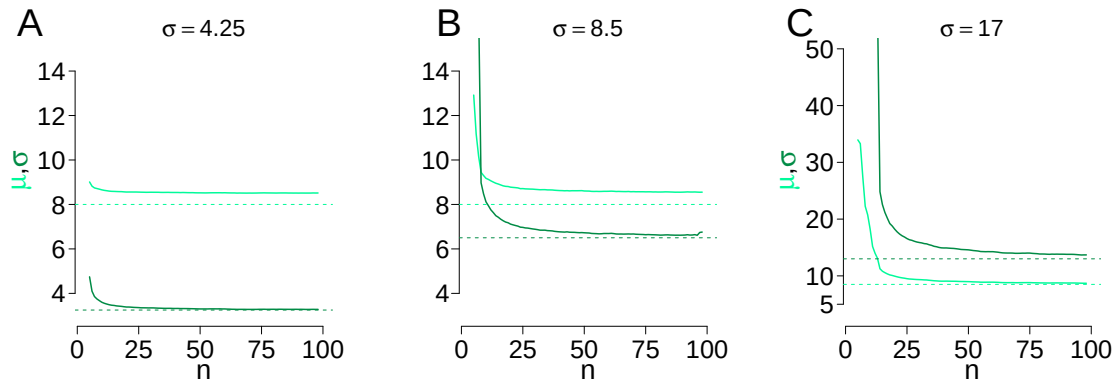

Figure 12.3: Drawback of using UMVU estimators for b and ν_0. *In the two-step simulation procedure explained above inverse Gaussian random variables are simulated. The UMVU estimates $\hat{\mu}^{UMVU}$ (light green) and $\hat{\sigma}^{UMVU}$ (green) of the second simulation are for different sample sizes n compared with the parameters μ and σ of the IG random variables of the first simulation printed as horizontal lines (which per construction should correspond to μ and σ of the IG random variables of step 2.). $\mu = 8$ is constant over the panels, whereas σ differs $\sigma = 4.25$ (A), $\sigma = 8.5$ (B), $\sigma = 17$ (C) causing different degrees of regularity of the inverse Gaussian distribution.*

12.1.3 Moment estimators

The moment estimators for the b, ν_0-parametrization of the IG distribution are given by

$$\hat{b}^{\text{mom}} = \frac{1}{2}\sqrt{\frac{\hat{\mu}^3}{\hat{\sigma^{\text{mom}}}^2}} \qquad \hat{\nu}_0^{\text{mom}} = \sqrt{\frac{\hat{\mu}}{\hat{\sigma^{\text{mom}}}^2}}$$

using the empirical standard deviation $\hat{\sigma}^{\text{mom}}$ (given in Section 9.3.1.3). This follows from Proposition 8.4. We will not use the moment estimators further as their relative bias and relative errors are larger compared to the ML estimators (data not shown, comparable to Figure 9.9).

12.2 Intermittent presentation: Parameter estimation

To estimate the HBMi parameter set $\Theta_{\text{HBMi}} = (b_S, \nu_S^*, b_U, \nu_U^*, \tilde{b}_S, \tilde{b}_U, \nu_B^*, \pi_{\text{start},S}^*)$ we maximize the log-likelihood of the model directly.

12.2.1 Direct numerical maximization of the log-likelihood

We start by discussing the key idea of the direct numerical maximization algorithm and continue by a theoretical justification including a proof of the representation of the likelihood. Then, details about scaling, constraints and starting values of the algorithm are given as well as remarks on the inclusion of censored dominance times and the estimation implementation. Finally, we explain that the assumption of constant drifts during blank display and presentation period has negligible effects for the parameter estimation of the HBMi.

12.2.1.1 Idea

The HBMi parameter set $\Theta_{\text{HBMi}} = (b_S, \nu_S^*, b_U, \nu_U^*, \tilde{b}_S, \tilde{b}_U, \nu_B^*, \pi_{\text{start},S}^*)$ is estimated using maximum likelihood. The likelihood L is given by

$$L(d_1, \ldots, d_n|\Theta_{\text{HBMi}}) \approx \alpha_S(n) + \alpha_U(n), \tag{12.5}$$

where the forward variable $\alpha_j(i) := \alpha_j(i|\Theta_{\text{HBMi}}) := \mathbb{P}(D_1^i = d_1^i, Y_i = j|\Theta_{\text{HBMi}})$ denotes the probability of observing $(d_1, \ldots, d_i)$ and being in state j at time i. Lemma 12.6 shows the correctness of equation (12.5). The approximation is due to the averaging of drifts during blank display and stimulus presentation. The forward variables can be derived recursively by (Rabiner, 1989; Turner, 2008)

$$\alpha_j(i) = \begin{cases} \pi_{\text{start},j}^* f_{2b_j/\nu_j^*, \sqrt{2b_j/\nu_j^{*3}}}^{\text{IG}}(d_i), & \text{if } i = 1, \\ f_{2b_j/\nu_j^*, \sqrt{2b_j/\nu_j^{*3}}}^{\text{IG}}(d_i) \sum\limits_{k \in \{S,U\}} \alpha_k(i-1)\tilde{p}_{kj}(d_{i-1}), & \text{if } i > 1, \end{cases} \tag{12.6}$$

with $j \in \{S, U\}$, which is shown in Lemma 12.5. Details on the maximization algorithm can be found in the following two subsections. After estimation of Θ_{HBMi}, the estimates $\hat{\nu}_S$, $\hat{\nu}_U$ and $\hat{\nu}_B$ can be obtained as follows using equation (11.2) and the estimate of ν_0 from (12.1)

$$\hat{\nu}_S = \frac{(l_p + l_b)\hat{\nu}_S^* - l_p\hat{\nu}_0}{l_b}, \qquad \hat{\nu}_U = \frac{(l_p + l_b)\hat{\nu}_U^* - l_p\hat{\nu}_0}{l_b} \qquad \text{and} \qquad \hat{\nu}_B = \frac{(l_p + l_b)\hat{\nu}_U^*}{l_b}.$$

12.2.1.2 Theoretical justification

In this subsection we first prove the correctness of the terms for the forward variables in equation (12.6). Then, we prove that the expression for the model likelihood given the set of model parameters Θ_{HBMi} in equation (12.5) is correct.
To derive terms for the forward variables and thereby prove equation (12.6), we adjust Lemma 9.12 a) properly.

Lemma 12.5. ***Forward variables in the HBMi***
It holds for $j \in \{S, U\}$

$$\alpha_j(1) = \pi_{start,j}^* f_{2b_j/\nu_j^*, \sqrt{2b_j/\nu_j^{*3}}}^{IG}(d_1) \text{ and}$$
$$\alpha_j(i+1) = f_{2b_j/\nu_j^*, \sqrt{2b_j/\nu_j^{*3}}}^{IG}(d_{i+1}) \sum_{k \in \{S,U\}} \alpha_k(i)\tilde{p}_{kj}(d_i) \text{ for } i = 1, \ldots, n-1.$$

Proof: The claim is shown inductively, where the case $i = 1$ is trivial. For $i \to i+1$ it holds

$$\begin{aligned} \alpha_j(i+1) &= \mathbb{P}(D_1^{i+1} = d_1^{i+1}, Y_{i+1} = j|\Theta_{\text{HBMi}}) \\ &= \mathbb{P}(D_{i+1} = d_{i+1}|D_1^i = d_1^i, Y_{i+1} = j, \Theta_{\text{HBMi}})\mathbb{P}(D_1^i = d_1^i, Y_{i+1} = j|\Theta_{\text{HBMi}}) \\ &= f_{2b_j/\nu_j^*, \sqrt{2b_j/\nu_j^{*3}}}^{\text{IG}}(d_{i+1}) \cdot \\ &\quad \sum_{k \in \{S,U\}} \mathbb{P}(D_1^i = d_1^i, Y_i = k|\Theta_{\text{HBMi}})\mathbb{P}(Y_{i+1} = j|Y_i = k, D_i = d_i, D_1^{i-1} = d_1^{i-1}, \Theta_{\text{HBMi}}) \\ &= f_{2b_j/\nu_j^*, \sqrt{2b_j/\nu_j^{*3}}}^{\text{IG}}(d_{i+1}) \sum_{k \in \{S,U\}} \alpha_k(i)\tilde{p}_{kj}(d_i), \end{aligned}$$

where in the third line the conditional independence and the Markov property for the HBMi (equations (11.8) and (11.9)) were applied. In the last line, we made use of the definitions of $\alpha_k(i)$ and $\tilde{p}_{kj}(d_i)$. □

Note that in the HBMi the joint probability of observing the i-th dominance time d_i and the state transition from $Y_i = k$ to $Y_{i+1} = j$ given the state $Y_i = k$ can be written as

$$\begin{aligned}\mathbb{P}(D_i = d_i, Y_{i+1} = j | Y_i = k) &= \mathbb{P}(D_i = d_i | Y_i = k) \cdot \mathbb{P}(Y_{i+1} = j | D_i = d_i, Y_i = k) \\ &\approx f^{\mathrm{IG}}_{2b_k/\nu_k^*, \sqrt{2b_k/\nu_k^{*3}}}(d_i)\tilde{p}_{kj}(d_i), \end{aligned} \tag{12.7}$$

where the approximation is due to the non-constant drifts. Now, we use this insight to write the model likelihood in matrix notation.
We denote the starting distribution by $\pi^*_{\mathrm{start}} = (\pi^*_{\mathrm{start},S}, \pi^*_{\mathrm{start},U})$, the emission matrix by $E(d_i)$ with

$$E(d_i) := \begin{bmatrix} f^{\mathrm{IG}}_{2b_S/\nu_S^*, \sqrt{2b_S/\nu_S^{*3}}}(d_i) & 0 \\ 0 & f^{\mathrm{IG}}_{2b_U/\nu_U^*, \sqrt{2b_U/\nu_U^{*3}}}(d_i), \end{bmatrix},$$

and the transition matrix $\tilde{T}(d_i)$ is defined as

$$\tilde{T}(d_i) := \begin{bmatrix} 1 - \Phi_{\nu_S^* d_i, \sqrt{d_i}}(b_S) & \Phi_{\nu_S^* d_i, \sqrt{d_i}}(b_S) \\ 1 - \Phi_{-\nu_U^* d_i, \sqrt{d_i}}(b_U) & \Phi_{-\nu_U^* d_i, \sqrt{d_i}}(b_U) \end{bmatrix},$$

where the entries are the state transition probabilities dependent on the dominance time d_i. Using these matrix notations and the idea shown in equation (12.7), the approximate complete likelihood $\tilde{L}$ (which neglects the averaging of drifts) is given by (for a similar expression for the HMM likelihood compare equation (9.10))

$$\begin{aligned}\tilde{L}(d_1, \ldots, d_n | \Theta_{\mathrm{HBMi}}) &= \pi^*_{\mathrm{start}} E(d_1)\tilde{T}(d_1)E(d_2)\tilde{T}(d_2)\ldots E(d_{n-1})\tilde{T}(d_{n-1})E(d_n)(1,1)^T \\ &= \pi^*_{\mathrm{start}} \prod_{j=1}^{n-1} \left(E(d_j)\tilde{T}(d_j)\right) E(d_n)(1,1)^T. \end{aligned} \tag{12.8}$$

Now, we prove the representation of the likelihood given in equation (12.5). To omit approximation signs, we use $\tilde{L}$ instead of L.

Lemma 12.6. ***Likelihood of the HBMi***
Let $(d_i)_{i=1,\ldots,n}$ be the observed data of a HBMi with parameter set $\Theta_{HBMi} = (b_S, \nu_S^*, b_U, \nu_U^*, \tilde{b}_S, \tilde{b}_U, \nu_B^*, \pi^*_{start,S})$. Furthermore, let $\alpha_j(S)$ and $\alpha_j(U)$ be the forward variables. Then, then approximate likelihood given in (12.8) *can also be written as*

$$\tilde{L}(d_1, \ldots, d_n | \Theta_{HBMi}) = \alpha_S(n) + \alpha_U(n).$$

Proof: The assertion is shown by induction over i. Let $i = 1$. We have

$$\alpha_S(1) + \alpha_U(1) = \pi^*_{\mathrm{start},S} f^{\mathrm{IG}}_{2b_S/\nu_S^*, \sqrt{2b_S/\nu_S^{*3}}}(d_1) + \pi^*_{\mathrm{start},U} f^{\mathrm{IG}}_{2b_U/\nu_U^*, \sqrt{2b_U/\nu_U^{*3}}}(d_1) = \pi^*_{\mathrm{start}} E(d_1)(1,1)^T.$$

Assume the assertion is fulfilled for a fixed i. We show the induction step $i \to i+1$:

$$
\begin{aligned}
&\alpha_S(i+1) + \alpha_U(i+1) \\
&\overset{\text{Lemma 12.5}}{=} (\alpha_S(i)\tilde{p}_{SS}(d_i) + \alpha_U(i)\tilde{p}_{US}(d_i)) f^{\text{IG}}_{2b_S/\nu_S^*, \sqrt{2b_S/\nu_S^{*3}}}(d_{i+1}) \\
&\quad + (\alpha_S(i)\tilde{p}_{SU}(d_i) + \alpha_U(i)\tilde{p}_{UU}(d_i)) f^{\text{IG}}_{2b_U/\nu_U^*, \sqrt{2b_U/\nu_U^{*3}}}(d_{i+1}) \\
&= (\alpha_S(i), \alpha_U(i)) \begin{bmatrix} \tilde{p}_{SS}(d_i) & \tilde{p}_{SU}(d_i) \\ \tilde{p}_{US}(d_i) & \tilde{p}_{UU}(d_i) \end{bmatrix} \begin{bmatrix} f^{\text{IG}}_{2b_S/\nu_S^*, \sqrt{2b_S/\nu_S^{*3}}}(d_{i+1}) & 0 \\ 0 & f^{\text{IG}}_{2b_U/\nu_U^*, \sqrt{2b_U/\nu_U^{*3}}}(d_{i+1}) \end{bmatrix} (1,1)^T \\
&= (\alpha_S(i), \alpha_U(i)) \tilde{T}(d_i) E(d_{i+1}) (1,1)^T \\
&\overset{\text{I.H.}}{=} \pi^*_{\text{start}} \prod_{j=1}^{i-1} \left(E(d_j)\tilde{T}(d_j) \right) E(d_i)\tilde{T}(d_i)E(d_{i+1})(1,1)^T = \pi^*_{\text{start}} \prod_{j=1}^{i} \left(E(d_j)\tilde{T}(d_j) \right) E(d_{i+1})(1,1)^T \\
&= \tilde{L}(d_1, \ldots, d_i, d_{i+1} | \Theta_{\text{HBMi}}),
\end{aligned}
$$

where in the next-to-last line we made use of the induction hypothesis $\alpha_S(i) + \alpha_U(i) = \pi^*_{\text{start}} \prod_{j=1}^{i-1} \left(E(d_j)\tilde{T}(d_j) \right) E(d_i)(1,1)^T$ which also writes as $(\alpha_S(i), \alpha_U(i)) = \pi^*_{\text{start}} \prod_{j=1}^{i-1} \left(E(d_j)\tilde{T}(d_j) \right) E(d_i)$. □

12.2.1.3 Details and starting values

Recall that the likelihood of the whole model given the data and the parameter vector Θ_{HBMi} is approximately

$$L(d|\Theta_{\text{HBMi}}) \approx \alpha_S(n) + \alpha_U(n),$$

using the forward variables $\alpha_j(i)$ derived recursively in equation (12.6). Note that we suppress dependence on the parameters Θ_{HBMi} for convenience. In practice, we need to avoid underflow when calculating $\alpha_j(i)$. To that end the forward variables are normalized such that $\sum_j \alpha_j(i) = 1$ for all time points i, using the following steps (e.g., Turner, 2008) and similar to the scaling for the HMM forward variables (page 98). For $j \in \{S, U\}$,

$$
\begin{aligned}
&\alpha^*_j(1) := \alpha_j(1), \qquad c(i) := \alpha^*_S(i) + \alpha^*_U(i), \qquad \tilde{\alpha}_j(i) := \alpha^*_j(i)/c(i), \\
&\alpha^*_j(i) := f^{\text{IG}}_{2b_j/\nu_j^*, \sqrt{2b_j/\nu_j^{*3}}}(d_i) \sum_{k \in \{S,U\}} \tilde{\alpha}_k(i-1)\tilde{p}_{kj}, \quad i > 1.
\end{aligned}
$$

The likelihood then derives as

$$L(d|\Theta_{\text{HBMi}}) \approx \prod_{i=1}^{n} c(i)(\tilde{\alpha}_S(n) + \tilde{\alpha}_U(n)) = \prod_{i=1}^{n} c(i), \quad \text{yielding} \quad \log L \approx \sum_{i=1}^{n} \log(c(i)). \quad (12.9)$$

Parameter estimation is then obtained by maximizing $\sum_i \log(c(i))$, which is a function of the model parameters Θ_{HBMi}. To that end we apply the Newton-type algorithm (Dennis and Schnabel, 1983) implemented in the `R`-function `nlm()` (explained on page 157). Alternatively the COBYLA algorithm (Powell, 1994) for maximization under non-linear constraints can be applied. Its idea and application is discussed in Appendix B.

Next, we discuss the set of starting values $\{b_S^{(s)}, \nu_S^{*(s)}, b_U^{(s)}, \nu_U^{*(s)}, \tilde{b}_S^{(s)}, \tilde{b}_U^{(s)}, \nu_B^{*(s)}\}$ for the Newton-type optimization algorithm. Let $\mathscr{U} := \{\hat{\mu}_{15}, \hat{\mu}_{30}\}$ and $\mathscr{O} := \{\hat{\sigma}_{15}, \hat{\sigma}_{30}, 1.15\hat{\sigma}_{30}\}$, where $\hat{\mu}_k$ and $\hat{\sigma}_k$ denote the empirical mean and standard deviation of all dominance times larger than k seconds. Thereby, we split the dominance times into longer and shorter ones by the fixed borders 15 or 30 seconds. Then, we choose the initial values for b_S and ν_S^* from the sets

$$b_S^{(s)} \in \{\sqrt{\mu^3/\sigma^2}/2 | \mu \in \mathscr{U}, \sigma \in \mathscr{O}\}, \qquad \nu_S^{*(s)} \in \{\sqrt{\mu/\sigma^2} | \mu \in \mathscr{U}, \sigma \in \mathscr{O}\}.$$

Depending on $\nu_S^{*(s)}$ and $b_S^{(s)}$, we choose $b_U^{(s)} \in \{0.01b_S^{(s)}, 0.05b_S^{(s)}, 0.15b_S^{(s)}\}$ (as the border in the unstable state should be remarkably smaller than b_S), $\tilde{b}_S^{(s)} \in \{b_S^{(s)}, 10b_S^{(s)}\}$, $\nu_U^*(s) \in \{1.01\nu_S^{*(s)}, 3\nu_S^{*(s)}, 7\nu_S^{*(s)}\}$ (as the drift in the unstable state should be larger than ν_S^*), furthermore $\nu_B^{*(s)} \in \{0.1, 3\}$ and $\tilde{b}_U^{(s)} \in \{-3, 0, 3\}$ as $\tilde{b}_U$ can be positive or negative. All these starting values were chosen also according to and have proven of value in extensive simulation studies.
The value for $\pi^*_{\text{start},S} = \mathbb{P}(Y_1 = S)$ is set to $\hat{\pi}^*_{\text{start},S} = 1$ if $d_1 \geq 45$, $\hat{\pi}^*_{\text{start},S} = 0$ if $d_1 \leq 15$, and $\hat{\pi}^*_{\text{start},S} = 1/2$ otherwise. Alternatively and comparable to the HMM the stationary distribution can be used for the initial distribution, thereby reducing the number of parameters by one. As this, however, requires numerical integration and increases the computational effort considerably and the differences between the two approaches were negligible we used the simpler rule.
The maximization algorithm is applied using all combinations of starting values. We then take the set of parameter estimates which yields the highest log-likelihood and fulfills the following constraints

$$\text{A) } \hat{\nu}_U \geq \hat{\nu}_S; \qquad \text{B) } 0 < \hat{b}_U \leq \hat{b}_S; \qquad \text{C) } \hat{\tilde{b}}_S > 0; \qquad \text{D) } \hat{\nu}_B > 0;$$
$$\text{E) } \hat{\mu}_S^* \approx 2\hat{b}_S/\hat{\nu}_S^* \geq 0.98\hat{\mu}_{15}; \qquad \text{F) } \hat{\sigma}_S^* \approx \sqrt{2\hat{b}_S/\hat{\nu}_S^{*3}} < 1.20\hat{\sigma}_{15}.$$

Constraints A) to D) result from the model assumptions, E) prevents dominance times smaller than 15 seconds to be considered for the estimation of the distribution of stable dominance times, analogously to the HMM procedure. Constraint F) prevents too big estimates of standard deviations, which would yield implausible results.
In cases in which only dominance times larger than 30 seconds are observed, we apply the algorithm described for the HBMc, where b_S, ν_S^* are estimated like in Section 12.1.1 and $\tilde{b}_S$ is set to zero. In cases in which only dominance times up to 30 seconds are observed, we proceed analogously, where b_U, ν_U^* are estimated like in Section 12.1.1 and set $\tilde{b}_U = 10^{10}$. In either case we set $\nu_B^* = 10$ and do not estimate the other variables.
To derive confidence intervals for the HMM parameters (block) bootstrap approaches are thinkable (e.g., Efron and Tibshirani, 1994; Scholz, 2007).

Nonlinear optimization using nlm()

The log-likelihood function (12.9) is maximized numerically using the `nlm()`-command in `R`. Here, we describe the Newton-type algorithm implemented in this function briefly and refer for any details to Dennis and Schnabel (1983). Note that the algorithm performs global minimization of a function $f : \mathbb{R}^n \to \mathbb{R}$ such that we minimize the negative log-likelihood. Traditionally, the Newton method is used to find roots of a given function. As a necessary condition for a global minimum of f is that the derivative (i.e., the gradient) vanishes at the

minimum, finding the minimum is equivalent to finding the root of its derivative. Now, assume we are in the k-th iteration step. The key idea is to improve the current estimate x_k as follows: $x_{k+1} = x_k + \lambda_k p_k$, where λ_k is a step width and p_k is a descent direction. Following Dennis and Schnabel (1983) p_k is chosen in each step as $p_k := -H_k^{-1}\nabla f(x_k)$, where H_k^{-1} denotes an inverse of the Hessian matrix and ∇ denotes the gradient. Note that in case of an unknown gradient or Hessian matrix numerical approximation methods are used. The step width is chosen by a backtracking line search (Algorithm 6.3.5 in Dennis and Schnabel (1983)) with $\zeta \in (0, 1/2), 0 < l < r < 1$:

$\lambda_k := 1$;
while $f(x_k + \lambda_k p_k) > f(x_k) + \zeta\lambda_k \nabla f(x_k)^T p_k$, **do**
$\lambda_k := \rho\lambda_k$ for some $\rho \in [l, r]$;
$x_{k+1} = x_k + \lambda_k p_k$;

The condition in the `while`-loop ensures that the decrease in the function is not too small compared to the step width. ζ is typically chosen as 10^{-4}. Detailed instructions how to choose ρ are given by Dennis and Schnabel (1983). The algorithm stops if the relative gradient is close to zero, the difference between two iterates is very small, or the number of iterations has exceeded some limit.

Censored dominance times

Including the censored last dominance time d_{n+1} into the estimation is straightforward. For $j \in \{S, U\}$ the forward variables $\tilde{\alpha}_j(1), \ldots, \tilde{\alpha}_j(n)$ remain unchanged, and $\alpha_j^*(n+1)$ is introduced follows

$$\alpha_j^*(n+1) = \left(1 - F^{\mathrm{IG}}_{2b_j/\nu_j^*, \sqrt{2b_j/\nu_j^{*3}}}(d_{n+1})\right) \sum_{j \in \{S,U\}} \tilde{p}_{ij}(d_n)\tilde{\alpha}_s^*(n)$$

and normed to obtain $\tilde{\alpha}_j(n+1)$. Thereby, $c(n+1) = \alpha_S^*(n+1) + \alpha_U^*(n+1)$. Then, the resulting log-likelihood $\sum_i \log(c(i))$ is maximized subject to the constraints A)-F) given above on page 157.

Remark on the estimation implementation

The computation of the forward variables $\alpha_j(i)$ in the estimation of the HBMi should – due to the `for`-loop – be transferred to `C++` with the inverse Gaussian and normal weights as input (as explained on page 100 for the HMM). The computational effort using a `R`- and a `C++`-function for the forward algorithm is presented in Figure 12.4. Again, the `C++`-implementation is remarkably faster.

12.2.1.4 Exact distribution of hitting times in the HBMi

We assume constant drifts ν_U^* and ν_S^* in the estimation procedure described here although per construction of the HBMi the drifts of P during the presentation phase and the blank display differ between ν_S, ν_U and ν_0. However, an incorporation of the different drifts increases the mathematical efforts and leads to very complicated mathematical terms not estimable using standard approaches. Nevertheless, our simplifying approach is justified by two reasons.

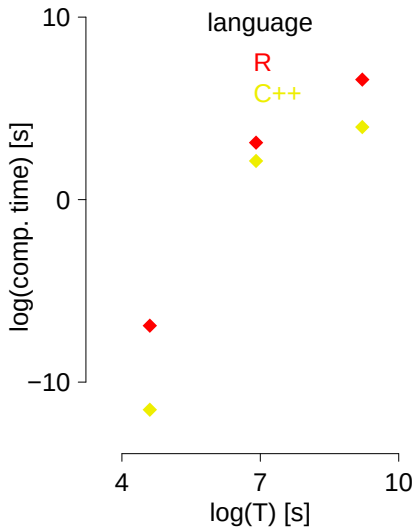

Figure 12.4: Comparison of the computation times for the estimation of the HBMi. *Red points show the mean computation time in ten trials with* `R` *and yellow points the mean computation times using* `C++`*. We used simulated response patterns of parameter combination C in Table 12.2. The axes are logarithmic due to the different magnitudes.*

First, compared to the overall mean of the hitting time in the stable state of, in most cases, more than 100 seconds, the proportion of a difference between hitting during blank display ($l_b = 0.8$ seconds in the experiment of Schmack et al. (2015)) and hitting during presentation ($l_p = 0.6$ seconds) is very small. In other words, because dominance times usually span multiple trials of duration $l_p + l_b$, the approximation is very close. In addition, the marginal distribution of P at multiples of such intervals $l_p + l_b$ is identical to the marginal distribution of a Brownian motion with drift ν_S^* at these time points, and the differences can only be observed in the meantime (as already explained in Section 11.2.3).
Second, the influence of the different drifts in the unstable state is larger as the dominance times are shorter. However, the start of a new dominance time relative to the start of the presentation of the stimulus is not fixed but also varies between the beginning of a presentation and the end of a blank display depending on the end of the last dominance time. Thus, the effects of different starting positions and faster drift during blank displays compensate each other resulting in a dominance time distribution similar to the one assuming a constant drift ν_U^* with comparable first moments. Moreover, the argument with the identical marginal distribution at multiples of intervals $l_p + l_b$ also holds during unstable phases.
As an example Figure 12.5 shows in panels A and C for the stable and the unstable phases of the response pattern type D (Table 12.2) the dominance times resulting from simulating the HBMi, where the drifts during blank display and presentation differ between ν_U, ν_S and ν_0. Additionally, in panels B and D the simulated dominance times when assuming a constant drift ν_S^* and ν_U^* are printed. We note that not only the differences in the means and the standard deviations are small (which are the parameters we intend to model) but also the differences in the shape of the distributions. This justifies again our simplifying assumption of constant drifts. Similar considerations hold for the non-constant drift of the background process.

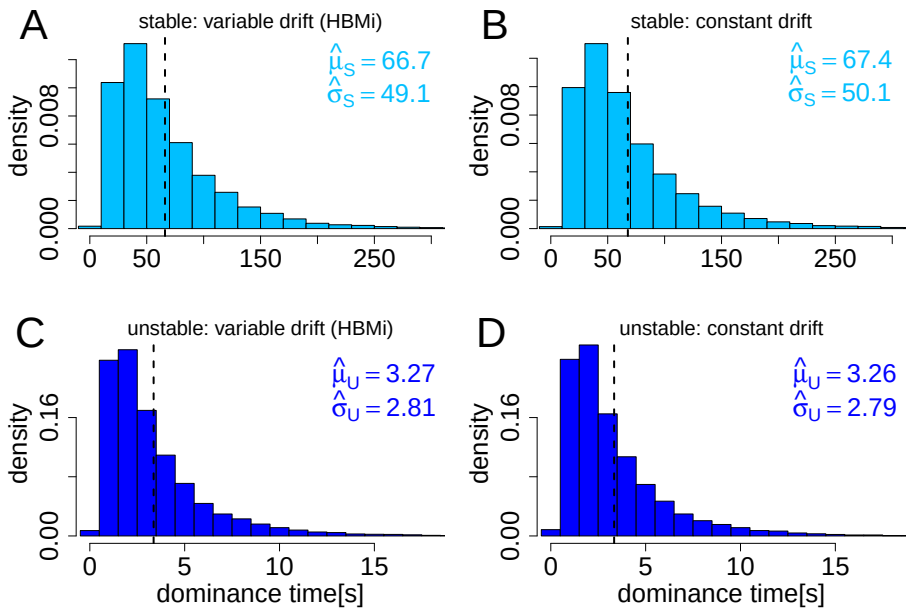

Figure 12.5: Example of empirical distributions of stable (A,B) and unstable (C,D) dominance times generated by the HBMi (A,C) with drifts ν_0, ν_S, ν_U and by simulations (B,D) assuming a constant drift ν_S^* and ν_U^*, respectively during blank display and presentation phase. *The parameters were $b_S = 5.42, \nu_S^* = 0.16, b_U = 1.06, \nu_U^* = 0.65, \nu_0 = 0.27, \nu_S = 0.01, \nu_U = 1.16$ (given by the subject D in Table 12.2, page 162). The sample means are printed in all four panels as dashed lines, and the estimated means and standard deviations are printed for each sample. For all plots 10000 simulations were used to estimate the histograms.*

12.2.2 ML estimators: Asymptotic distribution

Due to the close connection between the estimators for the HMM and the HBMi, comparable results concerning the asymptotic consistency and normality are expectable. However, technical assumptions will be necessary. We leave these theoretical analyses for future work.

12.3 Parameters of example response patterns

In Figure 9.1 (page 70) response patterns typical for continuous and intermittent presentation were shown. Here, we fit the HBM to these response patterns and show the estimated parameters. These are the same examples as used for the HMM in Section 9.5, and they are applied later on in this thesis for simulations.

12.3.1 Continuous presentation

Table 12.1 contains two estimated HBMc parameter combinations. We show in Figure 9.1 panels A and B the data where the parameters were estimated from and in Figure 9.2 A and B the corresponding histograms of dominance times.

panel	μ	σ	b	ν
A	10.50	8.18	2.08	0.40
B	6.69	3.58	2.42	0.72

Table 12.1: Estimated exemplary HBMc parameter combinations. *The corresponding data response patterns are shown in Figure 9.1 A and B (page 70) .*

12.3.2 Intermittent presentation

In Table 12.2 we show four estimated exemplary parameter combinations representing the response patterns described by the HBMi. The original processes are shown in Figure 9.1, and in Figure 9.2 C-F the corresponding histograms of dominance times are plotted.
In addition to the set of the original HBMi parameters, we use the set of derived parameters $(\mu^*_S, \sigma^*_S, \mu^*_U, \sigma^*_U, p^*_{SS}, p^*_{UU}, \pi^*_{\text{start},S})$ that are more easily comparable to the HMM parameters. The parameters were introduced in equations (11.4) and (11.7).

12.4 Precision of parameter estimates

The estimation precision in the HBMc is discussed in Section 12.4.1. Simulations to quantify the quality of the fitting procedure for the HBMi are performed in Section 12.4.2, where also a paragraph about censored dominance times is included.

12.4.1 HBMc

Simulation results for the HBMc are directly comparable to the simulated estimation precision results of the HMM for continuous presentation with inverse Gaussian distributed dominance times. Therefore, we refer to Section 9.6.2 (page 103) and note that sample size and CV are critical for the estimation.

panel	b_S	ν_S^*	b_U	ν_U^*	$\tilde{b}_S$	$\tilde{b}_U$	ν_B^*	$\pi^*_{\text{start},S}$
C	41.70	0.45	1.84	0.73	49.70	2.39	0.31	1.00
D	5.42	0.16	1.06	0.65	4.56	1.13	0.04	1.00
E	52.60	0.28	NA	NA	0.00	NA	10.00	1.00
F	13.50	0.38	1.00	0.38	110.30	0.77	1.08	1.00

panel	μ_S^*	σ_S^*	μ_U^*	σ_U^*	p_{SS}^*	p_{UU}^*	$\pi^*_{\text{start},S}$
C	186.50	30.50	5.01	3.06	0.66	0.97	1.00
D	67.18	50.78	3.26	2.78	0.36	0.79	1.00
E	372.30	68.30	NA	NA	1.00	NA	1.00
F	70.54	21.94	5.21	5.96	0.10	0.99	1.00

Table 12.2: Estimated exemplary HBMi parameter combinations. *The corresponding data response patterns are shown in Figure 9.1, panels C-F (page 70). The entry NA implies that only the parameters of the stable state were estimated as only dominance times larger than 30 seconds occur (compare Section 12.2.1.3).*

12.4.2 HBMi

Precision of parameter estimates

The variability of the parameter estimates in the HBMi is studied analogously to the HMM (compare Section 9.6), using the RE and the AE of the parameter estimates obtained in 1000 simulations of the 61 parameter combinations estimated from the empirical data set Schmack et al. (2015). For the border parameters $b_S, b_U, \tilde{b}_S, \tilde{b}_U$, we use the RE, while for the typically small drift parameters $\nu_S^*, \nu_U^*, \nu_B^*$, the AE is used. Again, one set of simulations uses the time horizon of the empirical data, $T_1 = 1200$ s (Figure 12.6 A), and a second simulation was performed using $T_2 = 3600$ s (Figure 12.6 B). According to the simulation results, the precision of parameter estimation in the given parameter range is not always satisfactory for the given parametrization $(b_S, b_U, \tilde{b}_S, \tilde{b}_U, \nu_S^*, \nu_U^*, \nu_B^*)$, yielding average errors (i.e., mean REs or AEs across all variables) smaller than 0.25 in only 24 out of 61 cases for the empirical time horizon T_1 and still only 44 out of 61 for the tripled sample size of T_2. This suggests that these raw parameters yield less reliable estimates because different combinations of b and ν can yield the same mean stable dominance time. In contrast, the set of derived parameters $(\mu_S^*, \sigma_S^*, \mu_U^*, \sigma_U^*, p_{SS}^*, p_{UU}^*)$ shows better properties. Figure 12.6 C and D show the median REs for $\mu_S^*, \sigma_S^*, \mu_U^*, \sigma_U^*$ and median AEs for p_{SS}^*, p_{UU}^* obtained in the 1000 simulations of length T_1 (panel C) and T_2 (panel D). Concerning this parametrization, 51 parameter combinations yielded average errors smaller than 0.25 across all variables for T_1, while as many as 58 out of 61 cases showed errors smaller than 0.25 for T_2. Large average errors mainly occur for small sample sizes $n < 10$ or large $p_{SS}^* > 0.8$ (panels E and F). These simulations suggest that the parametrization $(\mu_S^*, \sigma_S^*, \mu_U^*, \sigma_U^*, p_{SS}^*, p_{UU}^*)$ yields more reliable parameter estimates in the HBMi than the original parametrization of borders and drifts.
Note that it may happen that no estimate can be found that satisfies all constraints. In the 1000 simulations for 48 out of the 61 subjects this never happened, for seven cases it happened in less than one percent of the 1000 simulations, and for six subjects up to five percent of the estimates cannot be calculated. Mostly this is due to a small sample size with short as well as long dominance times.

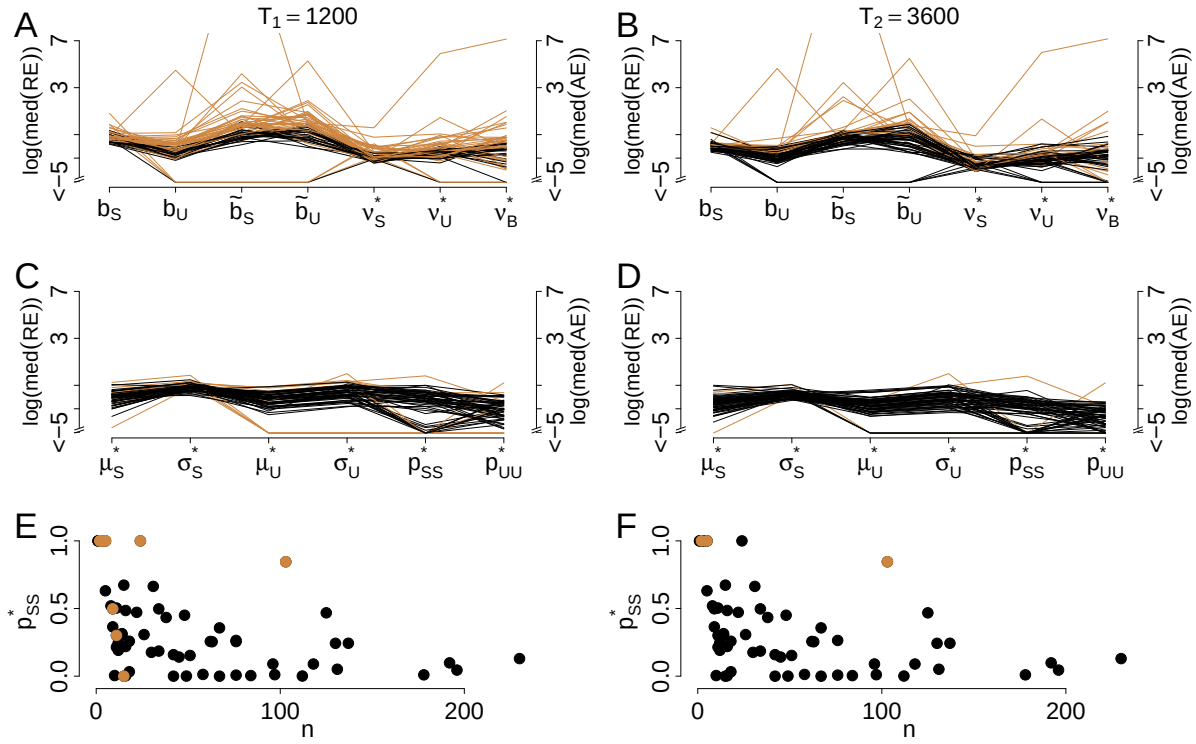

Figure 12.6: Precision of parameter estimates in the HBMi. *For each of the 61 parameter constellations from the sample data set, 1000 HBMi simulations were performed. (A) and (B): log(median(REs)) of the border parameters* $b_S, b_U, \tilde{b}_S, \tilde{b}_U$*, and log(median(AEs)) of the drift parameters* $\nu^*_S, \nu^*_U, \nu^*_B$ *with* $T = 1200$ *(A) and* $T = 3600$ *(B). (C) and (D): log(median(REs)) for the derived model parameters* $\mu^*_S, \sigma^*_S, \mu^*_U, \sigma^*_U$ *and log(median(AEs)) for the parameters* p^*_{SS} *and* p^*_{UU} *for* $T = 1200$ *(C) and* $T = 3600$ *(D). Parameter combinations with mean errors* < 0.25 *across all variables plotted in black. (E) and (F): Corresponding scatterplots of* p^*_{SS} *and* n *where the black points correspond to mean errors* < 0.25 *across the derived parameters.*

Censored dominance times: Precision of parameter estimates

The estimation precision of the estimation procedure including the censored dominance times (recall page 158) can be evaluated using the same parametric bootstrap as described above. The results are for most subjects comparable, i.e., the effect of including the censored last dominance time is very small. Only for the subjects whose response patterns are described using only the stable state the results for the non-censored estimation are better, i.e., yield smaller median errors. This can be explained by the fact that the corresponding sample sizes are small, and therefore the influence of the (less informative) censored dominance time is large.

12.5 Viterbi algorithm for the HBMi

What is the "single" best state sequence path of a HMM, i.e., the path maximizing $\mathbb{P}(Y_1^n = y_1^n, D_1^n = d_1^n|\Theta_{\text{HMM}})$? This question is answered by the Viterbi algorithm (Viterbi, 1967; Forney, 1973) using the estimated parameter set, i.e., after the parameter estimation. In this section we show that for the HBMi the same technique can be applied to estimate the most likely state sequence path Y_1^{n*}. Thus, we are able to estimate the hidden state of each dominance time given the estimated model parameters which is, for instance, important when comparing the stable dominance times before an estimated state change to the other stable dominance times. In the following, we first define the key variable and then present a brief summary of the Viterbi algorithm closely following Rabiner (1989). Third, the correctness of the Viterbi algorithm for the HBMi is proven. Fourth, the algorithm is evaluated in simulations of the HBMi.
Inductively we define for $j \in \{S, U\}$ and $i = 1, \ldots, n$ the variable $w_j(i)$ as follows

$$w_j(1) := \pi^*_{\text{start},j} f_j(d_1), \qquad w_j(i+1) := \left(\max_{k \in \{S,U\}} w_k(i) \tilde{p}_{kj}(d_i) \right) f_j(d_{i+1}). \tag{12.10}$$

In Proposition 12.7 we prove for the HBMi that it holds

$$w_j(i) = \max_{y_1, \ldots, y_{i-1}} \mathbb{P}(Y_1 = y_1, Y_2 = y_2, \ldots, Y_i = j, D_1^i = d_1^i|\Theta_{\text{HBMi}}),$$

i.e., that $w_j(i)$ gives the likelihood of the most likely path considering the first i observations and ending in state j at time i. Recall that $d_{i_0}^{i_1} := \{d_{i_0}, \ldots, d_{i_1}\}$ where $i_0 < i_1$ and similarly for D, y and Y.
After initializing the Viterbi algorithm consists of a recursion step, a termination step and state sequence backtracking. The recursion step contains the derivation of $w_j(i)$ as in (12.10), i.e., we search for each time the largest product of the likelihood of the current path and the transition probability to the next state. For each i and j the argument maximizing (12.10) has to be saved, for instance, by an array $\mathfrak{w}$. In the termination step of the algorithm we find the maximum entry of $w_k(n)$ and its argmax, i.e., the last state y_n^* of the most likely state path given all data. Then, we successively trace back in time to find the i-th state y_i^* of the most likely state path (using the array $\mathfrak{w}$).

The complete algorithm can be formalized as follows.

1. Initialization:
   - $w_j(1) := \pi^*_{\text{start},j} f_j(d_1), \qquad j \in \{S, U\}$
   - $\mathfrak{w}_j(1) := 0$
2. Recursion:
   - $w_j(i) := \max_{k\in\{S,U\}}(w_k(i-1)\tilde{p}_{kj}(d_{i-1}))f_j(d_i) \qquad 2 \leq i \leq n, j \in \{S, U\}$
   - $\mathfrak{w}_j(i) := \text{argmax}_{k\in\{S,U\}}(w_k(i-1)\tilde{p}_{kj}(d_{i-1}))$
3. Termination:
   - $L^* := \max_{k\in\{S,U\}} w_k(n)$
   - $y^*_n := \text{argmax}_{k\in\{S,U\}} w_k(n)$
4. State sequence backtracking:
   - $y^*_i := \mathfrak{w}_{y^*_{i+1}}(i+1), \qquad i = n-1, n-2, \ldots, 1$

In the implementation the Viterbi algorithm is quite similar to the forward algorithm (Section 9.4.1) except for the maximization over previous states performed in the recursion step for $w_j(i)$ which is done instead of summing as in Lemma 9.12 a).
Now, we prove the correctness of the Viterbi algorithm for the HBMi thereby for the sake of simplicity neglecting that due to the non-constant drift $f_j(d_i) \approx \mathbb{P}(D_i = d_i|Y_i = j)$ and $\tilde{p}_{kj}(d_i) \approx \mathbb{P}(Y_{i+1} = j|Y_i = k, d_i)$. Sometimes, we only write d_i or y_i instead of $D_i = d_i$ or $Y_i = y_i$ to abbreviate notation.

Proposition 12.7. ***HBMi: Viterbi recursion***
Given the HBMi parameters Θ_{HBMi} the joint probability of the most likely HBMi state path ending in state j at observation number i and all the observations up to observation number i is given by

$$\max_{y_1,\ldots,y_{i-1}} \mathbb{P}(Y_1^{i-1} = y_1^{i-1}, Y_i = j, D_1^i = d_1^i|\Theta_{HBMi}) = w_j(i)$$

for $i = 2, 3, \ldots, n$. For $i = 1$ it holds $\mathbb{P}(Y_1 = j, D_1 = d_1|\Theta_{HBMi}) = w_j(1)$.

Proof: We use the induction principle. For the base case, it holds

$$\begin{aligned} w_j(1) &= f_j(d_1)\pi^*_{\text{start},j} = \mathbb{P}(D_1 = d_1|Y_1 = j, \Theta_{\text{HBMi}})\mathbb{P}(Y_1 = j|\Theta_{\text{HBMi}}) \\ &= \mathbb{P}(Y_1 = j, D_1 = d_1|\Theta_{\text{HBMi}}) \end{aligned}$$

as claimed.

Now assume that the claim holds true for all times $1, \dots, i-1$. We show the induction step $i-1 \to i$ where we use the induction hypothesis in the second line and omit the condition Θ_{HBMi} in each $\mathbb{P}(\dots)$ for convenience

$$
\begin{aligned}
w_j(i) &= f_j(d_i) \max_{k\in\{S,U\}} \tilde{p}_{kj}(d_{i-1}) w_k(i-1) \\
&= f_j(d_i) \max_{k\in\{S,U\}} \tilde{p}_{kj}(d_{i-1}) \max_{y_1,\dots,i-2} \mathbb{P}(Y_{i-1}=k, Y_1^{i-2}=y_1^{i-2}, D_1^{i-1}=d_1^{i-1}) \\
&= \max_{k\in\{S,U\}} \max_{y_1^{i-2}} f_j(d_i)\tilde{p}_{kj}(d_{i-1}) \mathbb{P}(Y_{i-1}=k, Y_1^{i-2}=y_1^{i-2}, D_1^{i-1}=d_1^{i-1}) \\
&= \max_{k\in\{S,U\}} \max_{y_1^{i-2}} f_j(d_i) \mathbb{P}(Y_i=j|Y_{i-1}=k, D_{i-1}=d_{i-1}) \mathbb{P}(Y_{i-1}=k, Y_1^{i-2}=y_1^{i-2}, D_1^{i-1}=d_1^{i-1}) \\
&= \max_{k\in\{S,U\}} \max_{y_1^{i-2}} f_j(d_i) \mathbb{P}(Y_i=j|Y_{i-1}=k, D_1^{i-1}=d_1^{i-1}, y_1^{i-2}) \mathbb{P}(Y_{i-1}=k, y_1^{i-2}, d_1^{i-1}) \\
&= \max_{k\in\{S,U\}} \max_{y_1^{i-2}} f_j(d_i) \mathbb{P}(Y_i=j, Y_{i-1}=k, D_1^{i-1}=d_1^{i-1}, Y_1^{i-2}=y_1^{i-2}) \\
&= \max_{y_1^{i-1}} f_j(d_i) \mathbb{P}(Y_i=j, D_1^{i-1}=d_1^{i-1}, Y_1^{i-1}=y_1^{i-1}) \\
&= \max_{y_1^{i-1}} \mathbb{P}(D_i=d_i|Y_i=j) \mathbb{P}(Y_i=j, D_1^{i-1}=d_1^{i-1}, Y_1^{i-1}=y_1^{i-1}) \\
&= \max_{y_1^{i-1}} \mathbb{P}(D_i=d_i|Y_1^{i-1}=y_1^{i-1}, Y_i=j, D_1^{i-1}=d_1^{i-1}) \mathbb{P}(Y_i=j, D_1^{i-1}=d_1^{i-1}, Y_1^{i-1}=y_1^{i-1}) \\
&= \max_{y_1,\dots,y_{i-1}} \mathbb{P}(Y_1^{i-1}=y_1^{i-1}, Y_i=j, D_1^{i}=d_1^{i}).
\end{aligned}
$$

□

In the following y_i^* denotes the realization of the random variable Y_i^* for $i = 1, \dots, n$.

Proposition 12.8. ***HBMi: Viterbi traceback***
The final state of the most likely state path of a HBMi is $y_n^* = argmax_{k\in\{S,U\}} w_k(n)$.
If y_{i+1}^* *is the* $(i+1)$*-th state of the most likely state path, then*

$$y_i^* = \mathfrak{w}_{y_{i+1}^*}(i+1) = argmax_{k\in\{S,U\}} \mathbb{P}(Y_{i+1}^* = y_{i+1}^* | Y_i = k, D_i = d_i, \Theta_{HBMi}) w_k(i)$$

is the i*-th state of the most likely state path* $(i = 1, \dots, n-1)$.

Proof: First note that in the proof we omit the condition Θ_{HBMi} in each $\mathbb{P}(\dots)$ for convenience. By Proposition 12.7 we know that the last state of the most likely state sequence is given by

$$y_n^* = \text{argmax}_{k\in\{S,U\}} w_k(n) = \text{argmax}_{k\in\{S,U\}} \max_{y_1^{n-1}} \mathbb{P}(y_{1\dots n-1}, Y_n = k, d_{1\dots n}).$$

Now, let $i \in \{1, \dots, n-1\}$ and y_{i+1}^* be the $(i+1)$-th state of the most likely state path. In the following we show that $\text{argmax}_{k\in\{S,U\}} \mathbb{P}(Y_{i+1}^* = y_{i+1}^* | Y_i = k, D_i = d_i) w_k(i)$ is the i-th state of the most likely state path.

$$
\begin{aligned}
&\operatorname{argmax}_{k\in\{S,U\}}\mathbb{P}(Y^*_{i+1}=y^*_{i+1}|Y_i=k,D_i=d_i)w_k(i)\\
&=\operatorname{argmax}_{k\in\{S,U\}}\mathbb{P}(Y^*_{i+1}=y^*_{i+1}|Y_i=k,D_i=d_i)\max_{y_1^{i-1}}\mathbb{P}(Y_1^{i-1}=y_1^{i-1},Y_i=k,D_1^i=d_1^i)\\
&=\operatorname{argmax}_{k\in\{S,U\}}\max_{y_1^{i-1}}\mathbb{P}(Y^*_{i+1}=y^*_{i+1}|Y_i=k,D_i=d_i)\mathbb{P}(Y_1^{i-1}=y_1^{i-1},Y_i=k,D_1^i=d_1^i)\\
&=\operatorname{argmax}_{k\in\{S,U\}}\max_{y_1^{i-1}}\mathbb{P}(Y^*_{i+1}=y^*_{i+1}|Y_i=k,Y_1^{i-1}=y_1^{i-1},d_1^i)\mathbb{P}(Y_1^{i-1}=y_1^{i-1},Y_i=k,d_1^i)\\
&=\operatorname{argmax}_{k\in\{S,U\}}\max_{y_1^{i-1}}\mathbb{P}(Y^*_{i+1}=y^*_{i+1},Y_i=k,Y_1^{i-1}=y_1^{i-1},D_1^i=d_1^i)\\
&=\operatorname{argmax}_{k\in\{S,U\}}\left[\max_{y_{i+2}^n}\mathbb{P}(Y_{i+2}^n=y_{i+2}^n,d_{i+1}^n|y^*_{i+1})\right]\max_{y_1^{i-1}}\mathbb{P}(Y^*_{i+1}=y^*_{i+1},Y_i=k,Y_1^{i-1}=y_1^{i-1},d_1^i)\\
&=\operatorname{argmax}_{k\in\{S,U\}}\max_{y_1^{i-1}}\max_{y_{i+2}^n}\mathbb{P}(Y_{i+2}^n=y_{i+2}^n,d_{i+1}^n|y^*_{i+1})\mathbb{P}(Y^*_{i+1}=y^*_{i+1},Y_i=k,Y_1^{i-1}=y_1^{i-1},d_1^i)\\
&=\operatorname{argmax}_{k\in\{S,U\}}\max_{y_1^{i-1},y_{i+2}^n}\mathbb{P}(Y_{i+2}^n=y_{i+2}^n,d_{i+1}^n|y^*_{i+1},Y_i=k,y_1^{i-1},d_1^i)\mathbb{P}(y^*_{i+1},Y_i=k,y_1^{i-1},d_1^i)\\
&=\operatorname{argmax}_{k\in\{S,U\}}\max_{y_1^{i-1},y_{i+2}^n}\mathbb{P}(Y_{i+2}^n=y_{i+2}^n,d_{i+1}^n,y^*_{i+1},Y_i=k,Y_1^{i-1}=y_1^{i-1},d_1^i)\\
&=\operatorname{argmax}_{k\in\{S,U\}}\max_{y_1^{i-1},y_{i+2}^n}\mathbb{P}(Y_{i+2}^n=y_{i+2}^n,y^*_{i+1},Y_i=k,Y_1^{i-1}=y_1^{i-1},d_1^n)=\mathfrak{w}_{Y^*_{i+1}}(i+1)=y^*_i,
\end{aligned}
$$

where the last line is the i-th state of the most likely state path. □

In Figure 12.7 we present examples of the Viterbi path derived for the four response patterns presented in Figure 9.1, panels C-F (page 70). Here, the estimated paths (indicated by the background colors) agree closely with visual inspection as long dominance times are classified stable and short dominance times are estimated as unstable.

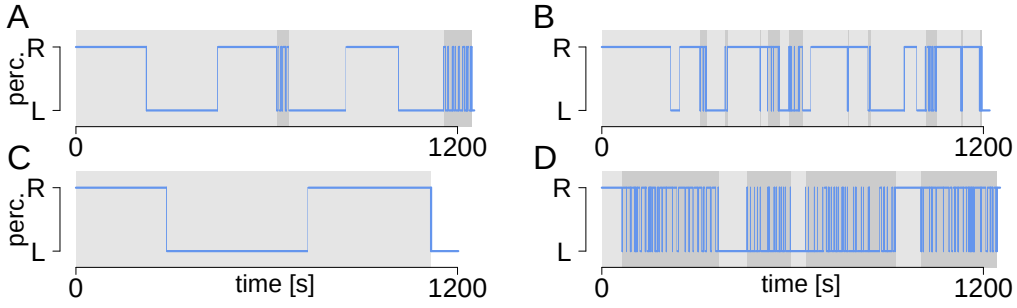

Figure 12.7: Estimated Viterbi paths. *Response patterns of the four subjects of Table 12.2 (page 162) together with the estimated Viterbi paths of the HBMi. Panel A corresponds to subject C, panel B to subject D and so on. Dominance times estimated as stable are colored light gray and dominance times estimated as unstable are colored in a darker gray. The last dominance time is censored and thus cannot be estimated by the Viterbi algorithm (white background). The estimated path corresponds to visual inspection in all four cases.*

Evaluation of the Viterbi algorithm

We briefly evaluate the Viterbi algorithm for the HBMi in simulations. Therefore, for each of the 61 intermittent response patterns in the data set Schmack et al. (2015) $n_0 = 1000$ HBMis are simulated, and the parameters as well as the Viterbi paths are estimated. As the underlying states are known in simulations, we can compare the Viterbi-estimated hidden states to the true states. We compute the quantity of false estimations η_k for each simulated response pattern $\{\Xi_k\}_{k=1,2,\ldots,n_0}$ as follows

$$\eta_k = \frac{|\{i : Y_i^k \neq \hat{Y}_i^k\}|}{n_k}, \tag{12.11}$$

where n_k is the number of dominance times in Ξ_k, $(Y_i^k)_{i=1,2,\ldots,n_k}$ denotes the hidden states and $(\hat{Y}_i^k)_{i=1,2,\ldots,n_k}$ denotes the estimated hidden states. Figure 12.8 shows for each subject the mean value of η_k in 1000 simulations. Only for six of the 61 subjects more than five percent of the states were estimated falsely (especially if the separation of stable and unstable distributions was not clear-cut) and the median over all subjects is 0.7%. We conclude that both the parameter estimation and the Viterbi algorithm for the HBMi yield convincing results.

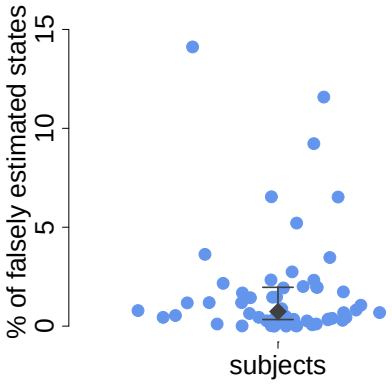

Figure 12.8: Evaluation of the Viterbi algorithm. *Mean percentage of falsely estimated states η_k (12.11) by the Viterbi algorithm for each subject in 1000 simulations together with the median (gray diamond) across all subjects and the 25%/75%-quantiles.*

Chapter 13

The HBM: Theoretical properties

Interpreting the perceptual changes as renewal points, the HBMc is an example of a renewal process, whereas the HBMi may be understood as an alternating renewal process (Section 8.2.3.1). As with the HMM in Chapter 10 we derive here theoretical results concerning the behavior of the point processes induced by the perceptual changes. These results can be used for investigation of differences between clinical groups.
In Section 13.1 we first derive the distribution and (asymptotic) expectation of the number of perceptual changes in a fixed interval during continuous presentation before deriving the marginal density of the perception process P. In Section 13.2 first-passage and steady-state results for the HBMi are given. Next, the number of changes as well as the residual time to the next perceptual change are investigated. Moreover, marginal densities of the perception and the background process are derived. Note that all results concerning the HBMi are only approximate due to the deviation between the assumed constant drift in theoretical results and the different drifts during blank display and presentation in the model. However, we omit approximation signs here for convenience.
The key results given in this chapter are the steady-state distribution (Corollary 13.11) and the theoretical (asymptotic) rate of changes of the HBMi (Proposition 13.13). Readers more interested in the application may skip all other parts of this chapter.
In this chapter we understand Ξ_{HBMc} and Ξ_{HBMi} as the point processes on the non-negative line generated by the points in time $(t_0, t_1, t_2, \ldots, t_n)$ of the perceptual reversals of the HBM for continuous and for intermittent presentation, respectively. There, we use $t_0 = 0$. Formally, for the set of realized dominance times $(d_1, d_2, \ldots, d_n)$ of a HBMc,

$$\Xi_{\text{HBMc}} := \{0\} \cup \{t \in \mathbb{R} | \sum_{i=1}^{k} d_i = t, k = 1, 2, \ldots, n\} = \{t_0, t_1, t_2, \ldots, t_n\}$$

and equivalently for the set of realized dominance times $(d_1, d_2, \ldots, d_n)$ of a HBMi

$$\Xi_{\text{HBMi}} := \{0\} \cup \{t \in \mathbb{R} | \sum_{i=1}^{k} d_i = t, k = 1, 2, \ldots, n\} = \{t_0, t_1, t_2, \ldots, t_n\}.$$

As with the HMM $\tilde{Y}_t := (\tilde{Y}_t)_{t\geq 0}$ is the hidden state at time t

$$\begin{aligned}\tilde{Y}_t &:= j \in \{S,U\} | \sum_{i=1}^{k} d_i \leq t < \sum_{i=1}^{k+1} d_i = t, Y_{k+1} = j, k = 0,1,2,\ldots,n-1,\\ &= Y_i \text{ on } t_{i-1} \leq t < t_i,\end{aligned}$$

with $\sum_{i=1}^{0} d_i := 0$. For a graph illustrating this definition, we refer to Figure 10.1 that shows these definitions for the Hidden Markov Model. Note again that $\tilde{Y}_t$ is an alternating renewal process with states S and U and thus also a regenerative process (Section 8.2.3.2).
In addition, note that Ξ_{HBMi} is not a continuous time Markov chain as the inverse Gaussian distribution is not memoryless (as explained in more detail on page 108).

13.1 Continuous presentation

In this section we start by computing results on the expectation and distribution of the number of perceptual reversals and on the residual time (Sections 13.1.1 and 13.1.2). Then, a result on the asymptotic marginal density of the perception process P is proven (Section 13.1.3).

13.1.1 Number of changes

Transferring the corresponding results for the HMMc (Proposition 10.1 and Corollary 10.2) to the HBMc, simple results for the number of changes in the HBMc in an interval of length $\Delta > 0$ can be stated. First, we assume that the interval starts with a perceptual change. Second, we relax this assumption and state an asymptotic result in Corollary 13.2. The crude stationarity of Ξ_{HBMc} in the limit is concluded. Recall that crude stationarity means that the number of changes in an interval only depends on its length and not on the starting point (Definition 8.14).

Proposition 13.1. ***Number of changes in the HBMc***
Let (b, ν_0) be the parameter set of a HBMc and $I(\Delta)$ be a right-open interval with length $\Delta \geq 0$ starting with a perceptual change. The number of perceptual changes in this interval $N^*(\Delta)$ has the following probability weights

$$w^*_\Delta(j) := \mathbb{P}(N^*(\Delta) = j) = \tilde{F}_{M_{\nu_0}(\Delta)}(2jb) - \tilde{F}_{M_{\nu_0}(\Delta)}(2(j-1)b),$$

for $j \geq 1$ and 0 else with $\tilde{F}_{M_{\nu_0}(t)}(m)$ as in (10.1). For $\Delta \to \infty$ it holds for the expected number of changes in the interval $I(\Delta)$: $\frac{\mathbb{E}[N^*(\Delta)]}{\Delta} \longrightarrow \frac{1}{2b/\nu_0}$.

Proof: As the HBMc just is a reparametrization of the HMMc this result is identical to Proposition 10.1. □

We skip the assumption of the interval $I(\Delta)$ beginning with a perceptual change and show an asymptotic result.

Corollary 13.2. ***Crude stationarity of the HBMc***
Contrary to Proposition 13.1 assume now that the start t of the right-open interval $I(\Delta)$ with length $\Delta \geq 0$ does not coincide with a perceptual change. Then, it holds

$$\lim_{t\to\infty} \mathbb{P}(N^*(\Delta) = j) = \begin{cases} \mathbb{P}(R^c > \Delta), & \text{if } j = 0, \\ \int_0^\Delta w^*_{\Delta-\Delta_r}(j) f_{R^c}(\Delta_r) d\Delta_r, & \text{if } j \geq 1, \end{cases}$$

with R^c as the asymptotic residual time with density $f_{R^c} = 1/(2b/\nu_0)(1 - F^{IG}_{2b/\nu_0, \sqrt{2b/\nu_0^3}})$ as given in the next Corollary 13.3 and w^*_Δ as given in Proposition 13.1.
For the expected value of changes, it again holds asymptotically

$$\frac{\mathbb{E}[N^*(\Delta)]}{\Delta} \xrightarrow[\Delta\to\infty]{} \frac{1}{2b/\nu_0},$$

and the resulting point process Ξ_{HBMc} is in the limit crudely stationary.

Proof: Analogous to the proof of Corollary 10.2. □

13.1.2 Residual time

The residual time, i.e., the time span until the next percept change, is the next issue. We show results for the density and the expectation.

Corollary 13.3. ***Residual time in the HBMc***
Let Ξ_{HBMc} be the point process of a HBMc with parameters (b, ν_0) and R^c be the asymptotic residual time. Its expectation is given by

$$\mathbb{E}[R^c] = \frac{1}{2\nu_0^2} + \frac{b}{\nu_0},$$

and the distribution has the density $f_{R^c}(x) = \frac{1}{2b/\nu_0}\left(1 - F^{IG}_{2b/\nu_0, \sqrt{2b/\nu_0^3}}(x)\right)$.

Proof: This follows by exchanging μ and σ in Corollary 10.3 by b and ν_0 using Proposition 8.6. □

13.1.3 Marginal density of P

In the HBM the perception is determined by the perception process $(P_t)_t$. Here, we focus on its marginal distribution and derive a limit result for $t \to \infty$ which however also holds for small t as we discuss. In Proposition 13.6 we show that the marginal limit distribution of P has also small weights outside the borders as overshooting is allowed. To simplify notation in the proof we introduce the **error function**. The error function is given by an integral (e.g., Abramowitz and Stegun, 1972).

Definition 13.4. ***Error function***
For $x \in \mathbb{R}$ the error function erf is defined as follows

$$erf(x) := \frac{2}{\sqrt{\pi}} \int_0^x \exp(-t^2) dt.$$

Remark 13.5. ***Connection of the error function to the normal distribution***
The error function is connected to the distribution function $\Phi(x)$ of the standard normal distribution (Abramowitz and Stegun, 1972), which can be shown via change of variables:

$$erf(x) = 2\Phi(\sqrt{2}x) - 1.$$

The name of the error function originates from its main application area (Kilian and Weber, 2003): In measurement theory the value of the error function at $\frac{x}{\sigma\sqrt{2}}$ gives for $x > 0$ the probability that a measurement has a distance of at most x from the mean value assuming normally distributed errors with standard deviation $\sigma > 0$.
Now, we are ready to state the proposition about the marginal density of P.

Proposition 13.6. ***Marginal density of P***
Let $(P_t)_t$ be the perception process in the HBMc with border b and drift ν_0 and $P_0 = -b$. $f_{P_t}(x)$ is the marginal density of the position P_t at a fixed time t. Letting $t \to \infty$ it holds

$$f_P(x) := \lim_{t\to\infty} f_{P_t}(x) = \begin{cases} \frac{1}{2b} - \frac{1}{4b}\exp(2\nu_0(x-b)) - \frac{1}{4b}\exp(-2\nu_0(x+b)), & \text{if } -b \le x \le b, \\ \frac{1}{4b}[\exp(-2\nu_0(x-b)) - \exp(-2\nu_0(x+b))], & \text{if } x > b, \\ \frac{1}{4b}[\exp(2\nu_0(x+b)) - \exp(2\nu_0(x-b))], & \text{if } x < -b. \end{cases}$$

Proof: The proof follows a case-by-case analysis.

First case: $|x| < b$
We seek to find an expression for $f_{P_t}(x)$ that is easy to handle. Let therefore E_t denote the distance covered by P_t, i.e., regardless of the sign of the drift E_t is the increment of the Brownian motion W (Model 11.1) in the interval $[0, t]$ plus $\nu_0 t$ (compare also Figure 13.1 for the exchange of the position P_t by the distance E_t). Moreover, let M_t denote the maximum distance reached until t. Note that different distances E_t lead to the same position x of the perception process (visualized in Figure 13.1 by the gray and red lines). In particular, starting in $-b$ a position x is reached when for $j = 1, 2, \ldots$ a distance of $x+b+4(j-1)b$ or $4jb-(x+b)$ is covered by the distance process. To consider the different drift signs of P, we have to claim that the maximum value M_t of the process has not exceeded the border $4(j-1)b + 2b$ in the first case of positive drift (because otherwise the sign of the drift would have changed such that the translation of P to E gets incorrect) and the border $4jb$ in the second case of negative drift. Therefore, it holds for $y := x + b$

$$f_{P_t}(x_t) = \sum_{j=1}^{\infty} \mathbb{P}(E_t = 4(j-1)b + y, M_t < 4(j-1)b + 2b) + \mathbb{P}(E_t = 4jb - y, M_t < 4jb), \tag{13.1}$$

where the substitution of x by y mainly is for notational reasons.
Next, we derive in step 1 expressions for the first and the second summand in equation (13.1). Then, we derive in step 2 upper and lower integral bounds for the infinite sum about these two summands using different inequalities for exponential functions. We will observe that the limits for $t \to \infty$ of the upper and the lower bound are identical such that the we can prove the assertion for the case $|x| < b$.

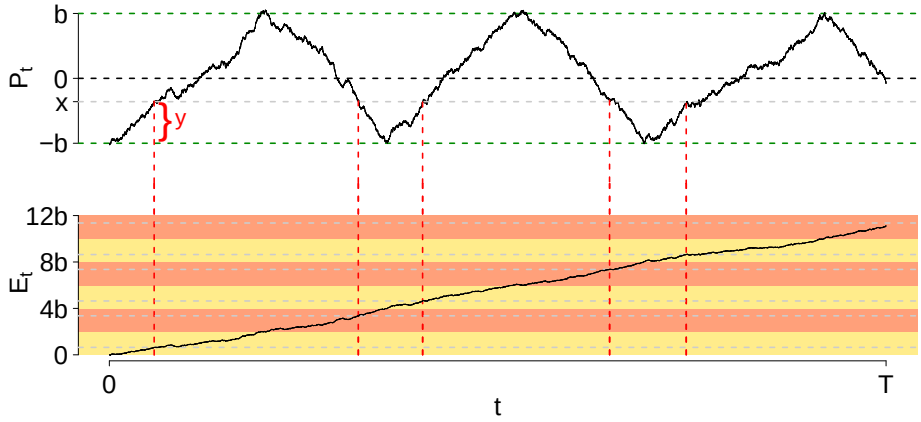

Figure 13.1: Transferring the perception process P_t (A) to the distance process E_t (B). *E_t is the distance P_t covered since the start of the experiment, i.e., regardless of the changes of the sign of the drift. One dominance time corresponds to a covered distance of $2b$. The variable $y := x + b$ is highlighted, and the position x is marked by a gray line in panel A. In panel B all distances leading to the position x are marked gray and the points in time where such a distance is reached are visualized by red lines.*

Step 1: Expressions for the summands in (13.1)
We need the following result (Theorem 7.2.1 in Shreve, 2004): For $w \leq m$ and $m \geq 0$ the joint density $\tilde{f}$ of the position W_t of a Brownian motion with drift ν_0 and its maximum M_t at time $t > 0$ is given by

$$\tilde{f}_{M(t),W(t)}(m,w) = \frac{2(2m-w)}{t\sqrt{2\pi t}} \exp\left(\nu_0 w - \frac{1}{2}\nu_0^2 t - \frac{1}{2t}(2m-w)^2\right).$$

Otherwise, $\tilde{f}_{M(t),W(t)}(m,w) = 0$.
Thus, it holds for the terms in equation (13.1)

$$\begin{aligned}
&\mathbb{P}(E_t = 4(j-1)b + y, M_t < 4(j-1)b + 2b) \\
&= \int_{4(j-1)b+y}^{4(j-1)b+2b} \frac{2(2m - 4b(j-1) - y)}{t\sqrt{2\pi t}} \exp\left(\nu_0(4(j-1)b + y) - \frac{1}{2}\nu_0^2 t \right. \\
&\qquad\qquad \left. - \frac{1}{2t}(2m - 4(j-1)b - y)^2\right) dm \\
&= -\frac{1}{\sqrt{2\pi t}} \exp\left(\nu_0(4(j-1)b + y) - \frac{1}{2}\nu_0^2 t - \frac{1}{2t}(2m - 4(j-1)b - y)^2\right)\Big|_{m=4(j-1)b+y}^{4(j-1)b+2b} \\
&= -\frac{1}{\sqrt{2\pi t}} \exp\left(-\frac{1}{2t}\left(-4m(4b(j-1)+y) + (4b(j-1) - t\nu_0 + y)^2 + 4m^2\right)\right)\Big|_{m=4(j-1)b+y}^{4(j-1)b+2b} \\
&= \frac{1}{\sqrt{2\pi t}} \exp\left(-\frac{1}{2t}(4(j-1)b - t\nu_0 + y)^2\right) - \frac{1}{\sqrt{2\pi t}} \exp\left(-\frac{1}{2t}\left(-4(2b + 4(j-1)b)(4b(j-1)+y)\right.\right. \\
&\qquad\qquad \left.\left. + (4b(j-1) - t\nu_0 + y)^2 + 4(2b + 4(j-1)b)^2\right)\right)
\end{aligned} \tag{13.2}$$

and

$$\begin{aligned}
&\mathbb{P}(E_t = 4jb - y, M_t < 4jb) \\
&\quad = \int_{4jb-y}^{4jb} \frac{2(2m - 4jb + y)}{t\sqrt{2\pi t}} \exp\left(\nu_0(4jb - y) - \frac{1}{2}\nu_0^2 t - \frac{1}{2t}(2m - 4jb + y)^2\right) dm \\
&\quad = -\frac{1}{\sqrt{2\pi t}} \exp\left(\nu_0(4jb - y) - \frac{1}{2}\nu_0^2 t - \frac{1}{2t}(2m - 4jb + y)^2\right)\Big|_{m=4jb-y}^{4jb} \\
&\quad = -\frac{1}{\sqrt{2\pi t}} \exp\left(-\frac{1}{2t}\left(-4m(4jb - y) + (-4jb + t\nu_0 + y)^2 + 4m^2\right)\right)\Big|_{m=4jb-y}^{4jb} \\
&\quad = \frac{1}{\sqrt{2\pi t}} \exp\left(-\frac{1}{2t}(-4jb + t\nu_0 + y)^2\right) \\
&\qquad - \frac{1}{\sqrt{2\pi t}} \exp\left(-\frac{1}{2t}\left(16jb(y - 4jb) + (-4jb + t\nu_0 + y)^2 + 64j^2b^2\right)\right). \qquad (13.3)
\end{aligned}$$

Step 2: Lower and upper bounds for the sums over (13.2) and (13.3)

We investigate the behavior of the sum over the first summand in (13.2). This infinite sum over j can be approximated by a lower and an upper integral bound. We explain this by using different inequalities for exponential functions. Note that $\exp(-(c\lfloor w\rfloor + a)^2) \leq \exp(-(cw+a)^2)$ for $cw + a \leq 0 \Leftrightarrow w \leq -a/c$ and $\exp(-(c\lfloor w\rfloor + a)^2) \leq \exp(-(cw - 1 + a)^2)$ for $cw + a > 1 \Leftrightarrow w > (1 - a)/c$. There, we use the floor function $\lfloor w\rfloor := \max\{k \in \mathbb{Z} \mid k \leq w\}$ and $w, c > 0, a \in \mathbb{R}$. With $w = z, c = 4b$ and $a = -4b + y - t\nu_0$ and the inequality $\exp(-(c\lfloor w\rfloor + a)^2) \leq \exp(0) = 1$ especially for $w \in (-a/c; (1 - a)/c]$ we find for the first summand of (13.2) the following upper bound

$$\begin{aligned}
&\frac{1}{\sqrt{2\pi t}} \sum_{j=1}^{\infty} \exp\left(-\frac{((j-1)4b - t\nu_0 + y)^2}{2t}\right) \\
&= \frac{1}{\sqrt{2\pi t}} \int_1^{\infty} \exp\left(-\frac{(\lfloor z\rfloor 4b - 4b + y - t\nu_0)^2}{2t}\right) dz \\
&= \frac{1}{\sqrt{2\pi t}} \left(\int_1^{\frac{t\nu_0 - y}{4b} + 1} \exp\left(-\frac{(\lfloor z\rfloor 4b - 4b - t\nu_0 + y)^2}{2t}\right) dz \right) \\
&\quad + \frac{1}{\sqrt{2\pi t}} \left(\int_{\frac{t\nu_0 - y}{4b} + 1}^{\frac{t\nu_0 - y + 1}{4b} + 1} \exp\left(-\frac{(\lfloor z\rfloor 4b - 4b - t\nu_0 + y)^2}{2t}\right) dz \right) \\
&\quad + \frac{1}{\sqrt{2\pi t}} \left(\int_{\frac{t\nu_0 - y + 1}{4b} + 1}^{\infty} \exp\left(-\frac{(\lfloor z\rfloor 4b - 4b - t\nu_0 + y)^2}{2t}\right) dz \right)
\end{aligned}$$

$$
\begin{aligned}
&\leq \frac{1}{\sqrt{2\pi t}} \left(\int_{1}^{\frac{t\nu_0 - y}{4b}+1} \exp\left(-\frac{((z-1)4b - t\nu_0 + y)^2}{2t} \right) dz + \int_{\frac{t\nu_0-y}{4b}+1}^{\frac{t\nu_0-y+1}{4b}+1} \exp(0) dz \right) \\
&\quad + \frac{1}{\sqrt{2\pi t}} \left(\int_{\frac{t\nu_0-y+1}{4b}+1}^{\infty} \exp\left(-\frac{((z-1/(4b)-1)4b - t\nu_0 + y)^2}{2t} \right) dz \right) \\
&= \frac{1}{\sqrt{2\pi t}} \frac{\sqrt{\pi t}}{\sqrt{32b}} \operatorname{erf}\left(\frac{1}{\sqrt{2t}} (4(z-1)b - t\nu_0 + y) \right) \Big|_{z=1}^{\frac{t\nu_0-y}{4b}+1} + \frac{1}{\sqrt{2\pi t}} \frac{1}{4b} \\
&\quad + \lim_{r\to\infty} \frac{1}{\sqrt{2\pi t}} \frac{\sqrt{\pi t}}{\sqrt{32b}} \operatorname{erf}\left(\frac{1}{\sqrt{2t}} (4(z-1/(4b)-1)b - t\nu_0 + y) \right) \Big|_{z=\frac{t\nu_0-y+1}{4b}+1}^{r} \\
&= \frac{1}{8b}(1 - \operatorname{erf}((y - t\nu_0)/\sqrt{2t})) + \frac{1}{4b\sqrt{2\pi t}} \qquad (13.4) \\
&\xrightarrow{t\to\infty} \frac{1}{4b},
\end{aligned}
$$

where we start the sum and the integral at 1, but effectively at 0 due to $j-1$ and $z-1$. Moreover, we use $\operatorname{erf}(0) = 0$ and $\lim_{x\to-\infty} \operatorname{erf}(x) = -1, \lim_{x\to\infty} \operatorname{erf}(x) = 1$ (e.g., Abramowitz and Stegun, 1972) and the abbreviation $\int_1^\infty f(x)dx := \lim_{X\to\infty} \int_1^X f(x)dx$ for arbitrary $f : \mathbb{R} \to \mathbb{R}$.
Concerning the lower bound for the first summand in (13.2), we use the inequalities
$\exp(-(c\lfloor w \rfloor + a)^2) \geq \exp(-(cw + a)^2)$ for $c\lfloor w \rfloor + a > 0$
and $\exp(-(c\lfloor w \rfloor + a)^2) \geq \exp(-(cw - 1 + a)^2)$ for $c\lfloor w \rfloor + a \leq 0$.
We conclude

$$
\begin{aligned}
&\frac{1}{\sqrt{2\pi t}} \sum_{j=1}^{\infty} \exp\left(-\frac{((j-1)4b - t\nu_0 + y)^2}{2t} \right) \\
&= \frac{1}{\sqrt{2\pi t}} \int_1^\infty \exp\left(-\frac{(\lfloor z \rfloor 4b - 4b - t\nu_0 + y)^2}{2t} \right) dz \\
&\geq \frac{1}{\sqrt{2\pi t}} \left(\int_1^{\lceil \frac{t\nu_0-y}{4b}+1 \rceil} \exp\left(-\frac{((z-1/(4b)-1)4b - t\nu_0 + y)^2}{2t} \right) dz \right) \\
&\quad + \frac{1}{\sqrt{2\pi t}} \left(\int_{\lceil \frac{t\nu_0-y}{4b}+1 \rceil}^{\infty} \exp\left(-\frac{((z-1)4b - t\nu_0 + y)^2}{2t} \right) dz \right) \\
&= \frac{1}{\sqrt{2\pi t}} \frac{\sqrt{\pi t}}{\sqrt{32b}} \operatorname{erf}\left(\frac{1}{\sqrt{2t}} (4(z-1/(4b)-1)b - t\nu_0 + y) \right) \Big|_{z=1}^{\lceil \frac{t\nu_0-y}{4b}+1 \rceil} \\
&\quad + \lim_{r\to\infty} \frac{1}{\sqrt{2\pi t}} \frac{\sqrt{\pi t}}{\sqrt{32b}} \operatorname{erf}\left(\frac{1}{\sqrt{2t}} (4(z-1)b - t\nu_0 + y) \right) \Big|_{z=\lceil \frac{t\nu_0-y}{4b}+1 \rceil}^{r}
\end{aligned}
$$

$$
\begin{aligned}
&= \frac{1}{8b}(1 - \operatorname{erf}((-1 - t\nu_0 + y)/\sqrt{2t})) \\
&\quad + \frac{1}{8b}\left(\operatorname{erf}\left(\frac{4(\lceil \frac{t\nu_0 - y}{4b} + 1\rceil - 1/(4b) - 1)b - t\nu_0 + y}{\sqrt{2t}}\right)\right) \\
&\quad - \frac{1}{8b}\left(\operatorname{erf}\left(\frac{4(\lceil \frac{t\nu_0 - y}{4b} + 1\rceil - 1)b - t\nu_0 + y}{\sqrt{2t}}\right)\right) \\
&\xrightarrow{t\to\infty} \frac{1}{4b},
\end{aligned}
$$

with the ceiling function $\lceil w \rceil := \min\{k \in \mathbb{Z} : k \geq w\}$.
Hence,

$$
\sum_{j=1}^{\infty} \frac{1}{\sqrt{2\pi t}} \exp\left(-\frac{1}{2t}(4(j-1)b - t\nu_0 + y)^2\right) \xrightarrow{t\to\infty} \frac{1}{4b}.
$$

Analogously we show

$$
\sum_{j=1}^{\infty} \frac{1}{\sqrt{2\pi t}} \exp\left(-\frac{1}{2t}(-4jb + t\nu_0 + y)^2\right) \xrightarrow{t\to\infty} \frac{1}{4b}
$$

which is the first summand in equation (13.3).
To bound the second summands in (13.2) and (13.3) we again require bounds for exponential functions. When using integrals to represent the sums over these summands, the argument is of the type $\exp(-(\lfloor z \rfloor^2 z_1 + \lfloor z \rfloor z_2))$ for $z_1 > 0, z_2 \in \mathbb{R}$ and $z > 0$. Depending on z_1 and z_2 we show two possibilities how to bound these expressions (one for small z, one for large z). First, we observe

$$
\exp(-(\lfloor z \rfloor^2 z_1 + \lfloor z \rfloor z_2)) \leq \exp(-(z^2 z_1 + z z_2)) \Leftrightarrow \lfloor z \rfloor^2 z_1 + \lfloor z \rfloor z_2 \geq z^2 z_1 + z z_2.
$$

For $z_2 \geq 0$ the display above never holds true. Assuming $z_2 < 0$ we obtain

$$
\lfloor z \rfloor^2 z_1 + \lfloor z \rfloor z_2 \geq z^2 z_1 + z z_2 \Leftrightarrow \frac{z_1}{z_2} \geq \frac{z - \lfloor z \rfloor}{\lfloor z \rfloor^2 - z^2} = \frac{-1}{\lfloor z \rfloor + z}. \tag{13.5}
$$

It follows $2z - 1 < \lfloor z \rfloor + z \leq 2z$, and therefore $z < -z_2/(2z_1)$ is a sufficient condition for strict inequality.
The second bound derives as

$$
\begin{aligned}
&\exp(-(\lfloor z \rfloor^2 z_1 + \lfloor z \rfloor z_2)) \leq \exp(-((z-1)^2 z_1 + (z-1) z_2)) \\
&\qquad \Leftrightarrow \lfloor z \rfloor^2 z_1 + \lfloor z \rfloor z_2 \geq (z-1)^2 z_1 + (z-1) z_2.
\end{aligned}
$$

For $z_2 \geq 0$ the display above always holds true. Assuming $z_2 < 0$ we obtain

$$
\lfloor z \rfloor^2 z_1 + \lfloor z \rfloor z_2 \geq (z-1)^2 z_1 + (z-1) z_2 \Leftrightarrow \frac{z_1}{z_2} \leq \frac{z - 1 - \lfloor z \rfloor}{\lfloor z \rfloor^2 - (z-1)^2} = \frac{-1}{\lfloor z \rfloor + z - 1}. \tag{13.6}
$$

It follows $2z - 2 < \lfloor z \rfloor + z \leq 2z - 1$, and therefore $z > -z_2/(2z_1) + 3/2$ is a sufficient condition for strict inequality.

Our aim is to find an upper border for the second summand in (13.2), which is

$$\sum_{j=1}^{\infty} \frac{1}{\sqrt{2\pi t}} \times \exp\left(-\frac{1}{2t}\left(-4(2b+4(j-1)b)(4b(j-1)+y)+(4b(j-1)-t\nu_0+y)^2+4(2b+4(j-1)b)^2\right)\right).$$

We abbreviate $m := -4(2b+4(z-1)b)(4(z-1)b+y)+(4(z-1)b-t\nu_0+y)^2+4(2b+4(z-1)b)^2$. Separating the terms with z^2 and z, we obtain as coefficient for the terms with z^2 in m the value $z_1 := 16b^2$ and for the coefficient for the terms with z the value $z_2 := -8bt\nu_0 - 8b < 0$. The infinite sum over the second summand in (13.2) hence can be bounded by an integral consisting of (at most) three parts. We need different parts as the bounds given below (13.5) and (13.6) state that different summands have to be bounded by different expressions. In the first part, we use the bound given due to (13.5), and in the third part we use the bound given following (13.6). Thus, we use values $N_1 := -z_2/(2z_1) = t\nu_0/(4b) + 1/(4b)$ as upper border of the first integral (if $N_1 > 1$) and $N_2 := -z_2/(2z_1) + 3/2 = t\nu_0/(4b) + 1/(4b) + 3/2$ as lower border of the third integral (which ensures the inequalities (13.5) and (13.6) to hold). The second part is just the integral between N_1 and N_2.

$$\begin{aligned}
&\sum_{j=1}^{\infty} \frac{1}{\sqrt{2\pi t}} \exp\left(-\frac{1}{2t}\left(-4(2b+4(j-1)b)(4b(j-1)+y)+(4b(j-1)-t\nu_0+y)^2\right.\right.\\
&\qquad\qquad \left.\left.+4(2b+4(j-1)b)^2\right)\right)\\
&= \int_1^{\infty} \frac{1}{\sqrt{2\pi t}} \exp\left(-\frac{1}{2t}\left(-4(2b+4(\lfloor z\rfloor-1)b)(4b(\lfloor z\rfloor-1)+y)+(4b(\lfloor z\rfloor-1)-t\nu_0+y)^2\right.\right.\\
&\qquad\qquad \left.\left.+4(2b+4(\lfloor z\rfloor-1)b)^2\right)\right) dz\\
&\leq \int_1^{\max(1,N_1)} \frac{1}{\sqrt{2\pi t}} \exp\left(-\frac{1}{2t}\left(-4(2b+4(z-1)b)(4b(z-1)+y)+(4b(z-1)-t\nu_0+y)^2\right.\right.\\
&\qquad\qquad \left.\left.+4(2b+4(z-1)b)^2\right)\right) dz\\
&\quad + \int_{\max(1,N_1)}^{N_2} \frac{1}{\sqrt{2\pi t}} dz\\
&\quad + \int_{N_2}^{\infty} \frac{1}{\sqrt{2\pi t}} \exp\left(-\frac{1}{2t}\left(-4(2b+4(z-2)b)(4b(z-2)+y)+(4b(z-2)-t\nu_0+y)^2\right.\right.\\
&\qquad\qquad \left.\left.+4(2b+4(z-2)b)^2\right)\right) dz
\end{aligned}$$

$$
\begin{aligned}
&= -\frac{1}{\sqrt{2\pi t}}\frac{\sqrt{\pi t}}{\sqrt{32b}}\exp\left(2\nu_0(y-2b)\right)\operatorname{erf}\left(\frac{-4b(z-1)+t\nu_0+y}{\sqrt{2t}}\right)\Big|_{z=1}^{\max(1,N_1)} + \frac{N_2-\max(1,N_1)}{\sqrt{2\pi t}} \\
&\quad - \lim_{r\to\infty}\frac{1}{\sqrt{2\pi t}}\frac{\sqrt{\pi t}}{\sqrt{32b}}\exp\left(2\nu_0(y-2b)\right)\operatorname{erf}\left(\frac{-4b(z-2)+t\nu_0+y}{\sqrt{2t}}\right)\Big|_{z=N_2}^{r} \\
&\leq \frac{1}{8b}\exp\left(2\nu_0(y-2b)\right)\left(1+\operatorname{erf}((-4b+t\nu_0+y)/\sqrt{2t})\right) + R_t + \frac{3}{2\sqrt{2\pi t}} \qquad (13.7) \\
&\xrightarrow{t\to\infty} \frac{1}{4b}\exp\left(2\nu_0(y-2b)\right).
\end{aligned}
$$

R_t includes the terms when plugging in the upper and the lower bound of the first and the third integral, respectively. R_t is proportional to $\operatorname{erf}(1/\sqrt{t})$ and thus vanishes for $t\to\infty$. The lower bound can be shown to be the same.
Analogously we compute for the second summand in (13.3)

$$
\sum_{j=1}^{\infty}\frac{1}{\sqrt{2\pi t}}\exp\left(\frac{-1}{2t}\left(16jb(y-4jb)+(-4jb+t\nu_0+y)^2+64j^2b^2\right)\right)\xrightarrow{t\to\infty}\frac{1}{4b}\exp\left(-2\nu_0 y\right).
$$

Finally, we have to adjust the terms with y properly (i.e., transform $y=x+b$ back to x) and arrive at

$$
f_P(x) = \frac{1}{2b} - \frac{1}{4b}\exp(2\nu_0(x-b)) - \frac{1}{4b}\exp(-2\nu_0(x+b)), \text{ if } -b\leq x\leq b.
$$

Thus, the first case of the assertion is proven.

Second and third case: $x > b$ and $x < -b$
Let $x > b$. We follow the same strategy as in the first case, i.e., find an expression for $f_{P_t}(x)$ and then bound it asymptotically by integrals. Concerning the distance E_t the process P_t covered this means that $4(j-1)b+2b$ has been crossed, but now the process is smaller than this border again. Moreover, P_t has not crossed the distance $4jb$ yet, as otherwise the drift direction would have changed again. With $x > b$ we therefore need the probability $\mathbb{P}(E_t = 4(j-1)b+3b-x, M_t \in (4(j-1)b+2b, 4jb))$. Again, we use a transformation $y := 3b-x$:

$$
\begin{aligned}
&\mathbb{P}(E_t = 4(j-1)b+y, M_t\in(4(j-1)b+2b,4jb)) \\
&= -\frac{1}{\sqrt{2\pi t}}\exp\left(\frac{-1}{2t}\left(-4m(4b(j-1)+y)+(4jb-t\nu_0+y)^2+4m^2\right)\right)\Big|_{m=4(j-1)b+2b}^{4jb} \\
&= \frac{1}{\sqrt{2\pi t}}\exp\left(\frac{-1}{2t}\left(-4(2b+4(j-1)b)(4b(j-1)+y)+(4jb-t\nu_0+y)^2\right.\right. \\
&\qquad\qquad \left.\left.+4(2b+4(j-1)b)^2\right)\right) \\
&\quad - \frac{1}{\sqrt{2\pi t}}\exp\left(\frac{-1}{2t}\left(-4(4jb)(4b(j-1)+y)+(4jb-t\nu_0+y)^2+4(4jb)^2\right)\right).
\end{aligned}
$$

As we already know, the infinite sum over the first summand in the latter display converges to $1/(4b)\exp(2\nu_0(y-2b))$ (as it is equivalent to the second summand in (13.2)). The sum over the second summand can be bounded by the same arguments as the sum over the second

summand in (13.2) (i.e., using (13.5) and (13.6)). We obtain $\frac{1}{4b}\exp(2\nu_0(y-4b))$ as lower and upper bound and do not the show the derivation in detail.
Interchanging $y = 3b - x$ by the position x above the border, we observe for $x > b$

$$\begin{aligned} f_P(x) &= \frac{1}{4b}(\exp(2\nu_0(b-x)) - \exp(2\nu_0(-b-x))) \\ &= \frac{1}{4b}(\exp(-2\nu_0(x-b)) - \exp(-2\nu_0(x+b))). \end{aligned}$$

Similarly, we obtain for $x < -b$

$$f_P(x) = \frac{1}{4b}(\exp(2\nu_0(x+b)) - \exp(2\nu_0(x-b))).$$

Thus, the assertion has been shown for all three cases. □

The perception process mainly fluctuates between the two borders $\pm b$. As, however, also overshooting is allowed, we analyze in Remark 13.7 the probability of exceeding the borders.

Remark 13.7. ***Probability of exceeding the borders***
Asymptotically, the probability for the perception process to be outside the borders is given for symmetry arguments by

$$\lim_{t\to\infty}\mathbb{P}(|P_t| > b) = 2\int_b^\infty \frac{1}{4b}(\exp(-2\nu_0(x-b)) - \exp(-2\nu_0(x+b)))dx = \frac{1}{4b\nu_0}[1-\exp(-4b\nu_0)].$$

This "overshooting"-probability ranges as claimed from 0 *to* 1*. It gets large for a small* $b\nu_0$ *as can be seen by regarding the function* $h(z) = 1/z(1-\exp(-z))$*. For* $z > 0$ *this function is monotonously decreasing from* 1 *to* 0*. In addition, we can relate the probability of overshooting the borders to the CV of the dominance times. It holds* $b\nu_0 = 0.5\mu^2/\sigma^2 = 1/(2CV^2)$*. Hence, highly irregular dominance time distributions with a large CV cause the perception process to be often outside the borders. In precise terms, we observe*

$$\lim_{t\to\infty}\mathbb{P}(|P_t| > b) = \frac{CV^2}{2}\left(1-\exp\left(-\frac{2}{CV^2}\right)\right).$$

Figure 13.2 compares the simulated marginal density of P_t in histograms with the theoretical density derived in Proposition 13.6. Different drift parameters ν_0 are chosen as well as two different points in time t to evaluate this asymptotic result.
In Figure 13.2 the dependence of the shape of the marginal distribution of P_t on the parameters is clearly visible. The first column (panels A and D) corresponds to typical parameters in the data set Schmack et al. (2015). Here, a bell-shaped density is derived with a small weight outside the borders $\pm b$. Already for the smaller $t = 20$ the fit is quite well (recall the length of recording $T = 240$ in the original data set). Decreasing the drift ν_0 increases the CV of the dominance times and thereby (Remark 13.7) increases also the probability to overshoot the borders as clearly is visible in Panels B and E. Here, the fit for the larger $t = 200$ is clearly better than for the smaller $t = 20$ (as also the mean dominance time is about 67 for this parameter combination such that often the upper border has not been reached at $t = 20$). Note that we have chosen a very extreme parameter ν_0 in these panels to illustrate the effect. Such an extreme CV is not observed in the data. The same holds for the small CV in panels C and F. There, the distribution between the borders is almost uniform as the drift is large

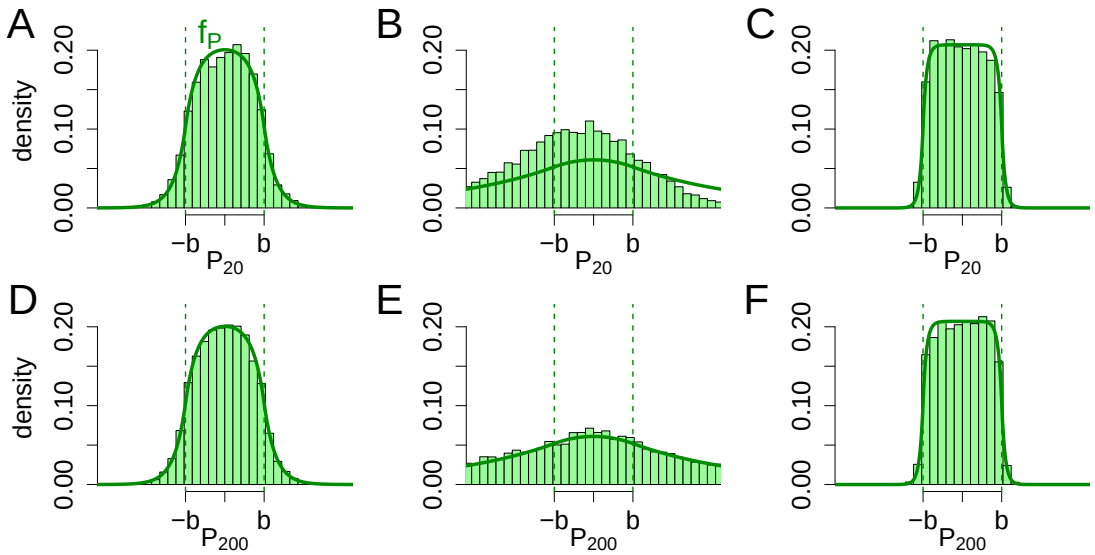

Figure 13.2: Comparison of the asymptotic marginal density $f_P(x)$ of P_t with simulated histograms at a fixed t. *The parameters are $b = 2.42$ and $\nu_0 \in \{0.72, 0.072, 2.42\}$, where ν_0 differs column by column. The parameters in the first column are the estimated parameters of subject B in Table 12.1 (page 161). In the first line (A-C), the empirical histogram at $t = 20$ is shown, where in the second line (D-F), the histogram at fixed $t = 200$ is plotted. 10000 simulations were used.*

allowing only small variability. Note that also for the quite extreme densities shown in panels B, C, E and F the fit of the asymptotic density is convincing.
The fast convergence of the empirical density toward the asymptotic density is due to the form of the error function (recall Remark 13.5 for its connection to the distribution function of the standard normal distribution). In the proof of Proposition 13.6, we let $t \to \infty$ in terms where t only occurs in the error function. Typical examples are the expressions in (13.4) and (13.7)

$$\frac{1}{8b}(1 - \operatorname{erf}((y - t\nu_0)/\sqrt{2t})) \xrightarrow{t\to\infty} \frac{1}{4b}$$
$$\frac{1}{8b}\exp\left(2\nu_0(y - 2b)\right)(1 + \operatorname{erf}((-4b + t\nu_0 + y)/\sqrt{2t})) \xrightarrow{t\to\infty} \frac{1}{4b}\exp\left(2\nu_0(y - 2b)\right),$$

where the limits $\lim_{x\to\infty} \operatorname{erf}(x) = 1$ and $\lim_{x\to-\infty} \operatorname{erf}(x) = -1$ are used. In Figure 13.3 we show that the terms with the error function (printed in the picture) in the aforementioned expressions converge very fast. For $t = 20$ both terms are close to +1 and -1, respectively.

13.2 Intermittent presentation

We derive results on the point process induced by the HBMi. For technical reasons the structure of this chapter differs slightly from the structure of Chapter 13.1. First, the relation to semi-Markov processes is discussed (Section 13.2.1). Next, first passage times as well as stationarity properties are derived (Section 13.2.2). Further, the number of perceptual reversals is investigated as well as the residual time (Sections 13.2.3 and 13.2.4). Additionally, in Section

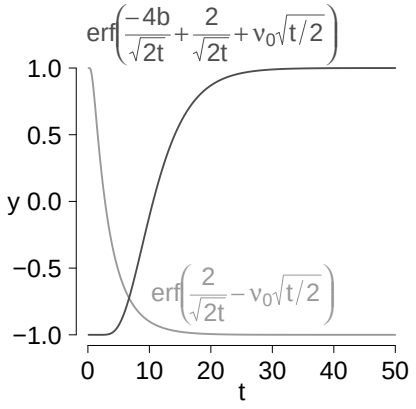

Figure 13.3: Convergence of the error function. *The error function for the two terms in equations* (13.4) *(light gray) and* (13.7) *(dark gray) depending on the time t. $b = 2.41$ and $\nu_0 = 0.72$ are chosen according to the estimated parameters of subject B in Table 12.1 and are the same as used for the first column in Figure 13.2. Moreover, we set $y := 2$. Larger absolute values for y slow the convergence toward ± 1 down, whereas smaller values speed the convergence up.*

13.2.5 marginal densities of the perception and the background process are computed. Recall that the key results are Corollary 13.11 about the steady-state distribution and Proposition 13.13 on the asymptotic rate of changes in the HBMi. Readers more interested in the application may skip all other parts of this section.

13.2.1 HBMi as semi-Markov process

The HBMi can be linked to the concept of semi-Markov processes (recall the introduction in Section 8.2.3.3) which is of importance in the theory of stochastic processes. The process $(\tilde{Y}_t)_{t\geq 0}$ denoting the state of the HBMi at time $t \geq 0$ constitutes a semi-Markov process (Definition 8.15, assuming known hidden states), and $(Y_i, (0, t_i))_{i\geq 1}$ is a Markov renewal process, where $(t_i)_{i\geq 1}$ are the perceptual reversal times and Y_i is the i-th hidden state. Here, we derive the key variables of this semi-Markov process. The entries of the semi-Markov kernel $Q(t)$ are given by

$$\begin{aligned} Q_{jk}(t) &= \mathbb{P}(D_{i+1} \leq t, Y_{i+1} = k | Y_i = j) = \mathbb{P}(Y_{i+1} = k | Y_i = j)\mathbb{P}(D_{i+1} \leq t | Y_{i+1} = k, Y_i = j) \\ &= p^*_{jk} \int_0^t f_{D_{jk}}(s) ds, \end{aligned} \tag{13.8}$$

where $f_{D_{jk}}(s)$ are the densities of the dominance times conditioned on the next state as derived in Lemma 11.3. In the context of semi-Markov processes the (D_{jk}) are the conditional sojourn times. In addition, $(Y_i)_{i\geq 1}$ is the embedded Markov chain.

13.2.2 First passage times, steady-state distributions and renewal results

In this section we focus first on the first passage times of the HBMi. These are defined like in Definition 10.4 with HMMi replaced by HBMi, Ξ_{HMMi} exchanged by Ξ_{HBMi} and $T^*_{ij}, \tilde{T}^*_{ij}$ instead of $T_{ij}, \tilde{T}_{ij}$, i.e.,

$$T^*_{ij} := \inf\{m \geq 2 : Y_m = j | Y_1 = i\} - 1, \qquad \tilde{T}^*_{ij} := \inf\{t > 0 : \tilde{Y}_t = j | \tilde{Y}_0 = i\}.$$

Then, we turn to the steady-state distributions. The steady-state distributions are of practical relevance, e.g., for the investigation of group differences between the control and the patients group in the data set Schmack et al. (2015). Note again that the following results are approximate due to the non-constant drifts of the perception process and the background process and that we omit approximation signs here for convenience.

Proposition 13.8. ***First passage and first recurrence times of the HBMi: Expectation***
Let p^*_{SS}, p^*_{UU} be defined as in equation (11.7) and μ^*_S, μ^*_U be as in equation (11.4). Moreover, $\mu^+_S, \mu^-_S, \mu^+_U$ and μ^-_U are defined as in Lemma 11.2.
Assume the HBMi starts with a perceptual reversal in the stable state S and $p^*_{SS} < 1$.
The expected first passage times of the unstable state U are approximately given by

$$\mathbb{E}[T^*_{SU}] = \frac{1}{1 - p^*_{SS}} \text{ and } \mathbb{E}[\tilde{T}^*_{SU}] = \frac{p^*_{SS}}{1 - p^*_{SS}}\mu^+_S + \mu^-_S = \frac{\mu^*_S}{1 - p^*_{SS}}.$$

Similar results hold for the first passage time of the stable state when starting with a perceptual change in the unstable state and $p^*_{UU} < 1$.
If $p^*_{SS} = 1$ or $p^*_{UU} = 1$, the corresponding expected first passage times are ∞.

If $\max(p^*_{SS}, p^*_{UU}) < 1$, the expected first recurrence time to the initial state is independent of the starting state approximately given by $\mathbb{E}[T^*_{SS}] = \mathbb{E}[T^*_{UU}] = \frac{1}{1-p^*_{SS}} + \frac{1}{1-p^*_{UU}}$ and
$\mathbb{E}[\tilde{T}^*_{SS}] = \mathbb{E}[\tilde{T}^*_{UU}] = \frac{p^*_{SS}}{1-p^*_{SS}}\mu^+_S + \mu^-_S + \frac{p^*_{UU}}{1-p^*_{UU}}\mu^+_U + \mu^-_U = \frac{\mu^*_S}{1-p^*_{SS}} + \frac{\mu^*_U}{1-p^*_{UU}}$.
If $\max(p^*_{SS}, p^*_{UU}) = 1$, the recurrence time is ∞.

Proof: The assertions for $\max(p^*_{SS}, p^*_{UU}) = 1$ are trivial. Therefore, we assume $\max(p^*_{SS}, p^*_{UU}) < 1$. As the lengths of stable dominance times are independent and the background process starts at zero at the beginning of each new dominance time, the number of visits to the stable state when starting in this stable state is a geometrically distributed random variable with success probability $1 - p^*_{SS}$. Thus, its expectation is given by $\mathbb{E}[T^*_{SU}] = \frac{1}{1-p^*_{SS}}$.
The length of a stable phase $\tilde{T}^*_{SU}$ is a random variable distributed like $\sum_{i=1}^{T^*_{SU}} D^S_i$, where $D^S_1, \ldots, D^S_{T^*_{SU}}$ denote the random stable dominance times. Given T^*_{SU}, we use linearity of expectation to compute the conditional expectation

$$\mathbb{E}\left[\sum_{i=1}^{T^*_{SU}} D^S_i | T^*_{SU}\right] = (T^*_{SU} - 1)\mu^+_S + \mu^-_S.$$

Now we take expectation over T^*_{SU} and use Corollary 11.4 to find

$$\mathbb{E}[\tilde{T}^*_{SU}] = \mathbb{E}\left[\sum_{i=1}^{T^*_{SU}} D^S_i\right] = \frac{p^*_{SS}}{1 - p^*_{SS}}\mu^+_S + \mu^-_S = \frac{\mu^*_S}{1 - p^*_{SS}}.$$

The assertions for T^*_{US} and $\tilde{T}^*_{US}$ can be shown using the same arguments. By the linearity of the expectations the claims about the expected first recurrences times follow. □

We derive the distribution of the first passage times as an additional result. For $\tilde{T}^*_{kj}$ we therefore sum over $f^i_{\tilde{T}^*_{kj}}(x)$ which are the densities of observing a phase of state k with i dominance times and length x followed by state j. Applying the law of total probability, the summation over i of $f^i_{\tilde{T}^*_{kj}}(x)$ gives the probability of a phase of state k with length x followed by a phase of state j.

Proposition 13.9. ***First passage and first recurrence times of the HBMi: Distribution***
a) Assume the HBMi starts with a perceptual reversal in the stable state S and $p^*_{SS} < 1$. The weights $w_{T^*_{SU}}$ of the first passage time of U are the weights of a Geometric distribution with parameter $p = 1 - p^*_{SS}$. The density $f_{\tilde{T}^*_{SU}}$ of the first passage time of the point process Ξ_{HBMi} is expressed using convolutions

$$f_{\tilde{T}^*_{SU}}(x) = \sum_{i=1}^{\infty} f^i_{\tilde{T}^*_{SU}}(x) = (1 - \tilde{p}_{SS}(x)) f^{IG}_{2b_S/\nu^*_S, \sqrt{2b_S/\nu^{*3}_S}}(x) + \sum_{i=2}^{\infty} \left((1 - \tilde{p}_{SS}) f^{IG}_{2b_S/\nu^*_S, \sqrt{2b_S/\nu^{*3}_S}} \right) * \left(\tilde{p}_{SS} f^{IG}_{2b_S/\nu^*_S, \sqrt{2b_S/\nu^{*3}_S}} \right)^{*(i-2)} (x), \quad (13.9)$$

if $x \geq 0$ and 0 otherwise. There, $\tilde{p}_{SS}(x)$ is given by (11.5).
Similar results hold for the first passage time of the stable state when starting with a perceptual change in the unstable state and $p^*_{UU} < 1$.
If $\max(p^*_{SS}, p^*_{UU}) = 1$, all finite weights vanish.

b) If $\max(p^*_{SS}, p^*_{UU}) < 1$, the weights $w_r(i)$ of the first recurrence time T^*_{SS} are $w_r(i) = 0$ if $i \leq 1$ and

$$w_r(i) = \sum_{j=1}^{i-1} w_{T^*_{US}}(j) w_{T^*_{SU}}(i - j),$$

else. The density $f_r(x)$ of the first recurrence time $\tilde{T}^*_{SS}$ is $f_r(x) = 0$ if $x < 0$ and

$$f_r(x) = \int_0^x f_{\tilde{T}^*_{US}}(y) f_{\tilde{T}^*_{SU}}(x - y) dy,$$

else.
If $\max(p^*_{SS}, p^*_{UU}) = 1$, the recurrence times are ∞.

Proof: First, we show a). The assertions for $\max(p^*_{SS}, p^*_{UU}) = 1$ are trivial. Therefore, we assume $\max(p^*_{SS}, p^*_{UU}) < 1$. As explained in the proof of Proposition 13.8, $\tilde{T}_{SU}$ is a geometrically distributed random variable with success probability $1 - p^*_{SS}$ which yields the assertion for $w_{T^*_{SU}}$.
We turn to the first passage time distribution of the unstable state by the point process Ξ_{HBMi}. To show the assertion a case-by-case analysis of the (random) number of dominance times in

the stable state T^*_{SU} is necessary. We explain the structure of $f^i_{\tilde{T}^*_{SU}}(x) := \mathbb{P}(\tilde{T}^*_{SU} = x, T^*_{SU} = i)$ for $i = 1$ and $i = 2$ in detail and then generalize to an arbitrary $i > 2$. In the last step of the proof we use the law of total probability $f_{\tilde{T}^*_{SU}}(x) = \sum_{i=1}^{\infty} \mathbb{P}(\tilde{T}^*_{SU} = x, T^*_{SU} = i) = \sum_{i=1}^{\infty} f^i_{\tilde{T}^*_{SU}}(x)$.
The stable phase ends after one dominance time ($T^*_{SU} = 1$) if at the time x of a border crossing by the perception process the background process is below $\tilde{b}_S$. Due to the independence of the two processes during one dominance time, we derive

$$f^1_{\tilde{T}^*_{SU}}(x) := \mathbb{P}(\tilde{T}^*_{SU} = x, T^*_{SU} = 1) = f^{\mathrm{IG}}_{2b_S/\nu^*_S, \sqrt{2b_S/\nu^{*3}_S}}(x)\Phi_{\nu^*_B x, \sqrt{x}}(\tilde{b}_S).$$

Now, assume that the stable phase of length x ends after two dominance times, i.e., $T^*_{SU} = 2$. This implies that at the end of the first dominance time with length x_1 ($0 < x_1 < x$) the background process is above the border $\tilde{b}_S$ (A) and, in contrast, at the end of the second dominance time with length $x - x_1$ the background process is below $\tilde{b}_S$ (B). Again, we make use of the independence of the two processes during one dominance time and the independence of two stable dominance times and need the convolution of the densities of events A and B:

$$\begin{aligned}
f^2_{\tilde{T}^*_{SU}}(x) &:= \mathbb{P}(\tilde{T}^*_{SU} = x, T^*_{SU} = 2) \\
&= \int_0^x f^{\mathrm{IG}}_{2b_S/\nu^*_S, \sqrt{2b_S/\nu^{*3}_S}}(x - x_1)\Phi_{\nu^*_B(x-x_1), \sqrt{x-x_1}}(\tilde{b}_S) f^{\mathrm{IG}}_{2b_S/\nu^*_S, \sqrt{2b_S/\nu^{*3}_S}}(x_1)(1 - \Phi_{\nu^*_B x_1, \sqrt{x_1}})(\tilde{b}_S)dx_1 \\
&= \int_0^x f^{\mathrm{IG}}_{2b_S/\nu^*_S, \sqrt{2b_S/\nu^{*3}_S}}(x - x_1)(1 - \tilde{p}_{SS}(x - x_1)) f^{\mathrm{IG}}_{2b_S/\nu^*_S, \sqrt{2b_S/\nu^{*3}_S}}(x_1)\tilde{p}_{SS}(x_1)dx_1 \\
&= \left((1 - \tilde{p}_{SS}) f^{\mathrm{IG}}_{2b_S/\nu^*_S, \sqrt{2b_S/\nu^{*3}_S}}\right) * \left(\tilde{p}_{SS} f^{\mathrm{IG}}_{2b_S/\nu^*_S, \sqrt{2b_S/\nu^{*3}_S}}\right)(x).
\end{aligned}$$

For $T^*_{SU} > 2$ we need $T^*_{SU} - 1$-fold convolutions (see Figure 13.4) following the same idea as explained for $T^*_{SU} = 2$, i.e., $T^*_{SU} - 1$ dominance times where the background process has crossed $\tilde{b}_S$ and the last dominance time where the background process is below its border (equation (13.9)).

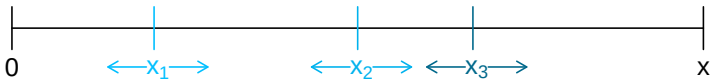

Figure 13.4: A stable phase of length $x > 0$ consisting of $T^*_{SU} = 4$ dominance times. *The perceptual changes occur at points in time $0 < x_1 < x_2 < x_3 < x$ which may vary as indicated by arrows.*

The assertion follows by the law of the total probability as explained above.
Now, we turn to b). By simple convolution arguments the claims about the first recurrences times follow. □

The first recurrence times can also be interpreted as life time distributions of a renewal process.

We illustrate Proposition 13.9. by comparing the theoretical density of the first passage time of the unstable state with the empirical density based on simulations. Therefore, we made use of the estimated HBMi parameters of subject C in Table 12.2 and simulated a HBMi with

10000 stable phases separated by unstable phases. For each stable phase we derived the length. The corresponding histogram is plotted in Figure 13.5 together with the theoretical density given in Proposition 13.9. We note that the theoretical and empirical density closely fit.

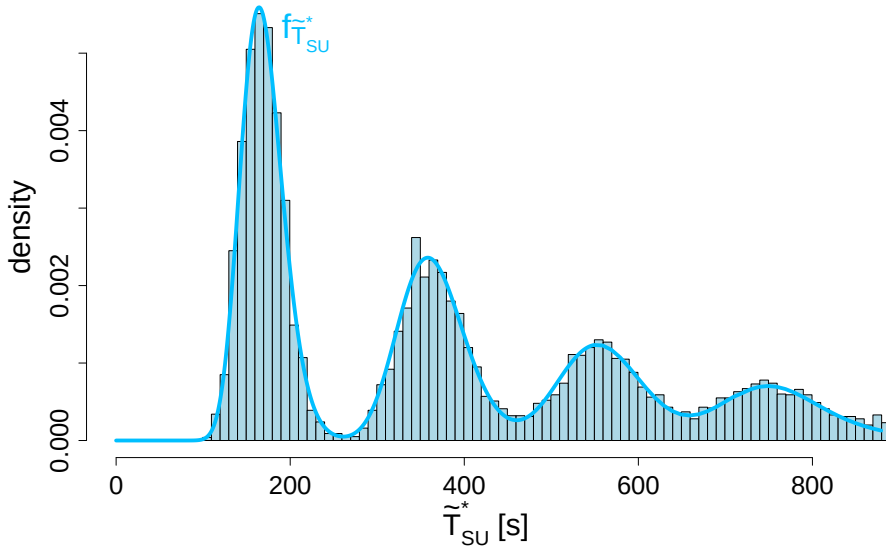

Figure 13.5: Comparison of the theoretical density $f_{\tilde{T}^*_{SU}}(x)$ (blue line, Proposition 13.9) of the length of a stable phase with a simulated histogram for parameter combination C (see Figure 9.1 [page 70] and Table 12.2).

Again, there exists a renewal equation for the distribution function of the first passage time of the process $\tilde{Y}_t$. Proposition 13.9 gives a solution of this equation.

Proposition 13.10. ***Renewal equation for the first passage time of the HBMi***
Regard the process $\tilde{Y}_t$. Let $G_{jk}(t) := \mathbb{P}(\tilde{T}_{jk} \leq t | \tilde{Y}_0 = j)$ describe the distribution function of the first passage time of state k starting in state j. It holds for $j, k \in \{S, U\}$, the semi-Markov kernel $Q(t)$ (equation (13.8)) and $t \geq 0$

$$G_{jk}(t) = Q_{jk}(t) + \int_0^t G_{jk}(t-x) dQ_{jj}(x).$$

Proof: This is Theorem 7.5 in Medhi (2009). □

Next, we analyze the stationary and steady-state distribution. Recall that the steady-state distribution $\tilde{\pi} = (\tilde{\pi}_S, \tilde{\pi}_U)$ denotes the probabilities of being in a given state at time t for $t \to \infty$, i.e., $\tilde{\pi}_S := \lim_{t\to\infty} \tilde{Y}_t = S$ as well as the long term relative time spent in the two states (equation (8.3)). Hence, $\tilde{\pi}_S$ is an important quantity to analyze group differences in the data set Schmack et al. (2015), and Corollary 13.11 is one of the key results stated in this chapter. To distinguish between the HBM and the HMM we now use stars as superscript for π and $\tilde{\pi}$.

Corollary 13.11. ***Stationary and steady-state distribution of the HBMi***
Let $(\mu_S^*, \sigma_S^*, \mu_U^*, \sigma_S^*, p_{SS}^*, p_{UU}^*)$ *be the derived parameter set of a HBMi. Assume* $\max(p_{SS}^*, p_{UU}^*) < 1$. *The stationary distribution* $\pi^* = (\pi_S^*, \pi_U^*)$ *of the underlying hidden state process is given by*

$$\pi^* = \left(\frac{p_{UU}^* - 1}{p_{SS}^* + p_{UU}^* - 2}, \frac{p_{SS}^* - 1}{p_{SS}^* + p_{UU}^* - 2} \right).$$

The steady-state distribution $\tilde{\pi}^* = (\tilde{\pi}_S^*, \tilde{\pi}_U^*)$ *with* $\tilde{\pi}_S^* := \lim_{t\to\infty} \mathbb{P}(\tilde{Y}_t = S)$, $\tilde{\pi}_U^* := \lim_{t\to\infty} \mathbb{P}(\tilde{Y}_t = U)$ *of the resulting point process* Ξ_{HBMi} *derives as*

$$\tilde{\pi}^* = \left(\frac{\frac{\mu_S^*}{1-p_{SS}^*}}{\frac{\mu_S^*}{1-p_{SS}^*} + \frac{\mu_U^*}{1-p_{UU}^*}}, \frac{\frac{\mu_U^*}{1-p_{UU}^*}}{\frac{\mu_S^*}{1-p_{SS}^*} + \frac{\mu_U^*}{1-p_{UU}^*}} \right). \tag{13.10}$$

If $p_{SS}^* = 1$, *we have* $\pi^* = \tilde{\pi}^* = (1, 0)$, *and if* $p_{UU}^* = 1$, *it holds* $\pi^* = \tilde{\pi}^* = (0, 1)$.

Proof: Assume $\max(p_{SS}^*, p_{UU}^*) < 1$. Note that the mean probability that the perception process remains in the stable state (i.e., is during the $i+1$-st dominance time stable given it is stable in the i-th dominance time) is given by p_{SS}^* if the i-th dominance time is unknown. Analogously p_{UU}^* is the mean probability to remain in the unstable state in case of an unknown i-th dominance time. These probabilities only depend on the current state. Therefore, we can interpret the hidden process $(Y_i)_{i\geq 1}$ as embedded Markov chain (compare also Section 13.2.1 about the interpretation as semi-Markov process). Assuming that P^* is the transition matrix of this Markov chain (with entries given by p_{jk}^* for $j, k \in \{S, U\}$) we know that π^* satisfies $\pi^* P^* = \pi^*$ (Section 9.1). By standard calculations it follows $\pi^* = \left(\frac{p_{UU}^* - 1}{p_{SS}^* + p_{UU}^* - 2}, \frac{p_{SS}^* - 1}{p_{SS}^* + p_{UU}^* - 2} \right)$.
To derive the steady-state distribution of Ξ_{HBMi}, we interpret Ξ_{HBMi} as regenerative process (compare Section 8.2.3.2). The life times $(\tilde{D}_i)_{i\geq 1}$ of the corresponding renewal process are given by the first recurrence times in the HBMi. The amount of time spent in state S during a life time then is just the first passage time of the state U when starting in S. Using equation (8.2) and Proposition 13.8, it follows directly

$$\tilde{\pi}_S^* = \frac{\mathbb{E}[\text{amount of time in state j during } \tilde{D}_1]}{\mathbb{E}[\tilde{D}_1]} = \frac{\mathbb{E}[\tilde{T}_{SU}]}{\mathbb{E}[\tilde{T}_{SS}]} = \frac{\frac{\mu_S^*}{1-p_{SS}^*}}{\frac{\mu_S^*}{1-p_{SS}^*} + \frac{\mu_U^*}{1-p_{UU}^*}}$$

and analogously for $\tilde{\pi}_U^*$.
The assertions for $\max(p_{SS}^*, p_{UU}^*) = 1$ are obvious. □

By equation (8.3) we know that the steady-state distribution also describes the long term relative time spent in the two states. Therefore, we now compare the theoretical relative time spent in the stable state with the empirical relative time spent in the stable state. 1000 response patterns for the four subjects given in Table 12.2 are simulated for $T \in \{1200, 3600\}$. The empirical value $\tilde{\pi}_S^{\text{emp}}$ is for each response pattern estimated as

$$\tilde{\pi}_S^{\text{emp}} := \frac{\sum_{i|Y_i=S} d_i}{T}. \tag{13.11}$$

Note that the hidden states Y_i are known as we simulate the response patterns. In Table 13.1 the mean and median of $\tilde{\pi}_S^{\text{emp}}$ for the two time horizons are compared with the theoretical values $\tilde{\pi}_S^*$ given by Corollary 13.11. We note that already for the comparatively small recording length in the data $T = 1200$ theoretical and empirical values agree quite closely.

		$T = 1200$		$T = 3600$	
subject	$\tilde{\pi}_S^*$	$\bar{\tilde{\pi}}_S^{\text{emp}}$	$\text{med}\tilde{\pi}_S^{\text{emp}}$	$\bar{\tilde{\pi}}_S^{\text{emp}}$	$\text{med}\tilde{\pi}_S^{\text{emp}}$
C	0.785	0.761	0.781	0.787	0.786
D	0.872	0.871	0.873	0.871	0.872
E	1.00	1.00	1.00	1.00	1.00
F	0.155	0.216	0.209	0.177	0.176

Table 13.1: Comparison of empirical and theoretical relative times spent in the stable state by the HBMi. *For the empirical steady-state distribution 1000 response patterns were simulated with the parameters given in Table 12.2 (page 162). Mean and median values of* (13.11) *are used for the comparison. The theoretical values are derived using* (13.10)*.*

The empirical validity of the stationary distribution π^* of the underlying Markov chain is comparable (data not shown).

Remark 13.12. ***Renewal results for the HBMi***
The results about the expected number of cycles in the HBMi, the renewal equations for Y_i and $\tilde{Y}_t$, the exact probability of being in the stable state and the probability generating function of the HBMi translate directly from the HMMi (Lemma 10.9, Proposition 10.10, Corollary 10.11 and Lemma 10.13). p_{SS} and p_{UU} have to be exchanged by p_{SS}^* and p_{UU}^*, respectively.

13.2.3 Number of changes

We focus on the rate of perceptual changes. The following proposition 13.13 is one key result of this chapter. It is, for instance, required to derive the asymptotic expected number of perceptual reversals in the HBMi when changing the length of the blank display. With a different length of the blank display $(\mu_S^*, \sigma_S^*, \mu_U^*, \sigma_S^*, p_{SS}^*, p_{UU}^*)$ change (as the mean drifts $\nu_S^*, \nu_U^*, \nu_B^*$ change). Proposition 13.13 enables us to derive the asymptotic expected rate of perceptual reversals dependent on the new parameter set.

Proposition 13.13. ***Rate of changes in the HBMi***
Let $(\mu_S^*, \sigma_S^*, \mu_U^*, \sigma_S^*, p_{SS}^*, p_{UU}^*)$ be the derived parameter set of a HBMi and $\Delta > 0$ be the length of an interval. If $\max(p_{SS}^*, p_{UU}^*) < 1$, it holds for the expected number of changes $N^*(\Delta)$ in this interval

$$\frac{\mathbb{E}[N^*(\Delta)]}{\Delta} \xrightarrow[\Delta\to\infty]{} \frac{2 - p_{UU}^* - p_{SS}^*}{(1 - p_{UU}^*)\mu_S^* + (1 - p_{SS}^*)\mu_U^*}. \tag{13.12}$$

If $p_{SS}^* = 1$, it holds

$$\frac{\mathbb{E}[N^*(\Delta)]}{\Delta} \xrightarrow[\Delta\to\infty]{} \frac{1}{\mu_S^*}$$

and analogously for $p_{UU}^* = 1$.
We define $\rho^{HBMi} := \lim_{\Delta\to\infty} \frac{\mathbb{E}[N^*(\Delta)]}{\Delta}$ as the (asymptotic) rate of changes.

Proof: Using Corollary 13.11 about the steady-state distribution, the proof is analogous to the proof of Proposition 10.14. □

The asymptotic rate of changes in the HBMi and the rate of changes in the data set Schmack et al. (2015) are compared in Figure 13.6 A. As with the HMM (compare Figure 10.5 on page 120) these rates are close together (mostly not more than 10% apart from each other). The same explanations as in the HMM case are possible for differences in the rates.
Panel B shows the comparison with the rate of changes in the data for the simulated rate of changes in the HBMi conditioning on the same (Viterbi-estimated) starting state and the same recording length as in the original data. As in contrast to the HMM not the transition probabilities directly are maximized, the model fit is a slightly worse compared to the HMM.

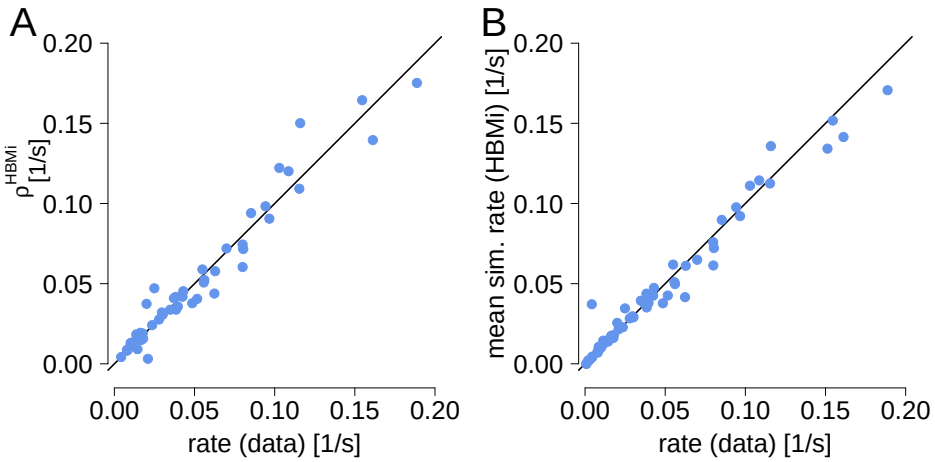

Figure 13.6: Comparison of the rate of changes between the HBMi and the data set Schmack et al. (2015). *In A the theoretical (asymptotic) rate ρ^{HBMi} (Proposition 13.13) is contrasted with the rate of changes in the data, and in B the mean rate of changes in 1000 simulations started in the same (Viterbi-estimated, Section 12.5) state as the original data is used ($T = 1200$).*

Additionally, we state results about the distribution of the number of perceptual changes in the HBMi. For technical reasons, we first assume an interval of length Δ starting with a perceptual change to state Proposition 13.14. In Proposition 13.15 we relax this assumption.

Proposition 13.14. ***Number of changes in the HBMi: Distribution I***
Let $\Theta_{HBMi} = (b_S, \nu_S^*, b_U, \nu_U^*, \tilde{b}_S, \tilde{b}_U, \nu_B^*, \pi_{start,S}^*)$ be the parameter set of a HBMi, π^* be its stationary distribution and p_{SS}^*, p_{UU}^* be defined as in equation (11.7).
Moreover, let $I(\Delta) := [t, t+\Delta)$ be an interval of length $\Delta \geq 0$ starting with a perceptual change and Y be a sequence of hidden states. The probability of a realization y covering $I(\Delta)$ with $|y| \geq 2$ states in $I(\Delta)$ is for $t \to \infty$ given by

$$\mathbb{P}(Y = y) = \pi_{y_1}^* \int_0^\Delta \left(1 - F^{IG}_{2b_{y_{|y|}}/\nu^*_{y_{|y|}}, \sqrt{2b_{y_{|y|}}/{\nu^*_{y_{|y|}}}^3}}(\Delta - s)\right) \begin{cases} g_{y_1}(s)ds, & \text{if } |y| = 2, \\ (g_{y_1} * \ldots * g_{y_{|y|-1}})(s)ds, & \text{if } |y| > 2, \end{cases} \tag{13.13}$$

where the following function is folded

$$g_{y_i}(s) := f^{IG}_{2b_{y_i}/\nu^*_{y_i},\sqrt{2b_{y_i}}/\nu^3_{y_i^*}}(s) \cdot \begin{cases} \Phi_{s\nu^*_B,\sqrt{s}}(\tilde{b}_{y_i}), & \text{if } y_{i+1} = U, y_i = S, \\ \Phi_{-s\nu^*_B,\sqrt{s}}(\tilde{b}_{y_i}), & \text{if } y_{i+1} = U, y_i = U, \\ 1 - \Phi_{s\nu^*_B,\sqrt{s}}(\tilde{b}_{y_i}), & \text{if } y_{i+1} = S, y_i = S, \\ 1 - \Phi_{-s\nu^*_B,\sqrt{s}}(\tilde{b}_{y_i}), & \text{if } y_{i+1} = S, y_i = U. \end{cases} \tag{13.14}$$

If $|y| = 1$*, we have*

$$\mathbb{P}(Y = y) = \pi^*_{y_1} \left(1 - F^{IG}_{2b_{y_1}/\nu^*_{y_1},\sqrt{2b_{y_1}/\nu^3_{y_1^*}}}(\Delta) \right). \tag{13.15}$$

The probability weights of the number of changes $N^*_c(\Delta)$ *of* Ξ_{HBMi} *in the interval* $I(\Delta)$ *(starting with a perceptual change) are then given by*

$$\mathbb{P}(N^*_c(\Delta) = j) = \sum_{y \in \mathfrak{Y}(\Delta):\ |y|=j} \mathbb{P}(Y = y), \tag{13.16}$$

where $\mathfrak{Y}(\Delta)$ *denotes all hidden state sequences starting with a perceptual change whose resulting point processes cover the interval* $I(\Delta)$*.*

Proof: In the first step of the proof, we take the probabilities $\mathbb{P}(Y = y)$ as given to show the assertion (13.16). In the second step of the proof, an explanation for the correctness of the expressions for $\mathbb{P}(Y = y)$ is provided.
Given a perceptual change at t, j changes in the interval $[t, t + \Delta)$ imply that the hidden state sequence y leading to the response pattern has a length of j (recall also Figure 10.6 on page 121 for an example). To compute the probability of j changes in the interval $I(\Delta)$, we therefore have to sum over all possible hidden state paths of length j, i.e.,

$$\mathbb{P}(N^*_c(\Delta) = j) = \sum_{y \in \mathfrak{Y}(\Delta) || y|=j} \mathbb{P}(Y = y).$$

Now, we focus on the derivation of $\mathbb{P}(Y = y)$. For $t \to \infty$ the probability weights of the first state of the interval are given by the stationary distribution π^*. Thus, the first factor of $\mathbb{P}(Y = y)$ is the stationary weight $\pi^*_{y_1}$ of the first state y_1.
$|y| = 1$ implies that no change occurs in the interval $[t, t + \Delta)$. This means that the perception process has not crossed the border b_S or b_U (depending on the hidden state) in this interval, i.e., (13.15) holds true.
For $j = |y| \geq 2$, we assume the last perceptual reversal occurring at time $t + s < t + \Delta$ (compare Figure 13.7). Then, no changes occur in $(t + s, t + \Delta)$. Thus, the perception process has not crossed its current border b_S or b_U in an interval with length $\Delta - s$. This event has the probability $1 - F^{\text{IG}}_{2b_{y_{|y|}}/\nu^*_{y_{|y|}},\sqrt{2b_{y_{|y|}}/{\nu^*_{y_{|y|}}}^3}}(\Delta - s)$. As the last perceptual change can occur at an arbitrary $t + s < t + \Delta$, we need the convolution defined in (13.13). The other $j - 1$ changes occur in the interval $[t, t + s)$. For all these perceptual changes it holds: The state remains stable or changes to stable if the current border $\tilde{b}_S$ or $\tilde{b}_U$ of the background process is crossed at the end of a dominance time (third and fourth case in (13.14)).

If the background process border is not crossed, the state remains or changes to unstable (first and second case in (13.14)). The function $g_{y_i}(s)$ in (13.14) considers for each pair (y_i, y_{i+1}) the length of dominance times and the hidden states. Folding it implies that we allow for arbitrary perceptual reversal times $t + s_1, t + s_2, \ldots, t + s_{j-2}, t + s$ with $t < t + s_1 < \ldots < t + s_{j-2} < t + s < t + \Delta$ (compare the arrows in Figure 13.7). □

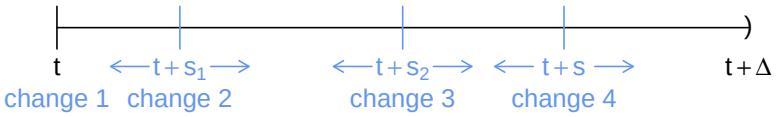

Figure 13.7: Visualization of the number of changes in the HBMi. *In this example $j = 4$ changes (marked by vertical bars) occur in the interval $I(\Delta)$ at times $t < t + s_1 < t + s_2 < t + s$ which are not fixed as indicated by arrows. There is no perceptual change in the interval $(t + s, t + \Delta)$.*

Next, we relax the assumption that the interval $I(\Delta)$ has to start with a perceptual change.

Proposition 13.15. ***Number of changes in the HBMi: Distribution II***
Let $I(\Delta) := [t, t + \Delta)$ be an interval of length $\Delta \geq 0$. The probability weights of the number of changes $N^*(\Delta)$ of Ξ_{HBMi} in the interval $I(\Delta)$ are then for $t \to \infty$ and $j \geq 1$ given by

$$\begin{aligned}
\mathbb{P}(N^*(\Delta) = j) = \tilde{\pi}_S^* \times & \\
& \left(\int_0^\Delta f_{R^S}(\Delta_S) \tilde{p}_{SS}^*(\Delta_S) \mathbb{P}(N_c^{*,S}(\Delta - \Delta_S) = j)/\pi_S^* \right. \\
& \left. + f_{R^S}(\Delta_S)(1 - \tilde{p}_{SS}^*(\Delta_S)) \mathbb{P}(N_c^{*,U}(\Delta - \Delta_S) = j)/\pi_U^* d\Delta_S \right) \\
& + \tilde{\pi}_U^* \times \\
& \left(\int_0^\Delta f_{R^U}(\Delta_U)(1 - \tilde{p}_{UU}^*(\Delta_U)) \mathbb{P}(N_c^{*,S}(\Delta - \Delta_U) = j)/\pi_S^* \right. \\
& \left. + f_{R^U}(\Delta_U) \tilde{p}_{UU}^*(\Delta_U) \mathbb{P}(N_c^{*,U}(\Delta - \Delta_U) = j)/\pi_U^* d\Delta_U \right),
\end{aligned}$$

where $N_c^{*,S}(\Delta)$ and $N_c^{*,U}(\Delta)$ denote the number of changes in an interval $I(\Delta)$ starting with a perceptual change in the stable or the unstable state, respectively (equation (13.16)), and $\tilde{\pi}_j^*$ denotes the steady-state probability of state j (Corollary 13.11). R^S and R^U are the asymptotic residual times in the stable and the unstable state as given in Proposition 8.12 with life time distributions $IG(\mu_S^*, \sigma_S^*)$ and $IG(\mu_U^*, \sigma_U^*)$.

$\tilde{p}^*_{SS}(\Delta_S)$ is the probability to remain stable given the residual time Δ_S and derives as

$$\begin{aligned}\tilde{p}^*_{SS}(\Delta_S) &:= \mathbb{P}\left(Y_2 = S | Y_1 = S, R^S = \Delta_S\right) \\ &= \int_{\Delta_S}^{\infty} \left(1 - \Phi_{\tilde{d}\nu^*_B, \sqrt{\tilde{d}}}(\tilde{b}_S)\right) \frac{f^{IG}_{2b_S/\nu^*_S, \sqrt{2b_S/\nu^{*3}_S}}(\tilde{d})}{1 - F^{IG}_{2b_S/\nu^*_S, \sqrt{2b_S/\nu^{*3}_S}}(\Delta_S)} d\tilde{d}. \end{aligned} \tag{13.17}$$

$\tilde{p}^*_{UU}(\Delta_U)$ is defined similarly.
For $j = 0$ we have

$$\mathbb{P}(N^*(\Delta) = 0) = \tilde{\pi}^*_S \mathbb{P}(R^S > \Delta) + \tilde{\pi}^*_U p \mathbb{P}(R^U > \Delta).$$

The point process Ξ_{HBMi} is asymptotically crudely stationary.

Proof: The proof mainly follows the same ideas as the proof of Proposition 10.16. Therefore, we only show that the expression for $\tilde{p}^*_{SS}(\Delta_S)$ in equation (13.17) holds true. First, we derive the density of the stable dominance time D^S_1 given its residual time Δ_S

$$f_{D^S_1 | R^S = \Delta_S}(\tilde{d}) = \frac{f_{A^S, R^S}(\tilde{d} - \Delta_S, \Delta_S)}{f_{R^S}(\Delta_S)} = \frac{f_{D^S_1}(\tilde{d})}{f_{R^S}(\Delta_S)\mathbb{E}[D^S_1]},$$

where A^S denotes the age (Definition 8.11), and the second equal sign follows by known results (e.g., Lemma 2.1 in Haviv, 2013).
Given this conditioned dominance time distribution we are able to derive the probability that the subject remains stable, i.e., that the background process is above $\tilde{b}_S$ at the end of the dominance time $\tilde{d}$. We integrate

$$\begin{aligned}\tilde{p}^*_{SS}(\Delta_S) &= \int_{\Delta_S}^{\infty} \mathbb{P}(B_{D^S_1} > \tilde{b}_S | D^S_1 = \tilde{d}, R^S = \Delta_S) f_{D^S_1 | R^S = \Delta_S}(\tilde{d}) d\tilde{d} \\ &= \int_{\Delta_S}^{\infty} \left(1 - \Phi_{\tilde{d}\nu^*_B, \sqrt{\tilde{d}}}(\tilde{b}_S)\right) \frac{f_{D^S_1}(\tilde{d})}{f_{R^S}(\Delta_S)\mathbb{E}[D^S_1]} d\tilde{d} \\ &= \int_{\Delta_S}^{\infty} \left(1 - \Phi_{\tilde{d}\nu^*_B, \sqrt{\tilde{d}}}(\tilde{b}_S)\right) \frac{f^{\mathrm{IG}}_{2b_S/\nu^*_S, \sqrt{2b_S/\nu^{*3}_S}}(\tilde{d})}{1 - F^{\mathrm{IG}}_{2b_S/\nu^*_S, \sqrt{2b_S/\nu^{*3}_S}}(\Delta_S)} d\tilde{d},\end{aligned}$$

where in the last line the density of R^S (Proposition 8.12) was plugged in. The same ideas are applicable to $\tilde{p}^*_{UU}(\Delta_U)$.
The asymptotic crude stationarity follows directly from the independence of the probability weights $\mathbb{P}(N^*(\Delta) = j)$ from t for $t \to \infty$. □

13.2.4 Residual time

Here, we derive the density and the expected value of the residual time, i.e., the time span until the next perceptual reversal in the HBMi.

Corollary 13.16. ***Residual time in the HBMi***
Let Ξ_{HBMi} be the point process of a HBMi with parameter set $\Theta_{HBMi} = (b_S, \nu_S^*, b_U, \nu_U^*, \tilde{b}_S, \tilde{b}_U, \nu_B^*, \pi_{start,S}^*)$ and asymptotic residual time R^{in}. Its expectation is given by

$$\mathbb{E}[R^{in}] = \tilde{\pi}_U^* \left(\frac{1}{2{\nu_U^*}^2} + \frac{b_U}{\nu_U^*} \right) + \tilde{\pi}_S^* \left(\frac{1}{2{\nu_S^*}^2} + \frac{b_S}{\nu_S^*} \right),$$

and the distribution has the density

$$f_R^{in}(x) = \frac{\tilde{\pi}_U^*}{2b_U/\nu_U^*} \left(1 - F^{IG}_{2b_U/\nu_U^*, \sqrt{2b_U/{\nu_U^*}^3}}(x) \right) + \frac{\tilde{\pi}_S^*}{2b_S/\nu_S^*} \left(1 - F^{IG}_{2b_S/\nu_S^*, \sqrt{2b_S/{\nu_S^*}^3}}(x) \right).$$

Proof: By substituting the mean and standard deviation parameters by the border and drift parameters (as in Proposition 8.6), the proof follows the same steps as the proof of Corollary 10.17. □

13.2.5 Marginal densities of the perception and the background process

Marginal density of *P*

As with the perception process in the HBMc, we derive the (approximate) asymptotic marginal density of the perception process for the HBMi.

Corollary 13.17. ***Marginal density of P***
Let $\Theta_{HBMi} = (b_S, \nu_S^*, b_U, \nu_U^*, \tilde{b}_S, \tilde{b}_U, \nu_B^*, \pi_{start,S}^*)$ be the parameter set of a HBMi. The limit of the marginal density $f_P(x)$ of the perception process is (approximately) given by

$$f_P(x) := \lim_{t\to\infty} f_{P_t}(x) \approx$$

$$\begin{cases}
\tilde{\pi}_S^* \left(\frac{1}{4b_S} [\exp(-2\nu_S^*(x - b_S)) - \exp(-2\nu_S^*(x + b_S))] \right) & \\
\quad + \tilde{\pi}_U^* \left(\frac{1}{4b_U} [\exp(-2\nu_U^*(x - b_U)) - \exp(-2\nu_U^*(x + b_U))] \right), & \text{if } x > b_S, \\
\tilde{\pi}_S^* \left(\frac{1}{2b_S} - \frac{1}{4b_S} \exp(2\nu_S^*(x - b_S)) - \frac{1}{4b_S} \exp(-2\nu_S^*(x + b_S)) \right) & \\
\quad + \tilde{\pi}_U^* \left(\frac{1}{4b_U} [\exp(-2\nu_U^*(x - b_U)) - \exp(-2\nu_U^*(x + b_U))] \right), & \text{if } b_U < x \leq b_S, \\
\tilde{\pi}_S^* \left(\frac{1}{2b_S} - \frac{1}{4b_S} \exp(2\nu_S^*(x - b_S)) - \frac{1}{4b_S} \exp(-2\nu_S^*(x + b_S)) \right) & \\
\quad + \tilde{\pi}_U^* \left(\frac{1}{2b_U} - \frac{1}{4b_U} \exp(2\nu_U^*(x - b_U)) - \frac{1}{4b_U} \exp(-2\nu_U^*(x + b_U)) \right), & \text{if } -b_U \leq x \leq b_U, \\
\tilde{\pi}_S^* \left(\frac{1}{2b_S} - \frac{1}{4b_S} \exp(2\nu_S^*(x - b_S)) - \frac{1}{4b_S} \exp(-2\nu_S^*(x + b_S)) \right) & \\
\quad + \tilde{\pi}_U^* \left(\frac{1}{4b_U} [\exp(2\nu_U^*(x + b_U)) - \exp(2\nu_U^*(x - b_U))] \right), & \text{if } -b_S \leq x < -b_U, \\
\tilde{\pi}_S^* \left(\frac{1}{4b_S} [\exp(2\nu_S^*(x + b_S)) - \exp(2\nu_S^*(x - b_S))] \right) & \\
\quad + \tilde{\pi}_U^* \left(\frac{1}{4b_U} [\exp(2\nu_U^*(x + b_U)) - \exp(2\nu_U^*(x - b_U))] \right), & \text{if } x < -b_S,
\end{cases}$$

with $\tilde{\pi}_S^*$ and $\tilde{\pi}_U^*$ as the steady-state distribution given in Corollary 13.11.

Proof: We decompose the density as follows

$$f_{P_t}(x) = \mathbb{P}(\tilde{Y}_t = S) f_{P_t|\tilde{Y}_t=S}(x) + \mathbb{P}(\tilde{Y}_t = U) f_{P_t|\tilde{Y}_t=U}(x).$$

Letting $t \to \infty$ we use the results of Corollary 13.11 (about the steady-state distribution $\tilde{\pi}^*$) and Proposition 13.6 (about the asymptotic marginal density of P in the HBMc as the (P)-process with an assumed constant drift ν_S^* or ν_U^* corresponds approximately to the (P)-process in the HBMc) to state the assertion. Now, we explain why the approximation signs occurs. Assume that the perception process is at b_S when the state changes to unstable. For simplification we assume that the perception process jumps back to b_S when the state gets stable again, i.e., the sign of the border does not change (in contrast to the true model behavior where the sign may change, see Model 11.1). Similar assumptions hold for a position of $-b_S$ and the unstable state, respectively. Using this approximation and conditioning on the stable or the unstable state, we are back in the situation of the perception process in the HBMc and can use the corresponding density to derive $f_{P_t|\tilde{Y}_t=S}(x)$ and $f_{P_t|\tilde{Y}_t=U}(x)$ (with adjusted drift and border parameters).
As the exact derivation of $f_{P_t}(x)$ would be lengthy and does not yield additional insights, and furthermore the approximation is close (e.g., Figure 13.8), we content ourselves with the approximation. □

An exemplary marginal density is shown in Figure 13.8 using the parameters of subject C in Table 12.2. The approximate theoretical density agrees closely with the empirical distribution (estimated in 1000 simulations), where the peak around zero is caused by the unstable state and the rather flat distribution for larger x-values is due to the stable state. Toward the borders $\pm b_S$ the density decreases like in the continuous case (Figure 13.2).

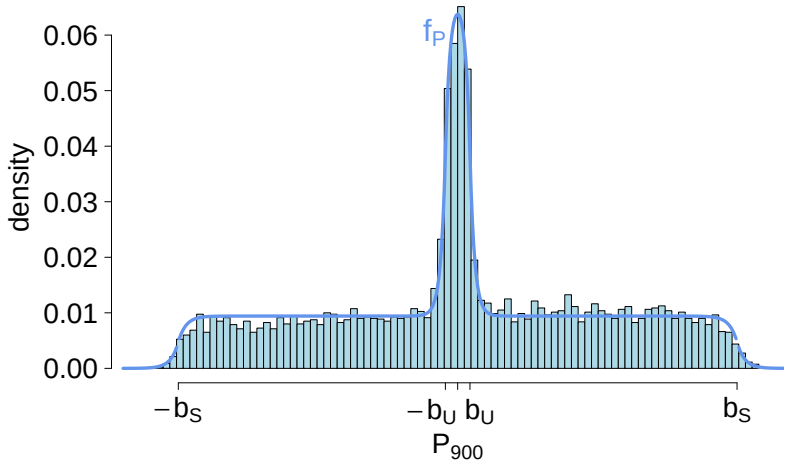

Figure 13.8: Comparison of the asymptotic marginal density $f_P(x)$ of P_t (blue line, Corollary 13.17) with an empirical histogram at $t = 900$ obtained from 1000 simulations. *The parameters are taken from parameter combination C (Table 12.2, page 162).*

Marginal density of B

Here, we discuss the asymptotic marginal density of the background process B.

Proposition 13.18. ***Marginal density of B***
Let $\Theta_{HBMi} = (b_S, \nu_S^*, b_U, \nu_U^*, \tilde{b}_S, \tilde{b}_U, \nu_B^*, \pi_{start,S}^*)$ be the parameter set of a HBMi with steady-state distribution $\tilde{\pi}^*$. The asymptotic marginal density of the background process B is given by

$$f_B(x) := \lim_{t\to\infty} f_{B_t}(x) = \tilde{\pi}_S^* \frac{1}{2b_S/\nu_S^*} \int_0^\infty \Phi_{\nu_B^* s, \sqrt{s}}(x) \left(1 - f^{IG}_{2b_S/\nu_S^*, \sqrt{2b_S/\nu_S^{*3}}}(s)\right) ds$$
$$+ \tilde{\pi}_U^* \frac{1}{2b_U/\nu_U^*} \int_0^\infty \Phi_{-\nu_B^* s, \sqrt{s}}(x) \left(1 - f^{IG}_{2b_U/\nu_U^*, \sqrt{2b_U/\nu_U^{*3}}}(s)\right) ds.$$

Proof: As we are asymptotically for $t \to \infty$ in the steady state, the perception process is with probability $\tilde{\pi}_S^*$ in the stable state and with probability $\tilde{\pi}_U^*$ in the unstable state. We use this and condition on the age of the current dominance time

$$\begin{aligned}
f_B(x) &= \lim_{t\to\infty} \mathbb{P}(Y_t = S) f_{B|Y_t=S}(x) + \lim_{t\to\infty} \mathbb{P}(Y_t = U) f_{B|Y_t=U}(x) \\
&= \lim_{t\to\infty} \mathbb{P}(Y_t = S) \int_0^\infty f_{B|Y=S,A=s}(x) f_{A|Y=S}(s) ds \\
&\quad + \lim_{t\to\infty} \mathbb{P}(Y_t = U) \int_0^\infty f_{B|Y=U,A=s}(x) f_{A|Y=U}(s) ds \\
&= \tilde{\pi}_S^* \int_0^\infty \Phi_{\nu_B^* s, \sqrt{s}}(x) \frac{\left(1 - f^{\text{IG}}_{2b_S/\nu_S^*, \sqrt{2b_S/\nu_S^{*3}}}(s)\right)}{2b_S/\nu_S^*} ds \\
&\quad + \tilde{\pi}_U^* \int_0^\infty \Phi_{-\nu_B^* s, \sqrt{s}}(x) \frac{\left(1 - f^{\text{IG}}_{2b_U/\nu_U^*, \sqrt{2b_U/\nu_U^{*3}}}(s)\right)}{2b_U/\nu_U^*} ds,
\end{aligned}$$

where we used Proposition 8.12 for the (asymptotic) density of the age and the property that the increments of the background process are normal distributed for a fixed s for the last equal sign. □

An exemplary marginal density of the background process is shown in Figure 13.9 using the parameters of subject C in Table 12.2. The theoretical density fits closely the empirical distribution (estimated in 1000 simulations), where the peak around zero is caused by the unstable state, and the rather flat distribution for larger x-values is due to $\tilde{b}_S$ being remarkably larger than $\tilde{b}_U$.

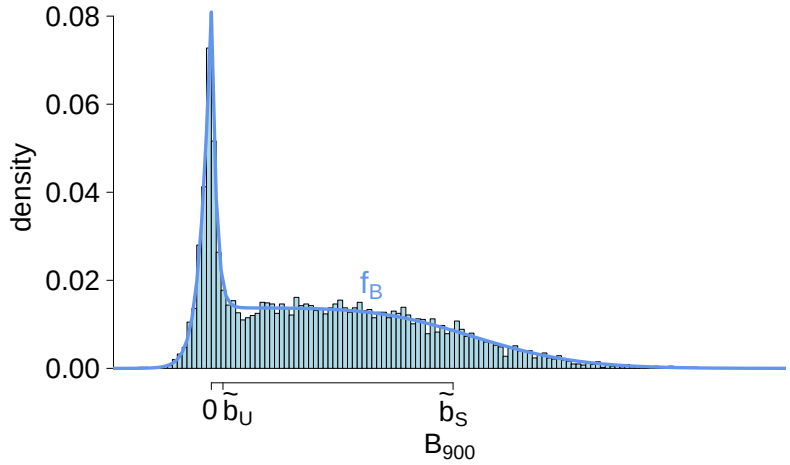

Figure 13.9: Comparison of the asymptotic marginal density $f_B(x)$ of B_t (blue line, Proposition 13.18) with an empirical histogram at $t = 900$ obtained from 1000 simulations. *The parameters are taken from parameter combination C in Table 12.2 (page 162).*

Chapter 14

Data analysis

In this chapter we apply the HMM and the HBM to the sample data set presented in Schmack et al. (2015) consisting of responses to continuous and intermittent stimulation obtained from each of 29 patients with schizophrenia and 32 healthy controls (Sections 14.1 and 14.2). As suggested in Schmack et al. (2015), missing responses during intermittent stimulation were replaced by their preceding responses because the reported percept typically persisted to the next available response. For both models we evaluate the model fit visually, perform model diagnostics and investigate group differences between the patients with schizophrenia and the control subjects. For the HMM for continuous presentation, we moreover show a reproducibility result, i.e., that the parameters μ and σ are highly correlated across subjects in two different recording sessions recorded by Schmack et al. (2013) (Section 14.1.5). Additionally, the advantage of the inverse Gaussian HMM compared to the Gamma HMM is analyzed (Section 14.1.3). All response patterns reported in Schmack et al. (2015) are visualized in Appendix A. In the last part of the chapter (Section 14.3), another data set (published in Weilnhammer et al., 2016) is presented, and the HBMc is fitted to this data set.

Statistical properties like the coefficient of variation of the dominance times or different correlation measures are often investigated in studies evaluating continuous stimulation with an ambiguous stimulus. Therefore, we analyze the response patterns during continuous presentation in Schmack et al. (2015) briefly with regard to the CV and correlation and compare the results to other studies. Moreover, we justify again the assumption of independent dominance times in the HMMc and the HBMc. While response patterns in the data set Schmack et al. (2015) were highly variable across subjects, the CV of dominance times (mean 0.79, SEM 0.04) was comparable as also reported in (Cao et al., 2016). Serial correlation of adjacent dominance times of the same percept was typically small (mean of Kendall's rank correlation $\bar{\tau} = 0.02$), and statistically significant on the 5% level in less than 7% of the cases, which is about chance level. Concerning long-term dependence (compare Pastukhov and Braun, 2011), deviations from the assumption of independent dominance times were not observed in 81% of the cases, and no differences were observed between the experimental groups ($p > .1$, Wilcoxon test). Long-term dependencies are analyzed using the Pearson correlation coefficient c_H between the dominance times and the cumulative history H as introduced in Pastukhov and Braun (2011). The history H is a function of the length and recency of previously dominated percepts. For each of the 57 subjects with at least five dominance times, c_H is estimated as explained in Pastukhov and Braun (2011). To assess statistical significance, 1000 data sets are obtained for each subject by permutation of the dominance

times to approximate the distribution of c_H under the null hypothesis of independent and identically distributed dominance times. Statistical significance on the 5% level is obtained by comparison of the empirical history c_H to the 95% quantile of the distribution of c_H derived from the permuted data sets. A correlation between the alternation rates in continuous and intermittent stimulation across subjects was not observed in either group, comparable to the results of Brascamp et al. (2009).

14.1 Hidden Markov Model

Here, we apply the Hidden Markov Model with IG distributed dominance times to the data set reported in Schmack et al. (2015). First, we investigate the goodness of fit visually (Section 14.1.1), then perform model diagnostics for the HMMi (Section 14.1.2) before showing that the IG HMM describes the data better than the HMM with Gamma-distributed dominance times (Section 14.1.3). In Section 14.1.4 we refine group differences between a group of patients with schizophrenia and a control group using the HMM parameters, and in Section 14.1.5 we show that the HMMc parameters of individuals across two different sessions are highly correlated (data from Schmack et al. (2013)).

14.1.1 Model fit

By fitting the HMM to response patterns in continuous and intermittent presentation as described in Section 9.3, the typical properties of the observed response patterns can be reproduced in simulations, including unimodal distributions for continuous presentation and changes between stable and unstable stages in intermittent presentation and a high variety of response patterns (Figure 14.1). For example, subject C shows rather regular stable phases, separated by unstable phases, while subject D shows an irregular response pattern, subject E shows only stable phases, while subject F shows almost only unstable phases. The parameter estimates of these example subjects are given in Tables 9.1 and 9.2. Note also that the response patterns of seven of the 61 subjects were described better by only one (stable or unstable) distribution than by the two-state HMM.
In addition to the good correspondence in the response patterns, no strong deviations could be observed from the model assumption of inverse Gaussian distributed dominance times (Figure 14.2).

14.1.2 Model diagnostics

The fitting procedure leaves the investigator with the estimated set of parameters $\hat{\Theta}_{\text{HMM}}$. Should we trust these parameters and thereby work with them for, e.g., comparison between parameter estimates or not? First of all, we recommend visual inspection of a number of simulated data with the same parameters (maybe ten) and comparison to the original data. In case the simulated data differ strongly from the original data because, e.g., unstable phases occur too often or the response pattern is too irregular, we recommend not working with the estimated parameters. Model diagnostics offer a more formal approach to answer the question if to trust the parameters.

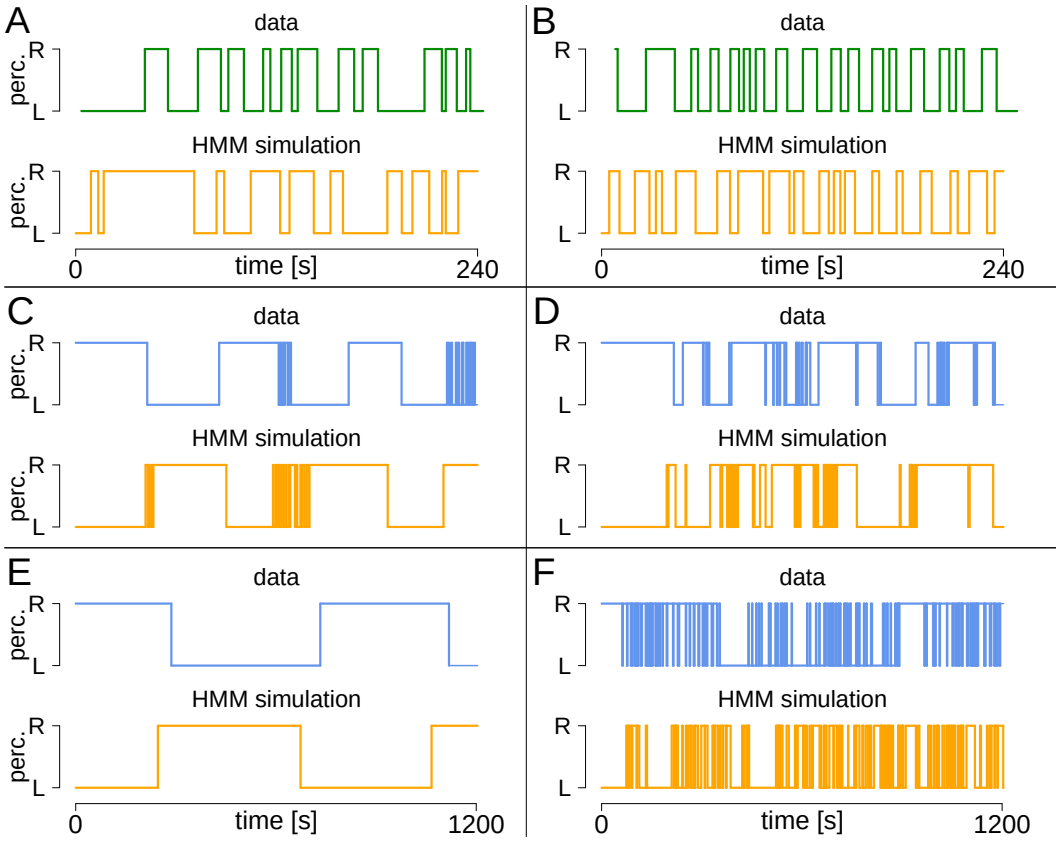

Figure 14.1: Comparison of empirical response patterns to patterns simulated with the HMM. *Examples of response patterns to continuous (green, A-B) and intermittent (blue, C-F) stimulation repeated from Figure 8.1 and corresponding simulations within the HMM (orange). The parameter estimates are given in Tables 9.1 and 9.2 (page 102), respectively.*

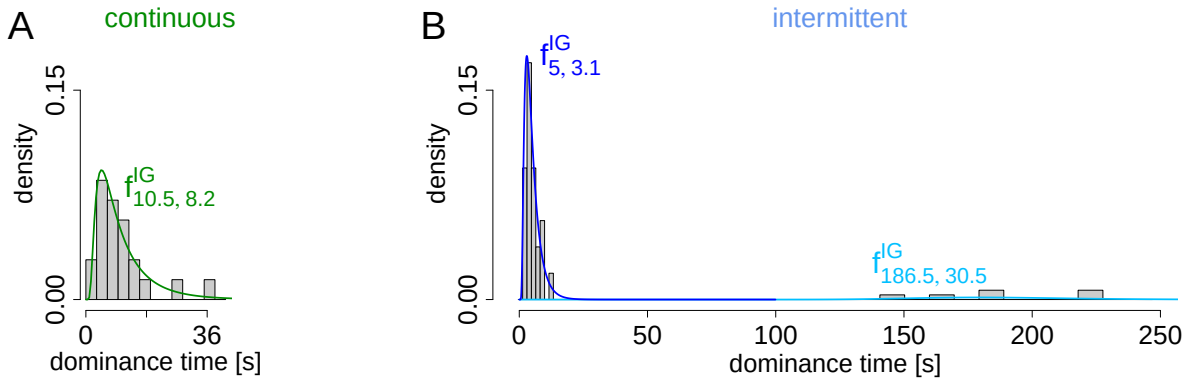

Figure 14.2: Comparison of distribution of dominance times with theoretical distribution. *The theoretical IG distribution in the HMM fitted to the empirical distribution of dominance times for continuous (A) and intermittent (B) presentation shown in Figure 14.1 A and C.*

In the literature several approaches for model diagnostics of HMMs are described. Here, we concentrate on the two-state HMM for intermittent presentation and focus on the idea of Altman (2004), who compares the empirical distribution function of dominance times $\hat{F}(y) = \sum_{i=1}^{n} \mathbb{1}_{d_i \leq y}/n$ with the parametric HMM estimate

$$F_{\Theta_{\text{HMM}}}(y) = \pi_S \cdot F_{S,\Theta_{\text{HMM}}}(y) + \pi_U \cdot F_{U,\Theta_{\text{HMM}}}(y),$$

where $F_{S,\Theta_{\text{HMM}}}(y)$ and $F_{U,\Theta_{\text{HMM}}}(y)$ describe the response distributions in the stable and the unstable state, respectively, and π_S, π_U are the weights of the stationary distribution (Corollary 10.8). If the model is specified correctly, a plot of $\hat{F}(y)$ against $F_{\Theta_{\text{HMM}}}(y)$ should be close to the main diagonal.
Figure 14.3 presents the comparison of the empirical and the model distribution functions for the four response patterns shown in Figure 9.1 panels C-F (page 70). For subjects A, B and D the fitting is satisfactory, especially when considering the small sample sizes in the data set. The response pattern of subject C only consists of three complete dominance times. Hence, the empirical distribution function only takes the values $0, 1/3, 2/3, 1$. As the model distribution function of an IG distribution is continuous, the comparison of the empirical and the model distribution function is difficult (panel C). For the majority of the subjects in the two data sets of Schmack et al. (2013, 2015) the empirical and the model distribution function agree closely (data not shown).

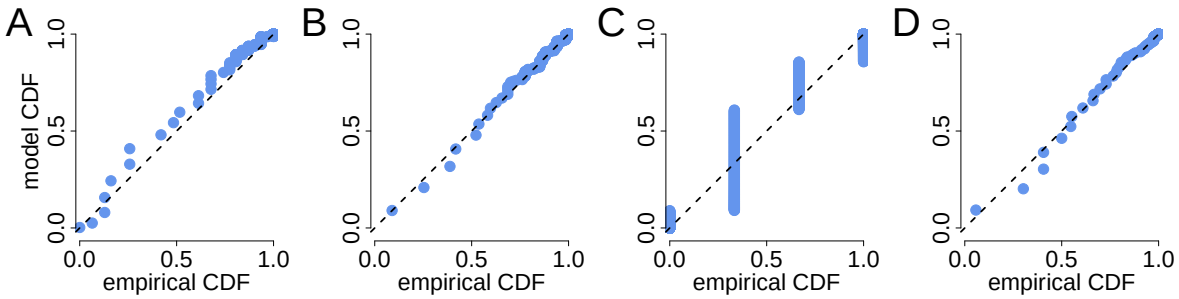

Figure 14.3: Comparison of the empirical with the HMM distribution functions. *The four exemplary response patterns shown in Figure 9.1 C-F (page 70) yield the HMM estimates of Table 9.2 (page 102) used here. Subject A here corresponds to panel C in the table and so on. Additionally, the main diagonal is plotted.*

Moreover, we briefly want to note that different types of tests exist to test the null hypothesis of a parameter set Θ_0 fitting to the data. The first type tests against the alternative of a parameter set Θ_1 describing the data and relies on the likelihood ratio for the two models (e.g., Giudici et al., 2000; Dannemann and Holzmann, 2008) where in our situation the distribution of the test statistic under the null hypothesis has to be simulated, or theoretical work is required. Such a test can be used to investigate the question if the estimated model for one subject may also explain the response data of another subject. Second, one may think of chi-square-type tests (Titman and Sharples, 2008) to test if Θ_0 describes the data well where the deviations of observations from their expectations are summed using chi-square statistics. Again, a simulation of the test statistic distribution would be necessary. Generally, one should keep in mind that more work is necessary to understand the different tests properly, that our sample sizes per subject possibly are too small for meaningful tests, and that tests should

always be carefully interpreted. Note that even if the HMM is not "correct" it maybe a valuable tool to approximate the data.
If the fitting procedure has not found a solution (i.e., no estimate satisfying the constraints A)-C) given on page 99 was found), the simulated data do not look convincing, or model diagnostics rather speak against the model, we should think about reasons and possible solutions:

- The model is not appropriate due to a completely discrepant structure of the data or due to non-stationarities. Thus, thinking about another model may be helpful.

- There are not enough events. This is an important issue given the small sample sizes analyzed in this thesis. However, increasing the recording length T is due to fatigue effects not always recommendable.

14.1.3 Comparison between Gamma and IG distribution

Throughout this thesis we have proposed to model the dominance times using the inverse Gaussian and not the Gamma distribution. To justify this, we compare in this subsection the fitting of these two distributions. First, we compare graphically the fitting of a Gamma and an inverse Gaussian distribution to exemplary dominance times distributions in continuous stimulation. In Figure 14.4 we note that the IG distribution visually fits the data slightly better than the Gamma distribution. To generalize this result, Figure 14.5 A shows the log-likelihoods of Gamma and inverse Gaussian distributions fitted to the dominance times during continuous stimulation in Schmack et al. (2015). In about 61% of the cases the IG model yielded a (slightly) larger log-likelihood than the model using Gamma-distributed dominance times, and in the other cases the Gamma-distribution yielded only slightly better results.

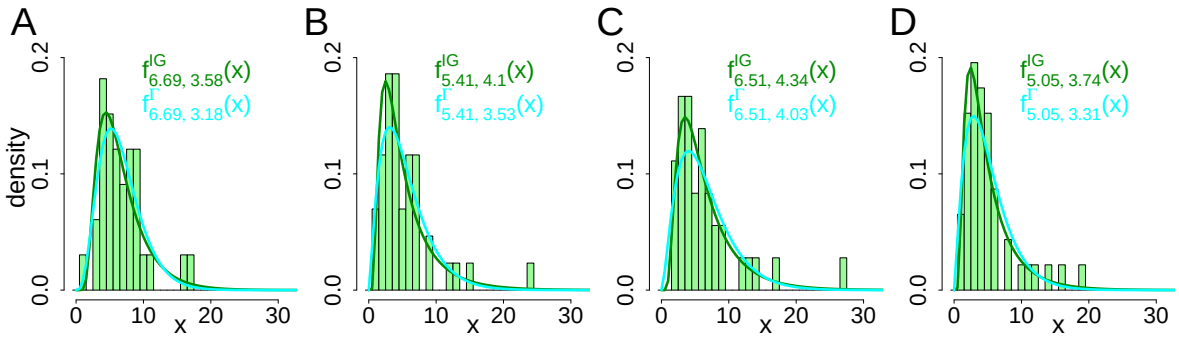

Figure 14.4: (A-D): Four examples of histograms of dominance times from Schmack et al. (2015) with densities of fitted Gamma (cyan) and inverse Gaussian distributions (green, both via maximum likelihood).

Comparing the two Hidden Markov Models for the response data to intermittent presentation note that except for two cases the model likelihood for all subjects is larger for the IG HMM than for the HMM with Gamma-distributed dominance times (shown in Figure 14.5 B).

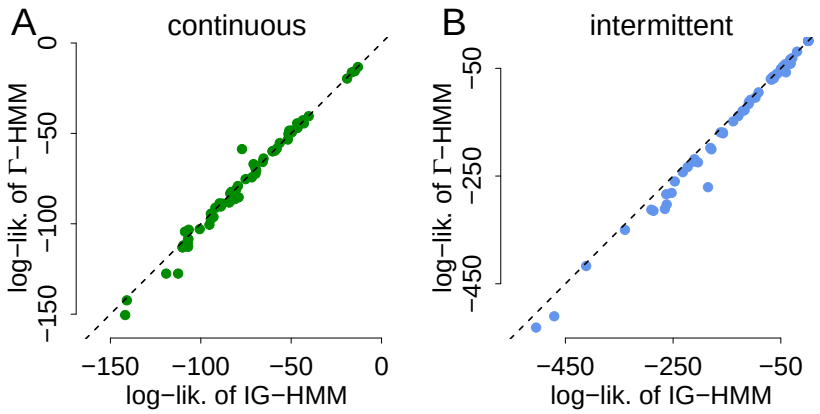

Figure 14.5: HMM log-likelihoods for the IG and the Gamma distribution. *(A) Comparison of the log-likelihoods of the inverse Gaussian- and the Gamma-HMM for continuous presentation. (B) Comparison of the log-likelihoods of the inverse Gaussian- and the Gamma-HMM for intermittent presentation. The main diagonal is added in both plots.*

14.1.4 Group differences

The HMM provides a relation between the underlying model parameters and the observed group differences reported in the introduction (Figure 8.2) and in Schmack et al. (2015). In the continuous case, the decreased alternation rate in the patients with schizophrenia is simply reflected in an increased mean dominance time $\hat{\mu}$ (Figure 14.6 A) in the one-state HMM. For intermittent presentation, we had observed an increased alternation rate in the patients with schizophrenia. The interpretation of this observation was not obvious due to the high variability of response patterns and particularly due to the fluctuation between stable and unstable state. The HMM provides a first explanation of this phenomenon by capturing important response properties in the parameter estimates, which showed the following group differences: In particular, the (expected) relative time spent in the stable state $\tilde{\pi}_S$, was higher in the control group (Figure 14.6 B, formula given in equation (10.2) in Section 10.2.2). As the main variable contributing to this difference, we observe that the probability $\hat{p}_{SS}$ to stay in the stable state was higher in healthy controls. In addition, the mean dominance time $\hat{\mu}_U$ in the unstable state was slightly larger in the patients with schizophrenia. The degree of statistical significance was highly similar to the one reported in Schmack et al. (2015) ($p < .1$ for $\hat{\mu}, \hat{\mu}_U, \hat{p}_{SS}$ and $\hat{\tilde{\pi}}_S$, two-sided Wilcoxon test).

Remark 14.1. ***Effect of direct maximization, censored dominance times, UMVU inspired estimation and the Gamma model***
The observed parameter differences also hold for the DNM estimation described in Section 9.4.2 and using the censored dominance times or the UMVU inspired approach. Moreover, using the same constraints concerning $\hat{\mu}_S$ and $\hat{\sigma}_S$ as for the HBMi (E) and F) on page 157) does not change the significance of results (but yields less reliable estimates as μ_U appears to be estimated too large). Using the assumption of Gamma instead of inverse Gaussian distributed dominance times also does not affect the estimated group differences considerably.

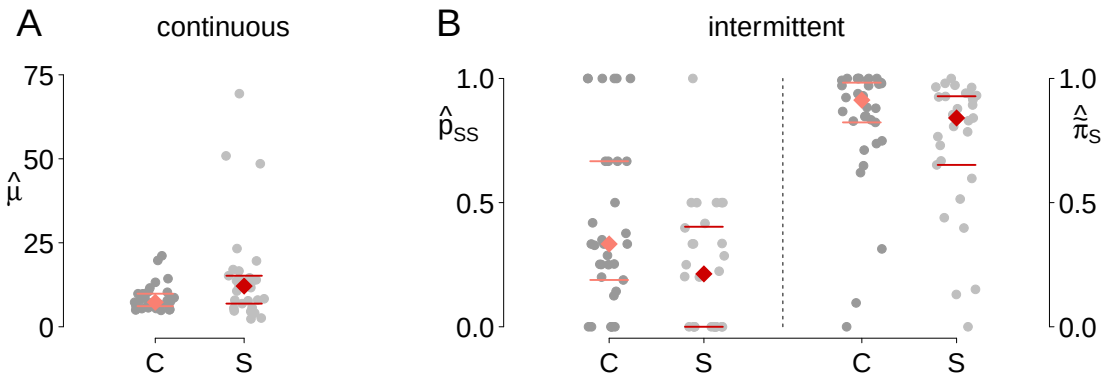

Figure 14.6: Differences in the HMM parameter estimates between subjects with schizophrenia and control subjects. *(A) $\hat{\mu}$ during continuous presentation and $\hat{p}_{SS}$ and $\hat{\tilde{\pi}}_S$ for intermittent presentation (B). Each gray dot indicates one individual participant's data, colored diamonds indicate medians, horizontal bars indicate 25%/75%-quantiles.*

14.1.5 Comparison of repeated trials

14.1.5.1 Results

The HMM approach also allows studying the reproducibility of response parameters of subjects across multiple sessions. Interestingly, the data set reported in Schmack et al. (2013) contains two separate sessions of continuous presentation for each of 105 healthy subjects (the first two training runs from Behavioral Experiment 2 as described in this previous work). These showed highly reproducible response patterns, i.e., a high correlation of parameter estimates of the IG distribution of the same individuals across different sessions (Figure 14.7). In addition, we also used a likelihood ratio test (Samanta, 1985, evaluated in the next subsection) to investigate for each subject the null hypothesis of equality of the parameters of two inverse Gaussian distributed samples with sample sizes n_1 and n_2, i.e., $H_0 : \mu_1 = \mu_2$ and $\sigma_1 = \sigma_2$. The likelihood ratio derives as

$$Q_n = \prod_{i=1}^{2} (n/n_i)^{n_i/2} \, (S_i/S)^{n_i/2},$$

with $S_i = \sum_{j=1}^{n_i} (d_{ij}^{-1} - \hat{\mu}_i^{-1})$ for $i = 1, 2$, $S_3 = n_1/\hat{\mu}_1 + n_2/\hat{\mu}_2 - n^2(n_1\hat{\mu}_1 + n_2\hat{\mu}_2)^{-1}$, $n = n_1 + n_2$ and $S = S_1 + S_2 + S_3$. Under H_0 the quantity $Q_n^* := -2(1 - 1/6[1/n_1 + 1/n_2] - 1/[12n]) \log Q_n$ is approximately chi-square distributed with two degrees of freedom. Thus, the test rejects the null hypothesis at level 5% if Q_n^* exceeds the 95%-th-quantile of the $\chi^2(2)$-distribution. In the sample data set, the likelihood ratio test did not reject the null hypothesis of equal parameter sets in 83 out of 105 subjects (about 79%). For a comparison, we performed 10000 permutations by randomly assigning a first trial of one subject to a second trial of another subject and performing the likelihood ratio tests on the permuted data sets. In the mean, the null hypothesis was not rejected in only about 36% of the randomly assigned pairs, with a maximum percentage across all permutations of 51%. The likelihood ratio test is evaluated in the next subsection concerning the dependence of the significance level and the test power on the sample sizes and the distribution parameters.

In summary, the response patterns of the same subject across multiple sessions showed a high degree of reproducibility, with a Pearson correlation coefficient of up to $r = 0.76$ between $\log(\mu_1)$ and $\log(\mu_2)$ (Figure 14.7). The similarity of response patterns for the same subject across multiple sessions was significantly higher than the similarity of response patterns between subjects.

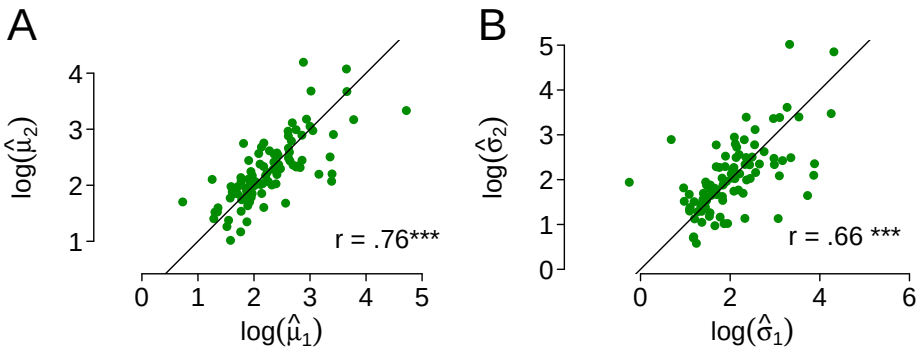

Figure 14.7: Reproducibility of response patterns. *Parameter estimates of* $\log(\mu)$ *(A) and* $\log(\sigma)$ *(B) of the IG distribution in two sessions with the same individuals, data set reported in Schmack et al. (2013). The logarithm was applied due to asymmetric distributions of the parameter estimates. Stars indicate highly significant* ($p < .0001$) *correlation of parameter estimates across different sessions.*

14.1.5.2 Evaluation of the likelihood ratio test by Samanta (1985)

The likelihood ratio test suggested by Samanta (1985) is an asymptotic test as the distribution of the test statistic Q_n^* is asymptotically chi-square. In the following, we investigate the empirical behavior of the test depending on the sample size $n_1 = n_2 = n$, the initial values μ_1, σ_1 and the factors of change $\mu_2/\mu_1, \sigma_2/\sigma_1$. For each sample size and parameter combination, we perform 1000 simulations consisting of n IG distributed random variables $X_1, X_2, \ldots, X_n$ with parameters μ_1, σ_1 and n IG distributed random variables $X_{n+1}, X_{n+2}, \ldots, X_{2n}$ with parameters μ_2, σ_2 and count how often the statistic Q_n^* exceeds for the random sample $X = (X_1, X_2, \ldots, X_{2n})$ the 95%-th-quantile of the $\chi^2(2)$-distribution, i.e., how often the null hypothesis is rejected. All sample sizes, parameter combinations and changes are shown in Figure 14.8. The parameters were chosen according to typical values in the data set Schmack et al. (2013).

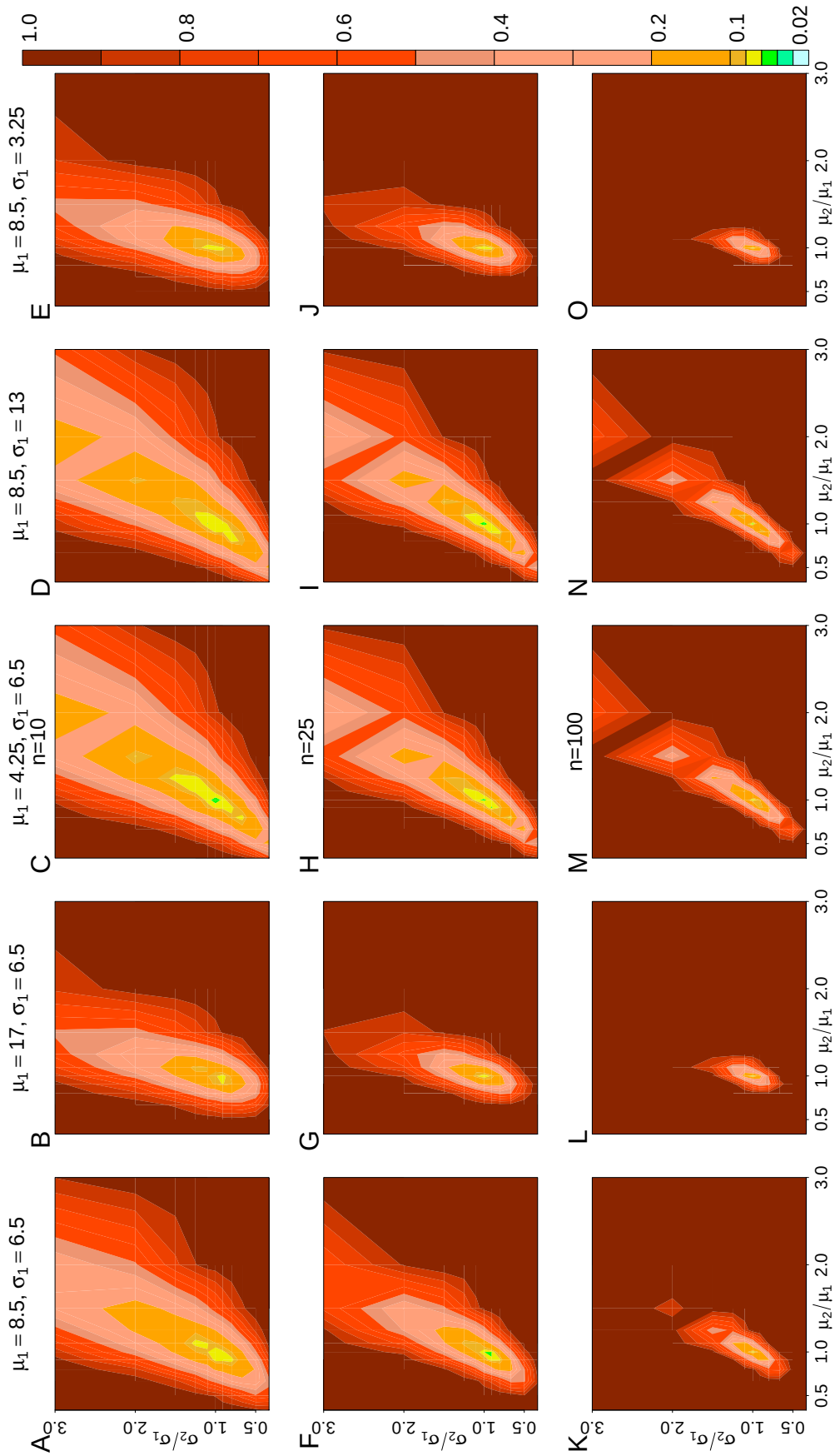
A
B
C
D
E
F
G
H
I
J
K
L
M
N
O
μ1 = 8.5, σ1 = 6.5
μ1 = 17, σ1 = 6.5
μ1 = 4.25, σ1 = 6.5
n=10
μ1 = 8.5, σ1 = 13
μ1 = 8.5, σ1 = 3.25
n=25
n=100
σ2/σ1
μ2/μ1
0.5
1.0
2.0
3.0
1.0
0.8
0.6
0.4
0.2
0.1
0.02

Figure 14.8: Simulated significance level and test power of the likelihood ratio test suggested by Samanta (1985) for different parameter combinations and magnitudes of changes in 1000 simulations. *In the first row (A-E) the sample size was $n = 10$, in the second row $n = 25$ (F-J) and in the third row $n = 100$ (K-O). The initial parameters were $(\mu_1, \sigma_1) \in \{(8.5, 6.5), (17, 6.5), (4.25, 6.5), (8.5, 13), (8.5, 3.25)\}$, where the initial values differ from column to column. The size of changes differs from $1/3$ to 3, where the point with no change neither in the mean nor in the variance shows the empirical significance level. The color coding is shown on the right.*

Four conclusions can be drawn from Figure 14.8:

- The empirical significance level (green/yellow points in Figure 14.8) ranges from $4.5-8.0\%$, mostly slightly above five percent.
- The test power increases with the sample size, which is a well-known effect in statistics.
- The test power increases with a decreasing CV$=\sigma/\mu$ as possibly a large irregularity overlaps the difference between the distributions.
- A change in the expectation μ is easier to detect than a change in the standard deviation σ (for instance, for $n = 25$ and $(\mu_1, \sigma_1) = (8.5, 6, 5)$ a change by the factor of 1.5 is detected with a probability of about 40 percent for σ and 94% for μ, see panel F) as changes in μ affect the mass of the distribution, and the standard deviation rather effects the tails. Hence, the parts of Figure 14.8 with smaller test power have an elliptic form.

To sum up, the likelihood ratio test of Samanta (1985) shows practical applicability also for rather small sample sizes ($n \approx 25$ as typical for the data Schmack et al. (2013)).

14.2 Hierarchical Brownian Model

Now, the Hierarchical Brownian Model is applied to the data set reported in Schmack et al. (2015). We start by assessing the goodness of fit visually (Section 14.2.1). Then, we perform model diagnostics for the HBMi (Section 14.2.2) before analyzing group differences in the HBM parameters between the patients and the controls in Section 14.2.3.

14.2.1 Model fit

Here, we use the parameter estimation described in Sections 12.1 and 12.2. Because the HBMc represents only a reparametrization of the one-state HMM, results are completely analogous for continuous presentation. Thus, a high variability of response patterns can be described with the two parametric distribution (see Figures 14.9 A and B), including also different means and variances of dominance times.
For intermittent presentation, the HBMi and the two-state HMM are similar, but also show a number of differences (see Section 14.1). As a first similarity to the two-state HMM, the HBMi can also describe and reproduce a high variety of response pattens (Figure 14.9 C-F). For example, these include highly regular stable states that may or may not be interrupted by short unstable phases (C,E) or response patterns with different degrees of regularity and different alternation rates (D, F). Note also that the response patterns to intermittent stimulation of six out of the 61 subjects were described better by the one-parametric HBMc as in these cases only long dominance times longer than 30 seconds occur (e.g., E).

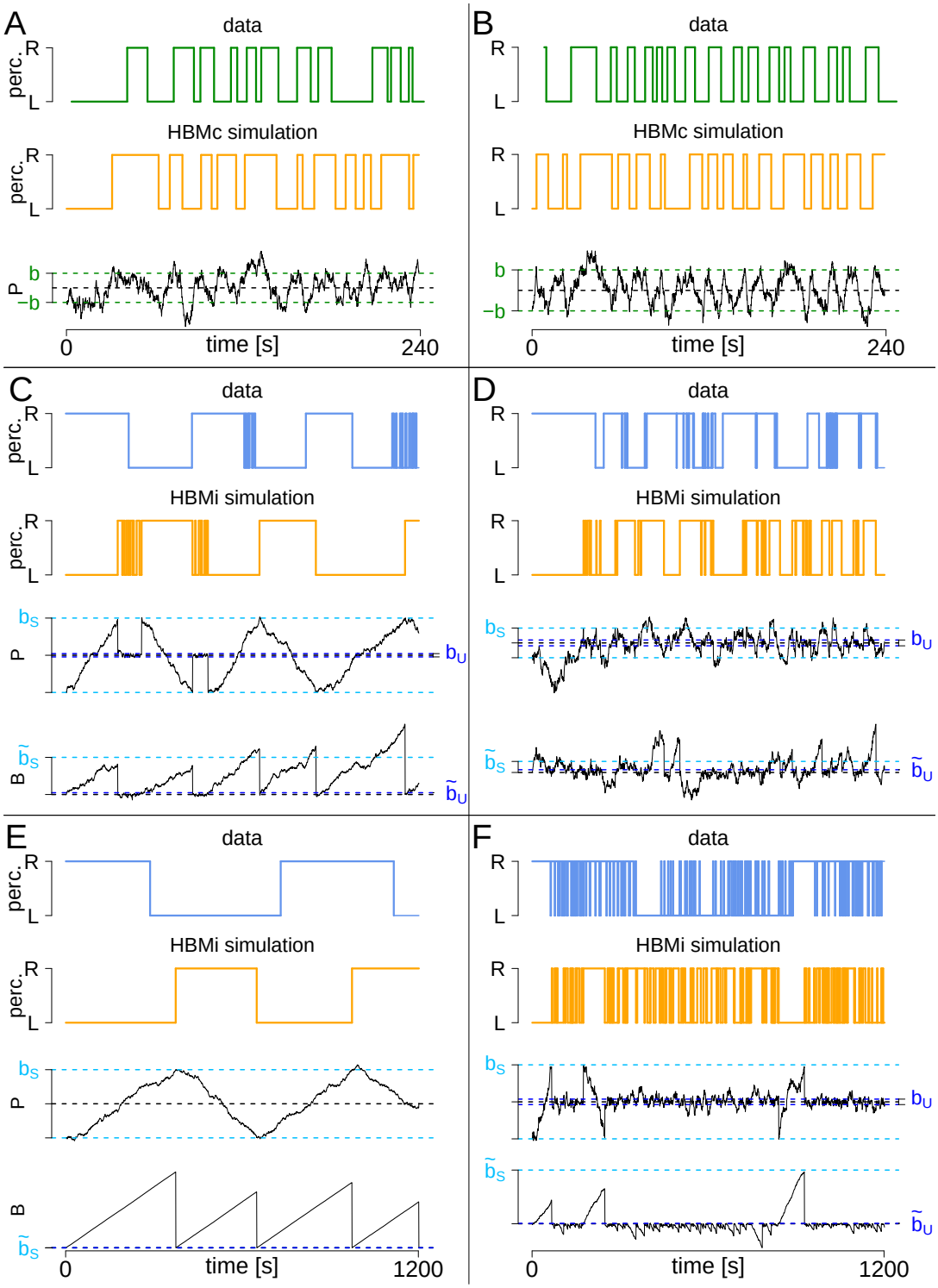
A
data
perc.
R
L
HBMc simulation
P
b
−b
0
time [s]
240
B
C
HBMi simulation
b_S
b_U
B
$\tilde{b}_S$
$\tilde{b}_U$
D
E
1200
F

Figure 14.9: Comparison of empirical response patterns to patterns simulated with the HBM. *Example empirical response patterns from Figure 8.1 and response patterns simulated by the HBM (orange). Responses to continuous and intermittent presentation are plotted in green and blue, respectively. The estimated parameters used for simulation are given in Tables 12.1 and 12.2 (page 162), respectively. (A) and (B) Continuous presentation and HBMc. (C)-(F) Intermittent presentation and HBMi. Below the orange response patterns, one can see the perception process P and (for the HBMi) the background process B corresponding to the respective simulation.*

In addition to the close description and reproduction of the patterns in the empirical data, one interesting additional aspect is captured by the HBMi, which cannot be described in the two-state HMM. As explained in Section 11.2.3, the probability of a transition from stable to unstable state decreases with the length of the dominance time in the HBMi. Indeed, the same observation can be made in the empirical data set, while this dependence cannot be captured within the HMM (Figure 14.11). Additionally, we show an example where a shorter stable dominance time before the state change is directly visible in both the data and the corresponding HBMi simulation and is printed on a yellow background (Figure 14.10).

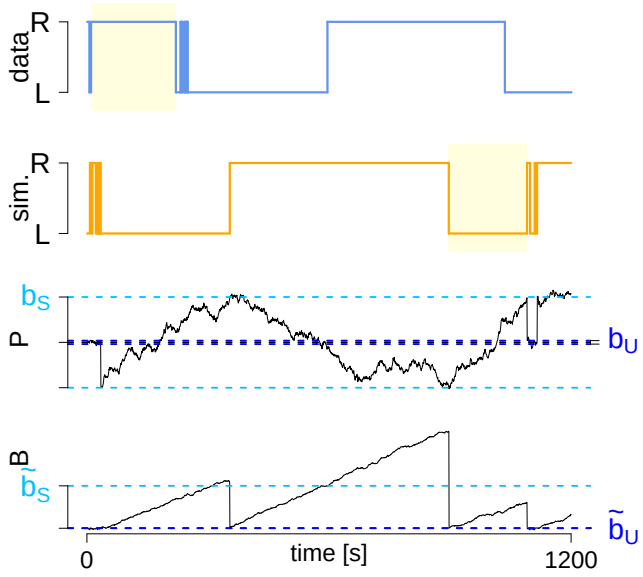

Figure 14.10: Example of a shorter dominance time before a state change from stable to unstable. *The shorter dominance time is printed on a yellow background and is visible in both the data (A) and the simulated response pattern of the HBMi (B) (using the estimated HBMi parameters from A).*

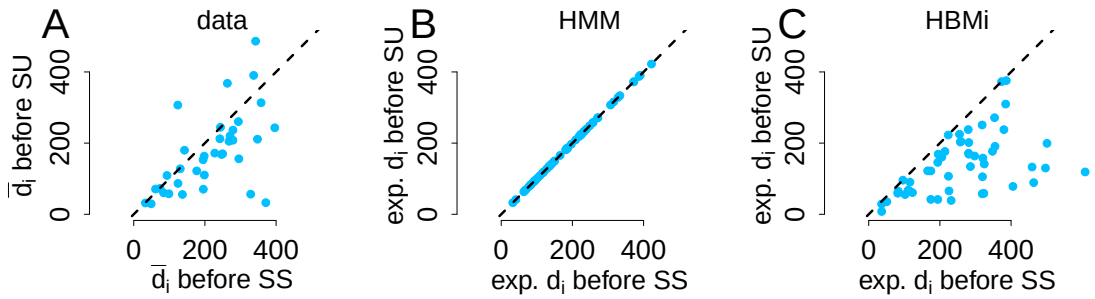

Figure 14.11: Mean dominance times in the stable state as a function of the successive state. *In the empirical data set, the mean dominance time before a state transition SU is shorter than the mean dominance time before SS (A). This observation can be reproduced in the HBMi (C), while the expected dominance time in the HMM (B) is equally long for intervals with and without transition, i.e., independent from transition between states. In the empirical data set (Schmack et al., 2015), the state transitions were estimated using the Viterbi paths (Section 12.5). Analogous results were obtained using a fixed threshold (All dominance times shorter than 15 seconds are classified as unstable and all dominance times larger than 45 seconds as stable. The other dominance times are classified as "no decision possible".) or the data set Schmack et al. (2013). For the HBMi, the expected dominance times were derived from the HBMi parameters according to Lemma 11.2. In the HMM, expected dominance times correspond to* $\hat{\mu}_S$.

14.2.2 Model diagnostics

As with the HMM the question of validity of the estimated parameter set arises. Again, we recommend comparing estimated and simulated data as well as the distribution functions using the approach of Altman (2004). For details see Section 14.1.2.
Figure 14.12 shows the comparison of the empirical and the HBMi distribution functions for the four response patterns shown in Figure 9.1 panels C-F (page 70). The same remarks as in Section 14.1.2 concerning the convincing fit for the three subjects A, B and D as well as for subject C with the small number of dominance times hold.

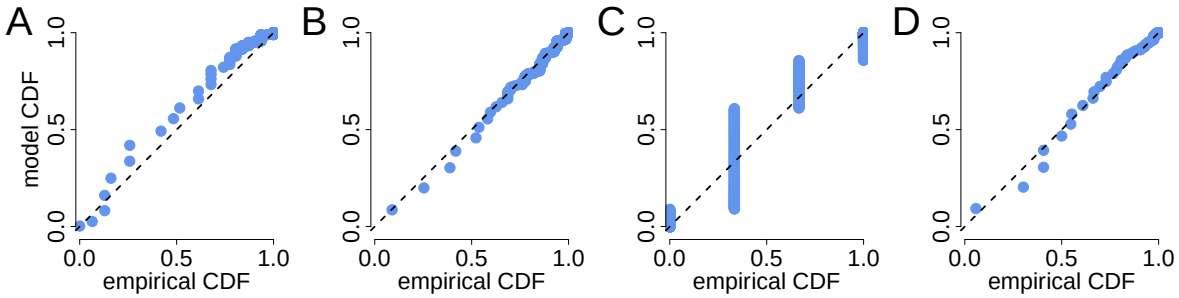

Figure 14.12: Comparison of the empirical and HBMi distribution functions. *The four exemplary response patterns shown in Figure 9.1 (page 70) yield in the HBMi estimates of Table 12.2 (page 162) used here. Panel A here corresponds to subject C in the table and so on. Additionally, the main diagonal is plotted.*

The same guidelines as on page 201 hold if the simulations or model diagnostics do not look convincing or no estimate satisfying the constraints A)-F) on page 157 has been found. Tests to check the model fit of an parameter set Θ_0 basing on the likelihood-ratio are conceivable as well as basing on chi-square statistics. However, we do not apply any test here.

14.2.3 Group differences

Due to the high correspondence of the HBMi response patterns with the empirical data and the neurophysiologically related parametrization, the HBMi provides potential additional links to underlying neuronal processes of the observed differences between control subjects and patients with schizophrenia in Schmack et al. (2015). Here, we consider three aspects related to continuous and intermittent stimulation and to the transition between these two conditions. First, concerning continuous stimulation, we note that the one-state-HMM with IG distributed dominance times and the HBMc yield identically distributed sequences of dominance times. Note that the mean dominance time $\hat{\mu}$ in the HMM (Figure 14.6A) therefore equals the corresponding value $2\hat{b}/\hat{\nu}_0$ in the HBMc. As a consequence, the results and interpretation were identical, i.e., the higher alternation rate of the control subjects during continuous presentation (Figure 8.2) was reflected in a smaller value of $2\hat{b}/\hat{\nu}_0$. When analyzing the individual parameters b and ν_0, we found no group differences in the drift ν_0, but a tendency for a larger neuronal pool b involved in sensory processing in the group of patients with schizophrenia (Figure. 14.13 A, $p < .1$, two-sided Wilcoxon test).

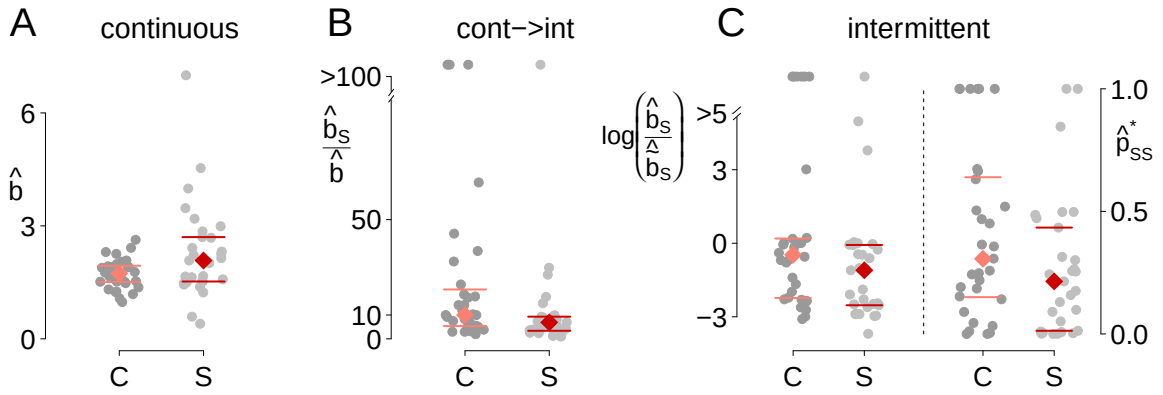

Figure 14.13: Group differences between patients with schizophrenia and control subjects in the HBM. *The HBMc parameter $\hat{b}$ (A) and the relation $\hat{b}/\hat{b}_S$ (B). (C): Differences in $\hat{b}_S/\hat{\tilde{b}}_S$ and $\hat{p}^*_{SS}$. The raw data together with the median (colored diamonds) and 25%- and 75%-quantiles are shown. All p-values of a two-sided Wilcoxon test were below .1. Recall that b can be interpreted as the size of the neuronal pool active during continuous presentation and b_S as the size of the neuronal pool being active in the stable state during intermittent presentation. $\tilde{b}_S$ is the border which the background process has to cross to remain stable.*

Second, regarding intermittent presentation, we focused on the derived parameters $(\mu^*_S, \sigma^*_S, \mu^*_U, \sigma^*_U, p^*_{SS}, p^*_{UU})$, which show correspondence to the HMM and good estimation properties, instead of testing the border and drift parameters individually. Similar to the HMM, we found an increased mean unstable dominance time in the group of patients with schizophrenia as compared to healthy controls. More importantly and also consistent with the HMM, we also found that patients with schizophrenia showed a decreased relative time

spent in S, $\tilde{\pi}_S^*$ ($p < .1$, two-sided Wilcoxon test, see eq. (13.10) in Section 13.2.2). Again, the probability p_{SS}^* to stay in the stable state seemed to be the main variable contributing to this difference, being significantly reduced in patients with schizophrenia (Figure. 14.13 C, $p < .1$, two-sided Wilcoxon test). In order to identify potential neurophysiological mechanisms underlying this group difference, we further investigated the components of p_{SS}^*. Noting that no difference was observed in the mean stable dominance time $\mu_S^* = 2b_S/\nu_S^*$ and in the relation ν_S^*/ν_B^* of the drift in stable state and the drift of the background process, one interesting parameter is $b_S/\tilde{b}_S$. Keeping all other parameters constant, an increase in this quantity means an increase in p_{SS}^* because the crossing of $\tilde{b}_S$ at the end of a stable dominance time, i.e., staying in the stable state, gets more likely. In the empirical data set, we found increased values of $b_S/\tilde{b}_S$ in the control group (Figure. 14.13 C, $p < .1$, two-sided Wilcoxon test). In terms of the potential neurophysiological interpretation, this would suggest an increased population size involved in stable perception processing as a potential main underlying mechanism.
Third, a similar observation resulted from the derived parameter b_S/b, which describes a transition of population sizes from continuous to intermittent stimulus processing. In the data set, we observed increased values of b_S/b for the control group (Figure 14.13 B) as compared to the group of patients with schizophrenia. Again, applying a potential neurophysiological interpretation, this would suggest that in the control group, the neuronal pool that is additionally recruited during intermittent presentation in stable states could be higher than in the group of patients with schizophrenia. Note that this result could not be obtained in the HMM, which does not explicitly describe a potential transition between continuous and intermittent presentation. However, note that this result should be interpreted carefully due to reduced estimation precision of the parameters $b_S/\tilde{b}_S$ and b_S/b.
In summary, this analysis of the HBM parameters suggests the following explanation for the observed phenomenon that the alternation rate of the perceived percepts is increased for patients with schizophrenia during intermittent stimulation, while being decreased during continuous stimulation. In general, the relative time spent in the unstable state was increased in patients with schizophrenia. According to the HBM, this was attributed to an increased probability of transition from the stable to the unstable state, which could be potentially related to a decreased recruitment of neurons in the stable state. More specifically, a larger neuronal pool is hypothesized to account for the increased stability, and we accordingly observe a smaller increase in the neuronal pool from continuous to intermittent stable presentation in the patients with schizophrenia, which is suggested by the HBM as a main mechanism for the observed group differences. This analysis of a potential underlying mechanism, explaining the observed group differences also in the transition from continuous to intermittent presentation, is a particular advantage of the HBM over the HMM, because the HBM provides mechanistic explanations and variables with potential neurophysiological interpretations.

Remark 14.2. ***Effect of the COBYLA algorithm, the censored dominance times and the constraints***
In this thesis, we also presented estimation approaches for the HBM using the COBYLA algorithm and using the censored last dominance times. The parameter differences found using the standard estimators above can also be observed for these other two estimation procedures. Moreover, omitting the constraints E) and F) (about μ_S^* and σ_S^*) for the HBMi on page 157 yields less reliable parameter estimates but also the same parameter differences observed when maximizing the likelihood under these constraints. Hence, the parameter differences are not due to an specific estimation procedure.

14.3 Dataset of Weilnhammer et al. (2016)

To show the applicability of our model, we fit the HBMc to another data set of responses to bistable stimulation presented in Weilnhammer et al. (2016). As the HMM for continuous presentation with IG distributed dominance times is directly comparable to the HBMc, one can alternatively fit the HMM.

Stimulus and data description

Lissajous figures (see, e.g., Figure 14.14) belong to the bistable stimuli as they are perceived as objects rotating in-depth and unpredictably changing their direction of rotation. They are generated by sinusoidally varying x- and y-values of 2D curves in the plane causing an increasing phase shift of the sinusoids (more details in Weilnhammer et al. (2016)).

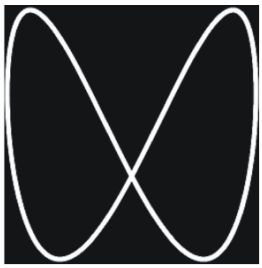

Figure 14.14: The intersection of two sinusoids with perpendicular axis and increasing phase-shift generates the Lissajous figure (from Weilnhammer et al., 2016, Creative Commons license).

Two factors (size and shifting frequency) of the Lissajous figure were varied in the aforementioned paper, resulting in four different conditions. In one run, each condition was presented for 80 seconds with five seconds of fixation in between and random order of conditions. All of the 18 participants completed 8-9 runs of the experiment. As the length of response patterns per run is thus very short, we focus on the overall distribution of dominance times per subject and/or per condition.

Data analysis and the HBMc model

The empirical dominance times show an one-peaked, right-skewed distribution resembling a Gamma or inverse Gaussian distribution. Our model can capture this kind of distribution, not only summed over all subjects, but also for the different conditions and the individual subjects as shown in Figures 14.16 and 14.17. In the figures the deviations between the simulated and the empirical histograms of dominance times are small. The HBMc moreover generates run response patterns closely matching the wide variety of empirical ones. In Figure 14.15 we present one example of an empirical response pattern during one run of 80 seconds duration and a simulated response pattern, closely fitting the true one.

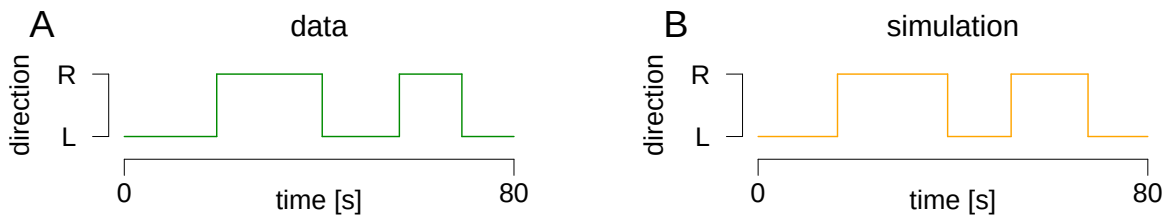

Figure 14.15: Comparison of an empirical (A) and a simulated (B) response pattern in one run of 80 seconds duration in the Lissajous experiment (Weilnhammer et al., 2016) and the HBMc, respectively.

We describe the parameter estimation briefly.

Parameter estimation

As each run only lasts 80 seconds, there is a number of runs where the perception does not change. Therefore, we treat these dominance times of length 80 as censored ones. The log-likelihood $\mathcal{L}$, which has to be maximized to estimate the HBMc model, is for the data $d = (d_1, \ldots, d_n)$ thus given by

$$\mathcal{L} = \sum_{i=1}^{n} \frac{1}{2} \log\left(\frac{4b^2}{\pi d_i}\right) \mathbb{1}_{d_i \leq 80} - \sum_{i=1}^{n} \frac{\nu_0^2}{2} \frac{(d_i - 2b/\nu_0)^2}{d_i} \mathbb{1}_{d_i \leq 80} + \sum_{i=1}^{n} \mathbb{1}_{d_i > 80} \log\left(1 - F^{IG}_{2b/\nu_0, \sqrt{2b/\nu_0^3}}(80)\right).$$

To maximize the latter display w.r.t. b and ν_0 the `nlm()`-command can be used with the moment estimates of b and ν_0 (Section 12.1.3, based only on the not-censored dominance times) as initial values.

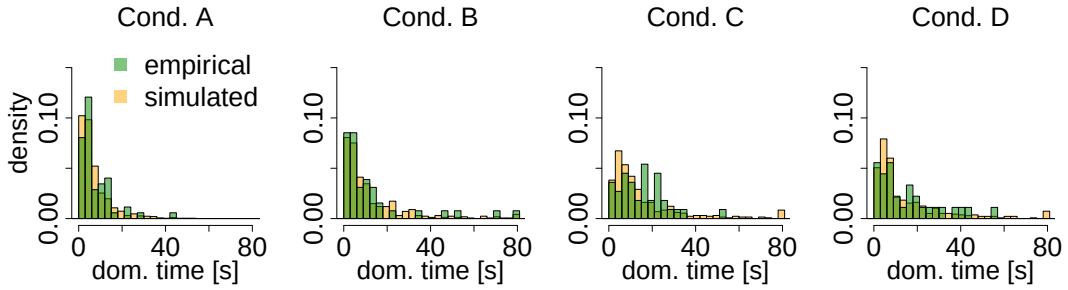

Figure 14.16: Comparison of the overall empirical distribution of dominance times in (Weilnhammer et al., 2016) and the simulated one in the HBMc for the four conditions for subject 1. *Parameters are fitted to the four conditions separately using all runs in the respective condition. 10000 runs were simulated for each condition.*

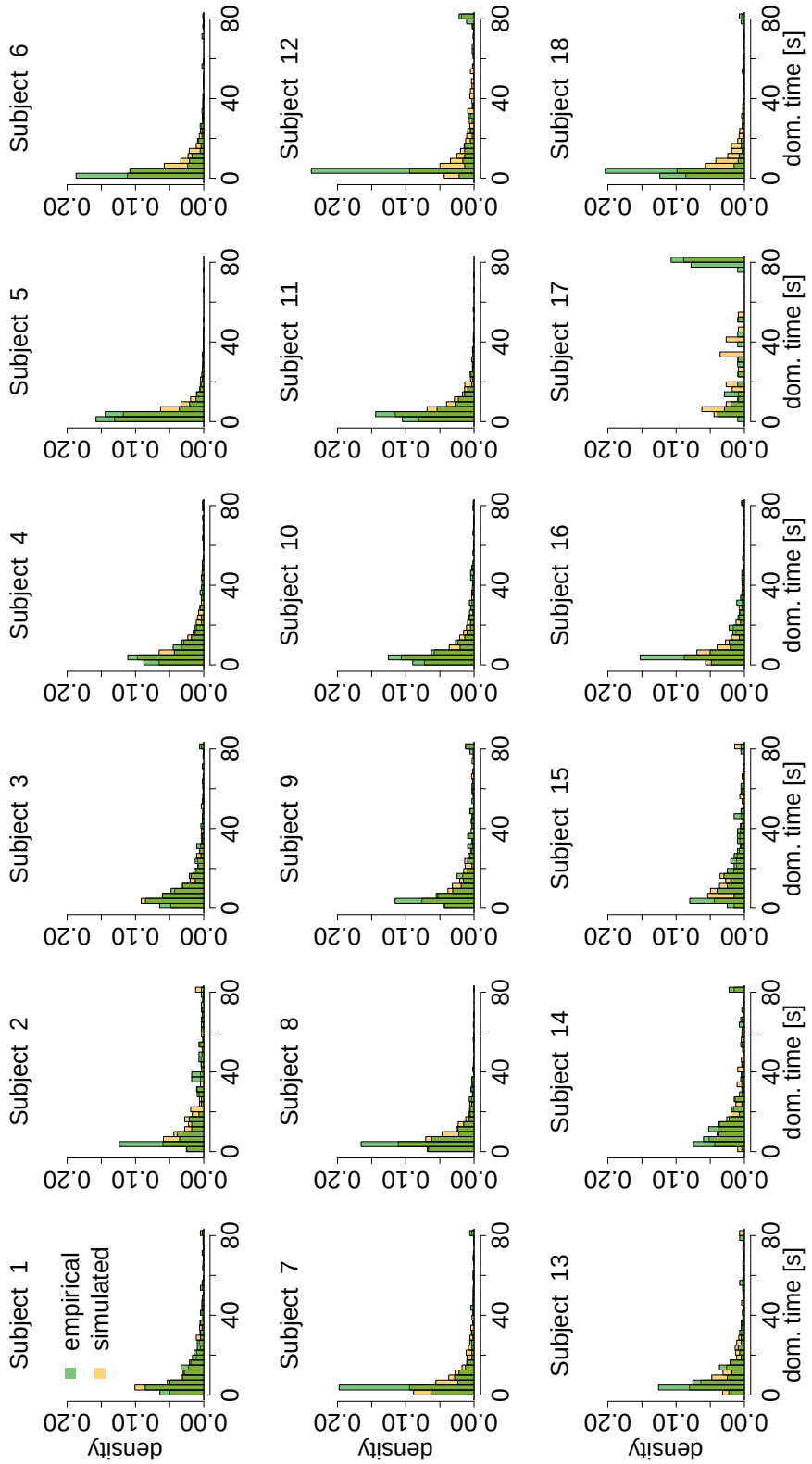

Figure 14.17: Comparison of the overall empirical distribution of dominance times in (Weilnhammer et al., 2016) and the simulated one in the HBMc for each of the 18 subjects. *Here, conditions and runs are not distinguished when fitting the parameters to the data of each subject. 10000 runs were simulated for each subject.*

Chapter 15

Summary and Discussion

In Section 15.1 a summary and discussion of this second part of the thesis is given (where we also relate our findings to other results in schizophrenia research), and in Section 15.2 the applicability of the HBMi as well as possible model extensions are discussed.

15.1 Summary and implications

In this part we have proposed a model framework for the description and analysis of perceptual responses to bistable stimuli. In particular, one aim was to describe a high number of observed patterns in responses to continuous and intermittent stimulation and the change in variability between the presentation types. The variety of patterns includes more or less regular dominance times during continuous stimulation and a switching between long and short dominance times, i.e., stable and unstable states, during intermittent stimulation, with a tendency for periodically occurring percept changes.
We started on a descriptive level, assuming that dominance times were generated by a simple HMM with only one state for continuous presentation and a stable and an unstable state in intermittent presentation. The HMM was sufficiently small to allow model fit to short empirical data sets (our third goal mentioned in the introduction on page 55) and could also describe the high variety of empirically observed response patterns in continuous and intermittent presentation (the first goal). Interestingly, it also revealed a high degree of reproducibility of response patterns of the same subject across different sessions. In addition, it allowed to relate observed group differences in the rate of percept alternations to HMM parameters, suggesting that especially the relative time spent in the stable state was reduced in the patients with schizophrenia. Mathematically, we derived for the first time the estimators for the HMM parameters in the framework of the Baum-Welch algorithm for inverse Gaussian distributed emissions.
Our second goal was to relate the observed response patterns and group differences to potential underlying mechanisms and thus, to build a link to models with detailed neurophysiological assumptions (Moreno-Bote et al., 2007; Brascamp et al., 2009; Gigante et al., 2009; Braun and Mattia, 2010; Pastukhov et al., 2013) that may not include all types or response patterns and/or may not allow fitting to short data sets. To that end, we proposed a hierarchical model of interacting Brownian motions (HBM). The HBM is based on the common assumption that the sequence of percept changes results from a competition of conflicting neuronal populations (Laing and Chow, 2002; Wilson, 2007; Brascamp et al., 2009; Gigante et al., 2009; Pastukhov

et al., 2013). Instead of modeling these in detail, we describe the activity difference by a Brownian motion P with drift ν_0 (Cao et al., 2016) between two borders $\pm b$, where the first hitting times of the borders indicate percept changes. These hitting times are inverse Gaussian distributed. Roughly speaking, the drift ν_0 could be considered related to the neuronal interactions within and between the populations, while the border b could be considered related to the population sizes. In order to describe responses to intermittent presentation, this mechanism is adapted in another population pair. These populations exhibit a corresponding background process B that evokes switching between stable and unstable states, similar to switching between the two percepts. In particular, B causes the perception process P to change parameters from small drift ν_S and large border b_S in the stable state to fast drift ν_U and small border b_U in the unstable state.
The HBM parameters can be related to the parameters of the HMM with inverse Gaussian distributed emissions. For the continuous presentation this is just a reparametrization, where for the HBMi the relation is not as straightforward. However, the models are highly similar in the sense that one subset of parameters describes the distributions of long and short dominance times and the other subset describes the transition probabilities between the hidden states. An important difference is that in the HBM the transition probabilities depend on the length of the current dominance time.
In addition, we derived properties of the point process induced by the perceptual changes of the HBMi including first-hitting times, distribution of the number of perceptual changes and stationarity properties. Most important, the expected relative time in the stable state was computed.
The HBM could be fitted nicely to the given empirical data set (i.e., fulfills the third goal), reproducing a high variety of response patterns to continuous and intermittent stimulation in healthy subjects and patients with schizophrenia (the first goal). The estimation for the HBMc applies maximum likelihood, and for the HBMi numerical maximization of the likelihood expressed in terms of forward variables is used. In particular, the model fit was improved over the descriptive HMM by reproducing shorter stable dominance times before a change to the unstable state. The HBM also provided more detailed explanations for the observed group difference that patients with schizophrenia showed higher alternation rates during intermittent stimulation, while percept alternation was decreased during continuous presentation. In particular, the HBM contains additional mechanisms of switching between stable and unstable state for intermittent presentation, which is assumed inactive during continuous presentation. The HBM, similar to the HMM, suggests an increased probability of switching to the unstable state for the patients with schizophrenia and thus, a longer relative time spent in the unstable state. The HBM also provides additional potential explanations related to the borders, or assumed population sizes, suggesting a higher increase from continuous (border b) to stable intermittent presentation (border b_S) in the healthy subjects. This is a first finding on the transition from continuous to intermittent presentation, which results from including both continuous and intermittent presentation in one model.

Connection to findings about schizophrenia These findings suggested by the HBM, which include a longer relative time spent in the unstable state for the patients with schizophrenia and a smaller population size involved in percept stabilization, are also in agreement with recent findings of Stuke et al. (2017). They studied the learning behavior of healthy subjects of whom the degree of delusional ideation (Peters et al., 1999) had been measured.

In compliance with earlier studies (for a review see Fletcher and Frith, 2009), they reported that subjects with larger delusion proneness made decisions on the basis of less information and were also less resilient against irrelevant information (compare also the literature about jumping to conclusions, e.g., Evans et al., 2015; Ross et al., 2015). In the present setting, the ambiguous stimulus represents a constant source of partly contradicting visual information (see also Hohwy et al., 2008; Weilnhammer et al., 2017). In that sense, the unstable state could be considered a state in which one is less resilient against this contradicting visual information, which yields a high rate of percept changes. The fact that the patients with schizophrenia spent more time in the unstable state is therefore highly consistent with the findings of Stuke et al. (2017). Moreover, this finding is also compatible with current models of schizophrenia in the framework of predictive coding (Adams et al., 2013) that propose a reduced top-down influence of stored predictions. However, it goes beyond previous work by highlighting the role of a background process that controls the balance between stable and unstable states in perceptual inference. In addition, the population sizes could be considered related to the amount of information taken into consideration to create a percept. Again, consistently with Stuke et al. (2017), we find, in the stable state, larger estimated population sizes, b_S, of the perceptual populations L and R in healthy controls than in patients with schizophrenia. Also, these population sizes are typically much larger than the population sizes in the unstable state ($b_S >> b_U$), which would be consistent with the notion that subjects in the unstable state need less information to change their perception.

15.2 Applicability and model extensions

The HBM may also be used to describe dominance times resulting from other experiments with ambiguous visual stimuli studying, e.g., motion-induced-blindness, binocular rivalry, moving plaids, the Necker Cube, orthogonal gratings or the house/face-paradoxon (e.g., van Ee, 2005; Cao et al., 2016) or also bistable auditory stimuli (Rankin et al., 2015). The HBM is, however, not designed for tristable stimuli, and transient stimulus manipulations as used in after-effect studies cannot be captured by the HBM in its current form. In different bistable settings, the HBM cannot be applied directly, but would allow for potential extensions. For example, in its present form, the HBM describes only balanced perception. However, it could be extended with respect to unbalanced bistable displays, e.g., for different eye contrasts during binocular rivalry (Brascamp et al., 2006), by choosing different drift parameters for the positive and the negative drift direction during presentation. Similarly, the drift could be chosen to vary as a function of attention (Pastukhov and Braun, 2007; Dieter et al., 2016) or as a function of long-term history (e.g., the cumulative history H proposed in Pastukhov and Braun (2011)). In studies on mixed perception during binocular rivalry (Gershman et al., 2012), one might use an additional border to define an intermediate range for the perception process in which mixed perception is described.
Possibly, the HBM could be connected to fMRI measurements. However, as the perception and the background process are assumed to represent differences in neuronal activities and as we only know their values at the time of perceptual changes, this connection might be a challenging task.
One should note that the HBMi in its current form is restricted to a duration of blank displays $l_b \leq l_p \cdot \nu_0/\nu_S$. For longer blank displays, the mean drift of P during stable states, ν_S^*, will be negative, yielding no perception change with high probability. However, it would be possible

to extend the model accordingly, assuming a temporal evolution in the drift parameters, given corresponding extended empirical observations. In addition, note that the border of the perception process is assumed to be b during continuous stimulation and b_S (or b_U) during intermittent stimulation. Therefore, an instantaneous change of intermittent to continuous presentation is not yet described. Here, we qualitatively assume that the border jumps very fast from b to b_S with the onset of a blank display, while going back slowly during stimulation. A transition from continuous to intermittent presentation would therefore instantly change the response pattern, while a reverse transition would gradually reverse the change back to the one-state process. Quantitative validation and fitting of this assumption would be interesting, but requires corresponding empirical observations, in which the length of the presentation period l_p is varied. This would also allow investigation of potential relations between the HBMc and HBMi parameters and thus, between the mechanisms assumed to underlie the identified group differences.

Concerning the impact of the duration of the blank display l_b, two aspects should be discussed. First, the HBM can theoretically reproduce a phenomenon reported earlier in Brascamp et al. (2009). Conditional that one percept has been present for a short while, the probability of a percept change rises with the blank duration l_b. In the HBMi, the same is observed during the unstable state with typically short dominance times: During the unstable state the drift in the blank displays, ν_U, is typically larger than the drift ν_0 during stimulation. Therefore, longer blank displays speed up P, thereby reducing perceptual stability.

Second, one interesting potential model extension is concerned with the relationship between the length of the blank display and the alternation rate. As reported earlier by Leopold et al. (2002); Brascamp et al. (2009); Gigante et al. (2009), the mean dominance time in intermittent presentation has been found to be a function of the relationship between the presentation length l_p (or "ON"-period) and the length of the blank display l_b (or "OFF"-period). Particularly, the dependence between l_b and the alternation rate is non-monotonic, as would be implied in the HBMi, but follows an inverted U-shape (Orbach et al., 1963; Kornmeier and Bach, 2004; Pastukhov and Braun, 2013) with a peak roughly at 0.4 s. Such an inverted U-shape would be possible in a model extension of the HBMi. As discussed in Section 11.2.1, the drift terms ν_S, ν_U only represent the mean drift across the period of blank display, which is sufficient and parsimonious in the given data set with fixed length of blank display. However, the model would be fully consistent with the assumption that the drifts change during the "OFF"-period, such that the mean drifts $\nu_S(l_b)$ and $\nu_U(l_b)$ are functions of the length of the blank display l_b. In Figure 15.1 A these mean drifts ν_S, ν_U decrease with l_b, where the stronger drifts at the beginning of the blank display could be effects of the recent stimulation. Panel B shows the resulting mean alternation rate, which has an inverted U-shape with a maximum around 0.4 s and shows increased stability under intermittent stimulation for $l_b > 0.7$. This increased stability is caused first by a small drift $\nu_S < \nu_0$ in that range. Second, it is also caused by the fact that the time interval l_b in which the background process B has positive drift is longer, leading to an increased probability to reach $\tilde{b}_S$ and thus, to stay in the stable state. Estimation of the functions $\nu_S(l_b)$ and $\nu_U(l_b)$ from a suitable data set with variable lengths of blank displays would be an interesting task.

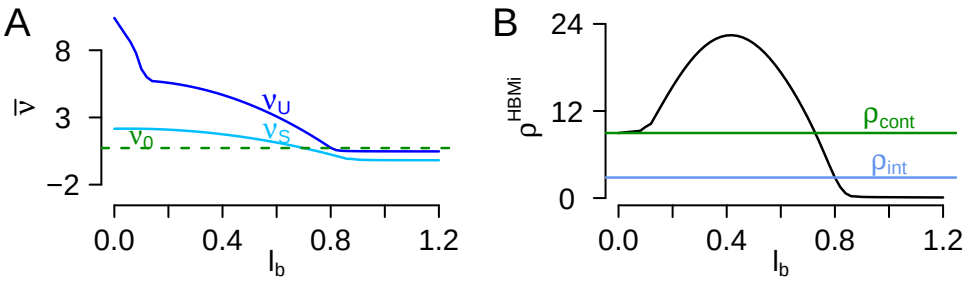

Figure 15.1: HBMi extension for different lengths of blank display. *Parameters derived for subject B and C in Tables 12.1 and 12.2, which is the same subject during continuous and intermittent presentation. (A) The mean drifts ν_S, ν_U decrease with the length of the blank display l_b. (B) The resulting mean alternation rate ρ^{HBMi} under intermittent stimulation (black) is derived using formula* (13.12) *(Section 13.2.3). Therefore, for each length of blank display l_b and the value of ν_S, ν_U as shown in panel A the mean drifts per second in the stable and the unstable state ν_S^*, ν_U^* and the mean drift of the background process ν_B^* are derived using equation* (11.2)*. The empirical mean alternation rates per minute of the subject during intermittent viewing with $l_b = 0.8$ and during continuous viewing are marked by blue and green lines, respectively.*

In summary, the proposed HBM intends to provide a link between empirical data analysis and mechanistic modeling. On the one hand, it aims at precisely describing the high variety of response patterns observed in perceptual responses to bistable stimuli. On the other hand, it aims at bridging the gap to detailed mechanistic models of bistable perception, allowing assumed processes to be fitted to short empirical data sets and thus, also the analysis of group differences. Various extension possibilities show a potential of the HBM to investigate related experimental contexts. By including both continuous and intermittent stimulation, the HBM can thus provide interesting new hypotheses on potential neuronal mechanisms of cognitive phenomena.

Chapter 16

Overall summary

The present thesis handles the description and analysis of point processes occurring in neuroscience, with a focus on the description and detection of different kinds of variability changes. It consists of two parts. In the first part, an existing method (MFT) for the test of rate homogeneity and the detection of rate change points in renewal processes was extended to the test of variance homogeneity of the life times and the detection of variance change points. The approach allows for the rate given by a step function, is non-parametric and can detect change points in multiple time scales. Under the null hypothesis of variance homogeneity limit processes for the corresponding filtered derivative process (which compares the estimated variances in two adjacent sliding windows) were derived which are called L in the case of rate homogeneity and $\widetilde{L}$ in the case of one rate change point. The two processes are both unit-variance centered Gaussian processes and differ only in the covariance structure around the rate change point, but in contrast to $\widetilde{L}$ the process L is independent of unknown process parameters. Hence, the rejection threshold is derived from L also with rate change points being present (as supported by simulation results). The necessity of estimating the rates before and including the rate change points in the procedure was explained. Simulations have shown that the procedure keeps the asymptotic significance level and that the detection probability of variance change points is considerably high. In an analysis of neuronal spike trains, several rate and variance change points were estimated.

In the second part of the thesis, response patterns to continuous and intermittent presentation of a bistable stimulus were modeled. Especially the difference between the unimodal distribution of dominance times during continuous presentation and the bimodal distribution during intermittent presentation, which can also be interpreted as change in variability, was of interest. First, a descriptive Hidden Markov Model with one or two hidden states was applied. Using the HMM the data set could be described nicely applying maximum likelihood estimation, and moreover, group differences observed in the response patterns of a healthy control group and a group of patients with schizophrenia could be refined. Second, a hierarchical Brownian model was used to allow for neuronal correlates. In this model perception arises from the competition between two conflicting neuronal populations. The activity difference between these groups of neuronal populations is modeled as Brownian motion with drift which fluctuates between two borders, where every first hitting time of a border implies a perceptual change and a change of the sign of the drift. For the intermittent presentation a second layer with competing populations encoding a stable and an unstable state is assumed. The model is estimated via the maximum likelihood method which also is applicable to the short data sets available from

experiments. Data are fitted closely and again the difference between the group of patients with schizophrenia and the group of controls is mainly explained by the patients spending less time in the stable state. The Viterbi algorithm allows estimating the points in time where the hidden regime changes from stable to unstable or vice versa. To conclude, the HBM connects precise data description and mechanistic models.

In summary, this work presented two approaches for dealing with point processes with different kinds of variability changes emerging in neuroscience. First, a widely applicable technique to detect change points in the first two moments of a point process was discussed, and second, a model linking empirical data analysis and mechanistic modeling for response patterns to bistable stimuli was presented. Thus, variance changes in point processes with a large number of events such as neuronal spike trains can be detected, and differences in the variability between short empirical point processes like response patterns can be described using the approaches developed in this thesis. To conclude, on the one hand, the thesis provides techniques that can be helpful for signal detection and as a preprocessing step for statistical analyses being sensitive to deviations from rate or variance stationarity. On the other hand, it introduces a mechanistic stochastic model closely describing the variability in response patterns to both continuous and intermittent stimulation by an ambiguous stimulus and thereby offers interesting new insights into potential neuronal mechanisms of visual perception.

Appendix A

The sample data set Schmack et al. (2015)

The main data set analyzed in Part II of this thesis was partly published in Schmack et al. (2015). The ambiguous stimulus (Figure 8.3) was presented continuously and intermittently to 61 subjects, where 29 were patients with schizophrenia and the other 32 a healthy control group. During intermittent presentation a presentation period of 0.6 seconds interchanged with a blank display period of 0.8 second (compare also Section 8.1 for a description of the experimental setup). As discussed, the response patterns to both continuous and intermittent stimulation vary widely between the subjects and groups. To give an overview, we show in Figure A.1 the response patterns to continuous presentation for all subjects and in Figure A.2 the response patterns to intermittent presentation. Note that the perception at the beginning of the experiment during continuous viewing is not known (as long as the subject does not press one button), and therefore the perception in Figure A.1 starts always at some time $t > 0$. The continuous data consist of the points in time a button was pressed and the button that was pressed. The intermittent data contain the times of stimulus onsets, the times where the stimuli were answered (if they were answered) and the button that was pressed. In the heading of each graph in Figures A.1 and A.2 we indicate if the subject belongs to the group of patients with schizophrenia or the control group. 68 subjects participated in the experiment but for different reasons only the data of 61 subjects were analyzed. Thus, some subject numbers are missing in Figures A.1 and A.2 (as Subject 3, Subject 6, etc.).
During continuous presentation the control group had more perceptual reversals, whereas during intermittent presentation the reverse holds true (Figure 8.2). Especially, the relative time spent in the stable state was significantly higher for the control group (Figures 14.6 and 14.13 for the HMM and the HBMi, respectively), which is also visible when comparing the response patterns of the two groups per eye (more long dominance times for the control group). The correlation between the alternation rates in continuous and intermittent stimulation across subjects was not significant in either group.

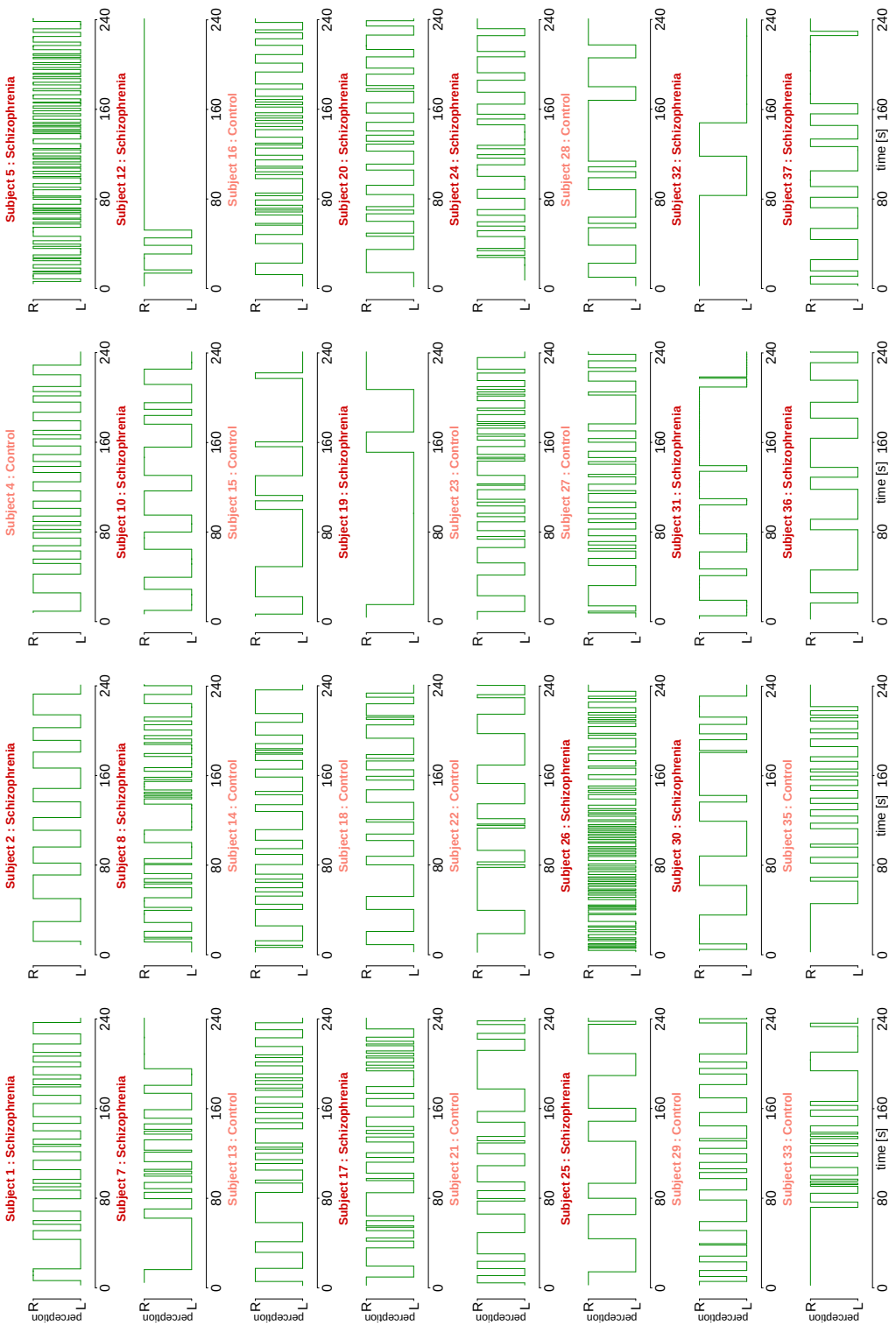
Subject 1 : Schizophrenia
Subject 2 : Schizophrenia
Subject 4 : Control
Subject 5 : Schizophrenia
Subject 7 : Schizophrenia
Subject 8 : Schizophrenia
Subject 10 : Schizophrenia
Subject 12 : Schizophrenia
Subject 13 : Control
Subject 14 : Control
Subject 15 : Control
Subject 16 : Control
Subject 17 : Schizophrenia
Subject 18 : Control
Subject 19 : Schizophrenia
Subject 20 : Schizophrenia
Subject 21 : Control
Subject 22 : Control
Subject 23 : Control
Subject 24 : Schizophrenia
Subject 25 : Schizophrenia
Subject 26 : Schizophrenia
Subject 27 : Control
Subject 28 : Control
Subject 29 : Control
Subject 30 : Schizophrenia
Subject 31 : Schizophrenia
Subject 32 : Schizophrenia
Subject 33 : Control
Subject 35 : Control
Subject 36 : Schizophrenia
Subject 37 : Schizophrenia
perception
R
L
0
80
160
240
time [s]

Figure A.1: Response patterns to continuous presentation of the stimulus for all 61 subjects differed by control or schizophrenia group (Schmack et al., 2015).

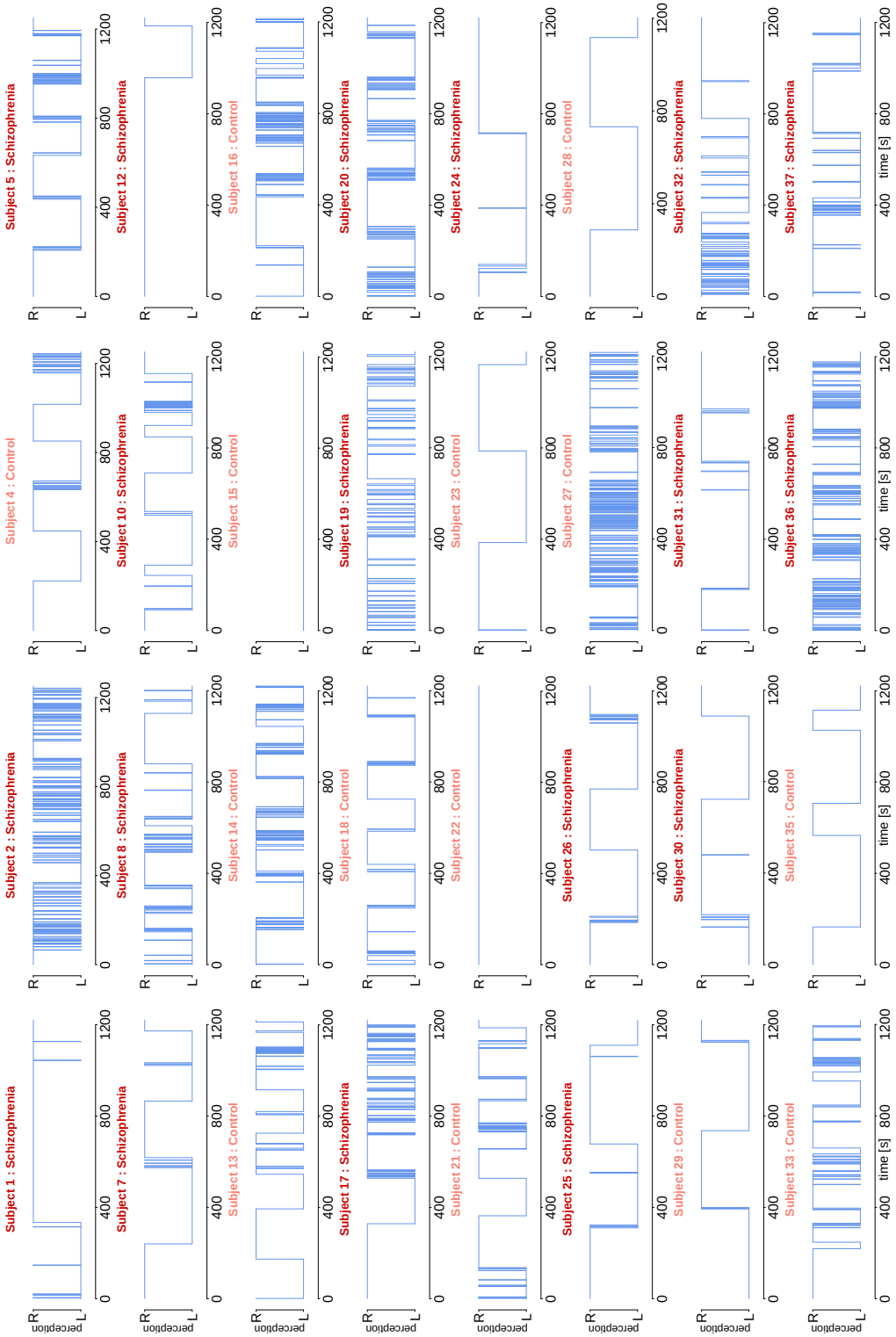
Subject 1 : Schizophrenia
Subject 2 : Schizophrenia
Subject 4 : Control
Subject 5 : Schizophrenia
Subject 7 : Schizophrenia
Subject 8 : Schizophrenia
Subject 10 : Schizophrenia
Subject 12 : Schizophrenia
Subject 13 : Control
Subject 14 : Control
Subject 15 : Control
Subject 16 : Control
Subject 17 : Schizophrenia
Subject 18 : Control
Subject 19 : Schizophrenia
Subject 20 : Schizophrenia
Subject 21 : Control
Subject 22 : Control
Subject 23 : Control
Subject 24 : Schizophrenia
Subject 25 : Schizophrenia
Subject 26 : Schizophrenia
Subject 27 : Control
Subject 28 : Control
Subject 29 : Control
Subject 30 : Schizophrenia
Subject 31 : Schizophrenia
Subject 32 : Schizophrenia
Subject 33 : Control
Subject 35 : Control
Subject 36 : Schizophrenia
Subject 37 : Schizophrenia
perception
R
L
0
400
800
1200
time [s]

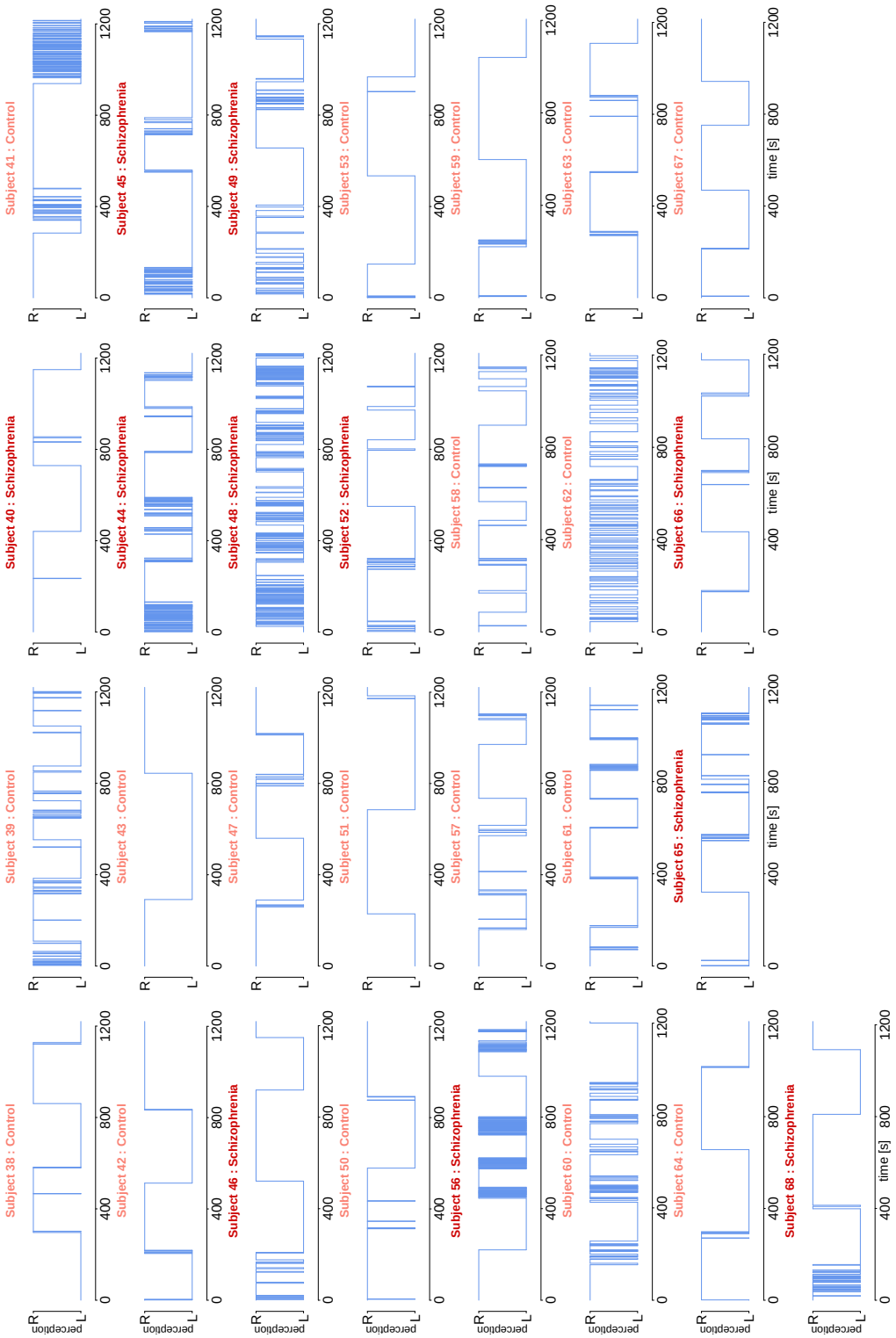

Figure A.2: Response patterns to intermittent presentation of the stimulus for all 61 subjects differed by control or schizophrenia group (Schmack et al., 2015).

Appendix B

The COBYLA algorithm

The COBYLA algorithm for optimization under non-linear constraints offers an alternative to the Newton-type approach used in this thesis for the direct numerical maximization of the HBMi log-likelihood as given in equation (12.9) on page 156. In contrast to the Newton-type approach (called by `nlm()` in `R`), it was directly constructed for constrained maximization with non-linear constraints. Recall that by using the `nlm()`-command we only accepted the solutions satisfying the constraints A)- F) on page 157. The COBYLA algorithm takes the constraints as input. In this appendix we present the idea of the COBYLA algorithm briefly (Section B.1) and then examine the estimation precision of parameter estimates for the HBMi using this algorithm (Section B.2) thereby also explaining why we do not use the COBYLA algorithm in practice. We use the same set of starting values as for the Newton-type algorithm (discussed in Section 12.2.1.3).

B.1 Idea

The COBYLA algorithm (constrained optimization by linear approximation) was invented by Powell (1994) to solve optimization problems that are constrained and where no derivatives exist. We describe the main ideas very briefly and refer for more details to Powell (1998, 2007). The goal is to minimize a function $f(x) : \mathbb{R}^n \to \mathbb{R}$ subject to $m \in \mathbb{N}$ (possibly non-linear) constraints $c_k(x) \geq 0, k = 1, \ldots, m$. Therefore, the function values $f(x_i), i = 1, \ldots, n$ at the vertices of a simplex are interpolated by a linear polynomial $L(x) : \mathbb{R}^n \to \mathbb{R}$, and the constraints are approximated by linear polynomials $l_k(x) \geq 0, k = 1, \ldots, m$. In each iteration step the linear program

$$\begin{aligned} &\min L(x) + \kappa[\max\left(-l_k(x), k = 1, \ldots, m\right)]_+ \\ &\text{s.t.} ||x - x_0|| \leq \rho_j \end{aligned}$$

is solved, where the subscript "+" denotes that the expression in the brackets is replaced by zero if it is negative. κ is a parameter, which may be increased from its initial value zero, x_0 is the vertice with the smallest value, i.e., $f(x_0) \leq f(x_i), i = 1, \ldots n$, $||\cdot||$ denotes the Euclidean norm, and ρ_j is a positive number, which may be reduced iteration-wise. The condition is introduced to prevent the linear approximations to be inaccurate. Moreover and particularly for the same reason, a lower bound Δ_j is imposed on ρ_j that is reduced only when the current value seems to prevent further progress. The new "best vertice" $\hat{x}_0$ replaces one of the old vertices of the simplex. The algorithm finishes when Δ_j becomes sufficiently small.

B.2 Precision of parameter estimates for the HBMi

We evaluate the estimation precision of the HBMi parameters applying parametric simulations as in Section 12.4.2 using the 61 estimated parameter constellations from the data set Schmack et al. (2015). The only difference is that we know use the COBYLA algorithm to estimate the parameters. Figure B.1 shows the results and is directly comparable to Figure 12.6 (page 163). For the original parameter set $b_S, \nu_S^*, b_U, \nu_U^*, \tilde{b}_S, \tilde{b}_U, \nu_B^*$ and the original recording length $T = 1200$ s only 18 parameter constellations yield smaller errors in the sense that the median error across the relative and the absolute errors was smaller than 0.25. For a recording length $T = 3600$ s 43 parameter constellation showed small errors. Regarding the set of derived parameters $\mu_S^*, \sigma_S^*, \mu_U^*, \sigma_U^*, p_{SS}^*$ and p_{UU}^* for $T = 1200$ s we observe 49 parameter constellations yielding small errors and for the larger $T = 3600$ s as much as 58 parameter combinations. Again the sample size n and the probability p_{SS}^* are critical for the estimation precision (panels E and F). These results are highly similar to the results obtained using the Newton approach implemented in the `nlm()`-function (Section 12.4.2). However, in a few cases the COBYLA algorithm (implemented in the `R`-package `nloptr`) does not stop and thereby causes a program crash. Therefore, we recommend to use the `nlm()`-function when estimating the HBMi parameters in practice.

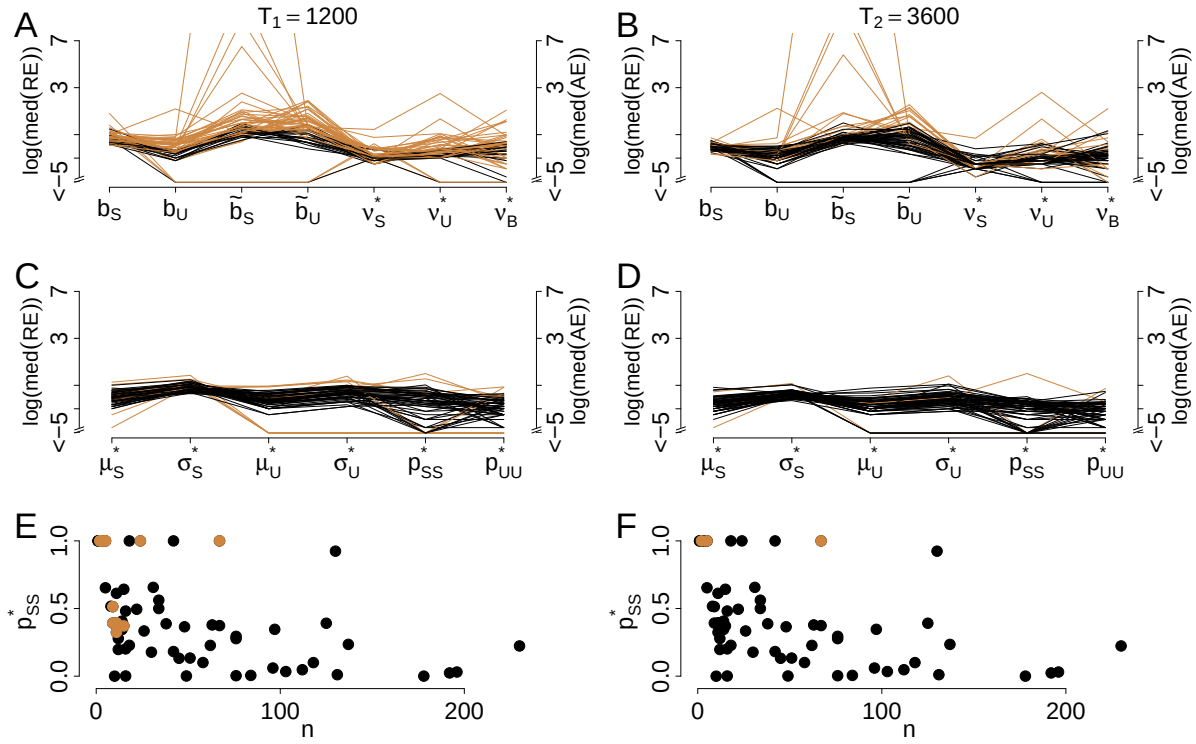

Figure B.1: Precision of parameter estimates in the HBMi using the COBYLA optimization. *For each of the 61 parameter constellations estimated from the sample data set, 1000 HBMi simulations were performed. (A) and (B): log(median(REs)) of the border parameters $b_S, b_U, \tilde{b}_S, \tilde{b}_U$, and log(median(AEs)) of the drift parameters $\nu_S^*, \nu_U^*, \nu_B^*$ with $T = 1200$ (A) and $T = 3600$ (B). (C) and (D): log(median(REs)) for the derived model parameters $\mu_S^*, \sigma_S^*, \mu_U^*, \sigma_U^*$ and log(median(AEs)) for the parameters p_{SS}^* and p_{UU}^* for $T = 1200$ (C) and $T = 3600$ (D). Parameter combinations with mean errors < 0.25 across all variables plotted in black. (E) and (F): Corresponding scatterplots of p_{SS}^* and n where the black points correspond to mean errors < 0.25 across the derived parameters.*

List of Figures

List of Tables

List of Notations and Abbreviations

AE	absolute error	103
$\alpha_j(i)$	forward variable denoting the probability of being in state j at time i and the data $d_1, \ldots, d_i$	56
a.s.	almost surely	13
A_t	age of a renewal process	65
b	border parameter in the HBMc	5
B	background process	129
$\beta_j(i)$	backward variable denoting the probability of the data $d_{i+1}, \ldots, d_n$ given state j at time i	91
BL	set of blank displays	129
b_S	HBMi border of P in the stable state	129
$\tilde{b}_S$	border B has to cross to remain stable	130
$\tilde{b}_U$	border B has to undershoot to remain unstable	130
b_U	HBMi border of P in the unstable state	129
BWA	Baum-Welch algorithm	55
χ_k	chi distribution with k degrees of freedom	78
χ_k^2	chi-square distribution with k degrees of freedom	78
cosh	cosinus hyperbolicus	80
CV	coefficient of variation	41
d_i	i-th dominance time	65
DNM	Direct Numerical Maximization	100
d_{SK}	Skorokhod metric	13
$d_{\|\|\cdot\|\|}$	metric induced by the supremum norm	13
$D[0,\tau]$	set of all càdlàg functions on $[0,\tau]$	13
EM	expectation maximization	90
erf	error function	171
$\mathbb{E}[X]$	expected value of X	13
F	distribution function	66

T_{ij}	first passage time of the state j starting in state i by the hidden state process	112
$\tilde{T}_{ij}$	first passage time of the state j starting in state i by the point process	112
UMVU	uniform minimum variance unbiased	69
$\mathbb{V}\mathrm{ar}(X)$	variance of X	13
W	Brownian motion (with drift)	11
Ξ_{HBMc}	point process generated by the HBMc	169
Ξ_{HBMi}	point process generated by the HBMi	169
Ξ_{HMMc}	point process generated by the HMMc	107
Ξ_{HMMi}	point process generated by the HMMi	107
ξ_i	i-th life time of a point process	10
$\xi_{j,k}(i)$	probability of being in states j and k at times i and $i+1$ given all data	91
Y_i	i-th state of a Markov chain/hidden state of the i-th dominance time	71, 107
$\tilde{Y}_t$	hidden state at time t	107
$\xrightarrow[\mathbb{P}]{}$	convergence in probability	13
$\xrightarrow[d]{}$	weak convergence	13
$*$	convolution	59

Bibliography

Abramowitz, M. and Stegun, I. A., editors (1972). *Handbook of Mathematical Functions with Formulas, Graphs, and Mathematical Tables*. Dover, New York.

Adams, R. A., Stephan, K. E., Brown, H. R., Frith, C. D., and Friston, K. J. (2013). The computational anatomy of psychosis. *Frontiers in Psychiatry*, 4:Article 47.

Albert, S. (2014). Ein Multiple-Filter-Test zur Detektion von Varianzänderungen in Erneuerungsprozessen. Master's thesis, Goethe University, Frankfurt a.M.

Albert, S., Messer, M., Schiemann, J., Roeper, J., and Schneider, G. (2017a). Multi-scale detection of variance changes in renewal processes in the presence of rate change points. *Journal of Time Series Analysis*, 38(6):1028–1052.

Albert, S., Schmack, K., Sterzer, P., and Schneider, G. (2017b). A hierarchical stochastic model for bistable perception. *PLoS Computational Biology*, 13(11):e1005856.

Altman, R. M. (2004). Assessing the goodness-of-fit of hidden markov models. *Biometrics*, 60(2):444–450.

Asmussen, S. and Glynn, P. W. (2007). *Stochastic Simulation: Algorithms and Analysis*. Springer, New York.

Aue, A. and Horváth, L. (2013). Structural breaks in time series. *Journal Of Time Series Analysis*, 34(1):1–16.

Barbu, V. S. and Limnios, N. (2008). *Semi-Markov Chains and Hidden Semi-Markov Models toward Applications*. Springer, New York.

Barndorff-Nielsen, O. E. (1978). Hyperbolic distributions and distributions on hyperbolae. *Scandinavian Journal of Statistics*, 5(3):151–157.

Barndorff-Nielsen, O. E. (1997). Normal Inverse Gaussian Distributions and Stochastic Volatility Modeling. *Scandinavian Journal of Statistics*, 24(1):1–13.

Basseville, M. and Nikiforov, I. (1993). *Detection of Abrupt Changes: Theory and Application*. Prentice Hall Information and System Sciences Series. Prentice Hall Inc., Englewood Cliffs, NJ.

Baum, L. E. and Petrie, T. (1966). Statistical inference for probabilistic functions of finite state markov chains. *The Annals of Mathematical Statistics*, 37(6):1554–1563.

Baum, L. E., Petrie, T., Soules, G., and Weiss, N. (1970). A maximization technique occurring in the statistical analysis of probabilistic functions of markov chains. *The Annals of Mathematical Statistics*, 41(1):164–171.

Beichelt, F. and Fatti, L. P. (2001). *Stochastic Processes and Their Applications*. CRC Press.

Berg, J., Tymoczko, J., and Stryer, L. (2007). *Biochemistry*. W. H. Freeman & Co., sixth edition.

Bertrand, P. R. (2000). A local method for estimating change points: the hat-function. *Statistics*, 34(3):215–235.

Bertrand, P. R., Fhima, M., and Guillin, A. (2011). Off-line detection of multiple change points by the filtered derivative with p-value method. *Sequential Analysis*, 30(2):172–207.

Bickel, P. J., Ritov, Y., and Rydén, T. (1998). Asymptotic normality of the maximum-likelihood estimator for general hidden markov models. *The Annals of Statistics*, 26(4):1614–1635.

Billingsley, P. (1968). *Convergence of probability measures*. John Wiley & Sons Inc., New York.

Bilmes, J. A. (1998). A Gentle Tutorial of the EM Algorithm and its Application to Parameter Estimation for Gaussian Mixture and Hidden Markov Models. Technical report, International Computer Science Institute.

Bingmer, M., Schiemann, J., Roeper, J., and Schneider, G. (2011). Measuring burstiness and regularity in oscillatory spike trains. *Journal of Neuroscience Methods*, 201:426–437.

Brascamp, J., Klink, P., and Levelt, W. (2015). The 'laws' of binocular rivalry: 50 years of levelt's propositions. *Vision Research*, 109:20–37.

Brascamp, J., van Ee, R., Noest, A., Jacobs, R., and van den Berg, A. (2006). The time course of binocular rivalry reveals a fundamental role of noise. *Journal of Vision*, 6(11):1244–1256.

Brascamp, J., van Ee, R., Pestman, W., and van den Berg, A. (2005). Distributions of alternation rates in various forms of bistable perception. *Journal of Vision*, 5(4):287–298.

Brascamp, J. W., Pearson, J., Blake, R., and van den Berg, A. (2009). Intermittent ambiguous stimuli: Implicit memory causes periodic perceptual alternations. *Journal of Vision*, 9(3):3, 1–23.

Braun, J. and Mattia, M. (2010). Attractors and noise: Twin drivers of decisions and multistability. *NeuroImage*, 52(3):740–751.

Brodsky, B. (2017). *Change-point analysis in nonstationary stochastic models*. CRC Press, Boca Raton, FL.

Brodsky, B. E. and Darkhovsky, B. S. (1993). *Nonparametric methods in change-point problems*, volume 243 of *Mathematics and its Applications*. Kluwer Academic Publishers, Dordrecht.

Brody, C. (1999). Correlations without synchrony. *Neural Computation*, 11:1537–1551.

Bulla, J. (2006). *Application of Hidden Markov Models and Hidden Semi-Markov Models to Financial Time Series*. PhD thesis, Georg-August-University of Göttingen.

Cao, R., Braun, J., and Mattia, M. (2014). Stochastic accumulation by cortical columns may explain the scalar property of multistable perception. *Physical Review Letters*, 113(9).

Cao, R., Pastukhov, A., Mattia, M., and Braun, J. (2016). Collective activity of many bistable assemblies reproduces characteristic dynamics of multistable perception. *The Journal of Neuroscience*, 36(26):6957–6972.

Cappé, O., Moulines, E., and Ryden, T. (2005). *Inference in Hidden Markov Models*. Springer, New York.

Casella, G. and Berger, R. L. (2002). *Statistical Inference*. Duxbury Press, second edition.

Chen, J. and Gupta, A. K. (1997). Testing and locating variance changepoints with application to stock prices. *Journal of the American Statistical Association*, 92(438):739–747.

Cohen, C. and Whitten, B. J. (1988). *Parameter Estimation in Reliability and Life Span Models*. CRC Press.

Cox, D. and Oakes, D. (1984). *Analysis of Survival Data*. Chapman and Hall/CRC.

Csörgö, M. and Horváth, L. (1997). *Limit theorems in change-point analysis*. Wiley Series in Probability and Statistics. John Wiley & Sons, Chichester. With a foreword by David Kendall.

Daley, D. J. and Vere-Jones, D. (1988). *An Introduction to the Theory of Point Processes*. Springer, Berlin.

Dannemann, J. and Holzmann, H. (2008). Likelihood ratio testing for hidden markov models under non-standard conditions. *Scandinavian Journal of Statistics*, 35(2):309–321.

Dayan, P. and Abbott, L. F. (2005). *Theoretical neuroscience: computational and mathematical modeling of neural systems*. The MIT Press, Cambridge.

Dempster, A., Laird, N., and Rubin, D. (1977). Maximum likelihood from incomplete data via the EM algorithm. *Journal of the Royal Statistical Society. Series B (Methodological)*, 39(1):1–38.

Dennis, J. E. and Schnabel, R. B. (1983). *Numerical Methods for Unconstrained Optimization and Nonlinear Equations*. Prentice-Hall, Englewood Cliffs, NJ.

Dette, H., Wu, W., and Zhou, Z. (2015). Change point analysis of second order characteristics in non-stationary time series. arXiv:1503.08610.

Dieter, K., Brascamp, J., D., T., and Blake, R. (2016). Does visual attention drive the dynamics of bistable perception? *Attention, Perception, & Psychophysics*, 78(7):1861–1873.

Eckley, I., Fearnhead, P., and Killick, R. (2010). *Bayesian Time Series Models*, chapter Probabilistic methods for time series analysis. Cambridge University Press, Cambridge, UK.

Efron, B. and Tibshirani, R. (1994). *An Introduction to the Bootstrap*. Chapman and Hall/CRC.

Eichinger, B. and Kirch, C. (2018). A MOSUM procedure for the estimation of multiple random change points. *Bernoulli*, 24(1):526–564.

Elliott, R. J., Aggoun, L., and Moore, J. B. (1995). *Hidden Markov models*, volume 29 of *Applications of Mathematics (New York)*. Springer-Verlag, New York. Estimation and control.

Ephraim, Y. and Merhav, N. (2002). Hidden markov processes. *Institute of Electrical and Electronics Engineers. Transactions on Information Theory*, 48(6):1518–1569. Special issue on Shannon theory: perspective, trends, and applications.

Evans, S. L., Averbeck, B. B., and Furl, N. (2015). Jumping to conclusions in schizophrenia. *Neuropsychiatric Disease and Treatment*, 11:1615–1624.

Farkhooi, F., Strube-Bloss, M., and Nawrot, M. P. (2009). Serial correlation in neural spike trains: Experimental evidence, stochastic modelling, and single neuron variability. *Physical Review E*, 79(2):021905.

Fletcher, P. C. and Frith, C. D. (2009). Perceiving is believing: a Bayesian approach to explaining the positive symptoms of schizophrenia. *Nature Reviews Neuroscience*, 10:48–58.

Forbes, C., Evans, M., Hastings, N., and Peacock, B. (2011). *Statistical Distributions*, chapter Chi Distribution. New York: Wiley, fourth edition.

Forney, G. (1973). The Viterbi algorithm. *Proceedings of the IEEE*, 61(3):268–278.

Fox, M., Ghallab, M., Infantes, G., and Long, D. (2005). Robot introspection through learned hidden markov models. *Artificial Intelligence*, 170(2):59–113.

Fox, R. and Herman, J. (1967). Stochastic properties of binocular rivalry alternations. *Psychophysiology*, 2(9):432–446.

Frick, K., Munk, A., and Sieling, H. (2014). Multiscale change point inference. *Journal of the Royal Statistical Society: Series B (Statistical Methodology)*, 76(3):495–580. With 32 discussions by 47 authors and a rejoinder by the authors.

Fryzlewicz, P. (2014). Wild binary segmentation for multiple change-point-detection. *The Annals of Statistics*, 42(6):2243–2281.

Gershman, S. J., Vul, E., and Tenenbaum, J. B. (2012). Multistability and perceptual inference. *Neural Computation*, 24(1):1–24.

Gigante, G., Mattia, M., Braun, J., and Del Giudice, P. (2009). Bistable perception modeled as competing stochastic integrations at two levels. *PLoS Computational Biology*, 5(7):e1000430.

Giudici, P., Rydén, T., and Vandekerkhove, P. (2000). Likelihood-ratio tests for hidden markov models. *Biometrics*, 56(3):742–747.

Gonon, F. (1988). Nonlinear relationship between impulse flow and dopamine released by rat midbrain dopaminergic neurons as studied by in vivo electrochemistry. *Neuroscience*, 24:19–28.

Grimmett, G. and Stirzaker, D. (2001). *Probability and random processes*. Oxford University Press, New York, third edition.

Grün, S., Diesmann, M., and Aertsen, A. (2002). Unitary events in multiple single-neuron activity. ii. non-stationary data. *Neural Computation*, 14(1):81–119.

Grün, S., Riehle, A., and Diesmann, M. (2003). Effect of cross-trial nonstationarity on joint-spike events. *Biological Cybernetics*, 88(5):335–351.

Grün, S. and Rotter, S., editors (2010). *Analysis of parallel spike trains*. Springer Series in Computational Neuroscience 7. Springer, New York.

Gut, A. (2009). *Stopped Random Walks*. Springer, New York, second edition.

Haviv, M. (2013). *A Course in Queueing Theory*. Springer, New York.

Hawkins, D. and Zamba, K. (2005). A change-point model for a shift in variance. *Journal of Quality Technology*, 37(1):21–31.

Hohwy, J., Roepstorff, A., and Friston, K. (2008). Predictive coding explains binocular rivalry: An epistemological review. *Cognition*, 108(3):687–701.

Horváth, L., Horvath, Z., and Huskova, M. (2008). Ratio test for change point detection. In *Beyond parametrics in interdisciplinary research*, volume 1, pages 293–304. IMS, Collections.

Hsu, D. A. (1977). Tests for variance shift at an unknown time point. *Applied Statistics*, 26(3):279–284.

Inclan, C. (1993). Detection of multiple changes of variance using posterior odds. *Journal of Business & Economic Statistics*, 11(3):289–300.

Inclan, C. and Tiao, G. (1994). Use of cumulative sums of squares for retrospective detection of changes of variance. *Journal of the American Statistical Association*, 89(427):913–923.

Iwase, K. and Seto, N. (1983). Uniformly minimum variance unbiased estimators for the inverse gaussian distribution. *Journal of the American Statistical Association*, 18(10):3587–3593.

Jandhyala, V., Fotopoulos, S., MacNeill, I., and Liu, P. (2013). Inference for single and multiple change-points in time series. *Journal of Time Series Analysis*, 34(4):423–446.

Johnson, D. H. (1996). Point process models of single-neuron discharges. *Journal of Computational Neuroscience*, 3(4):275–299.

Johnson, N. L., Kotz, S., and Balakrishnan, N. (1994). *Continuous univariate distributions*, volume 1 of *Wiley Series in Probability and Mathematical Statistics: Applied Probability and Statistics*. John Wiley & Sons, New York, second edition.

Kandel, E., Schwartz, J., and Jessell, T. (2000). *Principles of Neural Science*. McGraw-Hill, New York, fourth edition.

Kass, R. E., Ventura, V., and Brown, E. N. (2005). Statistical issues in the analysis of neuronal data. *Journal of Neurophysiology*, 94(1):8–25.

Khodadadi, A. and Asgharian, M. (2008). Change-point problems and regression: An annotated bibliography. *Collection of Biostatistics Research Archive (COBRA)*.

Kilian, U. and Weber, C., editors (2003). *Lexikon der Physik*. Spektrum Akademischer Verlag.

Killick, R., Eckley, I., Ewans, K., and Jonathan, P. (2010). Detection of changes in variance of oceanographic time-series using changepoint analysis. *Ocean Engineering*, 37(13):1120–1126.

Killick, R., Eckley, I., and Jonathan, P. (2013). A wavelet-based approach for detecting changes in second order structure within nonstationary time series. *Electronic Journal of Statistics*, 7:1167–1183.

Klenke, A. (2008). *Probability theory: a comprehensive course*. Springer, London.

Korkas, K. K. and Fryzlewicz, P. (2017). Multiple change-point detection for non-stationary time series using wild binary segmentation. *Statistica Sinica*, 27(1):287–311.

Kornmeier, J. and Bach, M. (2004). Early neural activity in Necker-cube reversal: Evidence for low-level processing of a gestalt phenomenon. *Psychophysiology*, 41(1):1–8.

Laing, C. R. and Chow, C. C. (2002). A spiking neuron model for binocular rivalry. *Journal of Computational Neuroscience*, 12(1):39–53.

Lang, S. (1997). *Undergraduate Analysis*. Springer-Verlag, New York, second edition.

Lavielle, M. and Moulines, E. (2000). Least-squares estimation of an unknown number of shifts in a time series. *Journal of Time Series Analysis*, 21(1):33–59.

Lawless, J. F. (1982). *Statistical Models and Methods for Lifetime Data*. John Wiley, New York.

Lehky, S. (1995). Binocular rivalry is not chaotic. *Proceedings of the Royal Society of London. Series B (Biological sciences)*, 259:71–76.

Lehmann, E. (1999). *Elements of Large-Sample Theory*. Springer, New York.

Lehmann, E. and Casella, G. (1998). *Theory of point estimation*. Springer-Verlag, New York, Berlin, Heidelberg, second edition.

Leopold, D. A. and Logothetis, N. K. (1999). Multistable phenomena: changing views in perception. *Trends in Cognitive Sciences*, 3(7):254–264.

Leopold, D. A., Wilke, M., Maier, A., and Logothetis, N. K. (2002). Stable perception of visually ambiguous patterns. *Nature Neuroscience*, 5(6):605–609.

Levelt, W. (1965). *On binocular rivalry*. PhD thesis, Soesterberg, The Netherlands: Institute for Perception.

Levelt, W. (1967). Note on the distribution of dominance times in binocular rivalry. *British Journal of Psychology*, 58(1):143–145.

Lévy, P. (1954). Processus semi-markoviens. *Proceedings of the International Congress of Mathematicians*, 3:416–426.

MacDonald, I. and Zucchini, W. (1997). *Hidden Markov and other models for discrete-valued time series*, volume 70 of *Monographs on Statistics and Applied Probability*. Chapman&Hall, London.

Maier, A., Wilke, M., Logothetis, N. K., and Leopold, D. A. (2003). Perception of temporally interleaved ambiguous patterns. *Current Biology*, 13(13):1076–1085.

Matteson, D. S. and James, N. A. (2014). A nonparametric approach for multiple change point analysis of multivariate data. *Journal of the American Statistical Association*, 109(505):334–345.

Medhi, J. (2009). *Stochastic Processes*. New Age International, third edition.

Messer, M. (2014). *A Multiple Filter Test for the Detection of Rate Changes in Renewal Processes with Varying Variance*. PhD thesis, Goethe University, Frankfurt a.M.

Messer, M., Albert, S., Plomer, S., and Schneider, G. (2017). MFT: The Multiple Filter Test for Change Point Detection. R package version 1.3 available via https://cran.r-project.org/package=MFT.

Messer, M., Albert, S., and Schneider, G. (2018). The multiple filter test for change point detection in time series. *Metrika*. accepted for publication.

Messer, M., Kirchner, M., Schiemann, J., Roeper, J., Neininger, R., and Schneider, G. (2014). A multiple filter test for change point detection in renewal processes with varying variance. *Annals of Applied Statistics*, 8(4):2027–2067.

Messer, M. and Schneider, G. (2017). The shark fin function - asymptotic behavior of the filtered derivative for point processes in case of change points. *Statistical Inference for Stochastic Processes*, 20(2):253–272.

Minka, T. P. (2002). Estimating a gamma distribution. Technical report, Microsoft Research.

Moreno-Bote, R., Rinzel, J., and Rubin, N. (2007). Noise-induced alternations in an attractor network model of perceptual bistability. *Journal of Neuophysiology*, 98(3):1125–1139.

Mörters, P. and Peres, Y. (2010). *Brownian Motion*. Cambridge University Press, Cambridge.

Murata, T., Matsui, N., Miyauchi, S., Kakita, Y., and Yanagida, T. (2003). Discrete stochastic process underlying perceptual rivalry. *NeuroReport*, 14(10):1347–1352.

Nam, C. F. H., Aston, J. A., Eckley, I., and Killick, R. (2015). The uncertainty of storm season changes: Quantifying the uncertainty of autoco- variance changepoints. *Technometrics*, 57(2):194–206.

Nawrot, M. P., Boucsein, C., Rodriguez Molina, V., Riehla, A., Aertsen, A., and Rotter, S. (2008). Measurement of variability dynamics in cortical spike trains. *Journal of Neuroscience Methods*, 169(2):347–390.

Necker, L. A. (1832). Observations on some remarkable optical phaenomena seen in switzerland; and on an optical phaenomenon which occurs on viewing a figure of a crystal or geometical solid. *The London, Edinburgh, and Dublin Philosophical Magazine and Journal of Science*, 1(5):329–337.

Noest, A., van Ee, R., Nijs, M., and van Wezel, R. (2007). Percept-choice sequences driven by interrupted ambiguous stimuli: A low-level neural model. *Journal of Vision*, 7(8):10, 1–14.

Noorossana, R. and Heydari, M. (2012). Change point estimation of a normal process variance with monotonic change. *Scientia Iranica*, 19(3):885–894.

Norris, J. (1998). *Markov Chains*. Cambridge Series in Statistical and Probabilistic Mathematics. Cambridge University Press, Cambridge, second edition.

Och, F. and Ney, H. (2003). A systematic comparison of various statistical alignment models. *Computational Linguistics*, 29(1):19–51.

Orbach, J., Ehrlich, D., and Heath, H. (1963). Reversibility of the Necker cube. i. an examination of the concept of "satiation or orientation". *Perceptual and Motor Skills*, 17:439–458.

Pandey, B. and Bandyopadhyay, P. (2012). Bayesian estimation of inverse gaussian distribution. arXiv:1210.4524v1.

Pastukhov, A. and Braun, J. (2007). Perceptual reversals need no prompting by attention. *Journal of Vision*, 7(10):5, 1–17.

Pastukhov, A. and Braun, J. (2011). Cumulative history quantifies the role of neural adaptation in multistable perception. *Journal of Vision*, 11(10):12, 1–10.

Pastukhov, A. and Braun, J. (2013). Structure-from-motion: dissociating perception, neural persistence, and sensory memory of illusory depth and illusory rotation. *Attention, Perception, & Psychophysics*, 75(2):322–340.

Pastukhov, A., Garcia-Rodriguez, P., Haenicke, J., Guillamon, A., Deco, G., and Braun, J. (2013). Multi-stable perception balances stability and sensitivity. *Frontiers in Computational Neuroscience*, 7(17):1–18.

Peters, E., Joseph, S., and Garety, P. (1999). Measurement of delusional ideation in the normal population: introducing the PDI (Peters et al. delusions inventory). *Schizophrenia Bulletin*, 25(3):533–576.

Powell, M. J. D. (1994). *Advances in Optimization and Numerical Analysis*, chapter A direct search optimization method that models the objective and constraint functions by linear interpolation, pages 51–67. Kluwer Academic, Dordrecht.

Powell, M. J. D. (1998). Direct search algorithms for optimization calculations. *Acta Numerica*, 7:287–336.

Powell, M. J. D. (2007). A view of algorithms for optimization without derivatives. Technical report, Cambridge University. DAMTP.

Pyke, R. (1961). Markov renewal processes: definitions and preliminary properties. *Annals of Mathematical Statistics*, 32(4):1231–1242.

Quiroga-Lombard, C., Hass, J., and Durstewitz, D. (2013). Method for stationarity-segmentation of spike train data with application to the pearson cross-correlation. *Journal of Neurophysiology*, 110(2):562–572.

Rabiner, L. R. (1989). A Tutorial on Hidden Markov Models and Selected Applications in Speech Recognition. *Institute of Electrical and Electronics Engineers. Transactions on Information Theory*, 77(2):257–284.

Rankin, J., Sussman, E., and Rinzel, J. (2015). Neuromechanistic model of auditory bistability. *PLoS Computational Biology*, 11(11):e1004555.

Rodionov, S. (2005). A sequential method for detecting regime shifts in the mean and variance. In *Large-Scale Disturbances (Regime Shifts) and Recovery in Aquatic Ecosystems: Challenges for Management Toward Sustainability*, Proceedings of 2005 UNESCO-ROSTE/BAS Workshop on Regime Shifts, pages 68–72.

Ross, R. M., McKay, R., Coltheart, M., and Langdon, R. (2015). Jumping to conclusions about the beads task? A meta-analysis of delusional ideation and data-gathering. *Schizophrenia Bulletin*, 41(5):1183–1191.

Ross, S. M. (1996). *Stochastic processes*. Wiley, New York.

Rubin, E. (1915). *Synsoplevede figurer*. PhD thesis, University of Copenhagen.

Rydén, T., Terasvirta, T., and Asbrink, S. (1998). Stylized facts of daily return series and the hidden markov model. *Journal of Applied Econometrics*, 13(3):217–244.

Samanta, M. (1985). On tests of equality of two inverse gaussian distributions. *South African Statistical Journal*, 19(2):83–95.

Schiemann, J., Klose, V., Schlaudraff, F., Bingmer, M., Seino, S., Magill, P. J., Schneider, G., Liss, B., and Roeper, J. (2012). K-atp channels control in vivo burst firing of dopamine neurons in the medial substantia nigra and novelty-induced behavior. *Nature Neuroscience*, 15(9):1272–80.

Schmack, K., Gòmez-Carrillo de Castro, A., Rothkirch, M., Sekutowicz, M., Rössler, H., Haynes, J.-D., Heinz, A., Petrovic, P., and Sterzer, P. (2013). Delusions and the role of beliefs in perceptual inference. *The Journal of Neuroscience*, 33(34):13701–13712.

Schmack, K., Schnack, A., Priller, J., and Sterzer, P. (2015). Perceptual instability in schizophrenia: Probing predictive coding accounts of delusions with ambiguous stimuli. *Schizophrenia Research: Cognition*, 2(2):72–77.

Schneider, G. (2008). Messages of oscillatory correlograms - a spike-train model. *Neural Computation*, 20(5):1211–1238.

Scholz, F. (2007). The bootstrap small sample properties. Technical report, University of Washington.

Schrödinger, E. (1915). Zur Theorie der Fall- und Steigversuche an Teilchen mit Brownscher Bewegung. *Physikalische Zeitschrift*, 16:289–295.

Seneta, E. (1981). *Nonnegative matrices and Markov chains*. Springer Series in Statistics. Springer-Verlag, New York, second edition.

Serfozo, R. (2009). *Basics of Applied Stochastic Processes*. Springer, Berlin Heidelberg.

Seshadri, V. (1993). *The Inverse Gaussian Applications: A Case Study in Exponential Families*. Oxford University Press.

Seshadri, V. (1999). *The Inverse Gaussian Distribution: Statistical Theory and Applications*. Springer, New York.

Shreve, S. (2004). *Stochastic Calculus for Finance II: Continuous-Time Models*. Springer, New York.

Smith, W. (1955). Regenerative stochastic processes. *Proceedings of the Royal Society. Series A*, 232(1188):6–31.

Staude, B., Grün, S., and Rotter, S. (2010). Higher-order correlations in non-stationary parallel spike trains: statistical modeling and inference. *Frontiers in Computational Neuroscience, 4*, 16.

Sterzer, P., Kleinschmidt, A., and Rees, G. (2009). The neural bases of multistable perception. *Trends in Cognitive Sciences*, 13(7):310–318.

Stuke, H., Stuke, H., Weilnhammer, V., and Schmack, K. (2017). Psychotic experiences and overhasty inferences are related to maladaptive learning. *PLoS Computational Biology*, 13(1):e1005328.

Titman, A. C. and Sharples, L. D. (2008). A general goodness-of-fit test for markov and hidden markov models. *Statistics in Medicine*, 27(12):2177–2195.

Turner, R. (2008). Direct maximization of the likelihood of a hidden markov model. *Computational Statistics and Data Analysis*, 52(9):4147–4160.

Tweedie, M. (1945). Inverse statistical variates. *Nature*, 155:453.

van der Vaart, A. (1998). *Asymptotic Statistics*, volume 3 of *Cambridge Series in Statistical and Probabilistic Mathematics*. Cambridge University Press, Cambridge.

van Ee, R. (2005). Dynamics of perceptual bi-stability for stereoscopic slant rivalry and a comparison with grating, house-face, and necker cube rivalry. *Vision Research*, 45(1):29–40.

Viterbi, A. (1967). Error bounds for convolutional codes and an asymptotically optimal decoding algorithm. *IEEE Transactions on Information Theory*, 13(2):260–269.

von Helmholtz, H. (1866). *Treatise on Physiological Optics*, volume 3. The Optical Society of America, Birmingham, AL.

Wald, A. (1944). On cumulative sums of random variables. *The Annals of Mathematical Statistics*, 15(3):283–296.

Walker, P. (1975). Stochastic properties of binocular rivalry alternations. *Perception & Psychophysics*, 18(6):467–473.

Watson, G. (1995). *A Treatise on the Theory of Bessel Functions*. Cambridge University Press, Cambridge, second edition.

Weilnhammer, V., Stuke, H., Hesselmann, G., Sterzer, P., and Schmack, K. (2017). A predictive coding account of bistable perception - a model-based fMRI study. *PLoS Computational Biology*, 13(5):e1005536.

Weilnhammer, V. A., Sterzer, P., and Hesselmann, G. (2016). Perceptual stability of the lissajous figure is modulated by the speed of illusory rotation. *PLoS One*, 11(8):e0160772.

Whitcher, B., Guttorp, P., and Percival, D. (2000). Multiscale detection and location of multiple variance changes in the presence of long memory. *Journal of Statistical Computation and Simulation*, 68(1):65–88.

Wilson, A. and Bobick, A. (1999). Parametric hidden markov models for gesture recognition. *IEEE Transactions on Pattern Analysis and Machine Intelligence*, 21(9):884–900.

Wilson, H. R. (2007). Minimal physiological conditions for binocular rivalry and rivalry memory. *Vision Research*, 47(21):2741–2750.

Yoon, B.-J. (2009). Hidden markov models and their applications in biological sequence analysis. *Current Genomics*, 10(6):402–415.

Young, G. and Smith, R. (2005). *Essentials of Statistical Inference*. Cambridge Series in Statistical and Probabilistic Mathematics. Cambridge University Press, Cambridge.

Zhao, W., Tian, Z., and Xia, Z. (2010). Ratio test for variance change point in linear process with long memory. *Statistical Papers*, 51(2):397–407.

German summary

Die vorliegende Dissertation widmet sich der Analyse und Modellierung von Punktprozessen, wie sie aus verschiedenen Experimenten in den Neurowissenschaften entstehen. Insbesondere wird ein Fokus auf die Beschreibung und Detektion von verschiedenen Arten von Variabilitätsänderungen innerhalb von Punktprozessen gelegt. Hierbei bilden die Zeitpunkte, zu denen Ereignisse stattfinden, Punktprozesse auf der (positiven) reellen Achse.

Ein prominentes Beispiel für die Anwendung von Punktprozessen in den Neurowissenschaften sind sogennante Spike Trains. Ein charakteristischer, kurzfristiger Anstieg im Membranpotential einer Nervenzelle (auch Neuron genannt) wird als "Spike" bezeichnet. Es wird Information durch die Übertragung elektrischer Signale zu benachbarten Zellen verarbeitet. Weder die Höhe noch die Dauer des Potentialanstiegs unterscheiden sich wesentlich, weshalb angenommen wird, dass die zeitliche Abfolge der Spikes – der Spike Train – die Basis der Informationsverarbeitung im Gehirn bildet (siehe z.B. Kandel et al., 2000). Die Auftrittszeitpunkte $(t_1, t_2, \ldots, t_n)$ der Spikes in einem Intervall $[0, T]$ (mit $0 < t_1 < t_2 < \ldots < t_n < T < \infty$) bilden den Spike Train und stellen im mathematischen Sinne einen Punktprozess auf der positiven reellen Achse dar. Die Analyse dieser Punktprozesse dient zum Verstehen der Funktionsweise des Nervensystems. Häufig werden dabei statistische Modelle auf der Basis von Erneuerungsprozessen verwendet (vgl. Johnson, 1996; Dayan and Abbott, 2005; Kass et al., 2005; Nawrot et al., 2008) und stationäre Modellparameter wie z.B. Rate oder Varianz der Lebenszeiten (auch Inter-Spike-Intervals genannt) angenommen. Statistische Analysen (wie beispielsweise serielle Korrelationen oder Koordination zwischen parallelen Spike Trains) können durch Verletzung dieser Modellannahmen verfälscht werden (Brody (1999); Grün et al. (2003); ein Beispiel eines simulierten Spike Trains mit nicht-stationärer Rate und Varianz findet sich in Abbildung 1). Es wurden daher eigens Techniken entwickelt, die auf separaten Analysen in Abschnitten mit stationären Parametern aufbauen (Grün et al., 2002; Schneider, 2008; Staude et al., 2010; Quiroga-Lombard et al., 2013). Diese Techniken verwenden Stufenfunktionen und zielen auf die Detektion der Change Points, d.h. der Strukturbrüche, ab.

Abbildung 1: Schematische Darstellung eines simulierten Spike Trains mit Strukturbrüchen in der Rate und in der Varianz

Außer der Verbesserung der Ergebnisse statistischer Analysen können detektierte Raten- oder Varianz Change Points auch direkt wertvolle Information beinhalten. So werden in Bingmer et al. (2011) verschiedene neuronale Feuermuster beschrieben, die mit Änderungen in der Variabilität verbunden sind. Dopaminerge Neuronen beispielsweise wechseln in ihrem

Feuermuster oftmals zwischen einem oszillatorischem Feuern geringer Rate und kurzen, so genannten burstigen Abschnitten mit hoher Feuerintensität. Diese burstigen Abschnitte stellen eine potenzielle Änderung in der Varianz dar und werdem mit einem erhöhten Dopaminausstoß in Verbindung gebracht (z.B. Gonon, 1988; Schiemann et al., 2012).

Zur Detektion von Change Points in der Rate (oder ähnlich gelagert von Change Points im Mittelwert von Folgen von Zufallsvariablen) gibt es vielfältige wissenschaftliche Arbeiten, wie z.B. Bertrand (2000); Lavielle and Moulines (2000); Bertrand et al. (2011); Frick et al. (2014); Fryzlewicz (2014); Matteson and James (2014); Messer et al. (2014); Eichinger and Kirch (2018). Einen generellen Überblick über das Feld der Change Point detection bieten die Übersichtswerke Basseville and Nikiforov (1993); Csörgö and Horváth (1997); Aue and Horváth (2013); Jandhyala et al. (2013); Brodsky (2017). Einige dieser Techniken können auch zur Detektion von Strukturbrüchen in der Varianz verwendet werden. Weitere Arbeiten zu diesem Thema stammen von Hsu (1977); Inclan (1993); Inclan and Tiao (1994); Chen and Gupta (1997); Whitcher et al. (2000); Killick et al. (2010); Zhao et al. (2010); Noorossana and Heydari (2012); Killick et al. (2013); Nam et al. (2015); Korkas and Fryzlewicz (2017). Einschränkend ist anzumerken, dass die meisten Methoden parametrisch sind, d.h. beispielsweise normalverteilte Zufallsvariablen annehmen, oder höchstens einen Change Point finden können. Eine zentrale Annahme ist zudem die einer stationären und teils sogar bekannten Rate. Zur Detektion simultaner Change Points in Rate und Varianz gibt es lediglich die anwendungsorientierten Arbeiten von Hawkins and Zamba (2005); Rodionov (2005). Weiterhin entwickelten Dette et al. (2015) einen statistischen Test für die Nullhypothese der Varianzhomogenität bei leicht variierendem Mittelwert.

Der erste Teil der vorliegenden Arbeit fokussiert sich daher auf eine Methode zur Erkennung von Change Points in der Rate und in der Varianz in Erneuerungsprozessen, die in verschiedenen Zeitskalen simultan oder separat auftreten können. In einem zweistufigen Verfahren soll dabei zunächst die Nullhypothese der Ratenhomogenität bei gewisser Variabilität der Varianz getestet und etwaige Raten Change Points detektiert werden. Im zweiten Schritt wird die Nullhypothese der Varianzhomogenität getestet und etwaige Strukturbrüche der Varianz sollen detektiert werden. Hierbei werden die Raten Change Points als Eingabe verwendet. Das nichtparametrische Verfahren ist auf eine Vielzahl an Lebenszeitverteilungen anwendbar und nicht auf die Alternative genau eines Change Points beschränkt.

Im zweiten Teil der Arbeit werden Punktprozesse resultierend aus Experimenten zur bistabilen Wahrnehmung untersucht. Beim Betrachten visueller Illusionen, die mehr als eine Art der Reizinterpretation zulassen (typischerweise zwei), treten unvorhersagbare Wechsel der Wahrnehmung auf. Die Zeitpunkte dieser Wahrnehmungswechsel bilden einen Punktprozess. Hierbei ist die Wechselrate höchst abhängig vom verwendeten Stimulus und weist große interindivuelle Unterschiede auf. Prominente Beispiele sind der Necker-Würfel (Necker, 1832) oder die Rubinsche Vase (Rubin, 1915). Darstellungen finden sich in Abbildung 2.

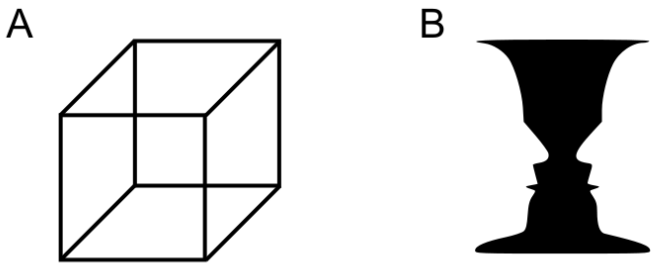

Abbildung 2: Necker-Würfel (A) und Rubinsche Vase (B). *Der Necker-Würfel kann entweder von oben oder von unten wahrgenommen werden. Die Rubinsche Vase kann als Vase oder als zwei sich anschauende Gesichter aufgefasst werden. Die Grafik wurde leicht überarbeitet von https://commons.wikimedia.org/wiki/File:Multistability.svg übernommen (Public Domain license).*

In dieser Arbeit werden Daten aus den Studien Schmack et al. (2013) und Schmack et al. (2015) verwendet. Den Teilnehmern dieser Studien wurde am Monitor eine Ansammlung von sich bewegenden Punkten gezeigt (Abbildung 3). Das "structure-from-motion" Phänomen bedingt, dass wir diesen Stimulus als drehende Sphäre mit nicht eindeutiger Drehrichtung wahrnehmen.

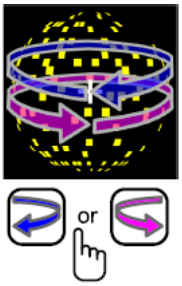

Abbildung 3: Stimulus aus Schmack et al. (2015). *Die Grafik unterliegt einer Creative Commons license.*

Den Studienteilnehmern wurde der Stimulus sowohl kontinuierlich als auch intermittierend, d.h. mit kurzen Phasen eines "blank displays" zwischen den Präsentationsphasen, vorgespielt. Die Zeitpunkte, zu denen die Teilnehmer einen wahrgenommenen Wechsel der Drehrichtung angaben, bilden die Punktprozesse, die im zweiten Teil der Arbeit betrachtet werden. Im Antwortverhalten lassen sich bemerkenswerte Unterschiede zwischen kontinuierlicher und intermittierender Präsentation feststellen (siehe Abbildung 4) mit einer Zunahme der Variabilität (gemessen an der mittleren Dominanzzeit, d.h. des mittleren Intervalls konstanter Wahrnehmung) hin zur intermittierenden Präsentation. Die Verteilung der Längen der Dominanzzeiten ist bei kontinuierlicher Stimulation meist eine rechtsschiefe unimodale Verteilung (Levelt, 1965; Brascamp et al., 2009) mit einem Mittelwert von ca. fünf Sekunden. Bei intermittierender Präsentation mit genügend langen "blank displays" hingegen beobachtet man einen Wechsel zwischen sehr langen, stabilen Dominanzzeiten von über eine Minute (Leopold et al., 2002; Maier et al., 2003) mit sehr kurzen, instabilen Dominanzzeiten von oft weniger als fünf Sekunden (Brascamp et al., 2009).

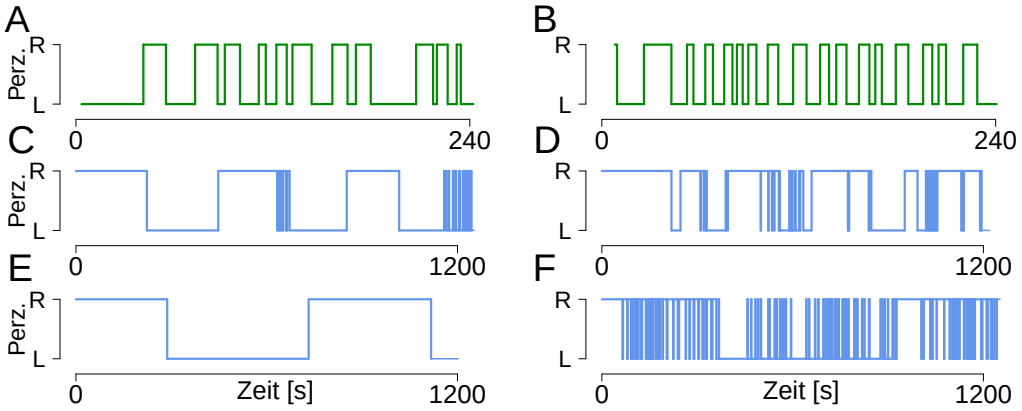

Abbildung 4: Antwortverhalten auf einen bistabilen Stimulus unter kontinuierlicher Präsentation (grün, A, B) und intermittierender Präsentation (blau, C-F). Die Daten stammen aus Schmack et al. (2015). *Es lässt sich eine große interindivuelle Variabilität der Antwortmuster feststellen.*

In der Literatur finden sich einige detaillierte mathematische Modelle zur Beschreibung bistabiler Wahrnehmung, die Eigenschaften wie die Verteilung der Dominanzzeiten bei kontinuierlicher Stimulation (Wilson, 2007; Gershman et al., 2012; Pastukhov et al., 2013; Cao et al., 2014, 2016; Weilnhammer et al., 2017) oder periodisches Verhalten und den Einfluss der Länge des blank displays bei intermittierender Stimulation (Brascamp et al., 2009; Gigante et al., 2009) erklären können. Oftmals wird hierbei eine Rivalität zwischen verschiedenen Wahrnehmungen zugeordneten Neuronenpopulationen angenommen (Laing and Chow, 2002; Wilson, 2007; Brascamp et al., 2009; Gigante et al., 2009; Pastukhov et al., 2013). Die Zunahme an Stabilität bei genügend langem blank display wird mittels multipler Zeitskalen für den Aufbau von Erinnerung modelliert (Brascamp et al., 2009; Gigante et al., 2009).

Aufgrund der Komplexität und Hochdimensionalität der Modelle stellen Parameteranpassungen an Realdaten eine Herausforderung dar, insbesondere unter Berücksichtigung der typischerweise kurzen Aufzeichnungslängen. Des Weiteren sind nur wenige Modelle dokumentiert, die sowohl kontinuierliche als auch intermitterende Stimulation abdecken (Wilson, 2007; Brascamp et al., 2009; Gigante et al., 2009).

Ziel des zweiten Teils dieser Arbeit ist es daher ein stochastisches Modell zu entwickeln, welches das beobachtete Verhalten in den beiden Stimulationsarten mit potenziell zugrundeliegenden Prozessen auf neuronaler Ebene in Verbindung bringt. Das Modell sollte dabei einerseits die große Variabilität der Antwortmuster zu kontinuierlicher und intermittierender Präsentation beschreiben. Andererseits sollte die Anzahl der Parameter klein genug sein um Modellanpassungen an Daten, die oftmals nur aus wenigen Dominanzzeiten bestehen, zu ermöglichen.

Nachfolgend werden die beiden Teile der Arbeit genauer erläutert.

Teil 1

Der in Teil 1 vorgestellte Test und Algorithmus basiert auf dem Multiple Filter Test (MFT) (Messer et al., 2014) und dem zugehörigen Multiple Filter Algorithmus (MFA). Diese wurden ursprünglich für die Detektion von Raten Change Points in Punktprozessen mit gewisser Variabilität der Lebenszeiten entwickelt. Der MFT testet zunächst die Nullhypothese der Ratenhomogenität. Wird diese verworfen, so werden Änderungen in der Rate mittels des MFA detektiert. Die Grundidee ist, Daten aus zwei angrenzenden Teilbereichen des Prozesses (Fenstern) heran zu ziehen, und auf deren Basis die passend skalierte Differenz der geschätzten Rate zu berechnen. Ist die Differenz groß, so spricht dies gegen eine stationäre Rate. Die Fenster werden zum einen vergrößert und zum anderen über den Prozess geschoben. Es werden die sogenannten filtered derivative Prozesse berechnet. Kleine Fenster können eher nah beieinanderliegende Change Points erkennen, während größere Fenster auch kleine Änderungen der Rate detektieren können. Das Maximum aller filtered derivative Prozesse dient als Teststatistik M, die mit einer Verwerfungsschwelle Q verglichen wird. Unter der Nullhypothese konvergieren die filtered derivative Prozesse schwach gegen Gaußsche Grenzprozesse $(L_{h,t})_t$, die von der verwendeten Fenstergröße h abhängen. Q wird als Quantil des Maximums über alle Grenzprozesse simuliert. Falls $M > Q$ wird die Nullhypothese der Ratenhomogenität verworfen.

Im ersten Teil der Arbeit wird der MFT erweitert, um auch Change Points in der Varianz der Lebenszeiten $(\xi_i)_i$ eines Erneuerungsprozesses zu finden. Statt der Rate wird nun die geschätzte Varianz in adjazenten und über den Prozess gleitenden Fenstern unterschiedlicher Größe verglichen (Kapitel 3). Für eine Fenstergröße h wird die Statistik

$$G := G_{h,t} := \frac{\hat{\sigma}^2_{\text{ri}} - \hat{\sigma}^2_{\text{le}}}{\sqrt{\widehat{\mathbb{V}\text{ar}}(\hat{\sigma}^2_{\text{ri}} - \hat{\sigma}^2_{\text{le}})}}$$

mit passenden Schätzern $\hat{\sigma}^2_{\text{le}}$ und $\hat{\sigma}^2_{\text{ri}}$ für die Varianz im linken bzw. rechten Teilfenster verwendet. Etwaige Raten Change Points werden dabei in der Varianzschätzung berücksichtigt.
Unter der Annahme der Varianz- und Ratenhomogenität wird in Theorem 3.4 gezeigt, dass der resultierende Gaußsche Grenzprozess L identisch zum Grenzprozess im Ratenfall ist, d.h. es wird die schwache Konvergenz

$$G \to L$$

in $(D[h, T-h], d_{SK})$ bewiesen (mit T als Zeithorizont). L ist definiert als

$$L := L_{h,t} := \frac{(W_{t+h} - W_t) - (W_t - W_{t-h})}{\sqrt{2h}},$$

wobei $(W_t)_t$ eine standard Brownsche Bewegung ist. Somit kann der Test und Algorithmus für die Varianzen analog zu den Raten angewendet werden. In Theorem 3.6 wird schließlich für die Situation eines Raten Change Points bewiesen, dass der Grenzprozess des filtered derivative Prozesses unter der Nullhypothese der Varianzhomogenität ein zentrierter Gaußscher Prozess $\widetilde{L}$ ist. Dieser unterscheidet sich lediglich in der Kovarianzstruktur in der Umgebung des Raten Change Points vom Prozess L. Der Grenzprozess im Falle mehrer Raten Change Points ist eng verwandt mit $\widetilde{L}$. Da $\widetilde{L}$ von unbekannten Prozessparametern abhängt, schlagen

wir vor, weiterhin den Prozess L zur Simulation der Verwerfungsschwelle Q zu verwenden. Dies wird auch von Simulationsresultaten unterstützt (Abschnitt 5.2). Die ausführlichen Beweise der beiden Theoreme finden sich in Kapitel 4. Hierbei sind das Anscombe-Donsker-Theorem (Theorem 4.1), continuous mapping sowie die Konsistenz der Schätzer für den Mittelwert μ und $\mathbb{V}\mathrm{ar}((\xi_i - \mu)^2)$ von zentraler Bedeutung. Der MFT lässt sich auch für den Test der Homogenität der k-ten Momente der Lebenszeiten verwenden unter Annahme der Homogenität aller niedrigeren Momente (Korollar 3.5).

In Kapitel 5 werden das Signifikanzniveau und die Testmacht des MFT bzw. MFA für die Varianzen in Simulationen untersucht. Der MFA kombiniert die von Einzelfenstern geschätzten Change Points und bevorzugt dabei die mit kleineren Fenstern detektierten Change Points. Mit einem genügend großen kleinsten Fenster in der Fenstermenge wird in den Simulationen das asymptotische Signifikanzniveau des MFT für weite Parameterbereiche eingehalten – auch bei zusätzlichen Raten Change Points (Abschnitte 5.1 und 5.2). Die Detektionswahrscheinlichkeit von Varianz Change Points wird von einer unbekannten, zu schätzenden Rate kaum beeinflusst und ist abhängig sowohl von der Stärke der Varianzänderung als auch von der Regularität des Prozesses (Abschnitt 5.3).

Schließlich werden MFT und MFA für die Rate und die Varianz in Kapitel 6 auf einen Datensatz von Spike Train Aufnahmen angewendet. Die Daten wurden als spontane Aktivität dopaminerger Neurone der Substantia nigra von anästhesierten Mäusen aufgenommen und in Schiemann et al. (2012) veröffentlicht. In ungefähr der Hälfte der Fälle werden beide Nullhypothesen von konstanter Rate und konstanter Varianz verworfen und multiple Raten und Varianz Change Points geschätzt.

Der erste Teil schließt mit einer Zusammenfassung in Kapitel 7. Hierbei wird betont, dass die vorgeschlagene Methode hilfreich bei der Change Point Detektion und Einteilung von Prozessen wie neuronalen Spike Trains in stationäre Abschnitte ist. Die Methode kann daher entweder im Sinne der Aufdeckung von Nichtstationaritäten oder als vorbereitender Schritt für statistische Analysen mit Stationaritätsannahmen dienen.

Veröffentlichte Inhalte: Dieser Teil der Arbeit ist größtenteils in Albert et al. (2017a) veröffentlicht. Die untersuchten Daten sind von Schiemann et al. (2012) publiziert. Der Code des Varianz-MFTs ist als Teil des Pakets `MFT` unter CRAN verfügbar (https://CRAN.R-project.org/package=MFT, Messer et al. (2017)).

Teil 2

Der zweite Teil der Arbeit behandelt die Modellierung des Antwortverhaltens auf bistabile Stimulation, wobei Daten aus Schmack et al. (2013, 2015) analysiert werden. Es soll u.a. die Zunahme an Variabilität von Antwortmustern auf kontinuierliche Stimulation hin zum Antwortverhalten auf intermittierende Stimulation beschrieben werden. In Kapitel 8 wird zunächst das Experiment genauer erläutert und eine Einführung in die wichtigsten Begriffe gegeben.

Zur Beschreibung der Daten wird in Kapitel 9 erstmals ein einfaches Hidden Markov Modell (HMM) verwendet, welches die beobachteten Antwortmuster mit wenigen Parametern

beschreibt. Im Falle kontinuierlicher Präsentation erzeugt ein Zustand unabhängige, identisch verteilte Dominanzzeiten, die entweder Gamma oder invers Gauß verteilt sind (mit Parametern μ und σ). Die Existenz von langen stabilen und kurzen instabilen Dominanzzeiten bei intermittierender Stimulation erfordert die Verwendung eines HMM mit zwei verborgenen Zuständen (siehe Abbildung 5). Parameter sind hier $\mu_S, \sigma_S, \mu_U, \sigma_U$ für die inverse Gauß (IG) Verteilung der Dominanzzeiten im stabilen (S) bzw. instabilen (unstable, U) Zustand sowie die Bleibewahrscheinlichkeiten p_{SS} und p_{UU}. Die Parameterschätzung baut für beide Stimulationsarten auf bekannten Methoden auf: Die Maximum-Likelihood-Methode und für die IG-Verteilung alternativ ein UMVU Schätzer (gleichmäßig bester erwartungstreuer Schätzer) wird beim HMM für die kontinuierliche Präsentation angewendet (Abschnitt 9.3), wobei zusätzlich die exakte Verteilung der ML-Schätzer unter IG-Verteilung hergeleitet wird. Das Resultat der Verteilung des Schätzers $\hat{\sigma}$ ist dabei originär in dieser Arbeit. Zum Schätzen der Parameter des HMM mit zwei Zuständen wird der Baum-Welch-Algorithmus (BWA, Baum and Petrie, 1966, basierend auf ML) verwendet (Abschnitt 9.4). Erstmals wird in der Arbeit dabei ein HMM mit invers Gauß verteilten Emissionen verwendet und die entsprechenden Parameterschätzer im Rahmen des BWA hergeleitet. Die Genauigkeit der Parameterschätzung wird in Abschnitt 9.6 für verschiedene Szenarien evaluiert. Hierbei ergeben sich trotz der geringen sample sizes zufriedenstellende Resultate.

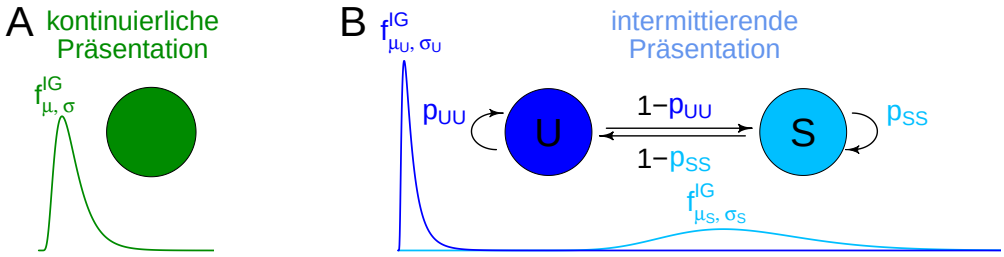

Abbildung 5: Ein HMM zur Beschreibung bistabiler Wahrnehmung. *(A) Ein Zustand induziert eine unimodale Verteilung der Dominanzzeiten unter kontinuierlicher Präsentation. (B) Zwei Zustände (S und U) emittieren lange und kurze Dominanzzeiten bei intermittierender Stimulation.*

In Kapitel 10 werden theoretische Eigenschaften der vom HMM erzeugten Punktprozesse von Wahrnehmungswechseln betrachtet. In Abschnitt 10.1 liegt der Fokus auf der kontinuierlichen Präsentation, während sich Abschnitt 10.2 dem HMM mit zwei Zuständen zur Modellierung des Antwortverhaltens während intermittierender Stimulation widmet. Es werden die Anzahl an Wechseln in einem Zeitintervall, Eintrittszeiten und Gleichgewichtszustände betrachtet. Ein bedeutendes Resultat (Korollar 10.8) betrifft hierbei die asymptotische Wahrscheinlichkeit, dass der verborgene Prozess $\tilde{Y}$ im stabilen Zustand ist

$$\tilde{\pi}_S := \lim_{t\to\infty} (\tilde{Y}_t = S) = \frac{\frac{1}{1-p_{SS}}\mu_S}{\frac{1}{1-p_{SS}}\mu_S + \frac{1}{1-p_{UU}}\mu_U},$$

die der erwarteten relativen Zeit im stabilen Zustand entspricht.

Das Hidden Markov Modell ist ein beschreibendes Modell und stellt keine Verbindung zu potenziell zugrundeliegenden Prozessen auf neuronaler Ebene her. Des Weiteren kann die

empirisch beobachtete Eigenschaft, dass stabile Dominanzzeiten vor einem Zustandswechsel zum instabilen Zustand kürzer sind, im HMM nicht modelliert werden. Daher wird in Kapitel 11 das sogenannte Hierarchische Brownsche Modell (HBM) vorgestellt, welches gleichzeitig die zugrundeliegende, aggregierte neuronale Aktivität und die beobachteten Antwortmuster beschreiben soll.

Zentrale Idee des HBM ist, dass das Wechseln der Wahrnehmung durch den Konflikt zweier Neuronenpopulationen hervorgerufen wird (vgl. z.B., Gigante et al., 2009). Um die Modellkomplexität gering zu halten, wird angenommen, dass sich der Prozess der Aktivitätsdifferenz (genannt perception process P) zwischen diesen beiden Populationen durch eine Brownsche Bewegung mit Drift beschreiben lässt (ähnlich wie in Cao et al., 2016). Weiterhin wird angenommen, dass dieser Prozess zwischen zwei Schwellen fluktuiert, wobei die ersten Übertrittszeiten über eine Schwelle einen Wechsel der Wahrnehmung und des Driftvorzeichens bewirken (Abbildung 6). Zur Beschreibung des Prozesses genügen folglich nur zwei Parameter, die Schwelle b und die Drift ν_0 (Abschnitt 11.1). Wir nehmen an

$$dP_t = S_t \nu_0 dt + dW_t, \qquad \text{mit} \qquad P_0 = -b,$$

wobei $(W_t)_t$ eine standard Brownsche Bewegung ist und $S_t := S(P_t, t)$ der Prozess des Driftvorzeichens mit Wert -1, falls P_t zuletzt b traf und Wert 1, falls P_t zuletzt $-b$ traf. Es gilt $S_0 := 1$. Die Dominanzzeiten sind somit durch die Treffzeiten der Schwellen gegeben. Als Treffzeiten einer Schwelle durch eine Brownsche Bewegung mit Drift sind die Dominanzzeiten invers Gauß verteilt (mit Parametern $2b/\nu_0$ und $\sqrt{2b/\nu_0^3}$ für die kontinuierliche Präsentation). Es gibt folglich eine einfache Beziehung zwischen den HBM Parametern für die kontinuierliche Stimulation und den entsprechenden HMM Parametern (unter der Annahme der invers Gauß-Verteilung im HMM).

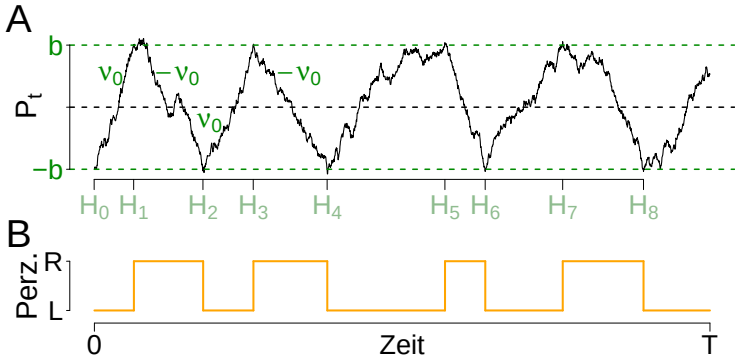

Abbildung 6: Das HBM für kontinuierliche Präsentation. *Die Übertrittszeiten (H_i) einer Brownschen Bewegung (schwarz, A) mit Drift $\pm\nu_0$ über Schwellen $\pm b$ induzieren Wechsel der Wahrnehmung (orange, B).*

Um die Antwortmuster auf intermittierende Stimulation im gleichen Modellrahmen darzustellen, wird in Abschnitt 11.2 ein hierarchisches Modell eingeführt. In diesem basiert das für diese Stimulationsart typische Wechseln zwischen stabilem und instabilem Zustand gleichfalls auf dem Konflikt von Neuronenpopulationen und dem Überschreiten einer Schwelle durch den Prozess der zugehörigen Aktivitätsdifferenz, der als background process B bezeichnet wird. Diese Differenz wird abermals durch eine Brownsche Bewegung modelliert (mit Drift Null

während Präsentationsphasen). Der background process bestimmt die Schwelle des perception process und dessen Drift während blank displays. Diese Drift und die Schwelle unterscheiden sich je nach verborgenem Zustand. Während Präsentationsphasen ist die Drift des perception process weiterhin durch ν_0 gegeben. Die weiteren Parameter sind nun die Schwellen b_S, b_U und Drifts ν_S, ν_U des perception process im stabilen bzw. instabilen Zustand sowie die Schwellen $\tilde{b}_S, \tilde{b}_U$ und die Drift ν_B des background process während blank displays. Unter gewissen Modellannahmen können die HBM Parameter mit den HMM Parametern verglichen werden (siehe Abschnitt 11.2.3). So gilt mit der mittleren Drift ν_S^* während stabiler Phasen für den Mittelwert μ_S^* und die Standardabweichung σ_S^* der Dominanzzeiten

$$\mu_S^* \approx 2b_S/\nu_S^* \quad \text{und} \quad \sigma_S^* \approx \sqrt{2b_S/{\nu_S^*}^3},$$

wobei die Approximation durch die Verwendung der mittleren Drift ν_S^* statt der sich unterscheidenden Drift ν_0 und ν_S begründet ist (die Auswirkungen dieser Vereinfachung sind vernachlässigbar). Ein analoges Resultat ist für die instabilen Phasen möglich. Weiterhin wird die Eigenschaft des HBM, dass die Übergangswahrscheinlichkeiten zwischen den Zuständen abhängig von der Länge der gegenwärtigen Dominanzzeit d_i sind, mathematisch analysiert. Für die Bleibewahrscheinlichkeit im stabilen Zustand gilt beispielsweise

$$\tilde{p}_{SS}(d_i) := \mathbb{P}(Y_{i+1} = S | Y_i = S, d_i) \approx 1 - \Phi_{\nu_B^* d_i, d_i}\left(\tilde{b}_S\right),$$

wobei Y_i der verborgene Zustand zur Zeit $i \geq 1$ ist, ν_B^* die durchschnittliche Drift des background process ist und $\Phi()$ die Verteilungsfunktion der Normalverteilung beschreibt. Die mittlere Bleibewahrscheinlichkeit p_{SS}^* erhält man durch Integration über die Länge der Dominanzzeit d_i wie folgt

$$p_{SS}^* \approx \mathbb{P}(X_S \geq \tilde{b}_S),$$

wobei X_S normal-invers Gauß-verteilt ist (Definition 8.9) mit Parametern $(0, \sqrt{{\nu_S^*}^2 + {\nu_B^*}^2}, \nu_B^*, 2b_S)$. Ähnliche Resultate gelten für den instabilen Zustand.

Die Parameterschätzung für das HBM wird in Kapitel 12 beleuchtet. Im Falle kontinuierlicher Präsentation kann abermals die Maximum-Likelihood-Methode verwendet werden (Abschnitt 12.1) und bei intermittierender Präsentation wird die Likelihood-Funktion L mittels Forward-Variablen $\alpha_j(i)$, die die Wahrscheinlichkeit der Beobachtungen $d_1, \ldots, d_i$ und des Zustands j zur Zeit i angeben, wie folgt bestimmt

$$L(d_1, \ldots, d_n) \approx \alpha_S(n) + \alpha_U(n)$$

und die resultierende log-likelihood numerisch maximiert (Abschnitt 12.2). n ist dabei die Anzahl der Dominanzzeiten. In Abschnitt 12.4 wird die Präzision der Parameterschätzung analysiert und gezeigt, dass auch kurze Datenstücke zu validen Schätzungen führen. Weiterhin wird in Kapitel 12.5 gezeigt, dass der Viterbi-Algorithmus zur Klassifikation der Dominanzzeiten als stabil und instabil für das HBM anwendbar ist.

Theoretische Resultate zum vom HBM induzierten Punktprozess folgen in Kapitel 13. Abermals werden die Anzahl der Wechsel, erste Treffzeiten und Gleichgewichtsverteilungen analysiert. Weiterhin werden Verbindungen des Prozesses zu bekannten stochastischen Prozessen wie Semi-Markov- oder regenerativen Prozessen betrachtet. Zudem werden marginale Verteilungen des perception und des background Prozesses hergeleitet.

Die Anwendung der beiden Modelle auf den Datensatz aus Schmack et al. (2013) und Schmack et al. (2015) erfolgt in den Kapiteln 14.1 und 14.2. Beide Modelle können auf die teils kurzen Datenstücke angepasst werden und sowohl die rechtsschiefe unimodale Verteilung der Dominanzzeiten während kontinuierlicher Präsentation als auch die bimodale Verteilung während intermittierender Stimulation wiedergeben. Zudem ermöglichen sie eine hohe interindividuelle Variabilität der Antwortmuster. Weiterhin lässt sich mit dem HMM eine hohe Reproduzierbarkeit des Antwortverhaltens während kontinuierlicher Präsentation zeigen (Figure 14.7), d.h. die Verteilungen der Dominanzzeiten des gleichen Probanden in zwei unterschiedlichen Versuchsdurchläufen ähneln sich stark. Das HBM erfüllt die in den Daten beobachtete Eigenschaft kürzerer stabiler Dominanzzeiten vor einem Zustandswechsel in den instabilen Zustand, wie in Figure 14.11 sichtbar ist. Des Weiteren können auch in den Daten beobachtete Unterschiede zwischen einer Kontrollgruppe und einer Gruppe von Patienten mit Schizophrenie in den Modellparametern des HMM und HBM identifiziert werden. Insbesondere ermöglicht das HBM die Verbindung zu potenziell zugrundeliegenden Prozessen im Gehirn. Im Wesentlichen trägt im Rahmen der Annahmen des HBM bei den Patienten eine geringere Anregung von Neuronen im stabilen Zustand während intermittierender Stimulation zu geringerer Stabilität der Wahrnehmung bei, während die Anzahl der beteiligten Neuronen bei kontinuierlicher Präsentation größer ist und somit hier im Vergleich zur Kontrollgruppe für erhöhte Stabilität der Wahrnehmung verantwortlich ist (Figure 14.13).

Ein Fazit in Kapitel 15 rundet den zweiten Teil ab. Das HBM bildet eine Brücke zwischen empirischer Datenanalyse und mechanistischen Modellen. Einerseits zielt es auf eine präzise Beschreibung der hohen Variabilität der Antwortmuster und der Varianzzunahme von kontinuierlicher zu intermittierender Präsentation ab, anderseits sollen potenziell zugrundeliegende neuronale Prozesse beschrieben werden. Verschiedene Erweiterungsmöglichkeiten zeigen das Potenzial des HBM, Ergebnisse verwandter Experimente zur multistabilen Wahrnehmung zu analysieren. Durch seine Anwendbarkeit auf kontinuierliche und intermittierende Stimulation können auf Basis des HBMs neue Hypothesen über potenzielle neuronale Mechanismen kognitiver Phänomene entwickelt werden.

Eine Darstellung der Daten aus Schmack et al. (2015) findet sich in Anhang A.

Veröffentlichte Inhalte: Weite Abschnitte des zweiten Teils der Arbeit (insbesondere Abschnitte der Kapitel 9, 11, 12, 14 und 15) sind in Albert et al. (2017b) veröffentlicht. Die untersuchten Daten sind von Schmack et al. (2013, 2015); Weilnhammer et al. (2016) publiziert.

Insgesamt betrachtet werden in dieser Arbeit zwei Ansätze zur Modellierung von Punktprozessen mit unterschiedlichen Arten an Variabilitätsänderungen vorgestellt. Im ersten Teil wird eine Methode zur Detektion von Change Points in Mittelwert und Varianzen von Lebenszeiten eines Punktprozesses präsentiert, während sich der zweite Teil einem mechanistische Modelle und empirische Datenanalyse verbindenden Ansatz zur Modellierung des Antwortverhaltens bistabiler Wahrnehmung widmet. Die Arbeit beinhaltet daher einerseits Techniken, die hilfreich für die Signaldetektion sein können und als vorbereitender Schritt für statistische Analysen, die auf Raten- und Varianzhomogenität beruhen, dienen können. Andererseits wird ein mechanistisches stochastisches Modell vorgestellt, welches die Variabilität in Antwortmustern auf kontinuierliche und intermittierende Stimulation mit einem bistabilen Stimulus abbilden kann und somit wertvolle, neue Hypothesen über potenzielle neuronale Mechanismen visueller Wahrnehmung liefert.